



A University of Sussex PhD thesis

Available online via Sussex Research Online:

<http://sro.sussex.ac.uk/>

This thesis is protected by copyright which belongs to the author.

This thesis cannot be reproduced or quoted extensively from without first obtaining permission in writing from the Author

The content must not be changed in any way or sold commercially in any format or medium without the formal permission of the Author

When referring to this work, full bibliographic details including the author, title, awarding institution and date of the thesis must be given

Please visit Sussex Research Online for more information and further details

IDENTIFICATION AND CHARACTERISATION OF A NOVEL INHIBITOR OF SERINE RACEMASE THROUGH A FRAGMENT- BASED DRUG DISCOVERY STRATEGY

A thesis submitted to the University of Sussex for the
degree of Doctor of Philosophy (DPhil)

By Chloe Rose Koulouris

OCTOBER 2017

Supervisor – John Atack
Sussex Drug Discovery Centre
School of Life Sciences, Uni. Sussex

Declaration

I hereby declare that this thesis has not been and will not be, submitted in whole or in part to another University for the award of any other degree.

Signed.....

C. R. Koulouris

Acknowledgements

First and foremost I would like to thank my supervisor, Prof. John Atack, for his continuous support, guidance, and expertise throughout the many highs and lows of this project. His persisting faith in me and sense of humour during my countless grumpy moments kept me going when I felt science was getting the better of me. I must also acknowledge the University of Sussex for graciously providing the funding that enabled my research on this exciting target.

I would like to thank my correspondents at Evotec, particularly Myron Smith and Michael Wood, for their invaluable perspective and advice regarding serine racemase, and for providing the resources that made this work possible. I must also extend my most sincere gratitude to those biologists — Sarah Walker, Gareth Williams, and Trevor Askwith — who helped me day-to-day in the lab, answering my incessant questions and giving advice on experiments, data, and life.

I am grateful to my parents, who have never understood what I do but have always been proud, loving, and supportive (both emotionally and financially). And thanks to all my siblings, whom I love, and will moan if I do not mention them.

There are many more I am indebted to. James Noble, for the crystallography expertise and for being fabulously James. Scott Henderson, the skilled chemist who diligently ordered and synthesised my SR inhibitors. Ryan West, for making me laugh and always being keen to answer my chemistry queries. Those friends who stuck around as I became more entrenched in my PhD and occasionally neglectful of them — Alex, Pheiffer, Sofia, Aisha. My roller derby team, for being a constructive outlet despite the injuries. All the other PhD students, for the camaraderie, humour, commiseration, and beer. A huge thank you to my best pal Yusuf Ali, for the procrastination, the motivation, the vindication, and of course, the zombie-killing catharsis.

And thank you to the Sussex Drug Discovery Centre, for being a home to me these past four years.

Abstract

The N-methyl-D-aspartate (NMDA) receptors (NMDAR) are a subtype of ionotropic glutamate receptors that are highly expressed in the central nervous system (CNS) and are involved in the excitatory synaptic transmission and synaptic plasticity that underpin many critical CNS functions. NMDAR dysfunction has been implicated in Alzheimer's disease, neuropathic pain, schizophrenia, and depression, among others. Most non-selective NMDAR antagonists (e.g. ketamine) have undesirable side-effects that restrict their clinical utility for relieving symptoms of neuropathic pain and treatment-resistant depression, but indirect modulators of NMDAR function offer the potential to have reduced side-effects relative to non-selective antagonists. One approach is to inhibit the production of the NMDAR co-agonist, D-serine, which is produced endogenously by conversion of L-serine to D-serine by the enzyme serine racemase (SR). Inhibitors of SR that reduce the production of D-serine may therefore have therapeutic benefits in disorders associated with NMDAR hyperfunction.

In this thesis, human SR (hSR) was expressed in a bacterial host and isolated to a high degree of purity (> 90%). The crystal structure of SR was solved in-house using the purified protein, to a resolution of 2.2 Å (in complex with malonate) and 1.9 Å (holoenzyme). To measure SR activity, a coupled biochemical assay was optimised, in which produced D-serine is degraded by D-amino acid oxidase (DAO) and the resulting H₂O₂ is quantified by a chemiluminescence reaction with HRP and luminol to produce light. Assay parameters such as K_m and IC_{50} were determined, and following further optimisation to enable medium-throughput screening, a single-point screen of 3000 fragments was performed to identify novel inhibitory hit matter. A final list of 61 specific hits was collated of fragments that did not exhibit nonspecific inhibition in a DAO counter screen, and demonstrated IC_{50} values against SR approximately 1 mM or below. These specific hits were characterised with biophysical methods adapted for SR (thermal shift, microscale thermophoresis) to determine binding affinities and structure stabilisation. Finally, via crystal soaking, the crystal structure of SR bound to an inhibitory fragment (K_D = 960 µM) was revealed to a resolution of 1.8 Å.

Table of Contents

Acknowledgements.....	ii
Abstract.....	iii
Contents.....	iv
List of Figures.....	ix
List of Tables.....	xii
Abbreviations.....	xiii

1 INTRODUCTION	1
1.1 GLUTAMATERGIC NEUROTRANSMISSION	1
1.1.1 THE GLUTAMATE SYNAPSE	2
1.1.2 GLUTAMATE RELEASE	2
1.1.3 GLUTAMATE TRANSPORTERS	3
1.2 GLUTAMATE RECEPTORS	6
1.2.1 METABOTROPIC GLUTAMATE RECEPTORS	6
1.2.2 IONOTROPIC GLUTAMATE RECEPTORS	8
1.2.3 DISTRIBUTION AND FUNCTION OF IGLURS	11
1.2.4 STRUCTURE OF IGLURS	12
1.3 NMDA RECEPTORS	16
1.3.1 UNIQUE CHARACTERISTICS OF NMDA RECEPTORS	16
1.3.2 LONG-TERM POTENTIATION AND LONG-TERM DEPRESSION	17
1.4 NMDA RECEPTOR PATHOPHYSIOLOGY AND PHARMACOLOGY.....	20
1.4.1 ROLE OF GLUTAMATE AND NMDA RECEPTORS IN DISEASE	20
1.4.2 SCHIZOPHRENIA.....	20
1.4.3 NEUROPATHIC PAIN.....	22
1.4.4 ALZHEIMER’S DISEASE	24
1.4.5 MAJOR DEPRESSIVE DISORDER.....	27
1.5 KETAMINE AS A THERAPEUTIC AGENT	29
1.5.1 RODENT STUDIES	30
1.5.2 HUMAN STUDIES.....	32
1.5.3 SIDE-EFFECT PROFILE OF KETAMINE	35
1.6 THERAPEUTIC APPROACHES TO MODULATING NMDA RECEPTOR FUNCTION	36
1.6.1 DIRECT EFFECTS ON NMDAR FUNCTION.....	36
1.6.2 AGONISTS AND PARTIAL AGONISTS	36
1.6.3 SUBUNIT-SPECIFIC NMDAR ANTAGONISTS.....	39
1.6.4 UNCOMPETITIVE ANTAGONISTS	41
1.6.5 INDIRECT EFFECTS ON NMDAR FUNCTION	43
1.6.6 TRANSPORTERS INHIBITORS	43
1.6.7 D-SERINE MODULATION	47
1.7 SERINE RACEMASE	50
1.7.1 DISCOVERY AND HISTORICAL CONTEXT	50
1.7.2 STRUCTURE OF SERINE RACEMASE	51
1.7.3 ENZYMATIC ROLE AND REACTION MECHANISM	54
1.7.4 FUNCTION OF SR <i>IN VIVO</i>	57
1.7.5 LINKING SR TO DISEASE.....	59
1.7.6 SERINE RACEMASE KNOCK-OUT MICE	61
1.7.7 SERINE RACEMASE INHIBITION	65
1.8 THE DRUG DISCOVERY PROCESS	71

1.8.1	TARGET IDENTIFICATION	71
1.8.2	TARGET VALIDATION	72
1.8.3	ASSAY DEVELOPMENT	73
1.8.4	HIT IDENTIFICATION.....	73
1.8.5	FRAGMENT-BASED DRUG DISCOVERY	74
1.8.6	HIT-TO-LEAD AND LEAD OPTIMISATION	75
1.9	AIM.....	76
2	RESULTS I: PROTEIN PRODUCTION AND PURIFICATION	77
2.1	INTRODUCTION	77
2.2	MATERIALS	81
2.2.1	PLASMIDS AND STRAINS	81
2.2.2	MEDIA	81
2.2.3	BUFFERS AND SOLUTIONS	81
2.2.4	ANTIBODIES	82
2.2.5	FURTHER MATERIALS, EQUIPMENT AND KITS	82
2.3	METHODS.....	83
2.3.1	MOLECULAR BIOLOGY	83
2.3.2	TRANSFORMATION OF COMPETENT CELLS.....	84
2.3.3	PREPARATION OF GLYCEROL STOCKS	84
2.3.4	EXPRESSION OF RECOMBINANT HUMAN SR	84
2.3.5	PROTEIN PURIFICATION	85
2.3.6	DETERMINATION OF PROTEIN CONCENTRATION.....	87
2.3.7	SODIUM DODECYL SULPHATE POLYACRYLAMIDE GEL ELECTROPHORESIS	87
2.3.8	WESTERN BLOT	88
2.3.9	MASS SPECTROMETRY	88
2.4	RESULTS.....	90
2.4.1	PLASMID SEQUENCING CONFIRMS PRESENCE OF SR GENE.....	90
2.4.2	IMAC PURIFICATION ISOLATES SR FROM LYSATE	90
2.4.3	OPTIMISATION OF SEC PURIFICATION.....	92
2.4.4	PURIFIED SR CHARACTERISED BY ANALYTICAL METHODS.....	98
2.4.5	MOLECULAR WEIGHT MARKERS IN SEC COLUMN	98
2.4.6	SR VISUALISED BY WESTERN BLOT	98
2.4.7	SR SEQUENCE CONFIRMED BY MASS SPECTROMETRY	101
2.4.8	SUMMARY OF SR PURIFICATIONS.....	103
2.5	DISCUSSION.....	104
3	RESULTS II: BIOCHEMICAL ASSAY DEVELOPMENT.....	107
3.1	INTRODUCTION	107
3.2	MATERIALS	111
3.2.1	REAGENTS	111
3.2.2	BUFFERS AND ASSAY SOLUTIONS	111
3.2.3	REAGENT SOLUTIONS.....	112
3.2.4	FURTHER MATERIALS, EQUIPMENT AND KITS	112
3.3	METHODS.....	113
3.3.1	GENERAL ASSAY PROCEDURE	113
3.3.2	PRE-TREATMENT OF L-SERINE	114
3.3.3	INITIAL EXPERIMENTS WITH AMPLITE RED	114
3.3.4	SR TIME COURSE.....	114
3.3.5	MICHAELIS-MENTEN CONSTANT, K_M	115
3.3.6	DIMETHYL SULFOXIDE TOLERANCE.....	115

3.3.7	DETERMINATION OF IC ₅₀	116
3.3.8	PRE-SCREENING PLATE TESTS.....	117
3.4	RESULTS.....	122
3.4.1	PRELIMINARY EXPERIMENTS WITH AMPLITE RED	122
3.4.2	L-SERINE TREATMENT REMOVES CONTAMINATING D-SERINE	122
3.4.3	D-SERINE STANDARD CURVE.....	124
3.4.4	EFFECT OF BUFFERS ON SR ACTIVITY	126
3.4.5	INFLUENCE OF TEMPERATURE AND BUFFER PH AND ON SR ACTIVITY	128
3.4.6	DTT ATTENUATES SR ACTIVITY	130
3.4.7	CHEMILUMINESCENCE REACTION IS IN EXCESS	131
3.4.8	SR ASSAY CAN BE TERMINATED BY EDTA	132
3.4.9	TRIS VS. PHOSPHATE BUFFER	134
3.4.10	TIME-DEPENDENCY EXPERIMENT.....	136
3.4.11	DETERMINATION OF MICHAELIS-MENTEN CONSTANT, K _M	136
3.4.12	SR TOLERANCE TO DMSO.....	139
3.4.13	DETERMINATION OF IC ₅₀ VALUES.....	139
3.4.14	OPTIMISATION OF PLATE TESTS.....	141
3.5	DISCUSSION.....	145
4	RESULTS III: BIOPHYSICAL METHODS.....	148
4.1	INTRODUCTION	148
4.1.1	THERMAL SHIFT	148
4.1.2	MICROSCALE THERMOPHORESIS (MST).....	149
4.1.3	ISOTHERMAL TITRATION CALORIMETRY (ITC)	151
4.2	MATERIALS	153
4.2.1	REAGENTS	153
4.2.2	BUFFERS AND SOLUTIONS	153
4.2.3	FURTHER MATERIALS, EQUIPMENT AND KITS	153
4.3	METHODS.....	154
4.3.1	THERMAL SHIFT	154
4.3.2	MST.....	154
4.3.3	ITC.....	157
4.4	RESULTS.....	160
4.4.1	THERMAL SHIFT: PROTEIN AND DYE CONCENTRATION	160
4.4.2	THERMAL SHIFT: DMSO TOLERANCE.....	162
4.4.3	THERMAL SHIFT: MALONATE BINDING STABILISES SR	162
4.4.4	MST: INFLUENCE OF BUFFERS AND CENTRIFUGATION	164
4.4.5	MST: OPTIMISATION OF SOFTWARE PARAMETERS.....	166
4.4.6	MST: DMSO AND MALONATE CONTROLS.....	166
4.4.7	MST: K _D DETERMINATION OF MALONATE	169
4.4.8	ITC: K _D DETERMINATION OF MALONATE	170
4.5	DISCUSSION.....	172
5	RESULTS IV: CRYSTALLOGRAPHY	174
5.1	INTRODUCTION	174
5.1.1	BACKGROUND TO SR CRYSTALLISATION.....	174
5.1.2	VAPOUR DIFFUSION: SITTING-DROP VS. HANGING-DROP	175
5.1.3	CO-CRYSTALLISATION VS. CRYSTAL SOAKING.....	175
5.1.4	MICROSEEDING	177
5.2	MATERIALS	178
5.2.1	CRYSTALLISATION REAGENTS	178

5.2.2	BUFFERS AND SOLUTIONS	178
5.2.3	COMMERCIAL SCREENS	178
5.2.4	OTHER MATERIALS, EQUIPMENT AND KITS	178
5.3	METHODS.....	180
5.3.1	PREPARATION OF PROTEIN SOLUTION	180
5.3.2	SITTING-DROP VAPOUR DIFFUSION	180
5.3.3	HANGING-DROP VAPOUR DIFFUSION	181
5.3.4	CRYSTAL SOAKING	181
5.3.5	SELECTION OF CRYSTALS	182
5.3.6	DATA COLLECTION AND STRUCTURE SOLUTION	182
5.4	RESULTS.....	183
5.4.1	CRYSTALLISATION WITH MALONATE	183
5.4.2	CRYSTAL STRUCTURE OF SR-MALONATE COMPLEX	185
5.4.3	CRYSTALLISATION OF THE SR HOLOENZYME	187
5.4.4	CRYSTAL STRUCTURE OF SR HOLOENZYME	188
5.4.5	REPETITION OF THE SR <i>HOLO</i> CRYSTAL	190
5.4.6	CRYSTALLISATION OF <i>HOLO</i> SR BY HANGING-DROP VAPOUR DIFFUSION	192
5.5	DISCUSSION	193
6	RESULTS V: ANALYSIS OF LITERATURE INHIBITORS	195
6.1	INTRODUCTION.....	195
6.2	MATERIALS	197
6.2.1	SR INHIBITORS.....	197
6.2.2	BUFFERS AND SOLUTIONS	197
6.2.3	REAGENT SOLUTIONS.....	197
6.2.4	FURTHER MATERIALS, EQUIPMENT AND KITS	198
6.3	METHODS.....	199
6.3.1	COMPOUND IC ₅₀ DETERMINATION	199
6.3.2	THERMAL DENATURATION ANALYSIS.....	199
6.4	RESULTS.....	200
6.4.1	IC ₅₀ VALUES FOR LITERATURE COMPOUNDS	200
6.4.2	THERMAL DENATURATION ANALYSIS OF LITERATURE COMPOUNDS	202
6.5	DISCUSSION	204
7	RESULTS VI: FRAGMENT SCREEN AND HIT VALIDATION.....	207
7.1	INTRODUCTION	207
7.2	MATERIALS	211
7.2.1	REAGENTS	211
7.2.2	FRAGMENT LIBRARIES	211
7.2.3	BUFFERS AND SOLUTIONS	211
7.2.4	FURTHER MATERIALS, EQUIPMENT AND KITS	212
7.3	METHODS.....	213
7.3.1	SR SINGLE-POINT FRAGMENT SCREEN	213
7.3.2	DAO COUNTER SCREEN.....	215
7.3.3	IC ₅₀ DETERMINATION OF FRAGMENT SCREEN HITS.....	215
7.3.4	FRAGMENT SCREEN DATA ANALYSIS.....	216
7.4	RESULTS.....	217
7.4.1	INITIAL SR SCREEN YIELDS >1000 HITS	217
7.4.2	DAO COUNTER SCREEN REDUCES HIT NUMBER TO 330.....	220
7.4.3	IC ₅₀ DETERMINATION OF THE HITS.....	223
7.4.4	BIOPHYSICAL HIT VALIDATION.....	225

7.4.5	THERMAL DENATURATION ANALYSIS OF FRAGMENT HITS	225
7.4.6	MST SINGLE-POINT ANALYSIS OF 61 HITS	228
7.4.7	MST K_D DETERMINATION OF FRAGMENT HITS	229
7.4.8	MST AGGREGATION AND FLUORESCENCE CONTROLS	232
7.4.9	ITC DIRECT TITRATION WITH FRAGMENTS	233
7.4.10	ITC DISPLACEMENT BINDING EXPERIMENTS	235
7.4.11	CO-CRYSTALLISATION OF FRAGMENT HITS	240
7.4.12	CRYSTAL STRUCTURE OF SR COMPLEX WITH 3-PYRIDIN-4-YL BENZOIC ACID	242
7.5	DISCUSSION	245
8	CONCLUSIONS AND FUTURE WORK	251
9	BIBLIOGRAPHY	254
10	APPENDIX	291
10.1	PROFILE OF PET-24A PLASMID	291
10.2	PUBLISHED SR BIOCHEMICAL ASSAYS	292
10.3	SR LITERATURE INHIBITORS	293
10.4	61 FRAGMENT INHIBITORS OF SR	297
10.5	CRYSTALLOGRAPHY RESULTS TABLES	302
10.5.1	SR-MALONATE COMPLEX	302
10.5.2	SR HOLOENZYME	303
10.5.3	SR COMPLEX WITH 3-PYRIDIN-4-YL BENZOIC ACID	303
10.6	RAMACHANDRAN PLOTS	304
10.6.1	SR-MALONATE COMPLEX	304
10.6.2	SR HOLOENZYME	305

List of Figures

Figure 1.1. The glutamate synapse.	5
Figure 1.2. Structure and domain organisation of the N-methyl-D-aspartate (NMDA) receptor.	12
Figure 1.3. Crystal structure of NMDA receptor and comparison with AMPA receptor.	15
Figure 1.4. Long-term potentiation and long-term depression.	19
Figure 1.5. The structure of human SR in complex with its orthosteric inhibitor malonate (PDB 3L6B).	53
Figure 1.6. Reaction mechanism of L-serine isomerisation by SR.....	56
Figure 2.1. Pairwise sequence alignment of hSR M1 CDS and its closest database match.	91
Figure 2.2. SDS-PAGE of fractions resulting from immobilised-metal affinity chromatography (IMAC) purification of SR.....	93
Figure 2.3. Initial SR SEC purifications resulted in high levels of protein aggregation...	95
Figure 2.4. Activity comparison of aggregate (Peak 1) and soluble (Peak 2) SR.	96
Figure 2.5. Addition of glycerol reduces SR aggregation during SEC purification.....	97
Figure 2.6. Analytical SEC with an ovalbumin marker to estimate molecular weight of purified SR.....	99
Figure 2.7. Human SR verified in the purified sample by chemiluminescence western blot.....	100
Figure 2.8. Peptide sequences from mass spectrometry analysis of purified SR.....	102
Figure 3.1. Principle of SR biochemical assay.	109
Figure 3.2. Plate maps for performing IC ₅₀ experiments in a 384-well plate with automation.	120
Figure 3.3. Pretreatment of commercial L-serine significantly reduces D-serine contamination.....	123
Figure 3.4. D-serine standard curves for determining the concentration of D-serine from the analytical signal, Relative Luminescence Units (RLU).	125
Figure 3.5. Comparison of SR activity in different buffer systems.....	127
Figure 3.6. Influence of incubation temperature and buffer pH on SR activity.	129

Figure 3.7. DTT attenuates the SR biochemical assay signal.....	131
Figure 3.8. Concentration-response curves for DAO, HRP, and luminol to determine the concentrations at which they were in excess.	133
Figure 3.9. EDTA effectively inhibits SR to act as a reaction stop.	134
Figure 3.10. Influence of buffer components on SR activity.....	135
Figure 3.11. Time-dependency experiments with different SR concentrations.	137
Figure 3.12. Michaelis-Menten plots of L-serine racemisation by SR.....	138
Figure 3.13. SR tolerance to dimethyl sulfoxide (DMSO).....	140
Figure 3.14. Inhibition of SR and DAO by control compounds.....	140
Figure 3.15. Effect of changing reader parameters on plate Z' scores.	143
Figure 4.1. Example trace from a thermal shift experiment using a Roche LightCycler®.	149
Figure 4.2. Example trace from an MST experiment using a NanoTemper Monolith NT.115.....	150
Figure 4.3. Fundamentals of an ITC experiment.	152
Figure 4.4. Example capillary scan from a NanoTemper Monolith NT.115.	156
Figure 4.5. Optimisation of SR and dye concentrations for the thermal shift assay....	161
Figure 4.6. DMSO tolerance of SR in the thermal shift assay.	163
Figure 4.7. Thermal denaturation analysis of SR with malonate and L-serine.....	164
Figure 4.8. Capillary scan of four buffer conditions for MST assay optimisation.....	165
Figure 4.9. MST analysis of SR at 20%, 40%, and 60% power.	167
Figure 4.10. MST analysis of SR in the presence of DMSO and malonate.	167
Figure 4.11. Normalised fluorescence of all controls from MST screen of potential SR inhibitors.....	168
Figure 4.12. Binding affinity curve of malonate and SR.....	169
Figure 4.13. Binding affinity of malonate for SR determined by ITC.....	171
Figure 5.1. Crystallisation of human SR with the inhibitor malonate.	184
Figure 5.2. X-ray crystal structure of human SR in complex with its orthosteric inhibitor malonate.....	186
Figure 5.3. Crystallisation pH screen of the SR holoenzyme.....	187
Figure 5.4. X-ray crystal structure of human SR holoenzyme and overlay with inhibitor-bound form.	189

Figure 5.5. Optimisation of microseeding crystallisation with SR holoenzyme.	191
Figure 5.6. Crystallisation of SR holoenzyme by hanging drop-vapour diffusion.	192
Figure 6.1. Inhibition curves for six SR literature inhibitors.....	201
Figure 6.2. Thermal denaturation analysis of literature SR inhibitors.	203
Figure 7.1. SR screening cascade.	210
Figure 7.2. Plate maps for the SR fragment screen.....	214
Figure 7.3. Z' scores of each plate from the SR fragment screen.	217
Figure 7.4. Percentage inhibition of SR activity by fragment molecules in the fragment screen.	219
Figure 7.5. Histogram of fragment molecule activity in the SR fragment screen.	219
Figure 7.6. Inhibition data for fragment hits in the DAO counter screen.	221
Figure 7.7. Correlation and distribution of SR-specific fragment hits.....	222
Figure 7.8. Inhibition data for SR-selective fragment hits.	224
Figure 7.9. Melting temperature shifts for SR incubated with fragment molecule hits.	226
Figure 7.10. Thermal denaturation analysis and melting point shifts (ΔT_m) of SR with four fragment hits.....	227
Figure 7.11. SR inhibitor malonate and 13 fragment hits demonstrating a significant F_{norm} shift in MST.....	229
Figure 7.12. K_D determination of SR fragment hits by MST.	231
Figure 7.13. MST analysis of F39 and associated aggregation and fluorescence controls.	232
Figure 7.14. ITC analysis of SR and three inhibitory fragment hits by direct titration.	234
Figure 7.15. ITC displacement experiment of SR with malonate and fragment inhibitors.	236
Figure 7.16. Thermodynamic parameters of SR-malonate binding in an ITC displacement experiment.	237
Figure 7.17. Co-crystallisation trials with SR and four inhibitory fragment hits.	240
Figure 7.18. Optimisation of SR co-crystallisation with hits F01 and F39 in Bis-Tris pH 6.	241
Figure 7.19. Crystallisation of SR and soaking with fragment inhibitors.	242

Figure 7.20. X-ray crystal structure of human SR bound to a novel fragment inhibitor, 3-pyridin-4-yl benzoic acid (F01).	244
Figure 10.1. Specific Ramachandran plots for SR-malonate complex generated by MolProbity.	304
Figure 10.2. Specific Ramachandran plots for SR holoenzyme generated by MolProbity.	305

List of Tables

Table 1.1. Glutamate receptor classes, subtypes, and overview of agonist/antagonist pharmacology.	10
Table 1.2. Overview of current SR inhibitors.	70
Table 2.1. Summary of all SR purifications, individual yields, and purpose of each batch.	103
Table 3.1. Percentage coefficient of variation (% CV) and Z' scores for positive (+ve) and negative (-ve) controls in plate test 1.	141
Table 3.2. Summary of plate test data from Figure 3.15.	144
Table 3.3. Summary of factors determined during optimisation of the SR coupled biochemical assay.	147
Table 6.1. Comparison of assay parameters from the present study and two reports on SR peptide inhibitors.....	205
Table 7.1. Thermodynamic parameters of SR-malonate binding in the absence and presence of fragment inhibitors.	237
Table 7.2. Summary profile of F01, the novel SR inhibitor and confirmed binder.....	245
Table 10.1. Features of pET-24a bacterial plasmid used for expression of SR.....	291
Table 10.2. Summary of SR coupled biochemical assays.	292
Table 10.3. Names and structures of reported SR inhibitors.....	293
Table 10.4. Fragment inhibitors of SR identified from medium-throughput screening.	297
Table 10.5. Data collection and validation statistics for SR-malonate complex.	302
Table 10.6. Data collection and validation statistics for SR holoenzyme.....	303
Table 10.7. Data collection and validation statistics for SR-F01 complex.....	303

Abbreviations

(His)6	Polyhistidine
ΔF_{norm}	Change in normalised fluorescence
ΔH	Enthalpy
ΔS	Entropy
5-HT	5-hydroxytryptamine
ACPD	1-amino-1,3-dicarboxycyclopentane
AD	Alzheimer's disease
ADP	Adenosine diphosphate
ALS	Amyotrophic lateral sclerosis
AMP	Adenosine monophosphate
AMPA	α -amino-3-hydroxy-5-methyl-4-isoxazolepropionic acid
AMPAR	AMPA receptor
AMPH	Amphetamine
AP-1	Activator protein 1
APP	Amyloid precursor protein
aSRCKO	Astrocytic serine racemase conditional knockout
ATD	Amino terminal domain
ATP	Adenosine triphosphate
BDNF	Brain-derived neurotrophic factor
CA1	<i>Cornu ammon 1</i>
cAMP	Cyclic adenosine monophosphate
CCG	(carboxycyclopropyl)glycine
cDNA	Complementary DNA
CDS	Coding DNA sequence
CE	Capillary electrophoresis
CHES	<i>N</i> -cyclohexyl-2-aminoethanesulfonic acid
CNS	Central nervous system
CONSIST	Cognitive and Negative Symptoms in Schizophrenia Trial
CRPS	Complex Regional Pain Syndrome
CTD	Carboxy-terminal domain
CV	Column volume
CV (%)	Coefficient of variation
Da	Dalton(s)
DAG	Diacylglycerol
DAO	D-amino acid oxidase
DISC1	Disrupted in schizophrenia 1
DLB	Dementia with Lewy bodies
DLS	Dynamic light scattering
DMSO	Dimethyl sulfoxide
DNA	Deoxyribonucleic acid
DP	Differential power
DTT	Dithiothreitol
<i>E. coli</i>	<i>Escherichia coli</i>

EAAT	Excitatory amino acid transporter
EC ₅₀	Drug concentration that gives half-maximal response
ECL	Enhanced chemiluminescence
EDTA	Ethylenediaminetetraacetic acid
EPSP	Excitatory postsynaptic potential
ERK	Extracellular signal-regulated kinase
FAD	Flavin adenine dinucleotide
FBDD	Fragment based drug discovery
fMRI	Functional magnetic resonance imaging
Fnorm	Normalised fluorescence
FPLC	Fast phase liquid chromatography
GABA	γ -aminobutyric acid
GDA	Glycyl dodecylamine
GlyT	Glycine transporter
GPCR	G-protein coupled receptor
GTI	Glycine transporter inhibitor
H ₂ O	Water
H ₂ O ₂	Hydrogen peroxide
HAM-D	Hamilton Depression Rating Scale
HCl	Hydrochloric acid
HEK	Human embryonic kidney
HEPES	4-(2-hydroxyethyl)-1-piperazineethanesulfonic acid
hERG	Human ether-à-go-go-related gene
HNK	Hydroxynorketamine
HPLC	High performance liquid chromatography
HRP	Horseradish peroxidase
hSR	Human serine racemase
HTS	High-throughput screening
IC ₅₀	Inhibitor concentration that reduces activity by half
IgG	Immunoglobulin G
iGluR	Ionotropic glutamate receptor
IMAC	Immobilised metal affinity chromatography
IP	Intraperitoneal
IP3	Inositol trisphosphate
IPF	Inhibitory protein factor
IPTG	Isopropyl β -D-1-thiogalactopyranoside
ITC	Isothermal titration calorimetry
IV	Intravenous
JNK	c-Jun N-terminal kinase
KA	Kainate
Kcat	Catalytic constant
K _D	Dissociation constant
kDa	kiloDaltons
K _i	Inhibition constant
K _m	Michaelis-Menten constant
KO	Knockout

L-DOPA	Levodopa/L-3,4-dihydroxyphenylalanine
L-EHA	L- <i>erythro</i> -hydroxyaspartate
LB	Lysogeny broth
LBD	Ligand binding domain
LDH	Lactate dehydrogenase
LDS	Lithium dodecyl sulfate
LEA/SENDAI	Subline of Long-Evans agouti rat
LED	Light-emitting diode
LIVBP	Leucine/isoleucine/valine-binding protein
LSOS	L-serine- <i>O</i> -sulfate
LTD	Long-term depression
LTP	Long-term potentiation
MADRS	Montgomery-Åsberg Depression Rating Scale
mAU	Milli absorbance units
MDD	Major depressive disorder
MES	2-(<i>N</i> -morpholino)ethanesulfonic acid
METH	Methamphetamine
mGluR	Metabotropic glutamate receptor
miRNA	Micro RNA
MOPS	3-(<i>N</i> -morpholino)propanesulfonic acid
mPFC	Medial prefrontal cortex
MRI	Magnetic resonance imaging
mRNA	Messenger RNA
MST	Microscale thermophoresis
MTS	Medium-throughput screening
Mw	Molecular weight
NaCl	Sodium chloride
NADH	Nicotinamide adenine dinucleotide
NBQX	2,3-dihydroxy-6-nitro-7-sulfamoyl-benzo[f]quinoxaline-2,3-dione
NCBI	National Centre for Biotechnology Information
NFPS	<i>N</i> -[3-(4'-fluorophenyl)-3-(4'-phenylphenoxy)propyl]sarcosine
NMDA	<i>N</i> -methyl-D-aspartate
NMDAR	NMDA receptor
NMR	Nuclear magnetic resonance
NO	Nitric oxide
NSAID	Non-steroidal anti-inflammatory drug
nSRCKO	Neuronal serine racemase conditional knockout
NTA	Nitrilotriacetic acid
OD 600	Optical density at 600 nm
PAINS	Pan-assay interference compounds
PAM	Positive allosteric modulator
PCP	Phencyclidine
PD	Parkinson's disease
PDB	Protein data bank
PDC	Pyrrolidine dicarboxylate
PDD	Parkinson's Disease Dementia

PEG	Polyethylene glycol
PFC	Prefrontal cortex
Phgdh	3-phosphoglycerate dehydrogenase
PICK1	Protein interacting with C-kinase 1
PIP2	Phosphatidylinositol (4,5)-bisphosphate
pKa	Association constant (logarithmic scale)
PKC	Protein kinase C
PLC	Phospholipase C
PLP	Pyridoxal phosphate
PNS	Peripheral nervous system
PTSD	Post-traumatic stress disorder
PVDF	Polyvinylidene difluoride
RFU	Relative fluorescence units
RISC	RNA-induced silencing complex
RLU	Relative luminescence units
RMSD	Root-mean-square deviation
RNA	Ribonucleic acid
Ro3	Rule-of-3
RT	Room temperature
<i>S. pombe</i>	<i>Schizosaccharomyces pombe</i>
SAR	Structure-activity relationship
SD	Standard deviation
SDS-PAGE	Sodium dodecyl sulphate polyacrylamide gel electrophoresis
SEC	Size-exclusion chromatography
SEM	Standard error of the mean
siRNA	Small inhibitory RNA
SLC	Solute carrier
SNP	Single nucleotide polymorphism
SOC	Super Optimal broth with Catabolite repression
SR	Serine racemase
SRCKO	Serine racemase conditional knockout
<i>SRR</i>	Serine racemase gene
T3MG	<i>Threo</i> -3-methylglutamate
TBOA	<i>Threo</i> - β -benzyloxyaspartate
TBST	Tris-buffered saline + Tween
Tg	Transgenic
THA	<i>Threo</i> - β -hydroxylate
Tm	Melting temperature
TMD	Transmembrane domain
TRD	Treatment-resistant depression
tRNA	Transfer RNA
UV	Ultraviolet
VGLUT	Vesicular glutamate transporter
WT	Wild-type

Abbreviations cont.Amino acids

Alanine	A	Ala	Leucine	L	Leu
Arginine	R	Arg	Lysine	K	Lys
Asparagine	N	Asn	Methionine	M	Met
Aspartate	D	Asp	Phenylalanine	F	Phe
Cysteine	C	Cys	Proline	P	Pro
Glutamate	E	Glu	Serine	S	Ser
Glutamine	Q	Gln	Threonine	T	Thr
Glycine	G	Gly	Tryptophan	W	Trp
Histidine	H	His	Tyrosine	Y	Tyr
Isoleucine	I	Ile	Valine	V	Val

Nucleic acids

A - Adenine C - Cytosine G - Guanine T - Thymidine U - Uracil

1 INTRODUCTION

The nervous system is dependent on synaptic transmission to process information and transmit signals between different parts of the body, in order to control both voluntary and involuntary processes (Purves *et al.*, 2001). This system is uniquely defined by the presence of neurons, which are distinguished from other cells by their ability to communicate with neighbouring cells via synapses — specialized contacts between neuronal membranes. The arrival of an action potential to the presynaptic neuron triggers an influx of Ca^{2+} ions and consequent fusion of vesicles with the membrane, causing the neurotransmitter within the vesicle to be released into the synapse. The neurotransmitter binds to and activates receptors on the postsynaptic neuron to cause an excitatory or inhibitory response, which can be either a rapid, transient action or a slower, modulatory response (Purves *et al.*, 2001). Glutamate, an amino acid, is the principle excitatory neurotransmitter in the mammalian brain, being present in over 50% of nervous tissue (Cooper, 2008). It has the ability to act on a number of different glutamate receptors to elicit a wide range of responses.

1.1 Glutamatergic neurotransmission

The role of glutamate as an excitatory neurotransmitter is well established, with studies first identifying this particular action in the 1950s (Hayashi, 1952). Nowadays glutamate is generally accepted to be the principle excitatory neurotransmitter in the vertebrate nervous system, with the ability to act postsynaptically, and to a lesser extent presynaptically, on two types of glutamate receptors: metabotropic and ionotropic (Vyklícký *et al.*, 2014). The ionotropic glutamate receptors can be further categorized into three families named according to their preferred agonists; *N*-methyl-D-aspartate (NMDA), α -amino-3-hydroxy-5-methyl-4-isoxazolepropionic acid (AMPA) and 2-carboxy-3-carboxymethyl-4-isopropenylpyrrolidine (kainate). In addition to its excitatory function, glutamate can also be used by the brain to synthesise γ -aminobutyric acid (GABA), the main inhibitory neurotransmitter of the mammalian nervous system.

1.1.1 The glutamate synapse

Grey matter is a major component of the central nervous system containing a high density of synapses and other structures such as neuronal cell bodies, dendrites, axons, glial cells and capillaries (Purves *et al.*, 2001). In $1\ \mu\text{m}^3$ of grey matter, there is about one glutamatergic nerve terminal (Harvey and Napper, 1991) surrounded by neuronal and glial structures that release glutamate and express glutamate receptors (Danbolt, 2001). The glutamate synapse could therefore be described as a complex network of various receptor types with different distributions across synapses, the extrasynaptic parts of neurons, and also glial cells (Fig. 1.1).

1.1.2 Glutamate release

Glutamate receptors are primarily found on the dendrites of postsynaptic neurons, where they bind glutamate released into the synaptic cleft from the presynaptic terminal. Glutamate is released from presynaptic terminals in vesicles (containing a glutamate concentration of $\sim 100\ \text{mmol/L}$) by a Ca^{2+} -dependent mechanism involving voltage-dependent Ca^{2+} channels (Meldrum, 2000). In general, neurotransmitter release is stimulated by Ca^{2+} influx through P/Q- ($\text{Ca}_v2.1$) or N-type Ca^{2+} channels ($\text{Ca}_v2.2$) and to a much lesser extent by R- ($\text{Ca}_v2.3$) and distantly related I-type Ca^{2+} channels (Ca_v1 family; Sudhof, 2004). Glutamate release can occur in two phases following Ca^{2+} influx: the initial rapid, synchronous component within $50\ \mu\text{s}$ of a Ca^{2+} current (Sabatini and Regehr, 1996), and the slower, asynchronous component continuing for over 1 s after the action potential owing to increased spontaneous neurotransmitter release (Goda and Stevens, 1994). It has also been suggested that some glutamate release might be non-vesicular, as it has been shown to occur in the presence of toxins that inhibit exocytosis (Jabaudon *et al.*, 1999).

As well as interacting with binding proteins (transporters and receptors) present in the synapse, glutamate may diffuse away from the synaptic cleft and interact with

metabotropic glutamate receptors along the spine and nerve terminal membranes, and this synaptic “overspill” may also reach glial glutamate transporters (Danbolt, 2001). The glutamate receptors and transporters may differ in their affinities for glutamate, their opening and inactivation times (receptors) and their transport efficiencies and ion conductances (transporters), which enables the released glutamate to reach various locations at various concentrations.

1.1.3 Glutamate transporters

Following glutamate release, it takes a matter of seconds for extracellular glutamate to build up if reuptake is blocked, as has been elegantly demonstrated with the glutamate uptake inhibitor threo- β -benzyloxyaspartate (TBOA; Jabaudon et al., 1999). Therefore, in order to prevent prolonged excitation, glutamate transporters remove glutamate from the synaptic cleft into the neuroglia and neurons. This reuptake ensures glutamate levels are kept low in the synapse after an action potential, and so terminates synaptic transmission. Without this process, glutamate levels would continue to increase, resulting in excitotoxicity — a process caused by excessive stimulation of neurons and influx of high levels of Ca^{2+} ions, leading ultimately to cell death. It is also important to keep the extracellular concentration of glutamate low to maintain a high signal-to-noise (background) ratio in both synaptic and extrasynaptic transmission, and to conserve the glutamate released for reuse.

The mammalian genome contains five genes (SLC1A1–3, 6 and 7) encoding the Excitatory Amino Acid (glutamate) transporters EAAT1–5 (Zhou and Danbolt, 2013). These transporters catalyse Na^+ - and K^+ -coupled transport of L-glutamate as well as L- and D-aspartate from the synapse back into the glia and neurons. EAAT1–3 function by exchanging one internal K^+ with one glutamate, three Na^+ and one H^+ on the external side of the membrane (Levy *et al.*, 1998). Three other genes (SLC17A7, SLC17A6, and SLC17A8) encode the vesicular glutamate transporters (VGLUTs 1–3), which pack glutamate into synaptic vesicles from the cell cytoplasm so that it can be released again into the synapse (Shigeri *et al.*, 2004).

The expression of EAAT1–5 show distinct neuroanatomical distributions, as demonstrated using either in situ hybridization or immunohistochemistry and western blot analyses. In general, EAAT1–3 are mostly abundant in the CNS but have been detected in some peripheral tissues such as the heart, liver, kidney, and intestines (Gegelashvili and Schousboe, 1998). EAAT1 and EAAT2 are found in glial cell membranes, although small amounts of EAAT2 can be found on neurones (Petr *et al.*, 2015). EAAT1 is predominantly expressed in the cerebellum, and EAAT2 in the brain and spinal cord with highest levels in the neocortex and hippocampus, where 5–10% EAAT2 is neuronal (Danbolt, 2001). EAAT2 is considered to mediate most (90%) of the glutamate uptake in the adult brain (Holmseth *et al.*, 2009). EAAT3 and EAAT4 are exclusively neuronal, with EAAT3 expressed throughout the forebrain and spinal cord, particularly in the hippocampus, basal ganglia, and cortical structures, and EAAT4 predominantly expressed in the cerebellum localised to Purkinje cells (Furuta *et al.*, 1997). Expression of EAAT5 is limited to photoreceptors and bipolar neurons in the retina (Pow and Barnett, 2000).

Glutamate transporters have been studied for their potential role in some pathological disease states using knockout mice of glutamate transporter proteins. Homozygous EAAT2 knockout mice became spontaneously epileptic at around three weeks of age and died shortly after (Tanaka *et al.*, 1997). The same effect was seen with knockout of astroglial EAAT2 but not neuronal EAAT2 (Petr *et al.*, 2015), suggesting astroglial EAAT2 is the main protector against excitotoxicity. EAAT4 knockout mice are viable and appear normal despite lacking glutamate transporter currents at Purkinje cell synapses (Huang *et al.*, 2004b), therefore its role is probably not critical. Targeted deletion of VGLUT1 in mice caused lethality three weeks after birth, and drastically reduced glutamatergic neurotransmission (Wojcik *et al.*, 2004) whereas homozygous VGLUT2 knockout mice were not viable at birth (Moechars *et al.*, 2006), implicating distinct developmental roles for VGLUT1 and VGLUT2. Heterozygous VGLUT2 knockout mice, which were viable, have been used to link VGLUT2-dependent glutamatergic signalling to neuropathic pain (Moechars *et al.*, 2006), epilepsy (Kang *et al.*, 2005, Schallier *et al.*, 2009), and amyotrophic lateral sclerosis (ALS; Wootz *et al.*, 2010).

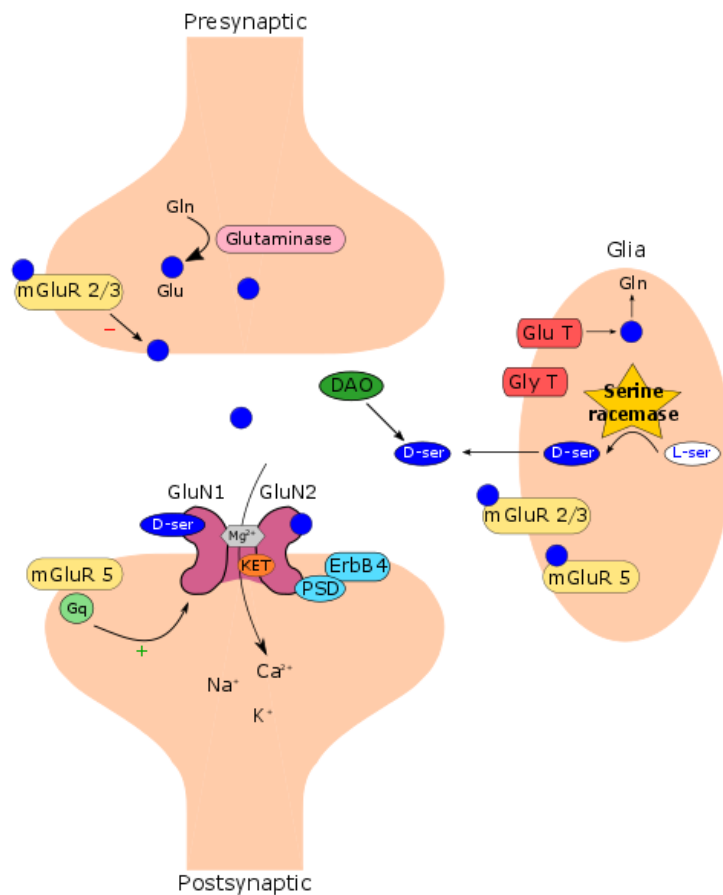


Figure 1.1. The glutamate synapse.

Glutamine (Gln) is converted to glutamate (Glu; blue circles) by glutaminase. Glutamate can bind to metabotropic type 2/3 (mGlu_{2/3}) and type 5 (mGlu₅) receptors to modulate glutamate neurotransmission, and to ionotropic N-methyl-D-aspartate (NMDA) receptors (NMDARs; pink, post-synaptic membrane) at the GluN2 subunit. Once the coagonist D-serine also binds at the GluN1 subunit and a depolarising current relieves Mg²⁺-dependent block, the channel opens and cations (Ca²⁺, Na⁺, K⁺) can diffuse into the post-synaptic terminal. NMDARs can be inhibited by the open channel blocker ketamine (KET). Membrane-spanning receptors such as mGluR5 and ErbB4 indirectly influence NMDAR function by interacting with the post-synaptic density (PSD). D-serine is produced from L-serine in glial cells by serine racemase, shuttled into the synaptic cleft, then eventually degraded by D-amino acid oxidase (DAO). Glutamate and glycine are removed from the synaptic cleft by glutamate transporters (Glu T; encoded by the EAAT1–5 genes) and glycine transporters (Gly T) respectively.

1.2 Glutamate receptors

As mentioned previously (section 1.1), glutamate has the ability to act on two different receptor families: ionotropic and metabotropic glutamate receptors (iGluR and mGluR, respectively). These two receptor classes are distinguished by their differing structures and mechanism of action. Hence, when activated by glutamate, iGluRs form an ion channel pore whereas mGluRs are G-protein coupled receptors (GPCRs) that rely on a signaling cascade involving G-proteins. The functional role and pharmacology of the receptors comprising these two families have been investigated and described in depth, by using selective ligands to elucidate their individual characteristics.

1.2.1 Metabotropic glutamate receptors

The family of mammalian mGluRs, which are members of the Class C GPCR superfamily, consists of eight subtypes (mGlu₁₋₈) that are classified into three groups according to their sequence homology, second messenger effects and/or pharmacology: Group I (mGlu₁ and mGlu₅), group II (mGlu₂ and mGlu₃), and group III (mGlu₄, mGlu₆, mGlu₇ and mGlu₈; Kew and Kemp, 2005). As part of the GPCR family, mGluRs have the classical seven transmembrane domain structure seen with other GPCRs (Bhave *et al.*, 2003), and act via G-proteins localized to the cell membrane linking to the activation of second messenger pathways and downstream signaling cascades. Group I mGluRs are usually linked to G_q/G₁₁ and initiate signalling cascades involving phospholipase C (PLC), inositol 1,4,5-trisphosphate (IP₃) and diacylglycerol (DAG; Willard and Koochekpour, 2013). Groups II and III mGluRs are linked to G_i/G_o and couple to the inhibition of adenylyl cyclase, the enzyme that catalyses the conversion of ATP to cAMP, thereby leading to a decrease in intracellular cAMP levels (Kew and Kemp, 2005).

In contrast to the rapid, ion flux-mediated effects produced by ionotropic glutamate receptors, mGluRs are responsible for slower, modulatory functions, such as inducing long-term changes in neuronal excitability by increasing intracellular Ca²⁺ (Willard and Koochekpour, 2013), and modulating synaptic transmission and plasticity. In addition,

the localization of mGluRs throughout the CNS, PNS and organ systems (including the epithelium, connective and muscle tissues) has suggested a role for mGluRs in homeostasis (Niswender and Conn, 2010).

An approach to develop novel therapies for psychiatric and neurological disorders is to selectively target individual mGluR subtypes that modulate specific cellular and neuronal functions. There is evidence to suggest targeting mGluRs in this way has a potential to treat several CNS disorders, such as depression, anxiety disorder, schizophrenia, pain disorders, epilepsy, Alzheimer's disease and Parkinson's disease (Niswender and Conn, 2010). Agonist activation of mGlu_{2/3} (found mainly presynaptically in cortical and limbic brain structures) in animal models of anxiety and psychosis results in suppression of excessive glutamate transmission, reduction of the activity of postsynaptic potentials, and reversal of abnormal behaviours (Dd and Marek, 2002). For instance, when Eli Lilly synthesised the first orally active mGlu_{2/3} agonist, LY354740, it was found to possess anticonvulsant and anxiolytic effects in rats (Monn *et al.*, 1997). Further tests in animals corroborated the anxiolytic effect of LY354740 (Helton *et al.*, 1998, Schoepp *et al.*, 2003), and demonstrated its ability to attenuate disruptions in cognition and locomotion in a PCP rat model of schizophrenia (Moghaddam and Adams, 1998, Cartmell *et al.*, 1999), inhibited withdrawal symptoms in morphine dependent mice (Klodzinska *et al.*, 1999), and reduced pain-induced behaviours in a rat model of neuropathic pain (Simmons *et al.*, 2002).

Further proof-of-concept of the therapeutic potential of targeting mGluRs has been obtained in preclinical studies of mGluR agonists related to LY354740 (Johnson *et al.*, 2017), including LY379268, LY379267, and LY389795 (Monn *et al.*, 1997). A potent and selective mGlu_{2/3} agonist with improved bioavailability, LY404039, has been shown to have broad preclinical efficacy with reduced undesirable side effects (such as sedation) across multiple animal models of anxiety and psychosis (Rorick-Kehn *et al.*, 2007, Fell *et al.*, 2008). Overall there seemed to be much promise that mGlu_{2/3} agonists could be a novel treatment for schizophrenia (Moghaddam, 2004, Conn *et al.*, 2009, Rotaru *et al.*, 2011). Accordingly, Eli Lilly developed LY-2140023, a methionine amide pro-drug of LY-404039, for the oral treatment of schizophrenia. The drug demonstrated

antipsychotic efficacy in a randomised, placebo-controlled, phase II clinical trial in patients with schizophrenia without eliciting side effects commonly observed with current antipsychotics, but unfortunately the results could not be replicated (Mezler *et al.*, 2010). A following phase II clinical trial was inconclusive, as LY-2140023 was no more efficacious than placebo, but the active control (olanzapine) did not separate from placebo either (Kinon *et al.*, 2011). Subsequently, LY-2140023 did not demonstrate any efficacy in patients with acute exacerbation of schizophrenia in a double blind, placebo controlled phase II clinical trial (Downing *et al.*, 2014), nor as an adjunctive treatment in schizophrenic patients being treated with a second-generation antipsychotic (Stauffer *et al.*, 2013). Despite these disappointing results, there is still much interest in modulating glutamatergic neurotransmission as a means to treat schizophrenia.

1.2.2 Ionotropic glutamate receptors

Ionotropic glutamate receptors (iGluRs) are categorized based on their pharmacological properties and are named to reflect their agonist selectivity as NMDA, AMPA, and kainate receptors. The distinct pharmacology of the three families can be explained in part by the fact there is only 20–30% (Traynelis *et al.*, 2010) amino acid sequence homology across the iGluR subunits each family.

Each iGluR has a homo- or heterotetrameric combination of receptor-specific subunits: GluA1–GluA4 for AMPA receptors (AMPA receptors), GluK1–GluK5 for kainate receptors, and GluN1, GluN2A–GluN2D, GluN3A and GluN3B for NMDA receptors (NMDARs; Traynelis *et al.*, 2010). The AMPAR subunits GluA1–GluA4 can arrange as homo- and heteromers, as can the kainate receptor subunits GluK1–GluK3, while GluK4 and GluK5 must be coexpressed with GluK1, GluK2, or GluK3 to form functional receptors. NMDARs are only functional in heteromeric configurations, requiring two obligatory GluN1 subunits to assemble with either two GluN2 subunits, or a combination of GluN2 and GluN3 subunits. In addition, NMDARs have been observed forming triheteromeric structures, in which the GluN1 subunits assemble with two different GluN2 subunits — for

example, GluN1/GluN2A/GluN2B — which creates the variation necessary to form NMDARs with specific functions and distribution profiles in the brain, although little progress has been made elucidating the exact functions of these triheteromeric structures.

Different subunit compositions create diversity in receptor properties, allowing receptors to fulfil a broader set of functions. For NMDARs in particular, the different compositions influence the kinetics and gating properties of the resulting NMDAR subtypes. For example, heteromeric NMDARs containing GluN2A or GluN2B have a higher conductance and sensitivity to Mg^{2+} blockade compared to heteromers containing GluN2C or GluN2D, and NMDARs containing a GluN3 subunit have an even greater reduction in Mg^{2+} blockade (Paoletti *et al.*, 2013). Further, GluN1/GluN2A have a higher open probability, lower sensitivity to glutamate and glycine, and faster deactivation kinetics compared to GluN1/GluN2C and GluN1/GluN2D receptors (Paoletti *et al.*, 2013). The distinct properties of NMDAR subtypes determine their respective contributions to synaptic functions such as long-term potentiation and long-term depression (section 1.3.2).

A summary of mGluR and iGluR subtypes, their transduction mechanisms, and putative agonists and antagonists is presented in Table 1.1.

Table 1.1. Glutamate receptor classes, subtypes, and overview of agonist/antagonist pharmacology.

Receptor		Receptor subtype	Gene name	Transduction mechanism	Agonists	Antagonists
Metabotropic	Group I	mGlu ₁	GRM1	G _q /G ₁₁ , activation of PLC, IP ₃ , DAG	Quisqualate ^a (S)-3,5-DHPG ^b	YM-298,198 ^p JNJ16259685 ^q
		mGlu ₅	GRM5			MPEP ^r
	Group II	mGlu ₂	GRM2	G _i /G _o , inhibition of adenylyl cyclase	DCG-IV ^c (2R,4R)-APDC ^d LY354740 ^e LY379268 ^f	APICA ^s EGLU ^t LY-341,497 ^u
		mGlu ₃	GRM3			
	Group III	mGlu ₄	GRM4	G _i /G _o , inhibition of adenylyl cyclase	L-AP4 ^g (RS)-PPG ^h	MPPG ^v
		mGlu ₆	GRM6			
		mGlu ₇	GRM7			
		mGlu ₈	GRM8			
Ionotropic	NMDA receptor	GluN1	GRIN1	Ca ²⁺ Na ⁺ K ⁺	GLYX-13 ⁱ D-serine ^j Glycine ^j D-alanine ^j ACPC ^j	DCKA ^w Conantokin ^x Ifenprodil ^y PCP/ketamine ^z Dizocilpine ^z Memantine ^{aa}
		GluN2A	GRIN2A			
		GluN2B	GRIN2B			
		GluN2C	GRIN2C			
		GluN2D	GRIN2D			
		GluN3A	GRIN3A			
		GluN3B	GRIN3B			
	AMPA receptor	GluA1	GRIA1	Na ⁺ (Ca ²⁺)	AMPA ^k Cl/Br-HIBO ^{l,m} ACPA ⁿ	NBQX ^{ab} Perampanel ^{ac}
		GluA2	GRIA2			
		GluA3	GRIA3			
		GluA4	GRIA4			
	Kainate receptor	GluK1	GRIK1	Na ⁺ (Ca ²⁺)	Kainate ^o (2S,4R)-methylglutamic acid ^o	CNQX ^{ad} NS102 ^{ae}
		GluK2	GRIK2			
		GluK3	GRIK3			
		GluK4	GRIK4			
		GluK5	GRIK5			

ACPA, (R,S)-2-amino-3-(3-carboxy-5-methyl-4-isoxazolyl)propionic acid; ACPC, 1-aminocyclopropane-1-carboxylic acid; AP4, L-2-amino-4-phosphonobutyric acid; APDC, (2R,4R)-4-aminopyrrolidine-2,4-carboxylate; CNQX, 6-cyano-7-nitroquinoxaline-2,3-dione; DCKA, 5,7-dichlorokynurenic acid; DHPG, (S)-3,5-dihydroxyphenylglycine; EGLU, (2S)-α-ethylglutamic acid; HIBO, (R,S)-4-(chloro/bromo)-homoibotenic acid; JNJ16259685, (3,4-dihydro-2H-pyrano[2,3-b]quinolin-7-yl)-cis-4-methoxycyclohexyl-methanone; MPEP, 2-methyl-6-(phenylethynyl)pyridine; MPPG, α-methyl-4-phosphonophenylglycine; NBQX, 2,3-dihydroxy-6-nitro-7-sulfamoyl-benzo[f]quinoxaline-2,3-dione; NS102, 5-nitro-6,7,8,9-tetrahydrobenzo[G]indole-2,3-dione-3-oxime; PPG, (R,S)-4-phosphonophenylglycine; YM-298,198, 6-amino-N-cyclohexyl-N,3-dimethylthiazolo[3,2-α]benzimidazole-2-carboxamide hydrochloride

a (Hinoi *et al.*, 2001); **b** (Wisniewski and Car, 2002); **c** (Ishida *et al.*, 1993); **d** (Schoepp *et al.*, 1995); **e** (Schoepp *et al.*, 1997); **f** (Monn *et al.*, 1997); **g** (Nakanishi, 1992); **h** (Gasparini *et al.*, 2000); **i** (Moskal *et al.*, 2005) partial agonist; **j** (Chen *et al.*, 2008), all GluN1 agonists; **k** (Vogensen *et al.*, 2000); **l** (Coquelle *et al.*, 2000); **m** (Bjerrum *et al.*, 2003); **n** (Strange *et al.*, 2006); **o** (Alt *et al.*, 2004); **p** (Kohara *et al.*, 2005) mGlu₁ noncompetitive; **q** (Lavreysen *et al.*, 2004) mGlu₁ noncompetitive; **r** (Gasparini *et al.*, 1999) mGlu₅ competitive; **s** (Ma *et al.*, 1999); **t** (Jane *et al.*, 1996); **u** (Li *et al.*, 2010); **v** (Bedingfield *et al.*, 1996); **w** (McNamara *et al.*, 1990) GluN1 competitive; **x** (Prorok and Castellino, 2007) GluN2 competitive/noncompetitive; **y** (Perin-Dureau *et al.*, 2002) GluN2B noncompetitive; **z** (Traynelis *et al.*, 2010) open channel blocker; **aa** (Rogawski and Wenk, 2003) open channel blocker; **ab** (Wilding and Huettner, 1996), competitive; **ac** (Rogawski and Hanada, 2013) noncompetitive; **ad** (Paternain *et al.*, 1996) competitive; **ae** (Johansen *et al.*, 1993) competitive.

1.2.3 Distribution and function of iGluRs

iGluRs are all ligand (glutamate)-gated ion channels that upon activation permit an influx of cations — either sodium, potassium, and/or calcium ions (Traynelis *et al.*, 2010). NMDARs deviate from this rule, as their activation requires binding by an additional co-agonist (glycine or D-serine) and the presence of a depolarising current (discussed further in section 1.3; Willard and Koochekpour, 2013). The influx of cations produces a depolarisation of the membrane potential, which if sufficient, triggers the firing of an action potential — the primary type of excitatory synaptic transmission throughout the CNS and PNS. The properties of this transmission, such as the amplitude and kinetic profile, are determined by the specific arrangement and combination of AMPA, NMDA, and kainate receptors at the synaptic and extrasynaptic sites, which also defines their role in synaptic physiology and gating kinetics (Lester *et al.*, 1990).

Kainate receptors are prevalent in the CNS grey matter, with a higher density expressed in the telencephalic structures and cerebellum (Monaghan and Cotman, 1982) and have roles at both pre- and postsynaptic sites. They have been demonstrated to have a role in mediating slow synaptic transmission at developing thalamocortical synapses, which then decreases as AMPA-mediated transmission increases, demonstrating a developmental form of LTP (Kidd and Isaac, 1999). Activation of kainate receptors is associated with short bursts of presynaptic activity, and in other cortical circuits they are largely expressed on inhibitory interneurons (Traynelis *et al.*, 2010). Additionally, kainate receptors are able to downregulate the release of GABA in the hippocampus by signalling via G-protein-coupled second messenger cascades to downstream effectors (Rodríguez-Moreno and Lerma, 1998).

In NMDARs, subunit heterogeneity is enhanced by alternative splicing of the gene encoding GluN1, giving rise to eight distinct isoforms (GluN1-1a–GluN1-4a and GluN1-1b–GluN1-4b; Paoletti *et al.*, 2013). The GluN1a isoforms are the result of alternative splicing of exons 21 and 22, creating carboxy-terminal domains of differing lengths, cell localisations, trafficking properties, and interactions with binding partners (Horak and

Wenthold, 2009). The GluN1b isoforms contain an insert of 21 amino acids in the amino-terminal domain, which affects the receptor kinetics, open probability, and agonist pharmacology (Vance *et al.*, 2012). The NMDAR subunits and their isoforms demonstrate well-characterised expression profiles and varying abundance levels.

1.2.4 Structure of iGluRs

The structure of iGluRs differs significantly from the typical arrangement of seven transmembrane domains seen in mGluRs and other GPCRs. Instead, they are composed of four subunits that form the channel, with each subunit sharing four well-conserved domains: the extracellular amino-terminal (ATD), ligand binding (LBD), transmembrane (TMD) and intracellular carboxy-terminal (CTD) domains (Traynelis *et al.*, 2010). Fig. 1.2 shows the domain arrangement of an NMDAR.

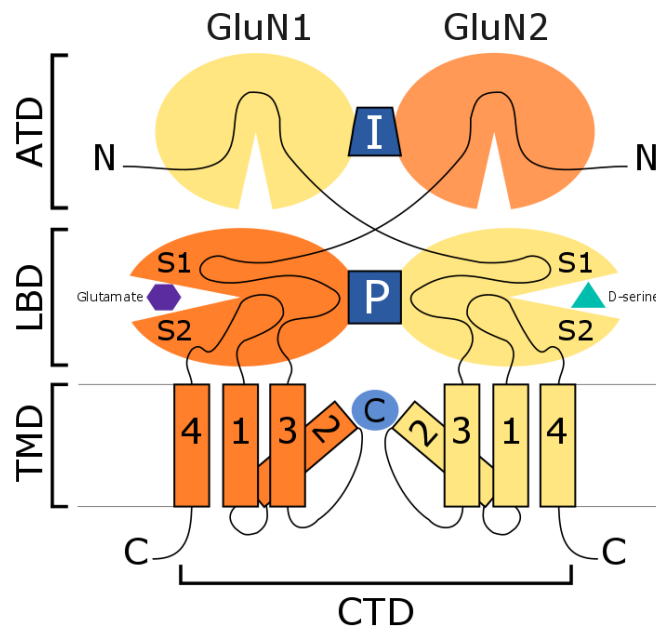


Figure 1.2. Structure and domain organisation of the N-methyl-D-aspartate (NMDA) receptor.

NMDAR subunits, as in other glutamate receptors, have a modular structure comprising: two large extracellular domains, the amino-terminal domain (ATD) and ligand-binding domain (LBD); a transmembrane domain (TMD) that forms part of the ion channel pore; and an intracellular carboxyterminal domain (C). The LBD is defined by two segments of amino acids, S1 and S2. The TMD is composed of three membrane-spanning helices (M1, M3, and M4) and a re-entrant loop (M2). I = ifenprodil binding site; P = proposed neurosteroids binding site; C = channel blocker site.

Much research has been dedicated to elucidating the structure of iGluRs due to their important role in neuronal function as well as CNS disorders such as depression, schizophrenia, stroke and Alzheimer's disease, among others. This structural determination began with the individual domains such as the water soluble ATD and LBD, with X-ray crystallography being used to solve the structures of these domains for various iGluR subunits in complex with agonist, antagonists, partial agonists and modulators (Karakas *et al.*, 2015). The first fully-intact structure for an iGluR — a rat homotetrameric GluA2 receptor in complex with antagonist — was not solved until ten years after that of the first LBD (Armstrong *et al.*, 1998, Sobolevsky *et al.*, 2009). Since then, several iGluR structures have been published describing the GluA2 receptor in different functional states, the GluK2 kainate receptor, and most excitingly, two recently published structures for the NMDA receptor.

The crystallographic studies of the rat GluA2 receptor, as solved by Sobolevsky and colleagues, has determined that the ATDs and LBDs are organized as a dimer of dimers with twofold symmetry perpendicular to the membrane plane, and the TMDs are arranged as a tetramer with fourfold rotational symmetry (Sobolevsky *et al.*, 2009). The extracellular ATD and LBD domains, as well as the TMDs, exhibit symmetry mismatch, which is due to the AMPA receptor containing two conformationally-distinct subunits — A/C and B/D subunits — which couple differently at the ion channel gate (Traynelis *et al.*, 2010). This means that the four homotetrameric subunits of the ATD and LBD, labeled A to D, will form AB and CD dimers at ATD, and AD and BC dimers at LBD (Sobolevsky *et al.*, 2009), and these distinct subunit-subunit contacts are thought to contribute to the overall function of the glutamate receptor. Further, they determined the AMPA receptor TMD consists of three transmembrane helices (M1, M3, and M4) and a membrane re-entrant loop (M2), which aligns with previous homology experiments predicting the pore structure would be similar to that of tetrameric K⁺ channels (Wo and Oswald, 1995, Kuner *et al.*, 2003).

Structural studies of NMDAR ATDs have indicated distinct architecture and subunit arrangement from those of other iGluRs. The NMDAR ATDs are structurally distinct from the ATD of other iGluR subunits with which they share relatively little sequence

identity. Moreover, the NMDAR ATDs are functionally distinct from other iGluR ATDs since they can accommodate allosteric modulator compounds and control gating properties (Furukawa, 2012). Combined with the extensive research carried out on NMDAR LBDs (Furukawa and Gouaux, 2003, Yao *et al.*, 2008, Vance *et al.*, 2011), predictions were made on the architecture of the NMDAR (Salussolia *et al.*, 2011, Riou *et al.*, 2012), which were confirmed when the structures of the rat (Fig. 1.3; Karakas and Furukawa, 2014) and frog (Lee *et al.*, 2014) GluN1a/GluN2B NMDAR structures were published. These structures, which share ~90% sequence identity with each other, allowed for the first full visualization of the overall NMDAR architecture.

The crystal structures reveal that, similar to the GluA2 AMPA receptor, the tetrameric NMDAR is organized as a dimer of dimers with an overall twofold axis of symmetry, with the receptor domains arranged with the ATD layer at the top, the LBD layer in the middle, and the TMD layer at the bottom (Lee *et al.*, 2014). The GluN1a and GluN2B subunits themselves assemble in a 1-2-1-2 (GluN1-GluN2-GluN1-GluN2) arrangement, and as in the AMPAR structure, feature a swapping of dimer pairs where the GluN1/GluN2B heterodimers are staggered between the ATD and LBD layers (Karakas and Furukawa, 2014, Lee *et al.*, 2014).

The most profound distinction from the GluA2 AMPAR structure is attributed to tight packing of the ATD and LBD in the GluN1a/GluN2B NMDAR, whereas these domains interact minimally in GluA2 AMPARs, which is a reflection of the low sequence identity and divergent pattern of dimeric arrangement between NMDAR and AMPAR ATDs (Karakas and Furukawa, 2014). Given that the ATD is known to regulate channel activity, such as channel open probability, in NMDARs (Yuan *et al.*, 2009) but not other iGluRs (Möykkynen *et al.*, 2014), the tight packing of LBDs and ATDs in NMDARs is consistent with this functional characteristic. At the TMD, the subunits exhibit pseudo-fourfold symmetry between the central M3 helices, and between the M4 helices of one subunit and M1 and M3 helices of the adjacent subunit, again similar to the GluA2 AMPAR and reminiscent of a K⁺ channel (Karakas and Furukawa, 2014). While undoubtedly an exciting development in the field of glutamate receptor pharmacology, a resolution of 3.7 Å and 4 Å for frog and rat respectively means some key sidechains

were not resolved, and a higher resolution structure will be required to identify the origin of unique NMDAR features, such as calcium permeability and magnesium block.

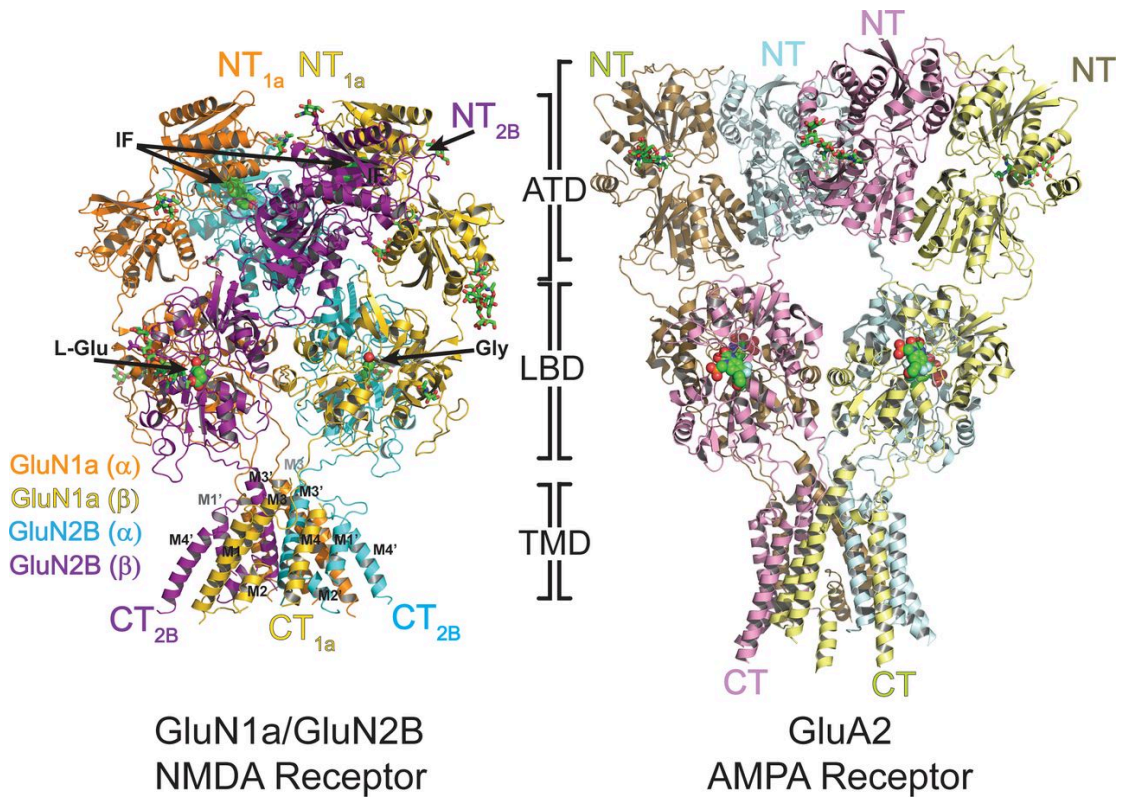


Figure 1.3. Crystal structure of NMDA receptor and comparison with AMPA receptor.

Overall structures of GluN1a-GluN2B NMDAR (left; PDB code 4PE5) and GluA2 AMPAR (right; PDB code 3KG2), arranged so that the tetramers of both receptors are in a similar orientation at the LBD layer. GluN1a and GluN2B subunits, labelled as GluN1a (α), GluN1a (β), GluN2B (α), GluN2B (β), are coloured orange, yellow, purple, and cyan, respectively. The amino terminal (NT) and carboxy terminal (CT) are located at the top and bottom, respectively. Ifenprodil, the GluN1/GluN2B-specific NMDAR antagonist, binds at the ATD heterodimer interfaces. The NMDAR agonists glycine (Gly) and L-glutamate (L-Glu) bind at their respective GluN1a and GluN2B LBDs, and are shown as green spheres. N-glycosylation chains are shown as green sticks. Both the NMDAR and AMPAR are assembled as a dimer-of-dimers at the extracellular region. The key difference in the overall structures of the two receptors arises from the tight packing of the ATD and LBD in GluN1a-GluN2B NMDARs, while in contrast, the ATD and LBD interact minimally in GluA2 AMPARs. Reproduced with permission from *Science*, Vol. 344 (6187) 992-7 (2014).

1.3 NMDA receptors

NMDA receptors have attracted considerable attention over the last few decades given their key role in neuronal plasticity (e.g., long-term potentiation and as a central component of the postsynaptic density) and excitotoxicity. There is on-going research on developing NMDAR antagonists that are able to block NMDAR activation, either by occluding the channel or inhibiting allosterically or indirectly, without inhibiting essential NMDAR function necessary for synaptic transmission and plasticity.

1.3.1 Unique characteristics of NMDA receptors

NMDA receptors are unique in that unlike other iGluRs, they are both voltage-dependent and ligand-gated. Moreover, activation requires the simultaneous binding of two different agonists: glutamate, which binds to GluN2, and glycine or D-serine, which binds to GluN1 (Kleckner and Dingledine, 1988). There are several other molecules that can activate NMDARs as co-agonists — although to a lower degree of specificity than glycine or D-serine — such as L-serine, D-alanine and L-alanine (Vyklíček et al., 2014). Studies have indicated that D-serine is the main coagonist at synapses while glycine is the coagonist at extrasynaptic NMDARs, which is supported by the differences in distribution between the two coagonists, as well as the preferential affinity of synaptic NMDARs for D-serine and extrasynaptic NMDARs for glycine (Papouin *et al.*, 2012).

In addition to their novel, co-agonist mechanism of activation, NMDARs exhibit a channel block by divalent cations such as Mg^{2+} , which is responsible for its voltage dependence. This is different to the typical voltage dependence seen in the voltage-gated family of ion channels; in this situation, the current flow through the NMDAR channel is physiologically blocked by Mg^{2+} , the strength of which increases when the membrane potential is hyperpolarized (Antonov and Johnson, 1999). A sufficient AMPAR-mediated depolarization of the membrane will dislodge the Mg^{2+} , allowing the flow of cations to be voltage-dependent (Qian and Johnson, 2002).

The combination of ligand-gating and voltage dependence contribute to the unique integrative functions of NMDARs and understandably has broad implications for various physiological and pathological processes reliant upon NMDAR activation, including neuronal development, cognition, behaviour, and nervous system pathology. Moreover, the fact that NMDARs require two forms of activation creates more avenues that can be targeted by pharmacological means in diseases underpinned by NMDAR dysfunction.

1.3.2 Long-term potentiation and long-term depression

Long-term potentiation (LTP) is an enduring enhancement in signal transmission and synaptic strength resulting from high frequency stimulation of a synapse. It was first described in detail by Terje Lømo, who studied signalling between the medial perforant path and granule cells of the dentate gyrus in the hippocampus of anesthetized rabbits. In the study, he observed that brief repetitive stimuli resulted in an increased efficiency of transmission in the cell synapses and a lasting enhancement of synapse strength (Lomo, 1971), in what is now considered an *ex vivo* model of the synaptic plasticity thought to underlie learning and memory. LTP has since been observed in a variety of neural structures, including the cerebral cortex, cerebellum and amygdala (Clugnet and LeDoux, 1990). Long-term depression (LTD), conversely, is an activity-dependent reduction in the efficacy of neural synapses, involving selective weakening of specific synapses — necessary to make it possible to encode new information (Massey and Bashir, 2007). Like LTP, it has been characterized in several areas of the brain — specifically the hippocampus and cerebellum.

Both LTP and LTD (Fig. 1.4) are generally considered to be processes mostly reliant upon the activity of NMDARs, although a unique form of developmental LTP has been described where synaptic transmission is initially mediated by slow kainate receptors, only to switch to AMPA-mediated transmission in the first postnatal week (Kidd and Isaac, 1999). It is NMDA and AMPA receptor-mediated LTP and LTD, though, that are

the most widely studied and considered to be the mechanism underpinning learning and memory.

LTP is induced when a train of action potentials induces glutamate release from the presynaptic nerve terminal, causing an AMPAR-mediated depolarisation of the postsynaptic membrane that results in a displacement of the Mg^{2+} block in the postsynaptic NMDAR. The combined effect of multiple action potentials and glutamate release maximizes Ca^{2+} influx, triggering the intracellular signalling cascades required to initiate strengthening of synaptic signalling (Lüscher and Malenka, 2012). In general, NMDAR activation that leads to a modest influx of Ca^{2+} will induce LTD, while strong activation of NMDARs resulting in a greater influx in postsynaptic Ca^{2+} will induce LTP (Malenka, 1994). The induction of LTP or LTD by presynaptically-released glutamate ensures that only synapses involved in the signal transmission will undergo plasticity, allowing for a level of specificity in which neural pathways are strengthened. NMDARs are an abundant component of the postsynaptic density (PSD), a postsynaptic specialisation containing glutamate receptors and associated cytoskeletal signalling proteins (Sheng, 2001). Here, the activity of NMDARs is regulated by tyrosine phosphorylation of the GluN2B subunit, and this phosphorylation increases during LTP (Rostas *et al.*, 1996).

The role of AMPARs in LTP and LTD was probed in experiments in the hippocampus of young animals that used high frequency stimulation to induce LTP in functionally silent synapses. These are glutamatergic synapses containing NMDARs but no AMPARs, and because AMPARs are needed for glutamate-mediated neurotransmission, the synapse is effectively rendered inactive (Purves *et al.*, 2001). It was found that induction of LTP instigated a conversion of these silent synapses into functional synapses, resulting from the insertion of AMPARs into the postsynaptic membrane (Isaac *et al.*, 1995, Liao *et al.*, 1995). Therefore, it is thought that while LTP is associated with increased movement of AMPARs from perisynaptic to synaptic sites, LTD involves the removal of AMPARs from the synapse, and it is this process that allows for sustained changes in synaptic efficacy (Lüscher *et al.*, 1999, Lüscher and Frerking, 2001).

The involvement of NMDARs, AMPARs, and their associated proteins in this type of plasticity means that a number of different disease states are thought to be linked to altered LTP and LTD. These include, for example, the loss of synaptic plasticity associated with Alzheimer's disease (Singh and Abraham, 2017), as well as depression, anxiety, addiction, PTSD, and neuropathic pain (Bliss and Cooke, 2011).

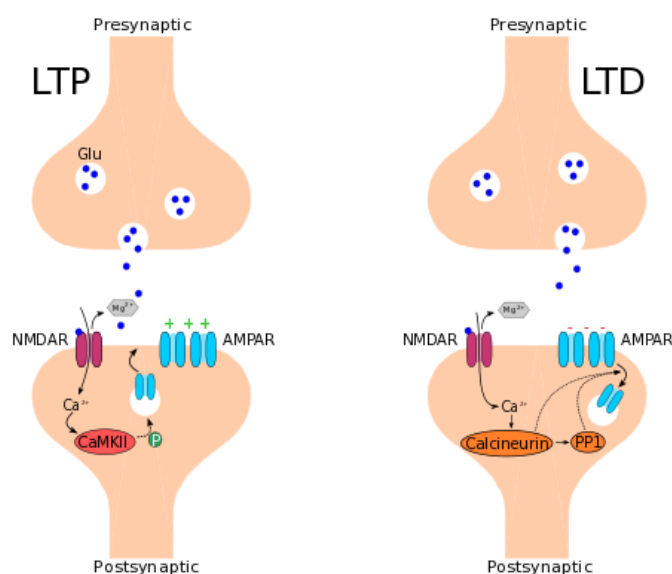


Figure 1.4. Long-term potentiation and long-term depression.

Long-term potentiation (LTP) is a long-lasting strengthening of signal transmission between two neurons. Repeated excitation of the presynaptic terminal causes glutamate release and subsequent NMDAR and AMPAR activation. Increased influx of Ca^{2+} activates Ca^{2+} /calmodulin-dependent kinase (CaMKII), which phosphorylates AMPARs to increase their activity and facilitate insertion of additional AMPARs into the membrane. Long-term depression (LTD) is a long-lasting decrease in synaptic strength. Persistent weak synaptic stimulation causes Ca^{2+} activation of calcineurin, which then activates protein phosphatase I (PPI), and both enzymes dephosphorylate AMPARs to trigger receptor internalisation.

1.4 NMDA receptor pathophysiology and pharmacology

1.4.1 Role of glutamate and NMDA receptors in disease

The integral biological role of glutamate signalling means altered glutamate neurotransmission has been implicated in various disease states. Here, the specific role of NMDAR signalling will be discussed.

1.4.2 Schizophrenia

Schizophrenia is a severe mental disorder characterised by positive (or psychotic) symptoms comprising delusions and hallucinations, negative symptoms such as social withdrawal, anhedonia, and lack of motivation, and cognitive symptoms including impairment to different types of memory, attention and learning (Kurtz *et al.*, 2001, Howes *et al.*, 2015). Schizophrenia has a fairly low lifetime prevalence of 0.7%, but is one of the major contributors to the global adult burden of disease (Whiteford *et al.*, 2013) due to the fact it usually presents in early adulthood with symptoms that tend to persist or fluctuate throughout life, despite treatment (Saha *et al.*, 2005). Although the underlying pathophysiology of the disease remains unknown, there is considerable pharmacological evidence for the dysfunction of both dopamine and glutamate neurotransmitters. Although the dopaminergic hyperfunction hypothesis, which is based upon the well described clinical efficacy of dopamine D2 receptor antagonists in treating the positive symptoms of schizophrenia, has dominated the field for several decades, more recent evidence has defined a role for the dysfunction of glutamatergic neurotransmission in the pathophysiology of schizophrenia.

The involvement of glutamate signalling in schizophrenia dates as far back as 1949 with reports of catatonic schizophrenic patients showing improved motor activity after being treated with glutamic acid (Kitzinger and Arnold, 1949). More recently, the glutamate dysfunction hypothesis has been refined to specifically implicate NMDARs. The theory arose from the observation that non-competitive NMDAR antagonists such

as phencyclidine (PCP), ketamine, and dizocilpine (MK-801) could produce effects resembling the positive and negative symptoms of schizophrenia (Krystal *et al.*, 1994, Javitt, 2007) and the cognitive deficits (Blot *et al.*, 2013) in healthy patients, as well as exacerbate the positive and negative symptoms in patients with schizophrenia (Lahti *et al.*, 2001). The wealth of supporting literature has led to NMDAR antagonists being used as a rodent model system of schizophrenia. Subsequently, rodent studies have demonstrated that administration of NMDAR antagonists are capable of producing neurochemical effects that reflect brain changes seen in schizophrenia. For example, studies using sub-chronic PCP treatment have resulted in parvalbumin-immunoreactive neuronal deficits in the hippocampus and prefrontal cortex of adult rats, as well as neurobiological deficits such as hypofrontality, a reduction in blood flow that is symptomatic of schizophrenia in humans (Neill *et al.*, 2014). Further, NMDAR antagonists have been used to elicit behavioural analogues of emotional blunting in mice (Noda *et al.*, 1995), and anhedonia and social withdrawal in rats (Baird *et al.*, 2008, Neill *et al.*, 2010). It is thought that the effects of NMDAR antagonists in animal studies are due to inhibition of NMDARs located on GABAergic interneurons, which are involved in regulating feedback inhibition on pyramidal glutamatergic neurons, leading to disinhibition of this feedback and an increase in hippocampal pyramidal cell firing (Lisman *et al.*, 2008).

The glutamate hypothesis of schizophrenia has been somewhat supported by post-mortem studies, which have identified reduced GluN1 subunit expression in the brain, but this may be due to impairments in receptor localisation, trafficking and downstream activation rather than a general deficit in receptor expression (Howes *et al.*, 2015). Recent genetic studies have identified several genes associated with schizophrenia that are involved in glutamatergic neurotransmission, most notably *GRIN2A* gene (which encodes for an NMDA receptor subunit) as well as the *GRM3* and *SRR* genes (which encode for the mGlu₃ receptor and serine racemase, respectively; Schizophrenia Working Group of the Psychiatric Genomics Consortium, 2014). Further insight into the role of glutamate in schizophrenia has been revealed by *in vivo* imaging studies, for example the use of proton magnetic resonance spectroscopy (1H-MRS) has identified a general increase in glutamate/glutamine levels in the prefrontal cortex and

basal ganglia of medication-free patients (Poels *et al.*, 2014) as well as an increase in glutamine in the anterior cingulate cortex of at-risk individuals and those with first-episode psychosis (Howes *et al.*, 2015).

The dopamine and glutamate hypotheses of schizophrenia are not mutually exclusive since schizophrenia is likely the result of the integrated effect of both altered dopaminergic and glutamatergic neurotransmission on the different symptom domains of schizophrenia. Nonetheless, the emergence of the role of glutamate in this disorder has encouraged the development of glutamatergic drug treatments for psychiatric disorders, which will be discussed further in section 1.6.

1.4.3 Neuropathic pain

Neuropathic pain has been defined by the International Association for the Study of Pain (IASP) as ‘pain caused by a lesion or disease of the somatosensory system’ (Jensen *et al.*, 2011). It is characterised by spontaneous on-going or shooting pain and amplified pain responses after both harmful and non-harmful stimuli, and can arise from a range of pathological conditions involving the brain, spinal cord, and peripheral nerves (Baron *et al.*, 2010). Neuropathic pain is distinct from inflammatory pain, which is caused by tissue injury arising from exposure to high intensity stimuli (Xu and Yaksh, 2011). Inflammatory pain typically improves as a function of the healing process and responds positively to NSAIDs and opiates, where by contrast, neuropathic pain cannot generally be alleviated by typical analgesics such as paracetamol (Gilron and Dickenson, 2014). With a limited choice of effective treatments, there is a continuing need to better understand the mechanisms that underpin neuropathic pain and develop improved therapies that are able to target this group of devastating conditions.

The symptoms of neuropathic pain have been linked to various factors, including inflammatory cytokines released from immune cells that may target the peripheral nerves, dorsal root ganglia and spinal cord (Marchand *et al.*, 2005, Watkins and Maier, 2005), disinhibition of GABAergic transmission at inhibitory dorsal horn interneurons

(Thompson *et al.*, 1993), and plastic changes in the spinal cord, possibly as a result of peripheral nerve injury (Costigan *et al.*, 2009). In addition to these, there is a considerable amount of evidence to suggest that NMDAR activation is involved in pain associated with peripheral tissue or nerve injury. There is also accumulating evidence that peripheral as well as central NMDARs contribute to nociception, therefore providing two potential levels of pharmacological intervention (Petrenko *et al.*, 2003).

It is generally thought that central NMDARs play a pivotal role in establishing the characteristics of neuropathic pain. The precise mechanism is central sensitisation, wherein the dorsal horn excitability increases and thus becomes more responsive to sensory input. This results in a state where a low-intensity, ordinarily non-harmful stimulus generates pain (allodynia) and noxious stimuli result in a more painful and prolonged pain response (hyperalgesia; Petrenko *et al.*, 2003). Sensitisation of the dorsal horn is likely caused by a process called 'wind-up', which is a frequency-dependent increase in the excitability of spinal cord neurons evoked by electrical stimulation of C-fibre primary afferent nerves (Zhou *et al.*, 2011). This process of wind-up and the subsequent sensitisation of dorsal horn neurons have been shown to be reduced by blocking NMDARs with antagonists including ketamine, memantine and MK-801 in rat models of neuropathy in which a selective ligation of the L5/L6 spinal nerves is used to produce a partial denervation of the hindpaw (Suzuki *et al.*, 2001). Further, in a rat model of neuropathic pain, GluN2B subunit specific antagonists such as ifenprodil were found to decrease the amplitude of NMDAR-mediated excitatory postsynaptic currents (EPSCs) recorded from dorsal horn neurons (Iwata *et al.*, 2007). In the same rat model, the GluN2B-selective antagonist Ro 25-6981 resulted in a dose-dependent anti-allodynic effect by inhibiting the C-fibre responses in dorsal horn neurons, and also inhibited LTP in these neurons when induced by high-frequency stimulation (Qu *et al.*, 2009). Together, these results implicate a role for GluN2B NMDARs in nociceptive transmission, dorsal horn sensitisation, and the development of long-term spinal excitability after nerve injury, highlighting the possibility of targeting GluN2B NMDARs in the treatment of neuropathic pain.

In addition, there have been a number of studies demonstrating that compounds such as L-701,324, MRZ2/576 and 5,7-dichlorokinurenic acid (DCKA), which are selective for the glycine/D-serine site on the obligatory GluN1 subunit of the NMDAR, are effective at reversing allodynia in spinal nerve ligated rats (Christoph *et al.*, 2005, Christoph *et al.*, 2006). Similar findings have been reported for the glycine/D-serine site antagonist GV196771 (Quartaroli *et al.*, 1999) and the pyridazinoquinolinetriones, a distinct class of glycine/D-serine site antagonists (Bare *et al.*, 2007).

However, despite the strong preclinical data, the efficacy of NMDAR antagonists in preclinical models of neuropathic pain has generally failed to translate into clinical efficacy in humans. For example, while GV196771 is effective in rat neuropathic pain models, it does not reduce the intensity of evoked pain in patients with neuropathic pain disorders (Wallace *et al.*, 2002). Similarly, another GluN2B-selective antagonist, radiprodil, was found to have no significant effect on the mean daily pain scores of patients compared to placebo in a 2010 Phase II randomised, double-blind clinical trial. On the other hand, the administration of ketamine in the treatment of neuropathic pain has yielded more definitive positive results, strongly linking glutamatergic signalling dysfunction to the pathophysiology of neuropathic pain (section 1.5).

1.4.4 Alzheimer's disease

Alzheimer's disease (AD) is a progressive neurodegenerative disorder that can occur in middle or, more commonly, old age, and is the most common cause of dementia, being responsible for 60–80% of cases (Hebert *et al.*, 2003). AD is characterised clinically by three groups of symptoms: cognitive dysfunction, which includes memory loss and language difficulties; psychiatric symptoms, which includes depression, hallucinations and delusions; and impairments to normal daily living, such as driving and dressing (Burns and Iliffe, 2009). Pathologically, there are two microscopic hallmarks of AD; the intracellular neurofibrillary tangles and the extracellular neuritic (or senile) plaques, which contain a core of amyloid peptide. There is considerable debate regarding which of these two pathological features is the key, disease-causing

lesion, the amyloid hypothesis being predominant over the last couple of decades. This postulates that extracellular amyloid beta ($A\beta$), a proteolytic cleavage product of the transmembrane protein amyloid-beta precursor protein (APP; Ray *et al.*, 2010), forms deposits in the brain that are fundamental to the progression of AD (Hardy and Allsop, 1991). On the other hand, the tau hypothesis proposes that AD is caused by abnormal, hyperphosphorylated tau proteins that cause the formation of neurofibrillary tangles inside neuronal cell bodies (Goedert *et al.*, 1991), ultimately leading to cell death (Chun and Johnson, 2007).

In addition to these pathological characteristics, there is considerable evidence of altered and dysfunctional neurotransmission contributing to the pathogenesis of AD, with the most affected being the cholinergic and glutamatergic systems (Neill, 1995). Understanding the role of the glutamatergic pathway in this disease state is therefore important when considering to what extent targeting NMDAR-mediated neurotransmission can be exploited in the treatment of AD.

In healthy brain, endogenous $A\beta$ has a critical role in synaptic plasticity and memory within the CNS (Puzzo *et al.*, 2011) but when present in excess has been shown to enhance neurotransmitter release probability at the synapse, which may lead to the compensatory synapse loss observed in AD (Abramov *et al.*, 2009). Pathologically elevated levels of large $A\beta$ oligomers may block neuronal glutamate uptake at the synaptic cleft, leading to elevated glutamate levels, and consequently increased activation of synaptic NMDARs (Esposito *et al.*, 2013) and extra-synaptic NMDARs (Rammes *et al.*, 2011). $A\beta$ oligomers can also directly activate NMDARs, particularly those with the GluN2A subunit (Texido *et al.*, 2011). Together, increased synaptic glutamate with additional activation of NMDARs by $A\beta$ can lead to Ca^{2+} -mediated excitotoxicity, oxidative stress, mitochondrial damage and ultimately neuronal death (Alberdi *et al.*, 2010).

The damaging effects caused by NMDAR overactivation include impairment of LTP (Walsh *et al.*, 2002, Wang *et al.*, 2002, Shankar *et al.*, 2008), enhancement of LTD (Li *et al.*, 2009), and internalisation of synaptic AMPARs and NMDARs (Snyder *et al.*, 2005,

Hsieh *et al.*, 2006). Eventually, increased activation of synaptic NMDARs induces receptor desensitisation and synaptic depression (Esposito *et al.*, 2013). Moreover, the A β -mediated downregulation of postsynaptic anchoring proteins (such as PSD-95 and synaptophysin) via suppression of GluN2A-containing NMDAR function and activation of GluN2B-containing NMDAR function causes respective induction of caspase-8 and caspase-3 apoptotic activity (Liu *et al.*, 2010).

The proposed overactivation of NMDARs in AD has led to the consideration of NMDAR antagonists as effective treatments for AD. Unfortunately, drugs that completely block NMDAR activity, such as ketamine, are accompanied with various severe CNS side effects such as hallucinations, anxiety, nausea, vomiting, and memory impairment (Muir and Lees, 1995). The only NMDAR antagonist approved for the clinical treatment of AD is memantine, a low affinity channel blocker that preferentially blocks NMDAR activity without disrupting normal activity, by entering the channel when it is excessively open and dissociating quickly to avoid it accumulating and interfering with normal synaptic transmission (Lipton, 2004). Memantine has also been demonstrated to reduce the levels of APP α (the secreted cleavage product of APP generated by α -secretase) and release of A β (Ray *et al.*, 2010), as well as protect against mitochondrial toxins and hypoxia (Volbracht *et al.*, 2006), and protect cholinergic neurones from inflammatory processes (Willard *et al.*, 2000).

Memantine represents an interesting paradigm shift away from other AD drugs in terms of its mechanism of action. It is only one of four approved pharmacotherapies for AD, the other three (donepezil, rivastigmine, galantamine) being cholinesterase inhibitors, which raise the level of acetylcholine (ACh) by inhibiting the enzyme that degrades it (Burns and Iliffe, 2009). Although memantine has been found in some clinical trials to improve cognitive impairment in people with moderately severe AD (Ströhle *et al.*, 2015), it can also be harmful to patients, with potential side-effects including drowsiness, weight gain, confusion, hypertension, and falling, and arguably not significantly improving the mental state of patients (Yang *et al.*, 2013).

The glutamatergic mechanism of action of memantine has formed part of the rationale for targeting NMDAR signalling as an approach to treat AD. For example, the GluN2B subunit-selective antagonist ifenprodil inhibits steady-state NMDAR currents evoked by polyamines (Kew and Kemp, 1998) and lacks the severe side effects seen with classical non-selective NMDAR blockers (Chenard *et al.*, 1995). Derivatives of ifenprodil, such as Ro 25-6981, have been studied as lead compounds in the development of new drugs for neurodegenerative disorders, and have led to the identification of GluN2B-selective antagonists such as CERC-301 and EVT-101 (Mony *et al.*, 2009) currently in clinical development for NMDAR-related pathologies including neuropathic pain (section 1.4.3), treatment-resistant depression (section 1.4.5) as well as AD.

1.4.5 Major depressive disorder

Major depressive disorder (MDD) is one of the most common psychiatric disorders, characterised by persistent low mood, often experienced with low self-esteem and inability to experience pleasure (anhedonia). MDD is associated with severe reductions in quality of life, impaired work productivity, reduced social functioning, and poor physical health (Katona and Katona, 2014). It is also accompanied by substantial economic costs, and is listed as the leading cause of disability worldwide in the WHO's Global Burden of Disease project (Whiteford *et al.*, 2013). Current treatment options are limited for acutely suicidal or severely depressed patients, with conventional treatments including cognitive behavioural therapy (Brown *et al.*, 2005), electroconvulsive therapy (Kellner *et al.*, 2005), and antidepressants (Szanto *et al.*, 2003).

The first-line antidepressants are selective serotonin reuptake inhibitors (SSRIs) which are moderately effective and slow to act, requiring 6–8 weeks of therapy to achieve relief from depression, as defined by a 50% reduction in depressive symptomology (Thase *et al.*, 2001). A twofold problem is created with SSRI treatment: patients suffer residual symptoms that increase their risk of relapse; and they are also discouraged from adhering to the treatment program by side effects that often manifest before

clinical benefit, including weight gain, sexual dysfunction, nausea, headache, and sleep disturbances (Rosenzweig-Lipson *et al.*, 2007). Only 30–40% of SSRI-treated patients achieve a full remission after a single course of antidepressants, and in addition to this, approximately one-third of patients with MDD suffer from treatment-resistant depression, which is characterised by an inadequate response to at least one antidepressant trial (Fava, 2003). This highlights the need for novel therapies with distinct mechanisms of action and improved side effect profiles.

The monoaminergic hypothesis for depressive disorders has been the dominant theory since the 1950s and is based on the fact that tricyclic antidepressants and monoamine oxidase inhibitors produce their beneficial effects on mood and anxiety by altering the pathways of monoamine neurotransmitters — dopamine, serotonin and noradrenaline. However, recent efforts to further understand the pathophysiology of depressive disorders have revealed a role of glutamate and its receptors in MDD, opening an avenue for next-generation treatments. For example, there have been numerous studies reporting changes in glutamate levels in the blood and cerebrospinal fluid in patients with MDD. In general, it has been observed that glutamate levels are significantly increased compared to healthy controls in the blood serum (Kim *et al.*, 1982) and in the plasma (Altamura *et al.*, 1993, Mauri *et al.*, 1998, Mitani *et al.*, 2006) with an apparent positive correlation between the levels of glutamate and severity of depression (Mitani *et al.*, 2006). After a 5-week period treatment with antidepressants, patients with MDD showed significantly decreased the levels of glutamate, as well as aspartate and taurine (Maes *et al.*, 1998). Although these findings appear to implicate glutamate in MDD, it should be acknowledged that peripheral glutamate does not necessarily reflect CNS neurotransmitter levels (Tremolizzo *et al.*, 2012).

Various post-mortem and *in vivo* studies on the brain have also indicated a link between glutamate signalling and the pathophysiology of MDD. For example, an examination of post-mortem brains from patients with MDD and bipolar disorder found an increased concentration of glutamate as well as D-serine in the frontal cortex (Hashimoto *et al.*, 2007). However, *in vivo* magnetic resonance spectroscopy (MRS) studies are somewhat conflicting in that on the one hand glutamate levels have been

reported to be significantly increased in the occipital cortex, while GABA levels were significantly decreased (Sanacora *et al.*, 2004) whereas groups using the same methods reported a reduction in glutamate/glutamine and GABA in prefrontal brain regions (Hasler *et al.*, 2007), the anterior cingulate cortex (Auer *et al.*, 2000) and the left amygdala (Michael *et al.*, 2003). It seems that while the exact mechanisms are unclear, a change in the excitatory-inhibitory neurotransmitter ratios might be responsible for some of the altered brain function in MDD, with inconsistencies among patients a result of their severity of depression, history of treatment, and genetics.

Several reports have investigated the potential genetic link between glutamate signalling and MDD. For example, in a microarray analysis of post-mortem mRNA from the cerebral cortex of MDD patients there was a downregulation of *SLC1A2* and *SLC1A3*, genes that encode for EAAT2 and 1, respectively (Choudary *et al.*, 2005) as well as glutamate-ammonia ligase, the enzyme that catalyses the synthesis of glutamine from glutamate (Choudary *et al.*, 2005, Bernard *et al.*, 2011), all of which are critical in synaptic glutamate clearance. Moreover, the mRNA of four glutamate receptor proteins was upregulated (*GRIA1*, *GRIK1*, *GRM1*, *GRM5*), as was *VGLUT2* in post-mortem MDD and bipolar brains compared to healthy controls (Bernard *et al.*, 2011). In a large-scale study on polymorphisms of *GRIN2B* (the gene encoding GluN2B), involving patients with (n=178) and without (n=612) treatment-resistant depression (TRD), as well as 779 healthy controls, it was found that *GRIN2B* contained a single nucleotide polymorphism (SNP) that was significantly associated with TRD, implying the gene confers susceptibility to TRD and may also be a genetic predictor for TRD in MDD patients (Zhang *et al.*, 2014a).

1.5 Ketamine as a therapeutic agent

The dissociative anaesthetic ketamine was first synthesised in the 1960s for use as a general anaesthetic as a safer, better tolerated alternative to phencyclidine (PCP; Domino, 2010). Now, more than fifty years later, there is a resurgence of interest in ketamine and its potential use as a therapeutic agent. Ketamine is able to rapidly cross

the blood-brain barrier to produce profound amnesiac effects and fast-onset analgesia (Schüttler *et al.*, 1987). Its rapid effects are reflected in its pharmacodynamics after intravenous administration, with a redistribution half-life of 7–15 min, clearance of $15 \text{ ml kg}^{-1} \text{ min}^{-1}$, and an elimination half-life of 2–3 h (Niesters *et al.*, 2014). The expanding literature on ketamine *in vivo* studies has suggested it is a useful drug for understanding the mechanisms of numerous CNS disorders. Ketamine has even been heralded by some as a ‘miracle drug’ for its efficacy in relieving symptoms in disorders relating to glutamatergic signalling dysfunction (Goel *et al.*, 2017).

1.5.1 Rodent studies

The idea that NMDAR antagonists might display antidepressant effects was first suggested in 1990, when in studies of rodents exhibiting behavioural depression it was observed that a competitive and non-competitive NMDAR antagonist caused clinically effective antidepressant effects in behavioural paradigms such as the forced swim and tail suspension tests (Trullas and Skolnick, 1990). Since then, a plethora of studies from several other groups have demonstrated NMDAR antagonists can be as effective as tricyclic antidepressants in preclinical antidepressant screening procedures (Paul and Skolnick, 2003).

In studies comparing the two isomers of ketamine, (*S*)- and (*R*)-ketamine, it was found using behavioural tests on mice models of depression that (*R*)-ketamine elicited a longer-lasting and more potent antidepressant effect compared to (*S*)-ketamine, and may possibly be free of the psychotomimetic effects typically associated with ketamine (Zhang *et al.*, 2014b, Yang *et al.*, 2015). There has been particular interest in (*S*)-ketamine (esketamine) by the pharmaceutical company Janssen, who are currently investigating its antidepressant potential in humans (section 1.5.2)

Several rodent models of neuropathic pain have been developed, usually involving ligation of certain nerves or inducing human disease phenotypes, such as diabetic neuropathy (Costigan *et al.*, 2009). Activation of peripheral NMDARs by intraplantar

local injection of glutamate or NMDA results in inflammatory pain behaviours in rats, demonstrated by a reduced latency in paw withdrawal when exposed to noxious heat, and this effect is attenuated when NMDAR antagonists such as ketamine and dizocilpine are administered peripherally (Jackson *et al.*, 1995). In a similar study but using a rat neuropathic partial nerve transection model, daily administration of ketamine led to a significantly decreased paw withdrawal response, as did nimodipine (calcium channel blocker) and imipramine (tricyclic antidepressant), indicating that several mechanisms contribute to the pathology of neuropathic pain (Hota *et al.*, 2007). Several studies of rodents that were administered intrathecal ketamine before undergoing nerve ligation have all demonstrated similar results, including decreased allodynia and decreased on-going pain for at least two weeks after ketamine administration and ligation (Burton *et al.*, 1999) and a relief of depression-like behaviours associated with induced neuropathic pain (Wang *et al.*, 2011). Ketamine also potentiated anti-allodynic effect when used in combination with spinal cord stimulation (Truin *et al.*, 2011) and in combination with electroacupuncture, which is known to stimulate the endogenous opioid system (Huang *et al.*, 2004a). Interestingly, ketamine may also exert its effects via μ -opioid receptors, as indicated in a study where μ -opioid receptor knockout mice displayed a lower pain threshold after ketamine administration, compared to wild-type mice (Sarton *et al.*, 2001).

Rodent studies of ketamine on models of other diseases have been less definitive. It has been reported that A β deposition was significantly reduced in the frontal cortex after repeated exposure to ketamine in the Tg2576 amyloid-overexpression mouse model of AD compared to control mice, indicating it may have a protective role (Quiroga *et al.*, 2014). In contrast, long-term ketamine administration has been shown to increase hyperphosphorylated tau protein in mice and monkeys, a hallmark of AD (Yeung *et al.*, 2010). The effects of IP infusion of subanaesthetic doses of ketamine (< 100 mg/kg) have been well documented in healthy rats, and include cognitive deficits, impaired short-term memory, increased locomotor activity, social behaviour deficits, and impaired spatial memory (Kotermanski *et al.*, 2013).

While ketamine shows promise in the treatment of neuropathic pain and TRD, it also reproduces the positive, negative, and cognitive symptoms of schizophrenia in healthy subjects, triggering a relapse in those with schizophrenia (Lahti *et al.*, 2001) and as such is often used in generating animal models of schizophrenia (Kotermanski *et al.*, 2013). The schizophrenic-like effects induced by ketamine inhibition of NMDARs might implicate NMDAR hypofunction as the source of glutamate neurotransmission dysfunction in schizophrenia. However, in recent years, there has been increasing evidence to suggest glutamatergic hyperfunction is actually critical in schizophrenia, and that developing treatments should focus on reducing rather than increasing presynaptic glutamate levels (Moghaddam, 2003). For example, systemic injections of NMDAR antagonists such as ketamine into conscious rats at subanaesthetic doses that impaired cognitive/PFC function were found to increase glutamate efflux in the PFC (Moghaddam *et al.*, 1997, Lorrain *et al.*, 2003), leading to abnormally high glutamate neurotransmission at non-NMDARs, particularly AMPARs (Moghaddam *et al.*, 1997). In addition, neuronal activity in the PFC was found to be generally increased in human fMRI studies of NMDAR antagonists (ketamine and PCP) that measured metabolic activation in PFC regions (Breier *et al.*, 1997, Vollenweider *et al.*, 1997). The most likely explanation for the paradoxical increase of cortical excitation caused by NMDAR antagonists such as ketamine is that inhibition of NMDARs decreases the activity of GABA interneurons, and ultimately increases the firing rate of pyramidal neurons (Homayoun and Moghaddam, 2007). Thus, NMDARs, which have a higher open probability in the more depolarised environment of interneurons (Maccaferri and Dingledine, 2002), may predominantly influence the activity of cortical interneurons by disinhibition of pyramidal neurons (Homayoun and Moghaddam, 2007).

1.5.2 Human studies

The first clinical proof-of-concept of ketamine as an antidepressant was conducted by Berman and colleagues, who discovered that that a single subanaesthetic dose (0.5 mg/kg) of ketamine administered by intravenous (IV) infusion over a 40-minute period produced a significant improvement within two hours compared to placebo, as

measured by the Hamilton Depression Rating Scale (HAM-D; Berman *et al.*, 2000). These effects have since been reproduced in larger trials of patients with TRD following a single (Zarate *et al.*, 2006, Murrough *et al.*, 2013) and repeated-dose (aan het Rot *et al.*, 2010, Messer *et al.*, 2010) IV infusion of ketamine, each reporting a reduction in depression symptoms as measured by the Montgomery-Åsberg Depression Rating Scale (MADRS) or HAM-D rating scale. As well as eliciting a profound antidepressant response, ketamine has been reported to be effective at relieving suicidal ideation (DiazGranados *et al.*, 2010, Price *et al.*, 2014).

Researchers at Janssen recently completed a double-blind clinical trial examining the safety and efficacy of esketamine in patients with TRD (Singh *et al.*, 2016). In the study, 30 patients were randomly assigned to receive placebo, or a lower (0.2 mg/kg) or higher (0.4 mg/kg) dose of esketamine. Two IV doses were administered during the double-blind phase, followed by a two-week follow-up wherein the patients could receive up to four additional open-label doses. The earliest antidepressant effect, as measured by change in MADRS, occurred two hours post-infusion, and both dose groups showed significant improvement in depressive effects over placebo within three days. Adverse effects did also occur, with the most common being headache, nausea, and temporary dissociation. The considerable evidence from clinical studies that support the efficacy of ketamine prompted Janssen to develop intranasal esketamine, which is currently in phase III clinical trials to assess its efficacy, optimal dosing and safety profile in the treatment of TRD (Janssen, 2017).

A preceding study of (*R*)- and (*S*)-ketamine administered by IV to healthy volunteers found that (*R*)-ketamine produced a state of relaxation and elation with no psychotic effects, as opposed to (*S*)-ketamine which produces psychotomimetic effects. Therefore, it may be possible NMDARs do not have a major role in the antidepressant effects of ketamine, which may be due to the potency of the isomers at different receptor systems (Zhang *et al.*, 2014b). Interestingly, this did seem to be the case with (*R*)-ketamine appearing to be more biologically active than (*S*)-ketamine, and moreover, the antidepressant activity associated with (*R*)-ketamine may have been mediated by its active metabolite (2*R*,6*R*)-hydroxynorketamine (HNK) via AMPARs

rather than NMDARs (Zanos *et al.*, 2016). It was also found that the greater antidepressant-like effect seen in female mice compared to male mice after ketamine treatment corresponded with greater (2S,6S;2R,6R)-HNK levels in the brains of female mice. Further, when the researchers deuterated (*R,S*)-ketamine to compare the effect of unmetabolised pharmacologically-active ketamine with the attenuated ketamine metabolites, there was a reduction of antidepressant effect and of metabolites in the brain, suggesting the antidepressant action of ketamine is mediated by its metabolites. Administration of the metabolites alone revealed that (2R,6R)-HNK had greater efficacy than (2S,6S)-HNK in the mouse learned helplessness paradigm, and was not self-administered, indicating a low drug abuse potential. The key finding of the study was that (2R,6R)-HNK did not affect NMDA-induced currents in a rat hippocampal slice model, but actually increased AMPA-mediated excitatory postsynaptic currents. Likewise, the antidepressant effects of (2R,6R)-HNK observed *in vivo* were independent of NMDAR inhibition but could be blocked by the AMPAR inhibitor NBQX, and ultimately led to increased expression of the AMPAR GluA1 and GluA2 subunits.

The therapeutic potential of ketamine in relieving symptoms of neuropathic pain has also been explored in the clinic. Ketamine administered by IV infusion has demonstrated efficacy at relieving pain in those suffering from complex regional pain syndrome (CRPS; Correll *et al.*, 2004, Kiefer *et al.*, 2008), a severe and debilitating neuropathic pain condition. In addition, when administered intranasally ketamine has been effective at relieving pain in various neuropathic pain conditions including CRPS, post-herpetic neuralgia, and polyneuropathy (Huge *et al.*, 2010). Other uncompetitive NMDAR antagonists, such as amantadine and dextromethorphan, have also demonstrated a reduction in neuropathic pain in postsurgical cancer patients (Pud *et al.*, 1998) and diabetic neuropathy (Nelson *et al.*, 1997), respectively. When administered peripherally by subcutaneous infusion, ketamine enhanced the local anaesthetic and analgesic effects of bupivacaine (a local anaesthetic) when administered postoperatively (Tverskoy *et al.*, 1996) and also demonstrated a dose-dependent decrease in hyperalgesia in neuropathic patients, as did the μ -opioid agonist alfentanil (Leung *et al.*, 2001). However, due to the differences in methods of administration and dosages, there has been little consistency in the longevity of the

analgesic effect, lasting anywhere from 45 minutes to three months (Niesters *et al.*, 2014). Of the few studies that examined the long-term effects of intravenous ketamine infusion for CRPS and spinal cord injury, the dosing ranged from daily IV infusion for 4 h (25 mg/h) over ten days (Schwartzman *et al.*, 2009), to a 100 h IV infusion of low-dose (20–30 mg/h) ketamine (Sigtermans *et al.*, 2009b) to a daily IV infusion of ketamine for 5 h (16 mg/h) over one week (Amr, 2010). A meta-analysis found the analgesic effect of ketamine persisted for at least four weeks, but eventually showed a rapid decline in effect that required retreatment (Niesters *et al.*, 2014). Ketamine has clear utility in treating chronic pain disorders, but there appears to be little consensus on the administration protocol.

1.5.3 Side-effect profile of ketamine

As previously mentioned, the most common CNS side effects of ketamine are psychotomimetic, often present at the doses used to treat chronic pain (20–30 mg/h, 80–100 mg total) and include perceptual alterations, delusions, paranoia, anxiety, disordered thinking, and a feeling of intoxication (Pomarol-Clotet *et al.*, 2006). Other CNS side effects include nausea/vomiting, blurred vision, dizziness, impaired motor function and memory deficits (Niesters *et al.*, 2014). There is also a risk that ketamine can indirectly stimulate the cardiovascular system, causing tachycardia, hypertension, and an increase in cardiac output (Sigtermans *et al.*, 2009a) and repeated ketamine infusions could elevate liver enzyme levels, leading to liver injury (Noppers *et al.*, 2011). The reputation of ketamine as a recreational drug means there is an abuse potential if it were to be expanded to treat other conditions, with there being a risk of suffering CNS side effects, physical harm, psychological dependence and tolerance, and urological disorders (Kalsi *et al.*, 2011). Considering these potential side effects, and the fact that repeated in-patient admission for IV administration is often required in clinical trials of ketamine, the therapeutic potential of other methods of modulating NMDAR function are currently being investigated.

1.6 Therapeutic approaches to modulating NMDA receptor function

The pharmacological complexity of NMDARs mean there are multiple methods of targeting NMDARs in the search for new and relevant therapeutic agents. These may take the form of classical direct inhibition, or increasingly, indirect inhibition.

1.6.1 Direct effects on NMDAR function

A direct approach to therapeutically targeting NMDARs may involve targeting specific parts of the receptor to modulate its function, such as with subunit-specific antagonists that bind to the glutamate site, partial agonists that bind to the D-serine site, or positive allosteric modulators (PAMs).

1.6.2 Agonists and partial agonists

Structure-activity studies have determined that glycine and related agonists such as L- and D-serine, L- and D-alanine bind to the LBD of GluN1, specifically at the cleft of the D1 and D2 domains (McBain *et al.*, 1989). This includes GluN1 partial agonists such as D-cycloserine and other cyclic analogues of glycine (Hood *et al.*, 1989, Sheinin *et al.*, 2001, Dravid *et al.*, 2010). Agonists of GluN2 include, naturally, NMDA — a synthetic amino acid derivative that mimics the action of glutamate specifically at NMDARs — while endogenous agonists include glutamate, D- and L-aspartate, homocysteate and cysteinesulfinate (Traynelis *et al.*, 2010).

Many clinical trials have investigated the therapeutic benefit of selectively potentiating NMDAR activity over other glutamate receptors by administering its co-agonists glycine and D-serine, particularly in disorders such as schizophrenia that have been associated with NMDAR hypofunction (Coyle and Tsai, 2004). In general, almost all of these clinical trials reported an improvement in the negative symptoms of schizophrenia (Shim *et al.*, 2008), particularly when glycine or D-serine were added to conventional antipsychotic drug treatments, although without any significant effect on

the positive symptoms and general psychopathology at low dosages (Javitt *et al.*, 1994). Other studies of high-dose glycine (60 g/day) support these findings (Shim *et al.*, 2008) and even suggest that high-dose glycine can improve cognitive symptoms (Heresco-Levy *et al.*, 1999) and to some extent, positive symptoms when added to antipsychotic drug therapy (Heresco-Levy and Javitt, 2004). Conversely, when the effect of glycine was examined in a larger patient population in the CONSIST¹ trial, there were no significant improvements for either cognitive or negative symptoms (Buchanan *et al.*, 2007). Two placebo-controlled, double-blind trials have reported that D-serine administration (30 mg/kg/day) significantly improved negative, positive, and cognitive symptoms when used as an add-on treatment to antipsychotic drugs (Tsai *et al.*, 1998, Tsai *et al.*, 1999) and in addition, a similarly-designed trial found that when D-alanine, a full glycine-site agonist, was administered (100 mg/kg/day) with antipsychotics, there was a significant improvement in negative and positive symptoms and general psychopathology in patients with treatment-resistant schizophrenia (Tsai *et al.*, 2006). The conclusions of these studies were promising but were not without caveats, such as the very high dose required to observe significant effects, relatively poor brain penetration, poor tolerability, and the presence of endogenous regulatory mechanisms that limit bioavailability of exogenously administered amino acids (Javitt, 2008, Traynelis *et al.*, 2010). Nevertheless, these studies have spurred interest in the development of novel NMDAR glycine site agonists and partial agonists.

One example is GLYX-13 (also known as rapastinel), a partial agonist that targets the glycine-binding site. In rat studies, GLYX-13 was able to act as a cognitive enhancer when tested with the Morris water maze and alternating T-maze tasks (Burgdorf *et al.*, 2011b) and produced antidepressant-like effects in several animal models of depression, without psychotomimetic side-effects (Burgdorf *et al.*, 2013). In a Phase II clinical trial of GLYX-13 on patients with MDD who had not responded to at least one other antidepressant treatment, a single IV dose (1–30 mg/kg) over 3–15 min improved depression scores within hours and lasted seven days on average. The antidepressant effect was not accompanied by psychotomimetic effects and was

¹ Cognitive and Negative Symptoms in Schizophrenia Trial (CONSIST)

generally well tolerated, with few mild or moderate side-effects reported by approximately 5% of subjects (Moskal *et al.*, 2014). GLYX-13 is starting Phase III clinical trials for TRD, and is accompanied by other glycine partial agonists in various stages of clinical development. This includes NRX-1074, which has demonstrated similar effects to GLYX-13 in preclinical trials but is considerably more potent and orally active. In 2015, a Phase II clinical trial was completed for an IV formulation of NRX-1074 in patients with MDD (NCT02067793) while a Phase I trial for an oral formulation has also recently been completed (NCT02366364). At the time of writing, the results for both had not been published.

The target engagement of GLYX-13 has been thoroughly examined. The group that first synthesised GLYX-13 used a radiolabeled form ($[^3\text{H}]$ GLYX-13) to determine the compound readily crossed the blood-brain barrier in rats, and found via electrophysiological experiments in frog oocytes that GLYX-13 could act as a co-agonist of NMDARs in the absence of glycine, an effect that was blocked by the glycine site selective antagonist 7-chlorokynurenic acid (Moskal *et al.*, 2005). In rat hippocampal slices, GLYX-13 reduced NMDAR-mediated synaptic currents in CA1 pyramidal neurons evoked by low frequency Schaffer collateral stimulation, but enhanced NMDAR currents during high frequency bursts of activity, corresponding to a respective suppression of LTD and enhancement of LTP (Zhang *et al.*, 2008). GLYX-13-mediated enhancement of LTP in hippocampal slices was also observed by others (Burgdorf *et al.*, 2011b). Analysis of hippocampal tissues from rats that had received a single IV dose (3 mg/kg) of GLYX-13 found facilitated LTP and increased whole-cell NMDAR current contributed by GluN2B-containing NMDARs, as well as increased mature spine density in the medial PFC and hippocampus (Burgdorf *et al.*, 2015). Ifenprodil, the GluN2B-selective allosteric antagonist, has been found to block GLYX-13 enhanced activation of burst-driven extrasynaptic NMDARs (Zhang *et al.*, 2008) and the GLYX-13-mediated improvement in positive emotional learning in rats (Burgdorf *et al.*, 2011a).

Studies on other glycine partial agonists have not been as obviously successful. D-cycloserine was initially studied for its potential as an antipsychotic, and from voltage-clamp experiments was thought to preferentially activate NMDARs containing the

GluN2C subunit (Sheinin *et al.*, 2001, Dravid *et al.*, 2010). D-cycloserine has been found to rescue weakened NMDAR activation in the CA1 cellular networks of aged rats (Billard and Rouaud, 2007), facilitate hippocampus-dependant learning in young adult rats (Thompson *et al.*, 1992), and enhance NMDAR-mediated excitatory postsynaptic potentials, facilitating synaptic plasticity of glutamatergic transmission via LTP and LTD induction (Rouaud and Billard, 2003). While early clinical trials suggested that D-cycloserine improved the negative symptoms of schizophrenia (Goff *et al.*, 1999), a subsequent meta-analysis of five trials, as well as the CONSIST trial which studied the effect of D-cycloserine in patients with schizophrenia, found that it had no efficacy on the negative symptoms or cognitive impairments (Tuominen *et al.*, 2005, Buchanan *et al.*, 2007). There have been mixed findings on the use of D-cycloserine in treating anxiety disorders; while several small-scale studies have supported its use in this application, later larger-scale studies have often showed weak or no effects (Otto *et al.*, 2015). One explanation for the observed variability has been attributed to differences in D-cycloserine dosages between trials. For instance, no improvement to immediate or delayed memory was found following weekly doses of 50 mg D-cycloserine in healthy participants (Otto *et al.*, 2009), yet hippocampus-dependent declarative learning was facilitated by a single 250 mg oral dose of D-cycloserine (Onur *et al.*, 2010). The discrepancy suggests D-cycloserine effects on hippocampal functioning may be dose-dependent, and accordingly a phase II clinical trial is being conducted to assess the effect of 250 mg D-cycloserine on improving therapeutic learning (NCT02376257). Overall, there does not appear to be any consistent or robust marker of target engagement to help interpret these data.

1.6.3 Subunit-specific NMDAR antagonists

Many competitive antagonists, so-called because they compete with endogenous ligands at their binding site, have been identified for both the GluN1 and GluN2 subunits. Both 7-chlorokynurenic acid (Birch *et al.*, 1988) and its analogue 5,7-dichlorokynurenic acid (DCKA; McNamara *et al.*, 1990) are examples of GluN1 antagonists — thought to work by interacting with the GluN1 LBD and stabilizing an

open-cleft formation — while (*R*)-2-amino-5-phosphonopentanoate (AP5) and its analogues are GluN2 competitive antagonists (Davies *et al.*, 1981). Subunit specificity with GluN2 competitive antagonists has been difficult to achieve due to the similarity of the molecular determinants that constitute the glutamate binding site. Conantokins are small endogenous peptides exhibiting both competitive and noncompetitive antagonist activity that have exhibited specificity for different GluN2 subunits (Prorok and Castellino, 2007) through binding to the glutamate binding pocket (Wittekindt *et al.*, 2001) so are being studied for rational design of drugs to treat NMDAR-related pathologies, including chronic pain, stroke, and seizure.

Subtype-selective noncompetitive antagonists also exist, characterized by binding to the NMDAR at a site distinct from the ligand-binding sites. These include ifenprodil, a phenylethanolamine selective for the GluN2B subunit that binds to the N-terminal leucine/isoleucine/valine-binding protein (LIVBP)-like domain of GluN2B (Perin-Dureau *et al.*, 2002). As well as ifenprodil, numerous other potent derivatives and subunit-selective non-competitive antagonists have been identified; GluN2B-selective antagonists in particular have been implicated in the treatment of a variety of neurological diseases. For example, ifenprodil has been shown to be neuroprotective in cases of ischemic brain injury in preclinical models (Wang and Shuaib, 2005), effective in inflammatory and neuropathic pain models in animals without accompanying motor effects (Chizh and Headley, 2005) and showed efficacy in animal models of Parkinson's disease, including rats (Nash *et al.*, 1999) and marmosets (Nash *et al.*, 2000).

Unfortunately, due to the additional activity of GluN2B antagonists such as ifenprodil and its analogue eliprodil at α 1-adrenergic receptors, 5-HT receptors, calcium channels and hERG potassium channels it has been difficult to develop these antagonists further, or else risk cardiovascular interactions (Lynch and Gallagher, 1996). This led to the development of several ifenprodil analogues with greater selectivity for GluN2B and the potential for reduced off-target interactions, including traxoprodil (CP-101,606, Pfizer) and Ro-25-6981, which have been tested in clinical trials with mixed results. Hence, traxoprodil was well tolerated and appeared to slightly improve the symptoms

and mortality rate of traumatic brain injury in a randomised, double-blind, placebo-controlled trial (Yurkewicz *et al.*, 2005), and in another trial on TRD it had a significant antidepressant effect but approximately half the patients experienced dissociative effects during intravenous infusion (Preskorn *et al.*, 2008). In the latter study, a 60% response rate (as measured by a reduction in HAM-D score) was seen in randomised non-responders treated with IV CP-101,606, compared to 20% for placebo, with 33% of patients meeting remission criteria in five days. While these initial studies seemed promising, further development of traxoprodil has been discontinued due to the continued potential risk of cardiovascular toxicity by potassium channel blockade, despite its improved specificity for GluN2B over previous subunit-selective NMDAR antagonists.

1.6.4 Uncompetitive antagonists

NMDAR uncompetitive antagonists act as open-channel blockers and require the receptor pore to be open in order for them to bind and block receptor activity. Inhibition increases with receptor activity and channel open probability, therefore uncompetitive antagonists can be considered use-dependent blockers.

The most notable of these NMDAR uncompetitive antagonists are the dissociative drugs PCP, its better-tolerated anaesthetic derivative ketamine, and dizocilpine (MK-801), a drug discovered by Merck. Dizocilpine has undergone extensive preclinical testing in rats for the potential treatment of diseases where NMDAR-related excitotoxicity may be a component, such as stroke, and Huntington's and Alzheimer's disease. Indeed, dizocilpine showed promise in protecting neuronal cell cultures and animal models from excitotoxic neurodegeneration following cellular trauma (Mukhin *et al.*, 1997), seizures (Ayala and Tapia, 2005), and spinal cord ischemia (Kocaeli *et al.*, 2005). Further, positive results with dizocilpine have been seen in animal models of depression (Maj *et al.*, 1992, Papp and Moryl, 1993, Yang *et al.*, 2016). In a PD rat model exhibiting L-DOPA-induced abnormal involuntary movements, high-dose dizocilpine (0.2–0.3 mg/kg) suppressed dyskinesia but worsened parkinsonism

(Paquette *et al.*, 2010), although another study on rats with lesions induced in the substantia nigra found dizocilpine (0.2 mg/kg) prevented impairment of working memory and dopaminergic degeneration (Hsieh *et al.*, 2012). The most significant drawback of dizocilpine is its lack of a robust safety profile in clinical trials, causing psychotomimetic effects such as hallucinations, as well as cardiovascular effects (Ellison, 1995). The observation that Olney's lesions, a form of neurotoxicity comprising neuronal vacuolation and mitochondrial breakdown, developed in rats treated with dizocilpine (Olney *et al.*, 1989) caused Merck to halt clinical development.

Currently the only clinically-approved NMDAR uncompetitive antagonist is memantine that is used to treat moderate to severe AD, and has been shown to improve quality of life for the patient and reduce caregiver burden (Doody *et al.*, 2004) and is generally well-tolerated (Areosa *et al.*, 2005). Memantine has shown additional efficacy treating patients with moderate to severe vascular dementia (Möbius and Stöffler, 2003), Parkinson's disease dementia (PDD) and dementia with Lewy bodies (DLB; Aarsland *et al.*, 2009) although it has not been clinically approved for these uses. Considering there is only once licensed treatment for PDD, rivastigmine, and no licensed treatments for DLB, it seems likely that targeting NMDAR neurotransmission could yield drugs to fill an unmet need with a novel mechanism of action. Memantine, while mechanistically similar to NMDAR channel blockers such as ketamine and PCP, displays distinct pharmacological characteristics including lower affinity and faster dissociation, which liken it more to the voltage-dependent Mg^{2+} that occludes NMDAR channels. Memantine may re-establish activity-dependent NMDAR channel block to maintain proper NMDAR functioning and limit excitotoxicity in AD, causing it to not exhibit the same severe cognitive side-effects (Danyysz *et al.*, 2000) as those caused by stronger blockers like ketamine and PCP.

NMDAR uncompetitive antagonists (as well as subunit specific antagonists) have the potential to reduce or prevent the development of neuropathic pain. Ketamine is particularly efficacious in the short-term treatment of post-operative pain, peripheral nerve disease, and spinal cord injury, in addition to its profound antidepressant effects (section 1.5.2), but the side effect profile of ketamine does mean it is not yet beneficial

as a long-term therapeutic agent until there is an improved administration protocol. The low-affinity NMDAR channel blocker remacemide has been studied in the treatment of acute ischemic stroke (Dyker and Lees, 1999), epilepsy (Wesnes *et al.*, 2009), Huntington's disease (Kieburz *et al.*, 1996), and Parkinson's disease. When remacemide was administered to patients with PD as an adjunct to dopaminergic therapy, some positive indications were observed but these results were not significant or robust enough to warrant further study (Shoulson *et al.*, 2001). Due to the lack of evidence that remacemide was an effective treatment for these diseases, its development has been discontinued, and currently there do not seem to be any new developments in the field of therapeutic NMDAR open channel blockers.

1.6.5 Indirect effects on NMDAR function

NMDA receptor antagonists, despite their potential to treat a variety of neurological conditions, have often failed in clinical trials due to their side effect liabilities or lack of therapeutic efficacy. This has led to an increased interest in developing approaches to modulating NMDAR function without directly targeting the receptor itself.

1.6.6 Transporters inhibitors

Glutamate is synthesised in the cytoplasm and stored in synaptic vesicles by VGLUTs (Reimer and Edwards, 2004) and is rapidly removed from the synapse after exocytosis by EAATs (Arriza *et al.*, 1994). Modulation of VGLUT expression or function may contribute to diseases including epilepsy, pain, and schizophrenia (Neale *et al.*, 2014). Likewise, altered expression of EAATs has been implicated in cerebral stroke, epilepsy, Alzheimer's disease, Huntington's disease, schizophrenia, and ALS (Shigeri *et al.*, 2004, O'Donovan *et al.*, 2017). Accordingly, these transporters are attractive targets for indirectly modulating NMDAR function for therapeutic benefit.

A number of VGLUT competitive inhibitors are amino acid analogues and include: glutamate analogues such as trans-ACPD (Winter and Ueda, 1993); quinoline and

quinoxaline analogues and derivatives such as 7-chloro-kynurenate (Bartlett *et al.*, 1998, Carrigan *et al.*, 2002); various azo dyes such as Trypan Blue, Evans Blue, Naphthol Blue Black, and Benzopurpurin 4B (Roseth *et al.*, 1998) as well as polyhalogenated fluoresceins and their derivatives, such as Rose Bengal (Ogita *et al.*, 2001); the endogenous molecule, inhibitory protein factor (IPF; Ozkan and Ueda, 1998); and tetrapeptide inhibitors such as D-Gln-L-Ile-D-Glu-L-Try (Patel *et al.*, 2007). These compounds vary in their potency and selectivity and often lack membrane permeability, with the exception of Rose Bengal, which is membrane permeable but not specific to VGLUT. Recently, a potent, VGLUT-specific inhibitor that is membrane permeable was identified — the diazo compound Brilliant Yellow, which has equivalent potency to Trypan Blue but is smaller and easily modifiable (Tamura *et al.*, 2014), meaning it may have potential as a prototype compound for novel drug therapies.

Likewise, an abundance of EAAT inhibitors have been identified, including: conformationally-constrained glutamate analogues such as (carboxycyclopropyl)glycine (CCG) compounds (Shimamoto and Ohfune, 1996); methyl-substituted glutamate analogues such as *threo*-3-methylglutamate (T3MG; Eliasof *et al.*, 2001); pyrrolidine dicarboxylate (PDC) derivatives such as L-*trans*-2,4-PDC, a competitive substrate of EAATs 1–4 (Arriza *et al.*, 1994, Fairman *et al.*, 1995); serine derivatives such as serine-*O*-sulphate (Arriza *et al.*, 1994); and aspartate derivatives such as *threo*- β -hydroxyaspartate (THA) and its derivatives (Shigeri *et al.*, 2001). As with VGLUT inhibitors, there have been challenges developing EAAT inhibitors that are potent and specific to EAAT subtypes, are non-transportable, and are soluble. Specificity is a particularly desirable goal because EAAT2 is heavily implicated in numerous disease states (O'Donovan *et al.*, 2017). Current inhibitors are mainly used to characterise EAATs in terms of their pharmacology, structure-function relationship, and roles *in vivo*, which will provide invaluable insight into transport mechanisms and facilitate the identification of a novel class of EAAT modulators with significant therapeutic potential.

An alternative target, which shows more promise in terms of having unique pharmacology and improved druggability, is inhibition of glycine reuptake to extend

co-agonist availability and activity at NMDARs. Extracellular levels of glycine at synapses are controlled by glycine transporters (GlyTs), of which there are two subtypes, GlyT1 and GlyT2 (Eulenburg *et al.*, 2005). Alternate promoter usage and/or splicing yields a further five variants of GlyT1 (GlyT1a, GlyT1b, GlyT1c, GlyT1d, GlyT1e) and three variants of GlyT2 (GlyT2a, GlyT2b, GlyT2c; Harvey and Yee, 2013). The two subtypes have distinct distribution patterns, with GlyT1 found in glial cells and some glutamatergic neurons at NMDAR-containing synapses in the spinal cord and forebrain (Cubelos *et al.*, 2005), and GlyT2 expressed neuronally at CNS regions enriched in glycinergic synapses, such as the spinal cord, brain stem, and cerebellum (Jursky and Nelson, 1995).

NMDARs are co-localised with GlyT1-type transporters that regulate localised glycine levels so can modulate NMDAR activity (Javitt, 2006), therefore inhibiting glycine reuptake may have the same therapeutic benefit of oral administration of glycine (section 1.6.2). The first indication that glycine transport inhibitors (GTIs) could modulate NMDAR function was when the glycine derivative glycyldodecylamide (GDA) reversed rodent hyperactivity induced by PCP inhibition of NMDAR function, which led to increased subcortical dopamine release (Javitt *et al.*, 1997). In the study, the increased extracellular glycine resulting from GlyT1 inhibition increased NMDAR activation to overcome the PCP effects. Further preclinical studies with the GlyT1 inhibitor NFPS (ALX/NPS-5407) has demonstrated its ability to enhance NMDAR-mediated neurotransmission in rat prefrontal cortical neurons both *in vitro* and *in vivo* (Chen *et al.*, 2003, Bridges *et al.*, 2008) which highlights its therapeutic potential.

Further GTIs have been developed with improved affinity and selectivity, such as Org24461 (and its active enantiomer Org-24598) and SSR504734. There is strong supporting evidence for their efficacy, particularly for SSR504734; in rodent studies, it has been shown to increase extracellular levels of glycine in the PFC (resulting enhanced glutamatergic neurotransmission), normalise activity in rat models of hippocampal and PFC hypofunctioning, reverse dizocilpine- and PCP-induced behaviours, increase extracellular dopamine in the PFC, and is effective in models of depression and anxiety (Depoortère *et al.*, 2005). Unfortunately the use of these

compounds — ALX/NPS-5407, Org24461/24598 and SSR504734 — in preclinical studies on animals has been associated with various side effects including ataxia, and decreased respiratory and motor activity (Lechner, 2006), although a newly-synthesised GTI, TASP0315003, appears to not have these effects (Chaki *et al.*, 2015).

A handful of clinical studies have been performed with sarcosine (*N*-methylglycine), a naturally occurring amino acid that is an intermediate of glycine metabolism and also a competitive inhibitor of GlyT1 (Zhang *et al.*, 2009). The first was a double-blind, placebo-controlled trial which examined the effects of sarcosine (2 g/day) as an add-on treatment for patients with schizophrenia, and found that patients receiving sarcosine showed significant improvements in their positive, negative, cognitive, and general psychiatric symptoms, as well as being well tolerated (Tsai *et al.*, 2004). Another study supported these findings and also found that sarcosine was an effective adjunctive therapy for those suffering with an acute exacerbation of symptoms, across all symptom domains (Lane *et al.*, 2005), although when tested on drug-free patients with schizophrenia, sarcosine was only weakly effective at reducing positive and negative symptoms (Lane *et al.*, 2008). Further clinical trials have indicated that sarcosine treatment may be able to relieve acute symptoms of obsessive-compulsive disorder (OCD) in drug-free patients (Wu *et al.*, 2011) as well as substantially improve depression scores in patients with MDD (Huang *et al.*, 2013).

There are now a number of novel GlyT1 inhibitors that have been tested in preclinical and clinical trials, such as animal studies with ASP2535 (Harada *et al.*, 2012) and TASP0315003 (Chaki *et al.*, 2015), and human studies with Org-25935 (Schoemaker *et al.*, 2014) and RG1678 (bitopertin), with studies on the latter being the most extensive and best-described. An initial trial of bitopertin promisingly showed a reduction in negative symptoms in patients with schizophrenia (Umbricht *et al.*, 2014) and a phase II/III trial showed a similar effect to the antipsychotic drug olanzapine in terms of improved readiness for hospital discharge after an acute schizophrenic episode (Bugarski-Kirola *et al.*, 2014). However, two subsequent phase III trials showed bitopertin had no significant effect on negative symptoms (Goff, 2014); a disappointing result as target engagement of bitopertin to GlyT1 was confirmed via displacement of

a GlyT1 PET ligand, [^{11}C]RO5013853, with occupancy levels reaching 85% at the highest dose (175 mg) of bitopertin (Martin-Facklam *et al.*, 2013). Clearly there are issues translating preclinical findings on GTIs to positive clinical results, as well as the typical challenges of finding a drug that has high specificity, efficacy, and brain penetrance. It is hoped that a new generation of GlyT1 inhibitors might exhibit higher potency, being effective at milligram-level dosing in contrast to the gram-level dosing required for sarcosine (Javitt, 2006) and thus will have genuine potential as compounds that can modulate NMDAR activity *in vivo*. Several pharmaceutical companies with interest in this target are also developing GlyT1 inhibitors, such as JNJ-17305600 and SSR-504734, a sarcosine-derivative structurally related to methylphenidate (Lechner, 2006).

1.6.7 D-serine modulation

D-serine is a functional and potent coagonist of NMDARs, being found in highest concentrations in the forebrain, hippocampus, and cerebral cortex (Schell *et al.*, 1995) in correlation with GluN2A/B subunit-containing NMDARs (Schell *et al.*, 1997). In contrast, glycine is the predominant NMDAR coagonist in the adult cerebellum and hindbrain (Schell *et al.*, 1997). Therefore, targeting D-serine metabolism may be a therapeutic method of indirectly modulating NMDAR function in certain regions of the brain. D-serine is metabolised endogenously by D-amino acid oxidase (DAO), which greatly diminishes NMDAR-mediated neurotransmission (Mothet *et al.*, 2000), so development of DAO inhibitors may also result in therapies that increase levels of endogenous D-amino acids as a way of enhancing NMDAR function (Horio *et al.*, 2009).

DAO *in vitro* and *in vivo* characterisation has been detailed extensively in the literature. Mutant rodent strains that have disorders in DAO resulting in abnormal DAO gene expression, have been used to investigate the impact of DAO on D-serine concentration. In the LEA/SENDAI strain, a subline of a strain with very low DAO expression, rats had no DAO activity, DAO protein or mRNA coding DAO (Konno *et al.*, 2009). These rats have large amounts of D-serine in forebrain structures — olfactory bulb, cerebral cortex, hippocampus, and hypothalamus — and drastically increased

levels of D-serine where high DAO activities are normally observed — cerebellum, medulla oblongata, and spinal cord — in relation to normal rats possessing DAO (Miyoshi *et al.*, 2011), which is consistent with the patterns observed in DAO knockout mice (Morikawa *et al.*, 2001, Hamase *et al.*, 2005). As D-serine levels are normally negligible in the adult cerebellum (Schell *et al.*, 1995), the mutant rat studies implicate an important role for DAO in controlling cerebellar D-serine. Indeed, it has been shown that D-serine in the immature cerebellum regulates LTD at synapses between parallel fibres and Purkinje cells (Kakegawa *et al.*, 2011) only during the developmental stage of the cerebellum, indicating a requirement to keep cerebellar D-serine levels low during adulthood.

Another mutant mouse strain lacking DAO activity (ddY/DAO⁻) showed a greater tolerance to pain across several nociceptive behavioural tests in comparison to normal ddY/DAO⁺ mice (Zhao *et al.*, 2008). In addition, intravenous application of sodium benzoate, a DAO competitive inhibitor (Bartlett, 1948) into mice having normal DAO activity, inhibited pain responses in these mice (Zhao *et al.*, 2008). These results are further supported by observations from a rat neuropathic pain model obtained by L5/L5 spinal ligation, which caused allodynia and increased DAO mRNA and DAO activity in the lumbar spinal cord. The allodynia was then blocked by intrathecal injection of sodium benzoate (Zhao *et al.*, 2010) suggesting a role for DAO in neuropathic pain.

Abnormal levels of D-serine, possibly caused by altered gene expression or aberrant homeostatic regulation, may contribute to the glutamate hypothesis of schizophrenia, and accordingly the link between DAO and schizophrenia has been investigated. This view was initially supported by the observation that serum levels of D-serine in patients with schizophrenia are significantly reduced (Hashimoto *et al.*, 2003), which is consistent with the twofold higher DAO activity seen in the post-mortem cortex of schizophrenic patients (Madeira *et al.*, 2008), but these observations were contradicted by later reports (Hons *et al.*, 2008). Rodent studies in models of schizophrenia are also conflicting; it has been reported that DAO inhibition was able to normalise PCP-induced prepulse inhibition and hyperlocomotion (Adage *et al.*, 2008)

but others were unable to replicate these effects (Smith *et al.*, 2009, Strick *et al.*, 2011). Similar conflicting evidence has also been seen in behavioural paradigms of DAO-null mice, possibly due to differences in genetic background, experimental setup, and methods employed (Yamanaka *et al.*, 2012). Furthermore, while several genome-wide association studies confirmed the link of DAO with schizophrenia (Corvin *et al.*, 2007, Ohnuma *et al.*, 2009, Roussos *et al.*, 2011), a seemingly equal number were unable to replicate these findings (Yamada *et al.*, 2005, Bass *et al.*, 2009, Jönsson *et al.*, 2009). While there have been no clinical studies of novel DAO inhibitors, a handful of double-blind, placebo-controlled trials using sodium benzoate as an add-on treatment for schizophrenia have showed significant improvement across symptom domains (Lane *et al.*, 2013, Lin *et al.*, 2015) and when used as a monotherapy for early-phase AD, substantially improved cognitive and overall functions of patients (Lin *et al.*, 2014).

Despite these contradictory reports, DAO is still a popular target for deriving new therapies for diseases related to NMDAR dysfunction. Specific novel inhibitors for DAO have only been identified relatively recently (Ferraris *et al.*, 2008, Sparey *et al.*, 2008, Duplantier *et al.*, 2009, Smith *et al.*, 2009). DAO certainly has a predominant role in modulating D-serine levels in glia of the cerebellum, and also glia of the cerebral cortex and hippocampus in the forebrain, although it also exists neuronally in the prefrontal cortex, hippocampus, and substantia nigra (Hamase *et al.*, 2005, Verrall *et al.*, 2007, Sasabe *et al.*, 2014). As DAO is mostly localised to white matter of the forebrain, D-serine levels in the neurons of this region are primarily controlled by serine racemase. This enzyme is responsible for producing almost all endogenous D-serine by conversion from L-serine, as well as possessing D-serine degrading activity that can modulate D-serine levels (Wolosker *et al.*, 1999b, Foltyn *et al.*, 2005) thus making it an appropriate drug target to indirectly modulate NMDAR function.

1.7 Serine racemase

As mentioned in section 1.3.1, two different endogenous coagonists are required to bind to and activate NMDARs: glutamate and D-serine (or glycine). D-serine is produced by the enzymatic conversion of L-serine to D-serine by serine racemase (SR), which also degrades L- and D-serine to pyruvate and ammonia. The following sections will review the characteristic features of SR and the literature that supports its potential as a novel drug target for modulating NMDAR activity.

1.7.1 Discovery and historical context

For a significant period of time, convention stated that D-amino acids were only found in bacteria whereas L-amino acids occurred almost exclusively in animal tissues, with the exception of occasional reports of D-amino acids that were either limited to invertebrates or dismissed as artefacts (or ‘unnatural isomers’; Corrigan, 1969). This was challenged with the discovery of large amounts of free D-serine in the vertebrate brain (Hashimoto *et al.*, 1992, Nagata *et al.*, 1994), which prompted further studies of the distribution, function, and origin of D-serine. While it had been reported that L-serine was the precursor to D-serine in experiments in rats using radiolabeled L-serine (Dunlop and Neidle, 1997), it was assumed that this would involve multiple steps rather than direct enzymatic conversion.

The answer to the source of D-serine was found when Wolosker and colleagues first purified SR from rat brain homogenates in 1999 and confirmed its ability to convert L-serine to D-serine with a simple chemiluminescence assay (Wolosker *et al.*, 1999b). In the same set of experiments, they identified that mammalian SR is a highly conserved enzyme with characteristics similar to those observed in SR partially purified from silkworms, such as an alkaline pH optimum and the requirement for the cofactor, pyridoxal 5'-phosphate (PLP; Uo *et al.*, 1998). Subsequent molecular cloning experiments showed that SR has a molecular weight of about 37 kDa, comprising of

340 amino acids, with a sequence identity to mouse SR of 88%, and a highly-conserved PLP binding region that is also found in the serine/threonine dehydratase family of proteins (De Miranda *et al.*, 2000). Human SR was then found to be discretely localised to brain regions high in endogenous D-serine, being particularly high in the white matter of the hippocampus and corpus callosum, with intermediate levels in the substantia nigra and caudate.

1.7.2 Structure of serine racemase

Since these initial experiments, much has been done to identify the structure of SR and the role of cofactors that influence its activity. In cellular extracts, the activity of mouse SR was highly stimulated by the addition of adenosine triphosphate (ATP), an effect that was potentiated by Mg^{2+} , although this stimulation did not require hydrolysis of ATP (De Miranda *et al.*, 2002). The combined effect of ATP and Mg^{2+} resulted in a fivefold increase in D-serine production, and chelation of Mg^{2+} and other divalent cations with EDTA caused strong inhibition of D-serine synthesis, suggesting that both Mg^{2+} and the nucleotide complex, Mg.ATP, are important for stimulating the activity of SR (De Miranda *et al.*, 2002). The high affinity of SR for ATP relative to ADP, the next highest affinity cofactor (respective K_m values of 3 and 100 μM), indicates that ATP is the most biologically relevant nucleotide that influences SR activity. It is also possible for Ca^{2+} to activate SR by binding at the same metal-binding site as Mg^{2+} (De Miranda *et al.*, 2002) but the ATP- Ca^{2+} complex has been shown to produce a twofold lower maximal activation and threefold higher EC_{50} than the ATP- Mg^{2+} complex (Bruno *et al.*, 2017). The relative concentrations of Mg^{2+} and Ca^{2+} are unlikely to make competition between the two ligands physiologically relevant, but both ATP- Mg^{2+} and ATP- Ca^{2+} complexes are capable of stabilising the tetrameric form of SR in comparison to the cations alone (Bruno *et al.*, 2017).

SR requires PLP as a cofactor, which is one of the active forms of pyridoxine (vitamin B6). PLP-dependent enzymes are found in all organisms, with PLP considered to have emerged very early in biological evolution (Christen and Mehta, 2001) and as such PLP-

dependent enzymes are very versatile, contributing to a large variety of enzymatic reactions including transamination, decarboxylation, β - and γ -eliminations and substitutions, as well as racemisation (Phillips, 2015). The PLP-dependent enzymes that are specifically involved in amino acid metabolism can be separated into four groups of paralogous proteins denoted as fold types I–IV, categorised by the similarity of their secondary structure (Jansonius, 1998). SR belongs to the fold-type II family, along with its closest homologue serine dehydratase (SDH).

Smith and colleagues were the first group to solve the crystal structure of human and rat SR, to a resolution of 1.5 and 2.1 Å respectively, in the presence of the orthosteric inhibitor malonate (Smith *et al.*, 2010). Both human and rat SR crystallised as a symmetric dimer. Human SR is composed of a large and small domain connected by a flexible loop domain that acts as a hinge; the large domain contains PLP and a seven-stranded twisted β -sheet surrounded by ten α -helices, while the small domain contains four central parallel β -sheets and three α -helices (two close to the domain interface, one on the solvent-exposed side). Of the 340 amino acids comprising SR, residues 1–68 and 157–340 compose the large domain, residues 78–155 compose the small domain, and residues 68–77 and 145–149 compose the flexible loop domain. A catalytic lysine residue (Lys-56) in helix 3 of the large domain forms an internal Schiff base (commonly called an internal aldimine) with the PLP region to covalently link it to SR. All the crystal structures available of SR in the PDB, across multiple species including human, contain Mn^{2+} or Mg^{2+} in the metal binding site, indicating a prominent role for divalent cations in stabilising the folding of SR. The Smith group had more success crystallising SR with the orthosteric inhibitor malonate (Fig. 1.5), which drastically improved crystal quality and diffraction data because the ligand-induced shift of the small domain stabilised the SR structure in a closed conformation.

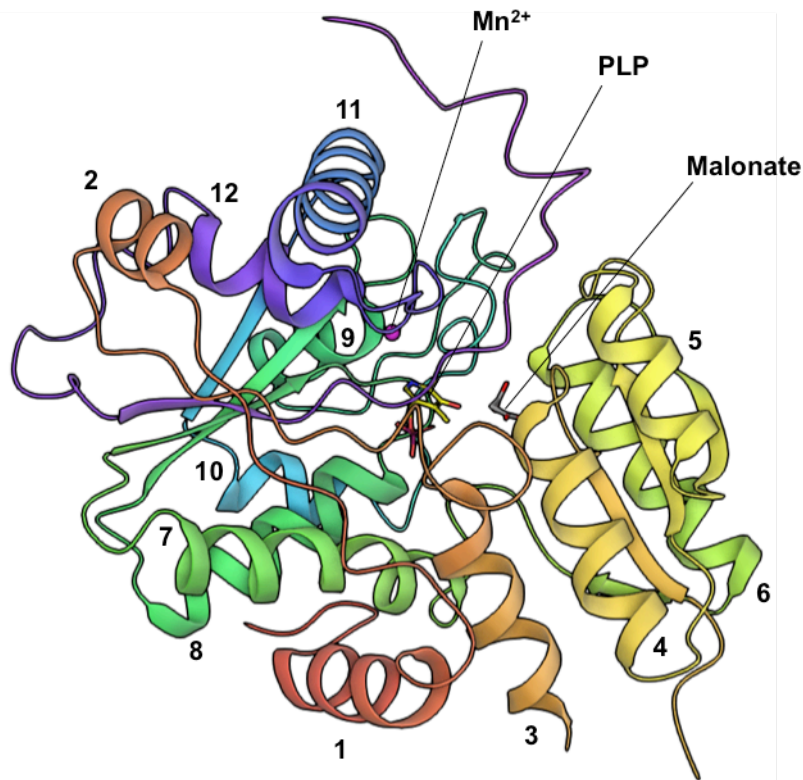


Figure 1.5. The structure of human SR in complex with its orthosteric inhibitor malonate (PDB 3L6B).

Image shown is of one SR monomer. Residues are coloured from red to violet, N-terminus to C-terminus, and all helices are numbered 1–12 based on the order they occur in the polypeptide sequence. The X-ray crystal structure of SR was solved by Smith *et al.* in 2010 and revealed that SR exists as a dimer, with each monomer comprising a large and small domain connected by a flexible loop region. The essential cofactor PLP is covalently bound to Lys56 as part of the large domain, and malonate binds in the active site at the interface of the two domains. SR is also dependent on binding of a divalent cation (Mn^{2+} here, but can also be Mg^{2+} or Ca^{2+}) to stabilise protein folding and increase activity. The small domain, which undergoes a ligand-induced conformational shift to orientate the ligand towards PLP, is comprised of helices 4, 5, and 6.

Only one published crystal structure offers a visualisation of the ATP binding site, in the yeast SR structure bound to the ATP analogue, AMP-PCP (PDB code 1WTC), and the authors determined its binding site is located at the domain interface (Goto *et al.*, 2009). Docking experiments onto the human SR structure using the AMP-PCP-containing yeast structure as a template determined that two molecules of ATP bind to human SR at the dimer interface, with both monomers contributing to the ATP/Mg²⁺ binding site (Jirásková-Vaníčková *et al.*, 2011).

1.7.3 Enzymatic role and reaction mechanism

While the production of D-serine is considered the main functional role of SR, the discovery of SR cofactors revealed SR is capable of catalysing another physiological reaction — the α,β -elimination of water from L-serine to form pyruvate and ammonia (De Miranda *et al.*, 2002). The elimination function reflects the homology of SR with serine dehydratases — enzymes which primarily produce pyruvate from L-serine — and suggests SR may have originated from a serine dehydratase gene and acquired serine racemisation, with its β -elimination activity being a relic from this evolutionary process (Wolosker and Mori, 2012). The physiological significance of this additional function of SR is unclear; while pyruvate has been shown to protect cells against oxidative damage and zinc neurotoxicity (Desagher *et al.*, 1997, Sheline *et al.*, 2000), the contribution of SR α,β -elimination to pyruvate levels is negligible compared to other processes such as glycolysis (Wolosker and Mori, 2012). It is possible that SR modulates D-serine levels, as it is also capable of catalysing the α,β -elimination of D-serine (Foltyn *et al.*, 2005). D-serine metabolism is primarily associated with the DAO enzyme (Hashimoto *et al.*, 1993) so the α,β -elimination function of SR may only be relevant in forebrain regions where DAO levels are reduced.

SR has little similarity to archetypal amino acid racemases, such as alanine racemase, again supporting the idea that its racemisation activity is a result of convergent evolution from an unrelated ancestor gene, serine dehydratase (De Miranda *et al.*, 2000). Indeed, the rate of racemisation of SR is about 100-fold lower than that of

alanine racemase, with a catalytic constant (K_{cat}) between 3–45 min^{-1} . In comparison to the efficiency of other enzymes this process is relatively slow, producing one molecule of D-serine in more than one second, but seems to correlate with the slow D-serine turnover in the brain (Dunlop and Neidle, 1997).

The proposed mechanism of the SR racemisation reaction (detailed schematic shown in Fig. 1.6) depends on two catalytic residues located on opposite sides of the PLP-conjugated plane: Lys56, which acts as a base, and Ser84, which acts as an acid. The PLP cofactor is connected to Lys56 via a Schiff base, and once L-serine binds to SR another Schiff base is formed between PLP and L-serine to produce an external aldimine separate from the active site. L-serine is deprotonated by Lys56 and a planar carbanionic intermediate is formed, then the substrate is protonated by Ser84 from the opposite plane to form D-serine.

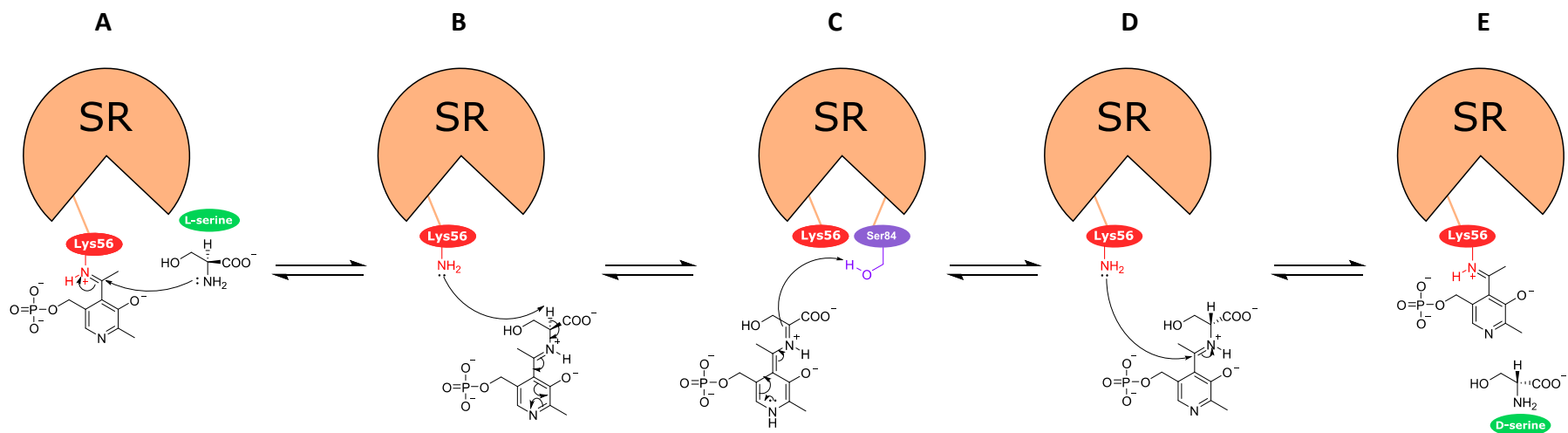


Figure 1.6. Reaction mechanism of L-serine isomerisation by SR.

(A) PLP is covalently bound to Lys56 via a Schiff base linkage. The α-amine of L-serine becomes deprotonated and carries out a nucleophilic attack on the carbon of PLP, followed by β-elimination of Lys56 to create a protonated Schiff base linkage between L-serine and PLP that is detached from the active site. (B) Lys56, present as the free amine, acts as a base to deprotonate the α-carbon of L-serine, causing double bond rearrangement of the Schiff base and loss of aromaticity to form a planar PLP intermediate. (C) Ser84, a residue in the active site, is moved into position to the opposite side of the PLP ring plane via an induced shift of the small domain. The planar Schiff base undergoes π-bond rearrangement and extracts a proton from Ser84, resulting in inversion of stereochemistry to form the D-isomer. (D) Lys56 carries out a nucleophilic attack on the PLP carbon, forcing π-electrons to transfer onto the nitrogen. Proton transfer results in the release of D-serine and reformation of the Schiff base linkage between PLP and Lys56. (E) SR returns to its native state and is able to accept another substrate.

1.7.4 Function of SR *in vivo*

With the initial purification of SR came an interest to identify which regions of the brain it was localised to, in order to understand the extent of the role SR has in D-serine metabolism and signalling. This was especially pertinent after findings that indicated D-serine is up to three times more potent than glycine as an NMDAR coagonist (Matsui *et al.*, 1995) and that selectively abolishing endogenous D-serine greatly reduced NMDAR activity in cell culture experiments (Mothet *et al.*, 2000), while the precise role and biosynthesis of D-serine remained unknown.

Accordingly, Wolosker and colleagues (the same group that initially purified SR) performed co-localisation experiments on rats to identify its expression pattern (Wolosker *et al.*, 1999a). They found that SR was expressed almost exclusively in the brain, particularly enriched in glial cells and reduced in neuronal cells, at levels that correlated with the high levels of endogenous D-serine in the brain. Further, they found that the distribution of SR closely mirrored that of D-serine, with highest concentrations of both being found in the forebrain, as well as in astrocytes throughout the cerebral cortex, dentate gyrus of the hippocampus, and corpus callosum. In contrast, negligible levels of D-serine and SR were present in the brainstem. SR was also found in areas of young rat brain where it is not found in the adult, such as the Bergmann glia of the cerebellum, which suggested that D-serine may have a role in the NMDA neurotransmission essential for neuronal development.

The overall enrichment of SR in glial cells in this study indicated that D-serine is formed in these cells rather than being synthesised in neurons and transported to glia, and indeed this theory was supported by several subsequent studies (Stevens *et al.*, 2003, Panatier *et al.*, 2006, Sasabe *et al.*, 2007). However, using *in situ* hybridisation it was then found that SR was predominantly expressed in rat brain neurons, especially in forebrain regions (Yoshikawa *et al.*, 2007) as well as the neuronal ganglion cells of the retina (Dun *et al.*, 2008, Takayasu *et al.*, 2008). Furthermore, immunohistochemical findings using polyclonal SR antibodies with improved sensitivity have suggested SR was actually localised to neuronal cells (Kartvelishvily *et al.*, 2006, Wolosker *et al.*,

2008), particularly in the cerebral cortex and hippocampal formation. This was based on numerous previous observations that high levels of D-serine are also present in neuronal cultures (Wolosker *et al.*, 2008, Rosenberg *et al.*, 2010). Further corroboration was provided by a report examining SR brain distribution, using novel SR knockout mice as negative controls to establish specificity of neuronal labelling (Miya *et al.*, 2008). The authors found SR was predominantly localised in pyramidal neurons of the cerebral cortex and hippocampal CA1 region, as well as in the GABAergic medium-spiny neurons of the striatum. Rather compellingly and in contradiction to earlier studies, they did not find any evidence of SR in the glia, a finding corroborated by the Allen Institute for Brain Science, who found negligible or no SR mRNA in astrocytes at the corpus callosum (Allen Institute for Brain Science, Lein *et al.*, 2007). The more recent findings that SR is also found to a lesser extent in astrocytes as well as in neurons in transgenic mice expressing eGFP (Ehmsen *et al.*, 2013) only adds further ambiguity, and suggests there may be a disparity in SR expression when comparing *in vitro* and *in vivo* techniques, spurring the need for confirmation in the form of SR knock-out mice models (section 1.7.6).

The evidence for neuronal SR would suggest that D-serine is predominantly found in neurons, but it is actually present in higher levels in astrocytes (Schell *et al.*, 1997, Kartvelishvily *et al.*, 2006, Williams *et al.*, 2006). Taking into account this information, a 'serine-shuttle' model was proposed by Wolosker to explain how the twofold enzymatic function of SR might contribute to modulating D-serine levels (Wolosker, 2011). In this model, D-serine is synthesised in neurons by SR using L-serine imported from astrocytes; after synthesis, D-serine is released into the extracellular medium and subsequently shuttled back to astrocytes where it is stored prior to activity-dependent release. The efficiency of the α,β -elimination reaction of SR is relatively high, which would explain why levels of D-serine are low in neurons expressing SR, and making astrocytes — which have low levels of SR — ideal for sequestering D-serine, where it is protected from degradation. The serine-shuttle model describes a complex interplay between neuron and astrocyte metabolism, and as such highlights the need for improved techniques in order to fully comprehend the role of D-serine in mediating

NMDAR activation, particularly in terms of the relative contribution of D-serine from neurones and astrocytes.

1.7.5 Linking SR to disease

The specific location of SR in the brain has yielded some insight into its physiological role. The enzyme D-amino acid oxidase (DAO) is largely responsible for D-serine catabolism in peroxisomes, but has minimal expression in forebrain areas, where SR is highly expressed. It is therefore possible that SR is able to regulate D-serine levels through its α,β -elimination activity. This is supported by the observation that D-serine levels in the forebrain are unchanged in mice expressing catalytically-inactive DAO (Hashimoto *et al.*, 1993) but is contradicted by recent findings that D-serine is localised to the same regions as SR, suggesting the α,β -elimination of SR is not predominantly responsible in altering D-serine levels (Ehmsen *et al.*, 2013). This latter experiment used mice with targeted deletion of 3-phosphoglycerate dehydrogenase (Phgdh), an enzyme involved in L-serine biosynthesis, to create mice significantly depleted of D-serine that could be used as specific negative controls; previous studies using antibody preadsorption as a negative control does not ensure specificity and may explain the variation in D-serine described as neuronal or glial.

SR-KO mice (section 1.7.6) are used as models for schizophrenia due to their NMDAR hypofunction and resulting morphological and behavioural changes. It is pertinent that in an extensive schizophrenia genome-wide association study, the *SRR* gene was identified as a possible genetic risk factor for schizophrenia (Schizophrenia Working Group of the Psychiatric Genomics Consortium, 2014), giving credence to the glutamate hypothesis of schizophrenia. However, earlier genetic analyses found varied results. The first examination of the genetic role of *SRR* revealed that human brain *SRR* transcripts consisted of four isoforms with one major species that were derived from alternative use of various 5' end exons, and that there was no significant association between *SRR* and schizophrenia in Japanese populations (Yamada *et al.*, 2005). In addition, no association was found between single-nucleotide polymorphisms (SNPs)

in the 5'-promotor region of the *SRR* gene and schizophrenia in a Russian population (Goltsov *et al.*, 2006), nor the 3' and central regions in a German population (Strohmaier *et al.*, 2007), a later Japanese population (Ohnuma *et al.*, 2009), and a Han Chinese population (Yu *et al.*, 2015). Another genetic analysis genotyped three SNPs of the 5' region of the *SRR* gene in patients with schizophrenia and found a significant excess of the IVS1a+465C allele of SNP5, thought to influence the promoter activity of the *SRR* gene and lower expression of SR (Morita *et al.*, 2007). The authors proposed the discrepancy was due to SNP5 being more associated with the paranoid- over disorganised-subtype of schizophrenia, and differences between the methods used by both groups. Others have found significant associations between SNPs in *SRR* and schizophrenia (Labrie *et al.*, 2009, Kim *et al.*, 2012, Luykx *et al.*, 2015, Van der Auwera *et al.*, 2016).

Results of genetic studies have been mixed, but there is some evidence that the aetiology of schizophrenia is linked to abnormal modulation of the NMDAR D-serine site, possibly mediated by SR. Changes in SR expression have been described in the post-mortem hippocampus and cortex of schizophrenic patients, with some studies observing a decrease (Bendikov *et al.*, 2007) and others an increase (Steffek *et al.*, 2006, Verrall *et al.*, 2007). Aberrant SR expression in schizophrenia is consistent with reports of diminished D-serine and elevated L-serine in the serum levels of patients (Hashimoto *et al.*, 2003). Further, the PFC of schizophrenic patients was found to have reduced expression of protein-interacting with kinase C (PICK1; Beneyto and Meador-Woodruff, 2006), which is genetically associated with schizophrenia (Fujii *et al.*, 2006) and binds to the C-terminus of SR to either modulate its activity, or increase phosphorylation of SR by PKC (Fujii *et al.*, 2006). Abnormalities in DISC1 have been consistently associated with psychiatric disorders (Brandon and Sawa, 2011) and accordingly mutant DISC1 has been shown to cause increased ubiquitination and degradation of astrocytic SR *in vivo* resulting from disruption of the normal physiological binding of DISC1 to SR (Ma *et al.*, 2013). The mice with mutant DISC1 had diminished D-serine concentrations and behavioural abnormalities consistent with NMDAR hypofunction (Ma *et al.*, 2013).

Aberrant SR and D-serine regulation may have a role in AD. Serum levels of D-serine and L-serine were found to be respectively lower and higher in patients with AD, indicating reduced activity of SR may contribute to the pathophysiology of AD (Hashimoto *et al.*, 2004). A β has been found to upregulate SR mRNA and protein and cause a corresponding increase in D-serine in hippocampal cell cultures (from the hippocampus of a transgenic mouse model of AD and human patients with AD) and rat microglia (Wu *et al.*, 2004, Madeira *et al.*, 2015). Similarly, secreted APP fragments have been proposed to transcriptionally induce SR, leading to increased steady-state levels of dimeric SR and elevated D-serine levels in microglia (Wu *et al.*, 2007). It has been suggested A β increases microglial transcription through JNK-dependent recruitment of AP-1 complex to the SR promoter (Wu and Barger, 2004). The overall elevation of SR mRNA and protein in microglia and AD hippocampus may contribute to excitotoxic neuronal cell death in AD because conditioned medium from A β -treated microglia is toxic to cultured hippocampal neurons, an effect that is prevented by the NMDAR D-serine site antagonist DCKA and by DAO degradation of D-amino acids (Wu and Barger, 2004, Wu *et al.*, 2004). This evidence is supported by observations that A β -induced neurotoxicity is attenuated in SR knockout mice (Inoue *et al.*, 2008).

1.7.6 Serine racemase knock-out mice

SR knock-out (KO) mice have been useful for probing the function of SR *in vivo*. The first SR-KO mouse strain was used as a negative control in double immunofluorescence staining experiments that revealed the predominant localisation of SR in neuronal cells (Miya *et al.*, 2008). In SR-KO mice, the most significant reduction of D-serine was in the forebrain, followed by the cerebellum and spinal cord (Miyoshi *et al.*, 2012), with D-serine being reduced to 10–20% that of wild-type (Inoue *et al.*, 2008, Miya *et al.*, 2008). The origins of the remaining D-serine remain inconclusive, with proposed alternative pathways including the glycine cleavage system (Iwama *et al.*, 1997), the hydrolysis of phosphoserine by phosphoserine phosphatase (Wood *et al.*, 1996), or exogenous D-serine from intestinal bacterial flora. In mice depleted of both SR and DAO, D-serine is drastically reduced (by 85%) in the cerebral cortex and hippocampus compared to

SR+DAO- mice, and also greatly reduced (by 50%) in the cerebellum and spinal cord, indicating D-serine is mostly synthesised by SR in these tissues (Miyoshi *et al.*, 2012), thereby emphasising the physiological role of SR in D-serine regulation in the brain. To quantify the contributions of astrocytes and neurons to SR and D-serine localisation, SR conditional knockout (SRCKO) mice with selective suppression of SR in astrocytes (α SRCKO) and in forebrain glutamatergic neurones (n SRCKO) were studied and revealed that while D-serine levels were decreased in n SRCKO mice, they remained unaffected in α SRCKO, implicating a more important role for neurons in producing D-serine (Benneyworth *et al.*, 2012). Despite this, the poor correlation between SR expression and D-serine levels in the mice in this study raises questions about the involvement of other pathways regulating D-serine, such as expression of SR in the liver, altered expression of DAO, and loss of SR α,β -elimination activity.

In regards to expression of NMDARs in SR-KO mice, the expression levels of GluN1, GluN2A and GluN2B, which are abundant in the forebrain, are comparable between SR-KO and WT mice (Inoue *et al.*, 2008). NMDAR-mediated neurotransmission is notably affected; SR-KO mice display impaired NMDA-dependent LTP, as well as slower decay kinetics of NMDAR-mediated EPSPs in whole-cell patch-clamp recordings in the Schaffer collateral and hippocampal CA1 of juvenile brain slices (Basu *et al.*, 2009). An analogous experiment found a significant reduction in the magnitude of LTP in n SRCKO mice but no change in the LTP of α SRCKO (Benneyworth *et al.*, 2012), suggesting that it is neuronal D-serine that primarily regulates synaptic plasticity. Activation of NMDARs leads to the formation of nitric oxide (NO) which nitrosylates and inactivates SR in a negative feedback loop (Mustafa *et al.*, 2007). In SR-KO mice NO formation and nitrosylation of its targets are substantially reduced, emphasising the importance of NMDAR activation by D-serine, and thus SR, in NO signalling (Mustafa *et al.*, 2010). SR depletion also protects against NMDAR-mediated excitotoxicity, indicating NMDA neurotransmission is diminished in SR-KO mice (Mustafa *et al.*, 2010).

SR-KO mice display observable changes in their behaviour, including a deficit in spatial memory formation compared to WT when evaluated in the Morris water maze and increased locomotor activity (Basu *et al.*, 2009). In a behavioural test that evaluates

episodic memory, SR-KO mice exhibited an abnormal pattern of preference for the order of events in distinct experiences in two separate tests (DeVito *et al.*, 2011) which could be a result of disrupted functioning of the PFC. This correlates with the observation that SR-KO mice have less complex dendrites with reduced spine density in the mPFC and abnormal apical dendrites of the pyramidal neurones (DeVito *et al.*, 2011) which is consistent with these neurones receiving projections from limbic regions where SR is highly expressed and the important role that D-serine plays in NMDAR signalling.

Overall, it is evident from SR-KO mice models that D-serine is especially important for cognitive function and NMDAR-mediated transmission. SR-KO mice have been used to study disorders associated with dysfunctional NMDAR signalling, such as neurodegeneration and schizophrenia. As well as displaying attenuated NMDA-induced excitotoxicity upon injection of NMDA into the cerebral cortex, SR-KO mice are also protected against $A\beta_{1-42}$ -induced neuronal damage when injected into the hippocampus (Inoue *et al.*, 2008). The neurotoxic derivatives of $A\beta_{1-42}$ are thought to contribute to the pathogenesis of Alzheimer's disease (Lambert *et al.*, 1998), so it is possible the observed effect implicates the involvement of D-serine in NMDAR-mediated neurotoxicity by $A\beta_{1-42}$ and neuronal death in AD (Inoue *et al.*, 2008). Taken together with the observation that D-serine is the dominant endogenous coagonist for NMDAR-excitotoxicity (Shleper *et al.*, 2005), and that $A\beta$ induces SR expression and stimulates the release of excitotoxic D-serine (Wu *et al.*, 2004), the case for D-serine and SR playing a role in neurodegeneration is strong. This makes SR-KO mice relevant models for studying other neurodegenerative diseases such as ALS and Huntington's disease. Accordingly, elevated levels of both D-serine and SR were observed in an ALS mouse model (Sasabe *et al.*, 2007) and where SR was also disrupted, ALS mice survived longer although show earlier symptom onset (Thompson *et al.*, 2012).

The relationship between glutamate signalling and neuropathic pain has been studied in SR-KO mice, which exhibited increased sensitivity to inflammatory pain (Tabata-Imai *et al.*, 2014) and aberrant decay times of NMDAR-mediated EPSCs in neurons of the central amygdala after injection of Freund's adjuvant to model arthritic pain (Maekawa

et al., 2012). It is thought that the chronic pain-induced behavioural changes observed in SR-KO mice are due to a reduction in D-serine in the amygdala, leading to decreased NMDAR-mediated neurotransmission in this area (Tsuzuki *et al.*, 2012).

SR-KO mice have been used as a mouse model of schizophrenia due to their NMDAR hypofunction and hippocampal deficits. As well as displaying decreased NMDAR activity and LTP, SR-KO mice also show morphological changes (including reduced hippocampal spines and dendritic volume), neurochemical changes (including decreased levels of miR-132 and BDNF, which regulate dendritic spine expression), and cognitive deficits (Balu *et al.*, 2013); all of which are associated with schizophrenia. That chronic D-serine treatment reverses the cognitive deficits attributed to reduced SR expression in these mice (Balu *et al.*, 2013, Balu and Coyle, 2014) suggests that positive allosteric modulation of SR could be a method of alleviating the currently poorly-treated cognitive and negative symptoms of schizophrenia by compensating for NMDAR hypofunction. Moreover, the effects of psychotomimetic drugs such as PCP, amphetamine (AMPH) and methamphetamine (METH) have been examined in SR-KO mice. Acute startle reactivity was increased in SR-KO mice when administered with PCP but not AMPH (Benneyworth *et al.*, 2011) and repeated administration of METH resulted in behavioural sensitisation in WT but not SR-KO mice (Horio *et al.*, 2012). The latter observation corresponded with an increase in ERK1/2 phosphorylation after METH administration in WT but not SR-KO mice, and a smaller METH-induced dopamine release in the nucleus accumbens of mice lacking SR (Horio *et al.*, 2012). SR-KO mice also demonstrated an inability to extinguish conditioned hyperactivity and responses to drug-associated stimuli after treatment with AMPH (Benneyworth and Coyle, 2012). Altogether, these results are consistent with the role of NMDAR hypofunction in the comorbidity of substance abuse seen in schizophrenia.

A key study for linking SR, D-serine and schizophrenia focuses on Disrupted-in-Schizophrenia-1 (DISC1), a gene which when disrupted has been found to be associated with schizophrenia, MDD and bipolar disorder (St Clair *et al.*, 1990, Millar *et al.*, 2000) and whose variants and polymorphisms have been linked to psychiatric disorders (Brandon and Sawa, 2011). A mouse model of selective and inducible DISC1

expression found that DISC1 acts as a scaffold that binds to and stabilises SR, but mutant DISC1 loses this function and instead binds to and depletes full-length DISC1, thereby facilitating ubiquitination and degradation of SR and decreased D-serine production (Ma *et al.*, 2013). Adult mice expressing mutant DISC1 exhibit behavioural abnormalities consistent with NMDAR hypofunction as a result of D-serine deficiency, such as greater responses to dizocilpine in open-field and pre-pulse inhibition of the acoustic startle tests (Ma *et al.*, 2013).

1.7.7 Serine racemase inhibition

The schizophrenia-like phenotype of SR-KO mice (impaired NMDAR-mediated neurotransmission and LTP, cognitive deficits, behavioural changes) might raise concern as to whether similar traits might be observed in patients treated with an SR inhibitor. It is important to remember this phenotype stems from glutamate *hypofunction* resulting from a downregulation of NMDAR activity comparative to wild-type, whereas an SR inhibitor would be used to treat conditions underpinned by glutamate *hyperfunction* (such as neuropathic pain and excitotoxicity) by aiming to reduce NMDAR neurotransmission to more typical levels. Moreover, the aim of an SR inhibitory drug would not be to completely abolish SR activity but to reduce it to a point at which it is therapeutically relevant. For instance, heterozygous (+/–) SR-KO mice have cortical D-serine levels that are 70% of wild-type (compared to 10% in the homozygote) and only moderately affected glutamatergic neurotransmission with respect to the homozygote (Basu *et al.*, 2009). With this in mind, the goal of an SR inhibitory drug would be to slightly reduce NMDAR activity while still enabling functional glutamatergic neurotransmission, which is currently not possible with many NMDAR antagonists (such as ketamine) that exhibit all-or-nothing degrees of inhibition.

The above considerations, in combination with the evidence for the role of NMDARs and D-serine in many CNS disorders, has formed the rationale for characterising and developing inhibitors of SR. Early experiments identified L-serine-O-sulfate (LSOS) as a SR inhibitor of D-serine synthesis (Panizzutti *et al.*, 2001) and naturally derivatives of L-

serine and LSOS were studied further, revealing several competitive inhibitors including glycine ($K_i = 1.63 \text{ mM}$), malonate ($K_i = 0.077 \text{ mM}$), and L-erythro-3-hydroxyaspartate (L-EHA; $K_i = 0.049 \text{ mM}$; Stríšovský *et al.*, 2005). A more comprehensive study of the effects of amino acids and their derivatives on SR activity found that glycine, and compounds related to aspartic acid such as L-aspartate, L-asparagine, and oxaloacetic acid, all act as substrate-mimetic SR inhibitors whereas sulfhydryl compounds such as L-cysteine can inhibit SR by reacting with PLP to form thiazolidine derivatives (Dunlop and Neidle, 2005). Substrate-product analogues have also been investigated for their inhibitory potential but with modest results. For example, α -(hydroxymethyl)serine exhibited linear mixed-type inhibition of SR from *S. pombe* ($K_i = 167 \text{ mM}$; Harty *et al.*, 2014).

Several novel inhibitors that are structurally distinct from L-serine were identified after high-throughput screening of a peptide library using a one-bead one-compound combinatorial approach. The inhibitors, which displayed a clear structural motif consisting of 3-phenylpropionic acid and histidine moieties, exhibited moderate potency (high micromolar K_i) towards human SR (Dixon *et al.*, 2006). Using a biochemical assay to evaluate enzyme kinetics, the authors concluded the inhibitors were slow binding and were competitive with respect to L-serine.

A new group of SR inhibitors was identified by Mori and colleagues, by multi-filter *in silico* screening of a 4 million compound database using one of the dipeptide-like SR inhibitors reported by Dixon *et al.* as the query molecule, then follow-up confirmation by *in vitro* enzyme assay (Mori *et al.*, 2014). The compounds identified from the screen contained an essential central amide structure with a phenoxy substituent, and substitution of parts of the structure for heavier halogen atoms such as bromine and iodine produced derivatives with improved inhibitory activity, binding affinity, and ligand efficiency. The inhibitors had IC_{50} values comparable to malonate and bore some structural resemblance to the bulky hydrophobic peptides identified previously (Dixon *et al.*, 2006). The Mori group investigated their inhibitors further by testing the most potent derivative in an *in vivo* assay to examine the effect on over-activation of NMDARs in the brain (Mori *et al.*, 2017). The authors used an Arc-Luc Tg hairless (HL)

mouse strain, in which brain activity could be detected by bioluminescence signal (Izumi *et al.*, 2017). Acute injection of kainate increased signal intensity in the brain of control mice owing to activation of high affinity KA-type glutamate receptors, but in mice orally administered the SR inhibitor beforehand, the intensity in regions of interest was reduced by about 1.4-fold. The results suggested the SR inhibitor suppressed neuronal activity-dependent Arc expression *in vivo* to regulate NMDAR overactivation.

Aside from these bulky hydrophobic peptides, most identified SR inhibitors are small molecules, indicating an inherent difficulty in targeting the tight cleft of the active site. Indeed, another novel family of SR inhibitors discovered through screening of structurally diverse small molecules are the hydroxamic acids, with the most potent being succinodihydroxamic acid ($IC_{50} = 90 \mu M$; Hoffman *et al.*, 2009a). Unfortunately, these inhibitors were non-specific, as their additional inhibition to other PLP-dependent enzymes suggested their mechanism of action was through PLP modification rather than targeting the active site.

As malonate is a selective and relatively potent SR inhibitor, Vorlová described a series of 20 malonate-based inhibitors of mouse SR including 2,2-dichloromalonate ($IC_{50} = 57 \mu M$), which is the most effective competitive SR inhibitor to date. The other inhibitors exhibited a wide range of potencies, from 2-hydroxymalonate ($IC_{50} = 94 \mu M$) to 2,2-bis(hydroxymethyl)malonate ($IC_{50} = 40 mM$; Vorlová *et al.*, 2015). A subsequent study aimed to find novel SR inhibitors by mimicking malonate with a cyclopropane scaffold, and presented a series of cyclopropane dicarboxylic acid derivatives that were tested by molecular docking and *in vitro* experiments. The few most potent inhibitors bind SR in the high micromolar range (Beato *et al.*, 2015), and while these are weaker than malonate-based compounds, they could still be used for the further development of more potent SR inhibitors.

As it has not yet been possible to find a SR inhibitor that inhibits with an IC_{50} below the micromolar range, some studies have focused on expanding the chemical space of existing hSR inhibitors to improve their potency. One group performed virtual screen

analyses and molecular modelling to elicit eight compounds with putative inhibitory activity, including two that are structurally diverse from any previously identified SR inhibitor (Dellafiora *et al.*, 2015). When evaluated in *in vitro* experiments on purified hSR, four of the eight exhibited a good inhibitory effect, but weak potency (59–70% inhibition, $K_i = 1.3\text{--}1.7\text{ mM}$), which are characteristics similar to inhibitors identified previously (Mori *et al.*, 2014, Beato *et al.*, 2015). The common characteristics of the active inhibitors include the presence of at least one carboxyl group that interacts with Ser83 — part of the substrate-binding loop in the active site — and a simultaneous binding to Arg135 at the top of the active site (Dellafiora *et al.*, 2015). Another group of SR inhibitors is composed of substrate-product analogues, which have limited efficacy unless there is a lot of space in the active site or the inhibitor is sufficiently flexible (Harty *et al.*, 2014) and considering the tight cleft of SR makes it a difficult target, there may be little potential for these types of inhibitors.

Regulation of SR activity via indirect inhibition has also been described. Mustafa and colleagues found that glial SR localised to membranes is physiologically inhibited by phosphatidylinositol (4,5)-bisphosphate (PIP_2), and this inhibition is relieved after mGluR activation leads to phospholipase C-mediated degradation of PIP_2 (Mustafa *et al.*, 2009). PIP_2 acts as a noncompetitive inhibitor by binding adjacent to the SR ATP site and preventing binding of ATP to SR, which is critical for regulating SR activity. This is supported by findings that when apyrase is used to hydrolyse the γ - and β -phosphate from ATP in cell extracts there is a resulting loss of SR activation (De Miranda *et al.*, 2002). These observations imply a potential for compounds designed to specifically target the ATP binding site as SR inhibitors.

The impact of SR inhibition on D-serine levels has been examined in a cellular model. When LSOS was added to a culture media of HEK293 cells expressing wild-type SR, it was found D-serine synthesis was largely inhibited, implying SR activity could be converted to an eliminase *in vivo* (Panizzutti *et al.*, 2001). Based on the findings of Panizzutti *et al.*, the first *in vivo* SR inhibitor study was performed in a rat model of arthritic pain. Intrathecal injection of LSOS and L-EHA decreased wind-up activity in normal and monoarthritic rats, producing antinociceptive effects in both rat groups, as

well as significantly lowering hyperalgesia in the monoarthritic rats (Laurido *et al.*, 2012). Subsequent injection of D-serine reinstated the hyperalgesia in monoarthritic rats and analgesia in normal rats, possibly implying that SR inhibitors can modulate D-serine and NMDAR activity levels *in vivo* as well as the development of chronic pain (Laurido *et al.*, 2012), but with the caveat that target engagement to SR was not ascertained in this study.

To conclude, the expanding area of SR inhibition has already produced much promising data that indicate targeting SR is a viable approach to modulating NMDAR activity, specifically for CNS disorders resulting from NMDAR overactivation such as excitotoxicity and neuropathic pain. However, it is not clear at this time whether inhibiting SR would have an overall positive therapeutic benefit in humans or not. For instance, SR-KO mice display cognitive deficits, while upregulating D-serine appears to have many of the same effects as ketamine, both of which surely have opposing mechanisms of action. It is probable there is a more complex relationship between D-serine production, SR activity, and NMDAR signalling, involving downstream signalling pathways and negative feedback loops. At present, knowledge in this field is expanding but is limited by the lack of highly potent and selective SR inhibitors that could drive the drug discovery process. It is the intention of this thesis to contribute to the development of a good tool compound that will be invaluable for conducting the critical target validation studies required prior to a formal drug discovery project.

Table 1.2. Overview of current SR inhibitors.

Group	Compound	Inhibition mode	Ref.
Serine analogues	L-serine- <i>O</i> -sulfate	Competitive/ substrate mimetic	a, b, c
	L-cysteine- <i>S</i> -sulfate		a
	β -chloro-L-alanine		a, c
	Homocysteic acid		a, c
Aspartate analogues	L-aspartate	Competitive	a
	L-asparagine		a
	L-erythro-3-hydroxyaspartate		a
	L-aspartate β -hydroxamate		d
Carboxylic acids	Malonic	Competitive	a
	Succinic		a
	Maleic		a
	L-malic		a
	Tartaric		a
	Dihydroxyfumaric		a
	Oxaloacetic acid	Product inhibition	a, c
Malonate derivatives	2-aminomalonate	Competitive	e
	2-fluoromalonate		e
	2-hydroxymalonate		e, f
	2,2-dichloromalonate		f
	2,2-bis(hydroxymethyl)malonate		f
Substrate-product analogues	α -(hydroxymethyl)serine	Substrate-product inhibition	g
Cyclopropane carboxylic acid derivatives	1,2-cyclopropanedicarboxylic acid	Competitive; related to malonate	h
Peptide inhibitors	Various; see Table 10.3	Malonate site/ dimer interface	i, j, k
Non-specific inhibitors	Sulfhydryl compounds (e.g. L-cysteine)	PLP modification	c
	Hydroxamic acids		d
Physiological modulators	PIP2 (physiological inhibitor)	Noncompetitive; Interferes with ATP binding	l
	GRIP	Activation; binds to SR	m
	PICK1	Inhibition; binds to SR and induces its PPN by PKC	n
	Golga3	Increases SR levels by preventing ubiquitylation	o
	Nitric oxide	Inhibition; induces S-nitrosylation of SR	p
	NADH	Inhibition; promotes ATP dissociation	q

ATP, adenosine triphosphate; Golga3, Golgin subfamily A member 3; GRIP, glutamate receptor-interacting protein; NADH, nicotinamide adenine dinucleotide; PICK1, protein interacting with C-kinase; PIP2, phosphatidylinositol 4,5-bisphosphate.

a (Strisovský *et al.*, 2005); **b** (Panizzutti *et al.*, 2001); **c** (Dunlop and Neidle, 2005); **d** (Hoffman *et al.*, 2009a); **e** (Jirásková-Vaničková *et al.*, 2011); **f** (Vorlová *et al.*, 2015); **g** (Harty *et al.*, 2014); **h** (Beato *et al.*, 2015); **i** (Dixon *et al.*, 2006); **j** (Mori *et al.*, 2014); **k** (Mori *et al.*, 2017); **l** (Mustafa *et al.*, 2009); **m** (Kim *et al.*, 2005); **n** (Fujii *et al.*, 2006); **o** (Dumin *et al.*, 2006); **p** (Mustafa *et al.*, 2007); **q** (Suzuki *et al.*, 2015).

1.8 The drug discovery process

The entire drug discovery process, from the point of inception through to filing and licensing of a compound by the regulatory authorities (e.g. FDA or EMA) is a complex process that can take 10–15 years and cost over \$1 billion (Hughes *et al.*, 2011). Normally a particular target will emerge with several years' worth of supporting evidence (e.g., genetic or pathological association with a disease, pharmacological validation in cellular or *in vivo* models that compounds targeting the protein of interest produce a disease-relevant phenotype) that to ensure it is worth the time and money invested in the process. Then, it will be subject to the preclinical stages of the drug discovery process either by the pharmaceutical industry or academic drug discovery centres to identify molecules that engage with this target and have suitable characteristics to make potential drugs. These key preclinical stages are: target identification and validation, assay development, high throughput screening, hit identification, lead optimization, and ultimately the selection of a candidate molecule for clinical development.

1.8.1 Target identification

Target identification requires a thorough understanding of the disease and would ideally yield a target that is efficacious, safe, and most importantly, 'druggable' — that is, accessible to drug molecules and is able to elicit a biological response both *in vitro* and *in vivo*. Often the aetiology of CNS disorders can be poorly understood, which limits the potential for selecting targets based solely on empirical evidence. Target identification may be achieved by a bioinformatics approach known as data mining to help identify, select, and prioritise targets (Yang *et al.*, 2009), phenotypic screening to identify therapeutically valuable compounds based on the phenotypic response of the subject (whether it be cell, tissue, or an entire organism; Szabo *et al.*, 2017), or simply by observing links between a particular disease and genetic polymorphisms, as seen in

familial AD wherein patients often have mutations in the APP or presenilin genes (Bertram and Tanzi, 2008).

1.8.2 Target validation

Here, the role of a target in disease must be clearly defined by generating cellular and/or *in vivo* data to support the hypothesis that modulation of the target produces a disease-relevant phenotype. The techniques employed range from the use of tool compounds to gather information about the target *in vitro* and *in vivo*, to whole animal models, to modulation of a desired target in disease patient. Target validation methods can include antisense technology to target mRNA, preventing translation and blocking synthesis of the protein of interest (Taylor, 1999), and a related approach of using small interfering RNA (siRNA) that, once integrated into an RNA-induced silencing complex (RISC), can base-pair to their target mRNA to induce cleavage of the mRNA and prevent it being translated (Castanotto and Rossi, 2009). Methods employing monoclonal antibodies have the advantage of neutralising the target protein more efficiently due to their ability to bind to a larger region of the protein, often with higher affinity, at unique epitopes outside of the often highly conserved active site (Hughes *et al.*, 2011). Perturbation of expression of the target gene by any of the above techniques, or by overexpression of cDNA and gene inhibition by a chemical compound, can produce valuable cellular model systems with the desired phenotype so the role of the target gene can be studied (Gashaw *et al.*, 2012).

Chemical genomics is an approach that aims to provide small molecules targeting every protein encoded by the genome (Zanders *et al.*, 2002), and has been largely made possible by developments in *in silico* technology to aid the synthesis of highly focused libraries containing structures with a high probability of interacting with ligand-binding sites on the target protein.

If possible, the relevance of a target in disease can be evaluated in knockout or transgenic animal models of the disease, assuming appropriate models exist. Animal

models can be useful because they allow the effect of gene manipulation to be observed in the phenotype of a whole animal and thus can yield insights into the function of genes and their role in disease *in vivo*. However, animal models are only of use if the molecular target has a human orthologue, and even then huge discrepancies can occur between species (Wendler and Wehling, 2010).

1.8.3 Assay development

An assay format needs to be developed to enable characterization of novel compounds and their potency against the target, which can then be used to develop structure-activity relationships (SARs). Generally, two types of assay are preferentially used: cellular assays, which depend on the creation of mammalian cell lines over-expressing the target of interest and are most applicable for membrane receptors, ion channels, and nuclear receptors (Michelini *et al.*, 2010); and biochemical assays, which are used to evaluate and characterise purified recombinant protein. Both generate different data, with cell-based assays giving a functional read-out if there is any compound activity, and biochemical assays measuring the affinity of the compound with the target protein, and enzyme activity. A number of requirements have to be met before an assay can be used for screening — data must be reproducible and repeat literature values where relevant, the assay signal must be robust, it needs to be quick, easy and cost-efficient to set up, and kinetic parameters must be established and reproducible (Hughes *et al.*, 2011).

1.8.4 Hit identification

A 'hit' compound is often defined as one that has a desired activity in a compound screen and whose activity is confirmed upon retesting. These hits may be identified by high throughput screening (HTS) which involves screening an entire compound library against the drug target in the previously established assay. This method requires automated laboratory machinery to achieve high throughput processing, so can generate hits with novel pharmacophores from large libraries of structurally diverse

compounds. On the other hand, knowledge-based screening involves selecting groups of molecules from the compound library that are more likely to have more activity at the protein target, based on knowledge of the target and chemicals with similar structures which are already known to have some activity at the target (Boppana *et al.*, 2009). The information obtained from knowledge-based screening has enabled the rapid development of computational screening methods that use known pharmacophores and molecular modelling to conduct virtual screens of compound databases, and is now considered a credible and complementary alternative to high-throughput biochemical compound screening (McInnes, 2007).

1.8.5 Fragment-based drug discovery

A newer approach, focusing on using much smaller molecules than in a standard compound library, has emerged as an important technique for many drug discovery organisations. Fragment-based drug discovery (FBDD) involves the generation of small molecular weight compound libraries that are screened at high concentration, often in conjunction with other techniques such as NMR and mass spectrometry to confirm hits. A significant advantage of FBDD is that screening with a fragment set is more likely to find new chemotypes that will bind to a target, because far fewer fragment molecules are required to span the chemical diversity space than with lead compounds; this is useful for popular targets where the surrounding literature may be saturated with identified compounds and so provides an additional approach to tackle the target. The other advantage of FBDD methods is that they can find chemotypes that bind to difficult targets, such as ones seemingly not very 'druggable' when put through HTS. This has particular relevance to SR, whose two domains form a very tight cleft that is not accessible to large molecular weight compounds, and has meant previous compound screens of SR in a biochemical assay system yielded no hits. Any fragments that are found to have weak interactions with the target protein are assessed using structural knowledge of the binding site to allow for optimization of these compounds with improved drug-like activity. These drug fragments are verified and evaluated before the most promising compounds are selected for hit-to-lead programmes.

1.8.6 Hit-to-lead and lead optimisation

In hit-to-lead, each hit is refined to try and produce more potent and selective compounds, with reduced off-target activities, and with reasonable pharmacokinetics that will allow them to be assessed in *in vivo* models. Lead optimisation is typically an iterative process consisting of making modifications to the hit compound structure to improve the activity and selectivity of the compound and comprehensively investigate SAR based on what structural information is known about the target and where the compound is binding. X-ray crystallography is an invaluable tool at this stage; crystallisation of the hit compound into the target protein would give insight into how to optimise favourable properties in lead compounds and improve deficiencies before being declared preclinical candidates.

1.9 Aim

The aims of this thesis were as follows. Firstly, to develop a biochemical assay for measuring SR activity that could be optimised to a medium-throughput screening format. Secondly, to conduct a fragment screen using this biochemical assay and, using a fragment-based drug discovery strategy, identify potential inhibitors of SR with desirable potencies. Thirdly, to confirm binding of any promising inhibitory hits using biophysical methods, principally X-ray crystallography. The overall aim of this thesis was to generate novel hit matter that could ultimately be used to drive medicinal chemistry efforts in the development of novel SR inhibitory compounds that have a greater potency than existing inhibitors, improved specificity, and a better safety profile over other glutamatergic modulators such as ketamine.

2 RESULTS I: PROTEIN PRODUCTION AND PURIFICATION

2.1 INTRODUCTION

The ability to express and purify a protein of interest is a key requirement for enabling drug discovery projects, which often comprise biochemical assay development, compound library screening, biophysical validation methods and crystallography. In many cases, including the current study, protein is produced in-house to circumvent the expense of repeatedly purchasing commercial samples. The large-scale protein generation described in this chapter consists of SR expression in a bacterial host, followed by two widely employed purification methods — immobilised-metal affinity chromatography (IMAC) and size-exclusion chromatography (SEC) — to achieve highly pure protein.

Bacterial expression systems such as *E. coli* are the predominant choice for large-scale protein production, due to their rapid growth and expression, ease of culture and gene modifications, low cost, and potential for mass production (Demain and Vaishnav, 2009). The use of bacterial expression systems in reports of recombinant SR expression has been almost unanimous since the method was first described (Foltyn *et al.*, 2005, Nagayoshi *et al.*, 2005, Strísovský *et al.*, 2005, Ohnishi *et al.*, 2008, Hoffman *et al.*, 2009b). The abundance of literature describing expression of recombinant SR in bacterial systems influenced the ultimate selection of an *E. coli* expression system for the experiments described in this chapter. Specifically, SR was expressed in *E. coli* BL21-CodonPlus (DE3)-RIL cells, which contain a chloramphenicol resistance gene and extra copies of the tRNA genes *argU* (AGA, AGG), *ileY* (AUA), and *leuW* (CUA). The extra codons mitigate the issue of codon bias, where translational problems may arise due to abundant rare codon clusters on the cloned heterologous gene, and low levels of corresponding tRNA codons in the bacterial expression host (Kane, 1995).

Selecting a suitable expression host is important because it is widely known that high-level expression of recombinant proteins in *E. coli* can lead to the formation of dense protein aggregates, commonly known as inclusion bodies (Singh *et al.*, 2015). It is possible to isolate inclusion bodies by low-speed centrifugation, but they will be heavily contaminated with *E. coli* cell wall and other membrane components (Palmer and Wingfield, 2004). It is therefore preferable to optimise the purification conditions such that the inclusion bodies are solubilised and refolded into native and biologically active protein. Previous reports suggest inclusion bodies can occur with SR; while one method of SR purification resulted in His-hSR being expressed in bacterial inclusion bodies, with 50% able to be refolded (Nagayoshi *et al.*, 2005), subsequent methods where hSR is expressed in BL21-CodonPlus (DE3)-RIL cells resulted in its purification directly from the soluble fraction (Dixon *et al.*, 2006, Hoffman *et al.*, 2009b).

IMAC is used to purify recombinant proteins containing a short affinity tag of six histidine residues, which is able to interact with a transition metal ion (Co^{2+} , Ni^{2+} , Cu^{2+} , Zn^{2+}) immobilised on a matrix (Bornhorst and Falke, 2000). The development of commercially available matrices such as nickel-nitrilotriacetic acid (Ni^{2+} -NTA) coupled to a solid support resin have improved protein yields and purity by preventing metal leaching from the matrix (Hochuli *et al.*, 1987). Histidine contains electron donor groups on its imidazole ring that readily form coordination bonds with the immobilised metal ions, making it possible to separate the target protein from solution that are subsequently eluted with high concentrations of competing imidazole (Porath, 1992). IMAC has the ability to yield 100-fold protein enrichments in a single purification step (Schmitt *et al.*, 1993), has been consistently used to successfully purify from numerous expression systems, including *E. coli* (Van Dyke *et al.*, 1992), and has proven efficacy at purifying proteins such as SR with polyhistidine tags. However, the potential for nonspecific binding to occur by histidine residues in contaminating proteins, or by nonspecific hydrophobic residues, means that achieving highly homogenous protein samples is only possible with additional purification techniques such as SEC.

SEC is used to separate proteins by their size as they pass through a column packed with SEC medium that consists of inert spherical particles containing pores. Superdex,

used here (M_w range 10–600 kDa), consists of dextran covalently attached to highly cross-linked agarose (GE Healthcare Life Sciences, 2017). Buffer pumped through the column is in equilibrium between the stationary phase (liquid in the pores) and mobile phase (liquid outside the particles). Small proteins and molecules diffuse more frequently into the bead pores so are delayed when passing through the column, causing the largest molecules to be eluted first and subsequent proteins to elute in order of decreasing size (Hong *et al.*, 2012). Detection by UV at 280 nm is predominantly used for SEC analyses, which gives a response for aromatic amino acids such as tryptophan (Hong *et al.*, 2012). As SEC separates proteins based on size, different oligomers and aggregated protein would be distinguishable by distinct peaks in the resulting UV chromatogram. For example, aggregates usually have a high molecular weight so are characterised by their elution in the void volume².

SEC purification has the additional benefit of improving and assessing protein homogeneity. For successful crystallisation, purified protein must be monodispersed — meaning that it exists in solution a single oligomeric species such as monomer or dimer — and it must be free of aggregates. To some extent, the monodispersity of the purified protein can be predicted from the shape of the SEC elution peaks; single symmetrical Gaussian peaks usually correspond to monodisperse protein, while wide asymmetrical peaks with shoulders or tailing edges signify polydisperse, unstable or unfolded protein (Ricker and Sandoval, 1996). In this case, the only way to confirm monodispersity is by dynamic light scattering (DLS). Knowing the dominant oligomeric species of SR also has particular relevance because the X-ray crystal structure of SR revealed it exists as a dimer (Smith *et al.*, 2010) and because previous studies have demonstrated SR is most active as a dimer (Wang and Barger, 2011).

The purification procedure outlined in this chapter was based on a pre-existing protocol and utilised a custom pET-24a plasmid containing the human SR gene linked to a polyhistidine tag. Both the protocol and plasmid were kindly provided by our

² The elution volume of molecules that are excluded from the gel filtration medium because they are larger than the largest pores in the matrix and pass straight through the packed bed.

collaborators at Evotec, who were the authors behind the seminal paper describing the first solved crystal structures of SR (Smith *et al.*, 2010). Their protocol gave several insights on the purification procedure with respect to optimising stability of SR, in particular the addition of pyridoxine to expression media for its ultimate formation into the PLP cofactor, the addition of SR cofactors (such as ATP and Mg^{2+}) to purification buffers, and the importance of maintaining protein solubility. The Evotec authors introduced cysteine-to-aspartate point mutations to two N-terminal surface-exposed residues, Cys2 and Cys6 (C2,6D), which were hypothesised to affect protein solubility (Smith *et al.*, 2010).

This chapter describes the protein expression and purification process utilised for large-scale generation of highly pure recombinant SR, from the initial steps of gene sequencing followed by transformation of *E. coli* with the pET-24a vector, to the expression of SR in liquid media, to the extraction and purification of SR from cell pellets. Also discussed are the optimisation steps taken to improve solubility of SR and thus increase the final yield, as well as the numerous quality control methods that were employed to confirm the presence and purity of SR, such as SDS-PAGE, western blot, and mass spectrometry. The methods described herein were imperative for characterising a protein and fostering confidence regarding its integrity, in order to form a solid foundation for medium-throughput screening, the primary purpose of this thesis.

2.2 MATERIALS

2.2.1 Plasmids and strains

Plasmids and strains	Supplier (product code)
BL21 CodonPlus (DE3)-RIL ultracompetent cells	Agilent (230245)
pET24a_SR M1 plasmid	Donated by Evotec (Abingdon, UK); contains two point mutations (C2,6D) and a (His ₆)-tag

2.2.2 Media¹

Media	Compounds	Supplier (product code)	Concentration
Preculture medium	LB broth	Sigma (L3022)	20 g/L
	Chloramphenicol	Sigma-Aldrich (C0378)	34 µg/mL
	Kanamycin	Sigma-Aldrich (60615)	50 µg/mL
Expression medium	LB broth	Sigma (L3022)	20 g/L
	Chloramphenicol	Sigma-Aldrich (C0378)	34 µg/mL
	Kanamycin	Sigma-Aldrich (60615)	50 µg/mL
	Pyridoxine ²	Sigma-Aldrich (P9755)	0.01%
LB agar	LB broth with agar	Sigma-Aldrich (L2897)	35 g/L
	Chloramphenicol	Sigma-Aldrich (C0378)	34 µg/mL
	Kanamycin	Sigma-Aldrich (60615)	50 µg/mL

¹ All media were autoclaved (121 °C, 15 min) for sterilisation. Antibiotics (and pyridoxine) were added once the temperature was below 55 °C.

² Pyridoxine pH adjusted to 7–8

2.2.3 Buffers and solutions³

Buffer	Compounds	Supplier (product code)	Concentration (mM)
Lysis buffer (Buffer A)	Tris-HCl pH 8	Sigma-Aldrich (154563)	50
	Sodium chloride	Sigma-Aldrich (S7653)	100
	Glycerol	Fisher Scientific (BP229)	10%
	Imidazole	Fisher Scientific (O3196)	10
	Magnesium chloride	Sigma-Aldrich (M8266)	2
	ATP*	Acros Organics (102800100)	1
	PLP	Sigma-Aldrich (P9255)	0.05
	Protease inhibitor tablet	Thermo Scientific (88265)	1 tablet per 50mL lysis buffer
	Benzonase Nuclease	Sigma-Aldrich (E1014)	5 units per mL
Equilibration and wash buffer (Buffer B)	Tris-HCl pH 8	Sigma-Aldrich (154563)	50
	Sodium chloride	Sigma-Aldrich (S7653)	100
	Imidazole	Fisher Scientific (O3196)	10
	Magnesium chloride	Sigma-Aldrich (M8266)	2
	ATP*	Acros Organics (102800100)	1
	PLP	Sigma-Aldrich (P9255)	0.05
Elution buffer (Buffer C)	Tris-HCl pH 8	Sigma-Aldrich (154563)	50
	Sodium chloride	Sigma-Aldrich (S7653)	100

	Imidazole	Fisher Scientific (O3196)	250
	Magnesium chloride	Sigma-Aldrich (M8266)	2
	ATP*	Acros Organics (102800100)	1
	PLP	Sigma-Aldrich (P9255)	0.05
SEC buffer (Buffer D)	Tris-HCl pH 8	Sigma-Aldrich (154563)	50
	Sodium chloride	Sigma-Aldrich (S7653)	100
	Glycerol	Fisher Scientific (BP229)	10%
	Magnesium chloride	Sigma-Aldrich (M8266)	1
	ATP*	Acros Organics (102800100)	1
	PLP	Sigma-Aldrich (P9255)	0.05
	DTT*	Fisher Scientific (BP172)	5
Towbin buffer	Tris base	Sigma-Aldrich (T1503)	25
	Glycine	Sigma-Aldrich (G8898)	192
	Methanol	VWR (85650.320)	20%
Tris-buffered saline (TBST)	Tris-HCl pH 7.5	Sigma-Aldrich (154563)	20
	Sodium chloride	Sigma-Aldrich (S7653)	150
	Tween-20	Sigma-Aldrich (P1379)	0.1%
ECL solution A ⁴	Tris-HCl pH 8.5	Sigma-Aldrich (154563)	100
	Luminol sodium salt	Sigma-Aldrich (A4683)	2.5
	Coumaric acid	VWR (ICNA0210257610)	0.4
ECL solution B ⁴	Tris-HCl pH 8.5	Sigma-Aldrich (154563)	100
	Hydrogen peroxide	VWR (L13235.AE)	0.02%

³ All buffers were filtered through a 0.22µm Whatman filter (GE Healthcare, 7184-004).

⁴ Kept in the dark at 4°C.

* Added on day of use.

2.2.4 Antibodies

Antibody	Supplier (product code)	Dilution used
Serine racemase rabbit polyclonal IgG (primary)	Santa Cruz Biotechnology	1:5000
Goat anti-rabbit IgG conjugated to HRP (secondary)	Santa Cruz Biotechnology	1:5000

2.2.5 Further materials, equipment and kits

Equipment	Supplier/manufacturer (product code)
Plasmid Miniprep Kit	Qiagen (12123)
IPTG	Generon (GEN-S-02122)
Phosphate-buffered saline	Life Technologies (18912-014)
Super Cobalt NTA affinity resin	Generon (Super-CoNTA100)
Ethanol	VWR (85651.320)
0.22µm Millex-GP filters	Merck Millipore (SLGPM33RS)
0.45µm Millex-HA filters	Merck Millipore (SLHAM33SS)
Vivaspin 15R centrifugal filters (10k MWCO)	Generon (VS15RH01)
NuPAGE® Novex® 4-12% Bis-Tris Protein Gels	Life technologies (NP0322BOX)
NuPAGE® MES SDS Running Buffer (20X)	Life technologies (NP0002)
NuPAGE® LDS sample buffer	Life technologies (NP0007)

Precision Plus Protein Dual Color Standards	Bio-Rad (1610374)
Ovalbumin SEC marker	Generon (615-0041)
BugBuster 10X	Novagen (70921)
Quick Coomassie Stain	Generon (GEN-QC-STAIN-IL)
PVDF Transfer membranes	Fisher Scientific (10384511)
CL-XPosure Film	Thermo Scientific (10465145)
In-gel Tryptic Digestion Kit	Thermo Fisher Scientific (89871)
HiLoad 26/600 Superdex 75 pg column	GE Healthcare (28989334)
Superdex 75 10/300 GL column	GE Healthcare (29148721)
Vibra cell Sonicator	Sonics (VCX500)
NanoDrop 2000	Thermo Scientific (N/A)
Avanti J-S26S XP centrifuge	Beckman Coulter (393124)
Allegra X-30R centrifuge	Beckman Coulter (A99470)
JLA 9.1000 rotor	Beckman Coulter (366754)
JA 25.50 rotor	Beckman Coulter (363055)
SX4400 rotor	Beckman Coulter (B01425)
C-DiGit® blot scanner	LI-COR (3600-00)

2.3 METHODS

2.3.1 Molecular biology

The pET-24a plasmid containing the SR gene also contains a T7 promoter and a gene encoding kanamycin resistance (for plasmid map, see Appendix). The SR gene encodes two cysteine-to-aspartate point mutations (C2,6D) in the protein sequence to improve protein solubility during the purification process (Smith *et al.*, 2010). The final protein is 340 amino acids in length, plus a 6-amino acid C-terminal polyhistidine (His₆)-tag for purification purposes. Plasmid sequencing was performed by Eurofins Scientific UK. Pairwise sequence alignments were carried out using EMBOSS Needle online tool (http://www.ebi.ac.uk/Tools/psa/emboss_needle/nucleotide.html) and alignment files were visualised using BoxShade.

The plasmid was transformed with *E. coli* BL21-CodonPlus (DE3)-RIL competent cells as part of a large-scale protein production. The SR-expressing cells obtained following the growth procedure were stored at -80 °C.

2.3.2 Transformation of competent cells

A 100 μL aliquot of competent cells was thawed on ice for 10 min, and 2 μL of β -mercaptoethanol (diluted 1:10 in dH_2O from kit stock solution) was added. The cells were incubated on ice for 10 min, after which 1 μL of the expression plasmid DNA (10 $\text{ng}/\mu\text{L}$) was added and the cells were incubated on ice for a further 30 min. The transformation reaction was then subjected to a heat pulse of 42 $^\circ\text{C}$ in a water bath for 20 s and incubated on ice for 2 min immediately after. Following the heat/cold shock, 0.9 mL of preheated (42 $^\circ\text{C}$) SOC medium³ was added and the reaction was incubated at 37 $^\circ\text{C}$ for 1 h with shaking at 220 rpm. Finally, using a sterile spreader, 150–200 mL of the transformed cells were spread onto LB plates containing chloramphenicol and kanamycin and incubated overnight at 37 $^\circ\text{C}$.

2.3.3 Preparation of glycerol stocks

A freshly transformed colony was picked with a sterile inoculation loop and placed into 10 mL LB medium (with antibiotics) and incubated at 37 $^\circ\text{C}$ overnight (16–18 h) with constant shaking at 200 rpm. The next day, 1 mL of the cell suspension was combined with 500 μL 50% glycerol (v/v) and each aliquot was stored in cryo-tubes at -80 $^\circ\text{C}$.

2.3.4 Expression of recombinant human SR

To prepare the preculture, a transformed colony was picked and inoculated into 200 mL LB supplemented with chloramphenicol (34 $\mu\text{g}/\text{mL}$) and kanamycin (50 $\mu\text{g}/\text{mL}$), which was then incubated at 37 $^\circ\text{C}$ overnight with constant shaking at 200 rpm. Cell density measurements were performed using the optical density at a wavelength of 600 nm (OD_{600}) to determine the number of cells present in the bacterial suspension. The OD_{600} of the preculture was measured in the morning and typically reached a

³ SOC (Super Optimal broth with Catabolite repression) is a nutrient-rich bacterial growth medium with added glucose. It is typically used for microbiological cultures and results in very high transformation efficiencies of plasmids.

value of approximately 2. If the OD₆₀₀ was not significantly below this value, 10 mL of the preculture was diluted into 1 L LB medium (1% v/v) in eight 2 L flasks, supplemented with the antibiotics and 0.01% pyridoxine. Pyridoxine is the precursor of pyridoxal phosphate (PLP) and is used by the expressing cells to produce PLP, the cofactor essential for the racemisation and β -elimination activity of SR.

The main cultures were incubated with shaking at 37 °C, 200 rpm, for approximately 3–4 h. The OD₆₀₀ was checked periodically until it reached 0.6–0.8, at which point the flasks were kept at 4 °C to stall growth until the end of the day. The cultures were then induced with 0.5 mM IPTG and incubated for a further 16 h overnight at 25 °C, 200 rpm. The cells were harvested by centrifugation at 8 500 $\times g$, 4 °C for 25 min (Avanti J-S26S XP centrifuge, JLA 9.1000 rotor, Beckman-Coulter) and the cell pellets were stored at -80 °C.

2.3.5 Protein purification

The isolation of SR from the cells was performed using a two-step purification process: immobilised metal ion affinity chromatography (IMAC) and size-exclusion chromatography (SEC), which are described in the following sections. Purification buffers are detailed in section 2.2.3, *Buffers and solutions*.

Cell lysis. The frozen cell pellets were thawed on ice and resuspended in ~150 mL cold lysis Buffer A. Cell lysis was performed in batches of 50 mL using a sonicator (Vibra cell, Sonics) at 40% amplitude, 30 s pulse on and 30 s pulse off for 2.5 min (total 5 min). Following this, cell debris was pelleted by centrifugation at 40 000 $\times g$, 4 °C, for 1 h (Avanti J-26 XP centrifuge, JA 25.50 rotor, Beckman-Coulter). The supernatant was collected immediately after and kept on ice.

IMAC purification. The resin used for IMAC purification was Super Cobalt NTA Affinity Resin (Generson). The histidines of the protein (His)₆-tag contain an imidazole side chain with an aromatic ring that binds to Co²⁺ ions immobilised with a linker to the

column matrix. Each time buffer was applied to the column, the resin was allowed to settle for 5 min. An empty column used for IMAC purification and was prepared by first rinsing with water to remove air bubbles, after which 8 mL resin suspension (in 20% ethanol) was added to the column. The ethanol was discarded in the flow-through and the column was washed with 10 CV (column volumes, i.e. resin volume used) water. The column was then washed with 10 CV Buffer B to equilibrate the resin. The supernatant from the *cell lysis* step was filtered (0.45 mm) and added to the column, which was then sealed and incubated at 4 °C with gentle rocking for 90–120 min for batch-binding of the protein to the resin.

After the resin had settled, the flow-through was collected, which should theoretically contain negligible levels of SR. The column was washed twice with 50 mL Buffer B and both fractions were collected. The protein was eluted with Buffer C, which has a high imidazole concentration (250 mM) to displace the SR-(His)₆ from the beads. The column was washed five times with 20 mL Buffer C with each fraction collected and kept on ice. The elution fractions were then analysed by SDS-PAGE and the fractions containing SR were pooled and concentrated to 10 mL using Vivaspin 15R centrifugal filter units with 10 kDa molecular weight cut-off (4000 × *g*, 4 °C, Allegra X-30R, SX4400 rotor).

SEC purification. A HiLoad 26/600 Superdex 75 prep grade column (GE Healthcare) connected to an ÄKTA-purifier fast protein liquid chromatography (FPLC) system (GE Healthcare) was used throughout the SEC purification process. One CV of the SEC column is equal to 320 mL. The column was first washed with 1 CV phosphate-buffered saline (PBS) then equilibrated with 2 CV Buffer D. The IMAC concentrate was then filtered (0.22 mm)⁴ and loaded onto the column using a 10 mL sample loop, where the eluate was collected in 2 mL fractions for the duration of 1 CV. The presence of protein was detected by UV at a wavelength of 280 nm, giving a readout with peaks signifying eluted proteins. The position of the peaks informed which fractions were collected and

⁴ Filtering with this pore size was essential to avoid particulate matter contaminating the SEC column. A filter with a bigger pore size of 0.45µM was used to filter the lysate supernatant due to the viscosity of the solution.

analysed by SDS-PAGE, and those found to be enriched with pure SR were pooled and concentrated until a desired concentration was reached ($4000 \times g$, 4 °C, Allegra X-30R, SX4400 rotor). Concentrated SR was aliquoted, flash-frozen in liquid nitrogen and stored at -80 °C. Analytical SEC was performed to determine the oligomeric form of the eluted SR; for this, ovalbumin (46 kDa) was used as a marker, and was loaded onto a Superdex 75 10/300 GL column (GE Healthcare) in conjunction with SR.

2.3.6 Determination of protein concentration

Protein concentration was measured in 1 μ L of sample using a NanoDrop 2000 UV-Vis spectrophotometer (ThermoFisher Scientific). The molecular weight (M_w) and extinction coefficient (ϵ) were taken from the ProtParam tool on the ExPASy online proteomics resource (<http://expasy.org/protparam>) and were included in the NanoDrop measurement. $M_w = 37.4$ kDa, $\epsilon = 29910 \text{ mol}^{-1} \text{ cm}^{-1}$.

2.3.7 Sodium dodecyl sulphate polyacrylamide gel electrophoresis

Fractions were assessed for the presence and purity of SR by SDS-PAGE, based on a process first described by Laemmli (Laemmli, 1970). Samples were denatured with NuPage® LDS (Lithium Dodecyl Sulfate) 4X sample buffer (Life Technologies) and heated at 95 °C for 3–5 min. Non-aqueous samples (such as whole-cell pellets) were first lysed with 1X BugBuster (Novagen) and incubated at room temperature (RT) for 30 min before being diluted with PBS and denatured using the same method. Sample volumes of 10–20 μ L were loaded in the wells with Precision Plus Protein™ Dual Color Standards (Bio-Rad). Electrophoresis was performed at a constant 200 V in 12- or 17-well NuPage® Novex® 4-12% BisTris protein gels, (Life Technologies) in conjunction with 20X MES SDS running buffer (Life Technologies) diluted to 1X. The bands were visualised using Quick Coomassie Stain (Generon) for between 15 min to 2 h and gels were destained overnight in distilled water.

2.3.8 Western blot

Purified SR was first analysed by SDS-PAGE at concentrations of 10, 50, and 100 ng per well, in conjunction with a Precision Plus Protein™ Dual Color stained protein ladder (Bio-Rad). PVDF membranes were cut to the same size as the gels and soaked in methanol for 5–10 min. The cassette was prepared by soaking it with the two mesh layers and two filter papers in prechilled Towbin buffer. Once the cassette was assembled, protein transfer onto the membrane was achieved with a constant voltage of 100 V for 30 min. To prevent non-specific interactions between the membrane and the antibodies, the membranes were incubated in TBST buffer + 5% non-fat dry milk and rocked for 2 h. For the primary antibody incubation (SR rabbit polyclonal IgG), the membrane was put in a 15 mL tube with 5 mL TBST + 5% milk and diluted antibody (1:5000) and incubated at 4 °C overnight with rocking. The membrane was washed for 30 min three times in TBST with rocking. The secondary antibody incubation (goat anti-rabbit IgG conjugated to HRP) was carried out as the primary incubation (1:5000) but for 1 h, and the membrane washed as before. The membrane was blot dried and transferred to Clingfilm where ECL reagent was pipetted on top (1:1 of A and B) and was sealed with Clingfilm after 2 min. The membrane was exposed to X-ray film in a cassette inside a darkroom for 3 min and the image developed using a C-DiGit® blot scanner (LI-COR).

2.3.9 Mass spectrometry

SR was analysed by SDS-PAGE and the bands were visualised with Quick Coomassie Stain (Generon). Bands were excised and were prepared for mass spectrometry with a trypsin digestion (In-Gel Tryptic Digestion Kit, ThermoFisher Scientific) according to the manufacturer protocol, which is briefly as follows: the destained band was reduced and alkylated to maximise the sequence coverage, then shrunk with acetonitrile. Activated trypsin was applied to the band and incubated for 15 min at RT. The Digestion Buffer provided by the kit containing 25 mM ammonium bicarbonate was added to the tube with the band and incubated overnight with shaking at 30 °C. The

trypsin was inactivated with the addition of trifluoroacetic acid and the samples were then ready for further analysis. Mass spectrometry was performed on an LTQ Orbitrap XL machine.

2.4 RESULTS

2.4.1 Plasmid sequencing confirms presence of SR gene

As a routine step in the interest of data integrity, the acquired pET-24a gene construct containing the SR (C2,6D) gene was sequenced to confirm the presence of the SR gene. The plasmid sequence was firstly subject to a BLAST nucleotide query and the results unanimously revealed that the plasmid contained a nucleotide sequence for *Homo sapiens* serine racemase, with a sequence homology of 99–100% depending on the transcript variant.

The plasmid sequence and the first transcript variant (accession number XM_011523974.2) were then directly compared via a pairwise sequence alignment using the EMBOSS Needle online tool. The sequence alignment (Fig. 2.1) showed an almost identical (99.5%) sequence identity between the plasmid sequence and the most closely matched transcript variant, with the exception of four nucleotide point mutations, TGT to GAT and TGC to GAC. These codon changes correspond to two cysteine-to-aspartate substitutions (C2D, C6D), which are unique to this gene construct. Based on this preliminary analysis, the subsequent expression and purification steps were carried out with confidence.

2.4.2 IMAC purification isolates SR from lysate

Following cell lysis and centrifugation, SR was purified from the soluble fraction. The solubilised SR was applied to a Co²⁺-NTA resin so the polyhistidine tag could bind to the beads. The column was washed twice with Buffer B, which contained a small amount (10 mM) of imidazole to remove non-binding proteins by eluting contaminants that are weakly bound to the column through non-specific binding or integral histidine residues. SR was then eluted with excess imidazole (250 mM) and collected in five fractions.

hSR_M1_pET-24a	1	ATGGATGCTCAGTATGACATCTCCTTTGCTGATGTTGAAAAAGCTCATATCAACATTCGA
hSR_XM_01152397	1	ATGGATGCTCAGTATGACATCTCCTTTGCTGATGTTGAAAAAGCTCATATCAACATTCGA
hSR_M1_pET-24a	61	GATTCTATCCACCTCACACCAGTGCTAACAAGCTCCATTTTGAATCAACTAACAGGGCGC
hSR_XM_01152397	61	GATTCTATCCACCTCACACCAGTGCTAACAAGCTCCATTTTGAATCAACTAACAGGGCGC
hSR_M1_pET-24a	121	AATCTTTTCTTCAAATGTGAACTCTTCCAGAAAACAGGATCTTTTAAGATTGCTGGTGCT
hSR_XM_01152397	121	AATCTTTTCTTCAAATGTGAACTCTTCCAGAAAACAGGATCTTTTAAGATTGCTGGTGCT
hSR_M1_pET-24a	181	CTCAATGCCGTCAGAAGCTTGGTTCCTGATGCTTTAGAAAGGAAGCCGAAAGCTGTTGTT
hSR_XM_01152397	181	CTCAATGCCGTCAGAAGCTTGGTTCCTGATGCTTTAGAAAGGAAGCCGAAAGCTGTTGTT
hSR_M1_pET-24a	241	ACTCACAGCAGTGGAAACCATGGCCAGGCTCTCACCTATGCTGCCAAATTGGAAGGAATT
hSR_XM_01152397	241	ACTCACAGCAGTGGAAACCATGGCCAGGCTCTCACCTATGCTGCCAAATTGGAAGGAATT
hSR_M1_pET-24a	301	CCTGCTTATATTGTGGTGCCCCAGACAGCTCCAGACTGTAAAAAACTTGCAATACAAGCC
hSR_XM_01152397	301	CCTGCTTATATTGTGGTGCCCCAGACAGCTCCAGACTGTAAAAAACTTGCAATACAAGCC
hSR_M1_pET-24a	361	TACGGAGCGTCAATTGTATACTGTGAACCTAGTGATGAGTCCAGAGAAAATGTTGCAAAA
hSR_XM_01152397	361	TACGGAGCGTCAATTGTATACTGTGAACCTAGTGATGAGTCCAGAGAAAATGTTGCAAAA
hSR_M1_pET-24a	421	AGAGTTACAGAAGAAACAGAAGGCATCATGGTACATCCCAACCAGGAGCCTGCAGTGATA
hSR_XM_01152397	421	AGAGTTACAGAAGAAACAGAAGGCATCATGGTACATCCCAACCAGGAGCCTGCAGTGATA
hSR_M1_pET-24a	481	GCTGGACAAGGGACAATTGCCCTGGAAGTGCTGAACCAGGTTCCCTTGGTGGATGCACTG
hSR_XM_01152397	481	GCTGGACAAGGGACAATTGCCCTGGAAGTGCTGAACCAGGTTCCCTTGGTGGATGCACTG
hSR_M1_pET-24a	541	GTGGTACCTGTAGGTGGAGGAGGAATGCTTGCTGGAATAGCAATTACAGTTAAGGCTCTG
hSR_XM_01152397	541	GTGGTACCTGTAGGTGGAGGAGGAATGCTTGCTGGAATAGCAATTACAGTTAAGGCTCTG
hSR_M1_pET-24a	601	AAACCTAGTGTGAAGGTATATGCTGCTGAACCCCTCAAATGCAGATGACTGCTACCAGTCC
hSR_XM_01152397	601	AAACCTAGTGTGAAGGTATATGCTGCTGAACCCCTCAAATGCAGATGACTGCTACCAGTCC
hSR_M1_pET-24a	661	AAGCTGAAGGGGAAACTGATGCCCAATCTTTATCCTCCAGAAACCATAGCAGATGGTGTC
hSR_XM_01152397	661	AAGCTGAAGGGGAAACTGATGCCCAATCTTTATCCTCCAGAAACCATAGCAGATGGTGTC
hSR_M1_pET-24a	721	AAATCCAGCATTGGCTTGAACACCTGGCCTATTATCAGGGACCTTGTGGATGATATCTTC
hSR_XM_01152397	721	AAATCCAGCATTGGCTTGAACACCTGGCCTATTATCAGGGACCTTGTGGATGATATCTTC
hSR_M1_pET-24a	781	ACTGTCACAGAGGATGAAATTAAGTGTGCAACCCAGCTGGTGTGGAGAGGATGAAACTA
hSR_XM_01152397	781	ACTGTCACAGAGGATGAAATTAAGTGTGCAACCCAGCTGGTGTGGAGAGGATGAAACTA
hSR_M1_pET-24a	841	CTCATTGAACCTACAGCTGGTGTGGAGTGGCTGCTGTGCTGTCTCAACATTTTCAAAC
hSR_XM_01152397	841	CTCATTGAACCTACAGCTGGTGTGGAGTGGCTGCTGTGCTGTCTCAACATTTTCAAAC
hSR_M1_pET-24a	901	GTTTCCCCAGAAGTAAAGAACATTGTATTGTGCTCAGTGGTGGAATGTAAA
hSR_XM_01152397	901	GTTTCCCCAGAAGTAAAGAACATTGTATTGTGCTCAGTGGTGGAATGTAAA

Figure 2.1. Pairwise sequence alignment of hSR M1 CDS and its closest database match.

The pET-24a plasmid was sequenced and a BLAST nucleotide search found closest identity matches from the NCBI database. The plasmid sequence was aligned with a hSR transcript variant (XM_011523974.2) to give a 99% sequence match, aside from the GAT-TGT and GAC-TGC mutations corresponding to two cysteine to aspartate point mutations.

Analysis of all the purification fractions was performed by SDS-PAGE and the gel is presented in Fig. 2.2. Bands at approximately 37 kDa, the molecular weight of SR, appear in almost all of the lanes. It was to be expected that small amounts of SR would remain in the whole-cell insoluble fraction and the unbound fraction because it is difficult to solubilise all available protein once removed from within the cellular environment, and contaminating proteins can compete with the target protein during incubation with the IMAC resin to prevent binding. Most impurities were removed in the first wash fraction, and SR was eluted primarily in the first three elution fractions. The dense bands at approximately 37 kDa in the elution fractions indicate the presence of concentrated SR, so those most enriched (usually E1, E2 and E3) were pooled and concentrated to 10 mL prior to loading onto the SEC column. The faint bands at approximately 74 kDa correlate with the molecular weight of dimeric SR; it is not unusual for trace amounts of oligomeric or aggregated protein species to remain after SDS-PAGE, even under denaturing conditions. Other bands that appear in the elution fractions could be contaminating proteins that survived the relatively crude process of IMAC purification, or degraded SR.

2.4.3 Optimisation of SEC purification

The protein purity achieved with IMAC purification would be suitable for assay development, but the much greater degree of purity (>95%) required for crystallography is only achieved by additional SEC purification. Ideally a singular, isolated peak of pure protein would appear in the UV trace, but often they may coincide with other peaks; these may reflect aggregated protein, or a different oligomeric form of the target protein. The aggregation peaks are discernable by their presence in the void volume (the first 30% of the column volume), where they elute first due to their high molecular weight.

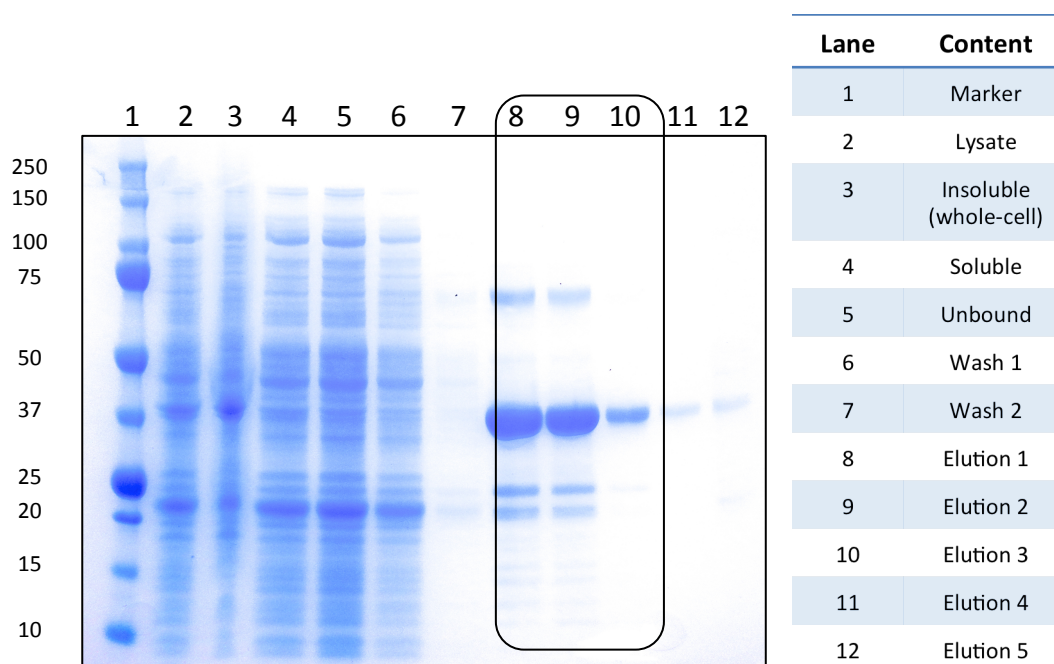


Figure 2.2. SDS-PAGE of fractions resulting from immobilised-metal affinity chromatography (IMAC) purification of SR.

SR was released from lysed *E. coli* BL21 CodonPlus (DE3)-RIL cells (2), and the whole-cell (3) and soluble cytosolic (4) fractions were separated by centrifugation. After batch-binding with Co^{2+} -resin, the soluble fraction was removed from the IMAC column and checked for trace amounts of unbound SR (5). The column was washed twice with SR equilibration buffer, giving two 75 mL fractions (6 & 7). SR was finally eluted with a high-imidazole buffer, giving five 18 mL fractions (8, 9, 10, 11 & 12). The lysate, soluble, and insoluble fractions were first diluted with PBS prior to analysis. Highly concentrated bands at approximately 37 kDa indicate the presence of SR; the fractions within the framed region were pooled for size-exclusion chromatography.

In initial experiments, a large aggregation peak appeared in the UV trace during SEC purification (Fig. 2.3A), almost equal-sized to the purified SR peak and so representative of a significant amount of protein that had been lost to aggregate. Samples of the fractions of both these peaks were analysed by SDS-PAGE, and from the resulting gel in Fig. 2.3B it can be seen that there was an obvious difference in the protein quality between two peaks. The second (purified SR) peak yields much cleaner and more distinct bands in the region of the Mw of SR (~37 kDa) compared to the first (aggregate) peak, the bands of which are not as discernable, possibly due to incomplete denaturation of all aggregated SR or simultaneous aggregation with other contaminating proteins.

The fractions of both peaks were pooled separately and concentrated to 11.6 mg/mL (peak 1) and 19.1 mg/mL (peak 2). The activity of the two SR samples was then directly compared in the coupled biochemical assay (refer to Fig. 3.1). A 1 h time course was performed with both and the results are shown in Fig. 2.4. The difference between the activities of the two SR samples was immediately obvious from the data, with soluble SR demonstrating an approximately fivefold greater activity than the aggregated protein sample. This disparity suggested that a significantly smaller proportion of the presumed aggregate was active, aligning with the species of SR (aggregate or soluble) that was expected in each sample.

It was clear from the SEC analysis and biochemical assay data that alterations needed to be made to the purification conditions to improve SR solubility, thereby reducing aggregation and maximising the overall yield of purified SR. Glycerol is well-known to prevent aggregation during protein purification, possibly by inhibiting protein unfolding and stabilising aggregation-prone intermediates by electrostatic interactions (Vagenende *et al.*, 2009). Therefore, the purification was repeated with 10% glycerol included in the lysis and SEC buffers, and a drastic improvement was observed in the relative proportions of aggregate to soluble SR. The UV trace in Fig. 2.5A shows a large, singular SR peak that eluted at the same volume as the soluble SR peak in Fig. 2.3A (≈ 138 mL) accompanied by a small shoulder peak in the void volume (115 mL).

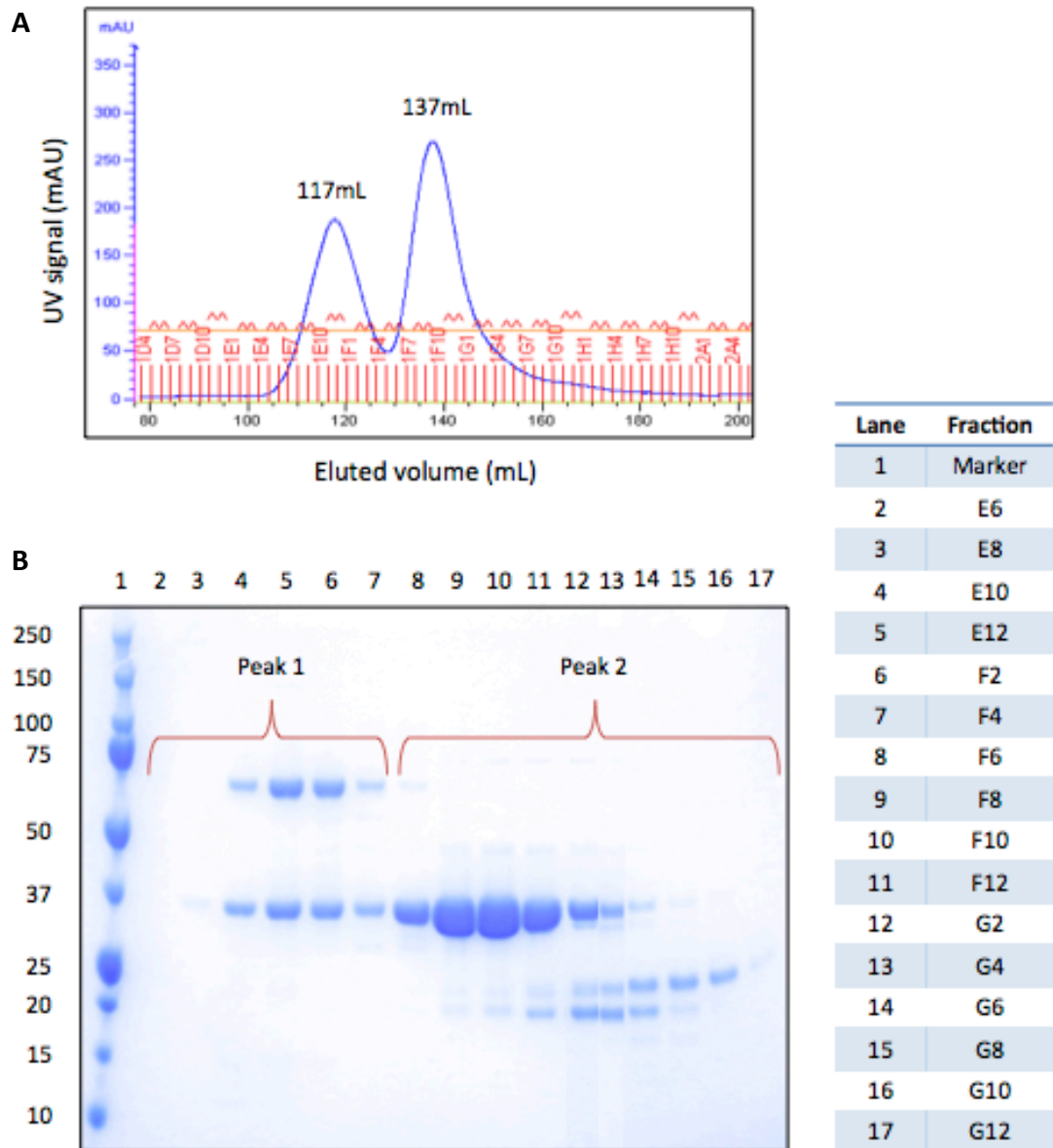


Figure 2.3. Initial SR SEC purifications resulted in high levels of protein aggregation.

(A) UV chromatogram detected at 280 nm of the fractions eluted from the SEC column; each 2 mL fraction was eluted into a 96-well plate and the well positions are shown the red lettering above the x-axis. Peak 1 (aggregate) eluted at 117 mL and Peak 2 (soluble protein) eluted at 137 mL. **(B)** The fractions corresponding to the each peak were analysed by denaturing SDS-PAGE and bands at approx. 37 kDa can be attributed to SR. Highly concentrated SR was present in the Peak 2 fractions while low quality SR was present in the Peak 1 fractions. The fractions of each peak were pooled separately and concentrated prior to storage at -80 °C.

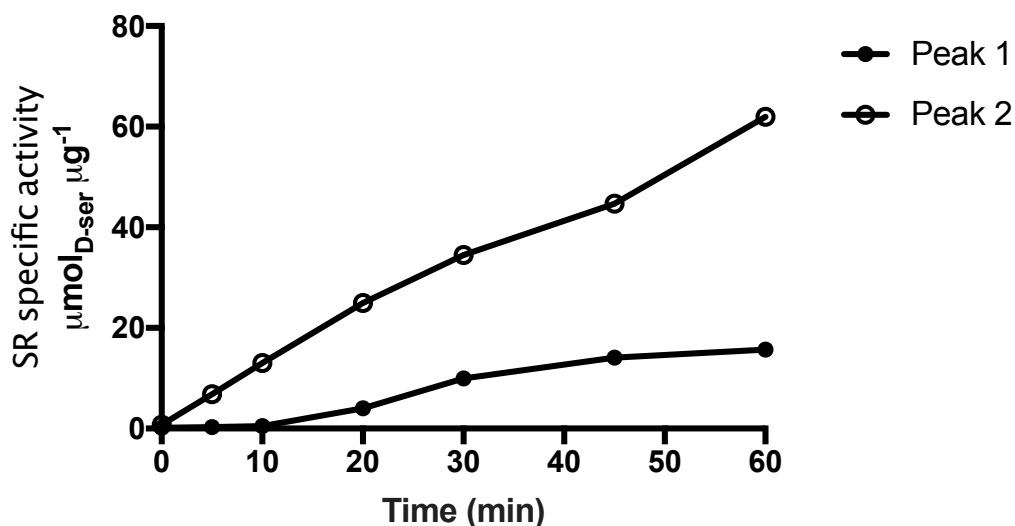


Figure 2.4. Activity comparison of aggregate (Peak 1) and soluble (Peak 2) SR.

The two species were separated following SEC purification and assessed in a 1 h time course in the SR coupled biochemical assay. The soluble SR isolated from Peak 2 had an approximate fivefold greater level of activity than the SR isolated from Peak 1, suggesting there is significantly less correctly folded and biologically active SR in the aggregate sample. The assay was performed with 2.5 μM SR and 2 mM L-serine substrate, and the reaction was stopped with 2 mM EDTA. The D-serine produced in the assay was catabolised by 1 U/mL DAO and the resulting H₂O₂ was quantified by a chemiluminescence reaction with 0.5 U/mL HRP and 50 μM luminol. The luminescence signal was read using a BMG PHERAstar. Data points are the mean of three replicates.

Moreover, the SDS-PAGE analysis of the fractions corresponding to the soluble peak (Fig. 2.5B) shows bands of highly concentrated, ultra pure SR that correlate with the increase in solubilised SR between the two SEC purifications, as indicated by the increase in UV signal (270 mAU to 430 mAU). SR consistently purified in this manner in successive experiments, and from each only the purest fractions of the soluble peak were isolated and concentrated for further use.

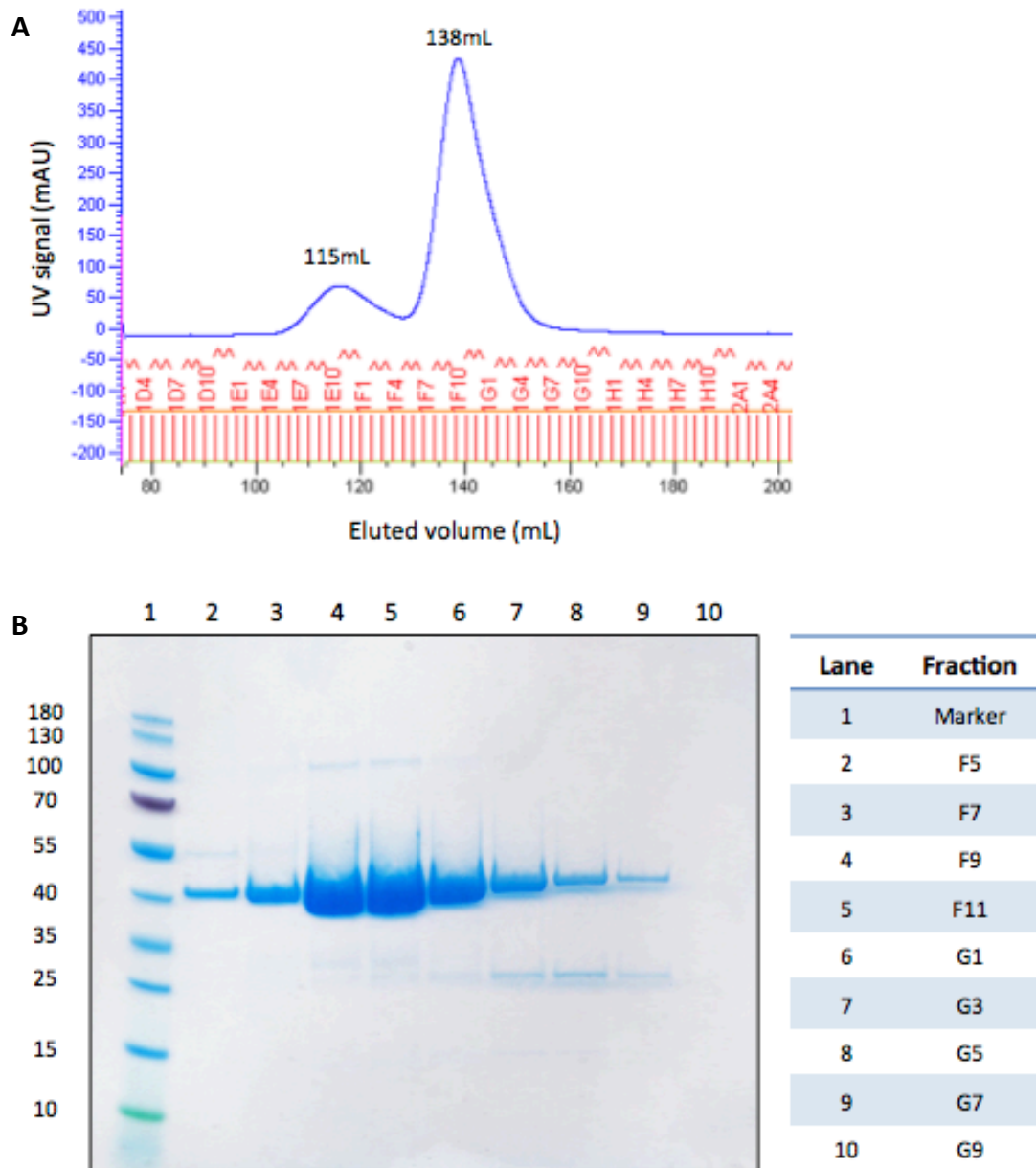


Figure 2.5. Addition of glycerol reduces SR aggregation during SEC purification.

(A) UV chromatogram detected at 280 nm of the fractions eluted from the SEC column. Peak 1 (aggregate) eluted at 115 mL and Peak 2 (soluble protein) eluted at 138 mL. (B) The fractions corresponding to the main peak were analysed by SDS-PAGE. The purest fractions containing SR were pooled and concentrated prior to storage at -80 °C.

2.4.4 Purified SR characterised by analytical methods

Although stringent procedural standards were maintained throughout this purification, there is always a possibility that contaminating proteins could be isolated as well as or in lieu of SR. The following techniques were applied to purified SR in the interest of quality control and characterisation.

2.4.5 Molecular weight markers in SEC column

The oligomeric species of a protein can be estimated by running markers of a specific molecular weight through a SEC column with a small amount of purified protein and observing the order in which they elute. It is a relevant application here as the SDS-PAGE experiments (Fig. 2.2, 2.3 and 2.5) would have denatured dimeric SR. A 46 kDa ovalbumin marker was loaded onto the column with purified SR, and Fig. 2.6 shows the resulting UV chromatogram of the proteins detected. The SR peak eluted before the ovalbumin marker, and as larger proteins elute from the SEC column first it can be reasonably concluded that the sample of purified SR had a greater molecular weight than 46 kDa. This suggests the SR peak corresponded to its dimeric form (74 kDa), although this is a qualitative assessment and not definitive.

2.4.6 SR visualised by western blot

Western blot utilises antibodies that are specific to a unique epitope on the target protein in order to detect specific proteins in a sample. In this case, the epitope of the SR antibody corresponded to amino acids 191–340 mapping at the C-terminus of the protein. Three concentrations of SR (10 ng, 50 ng, and 100 ng) were run on an electrophoresis gel and analysed by chemiluminescent western blot (Fig. 2.7), revealing two bands in the regions expected at approximately 37 kDa and 74 kDa, which correspond to the molecular weight of the SR monomer and dimer. Small bands of protein degradation (20–25 kDa) correspond to those seen in Fig. 2.2 and 2.3.

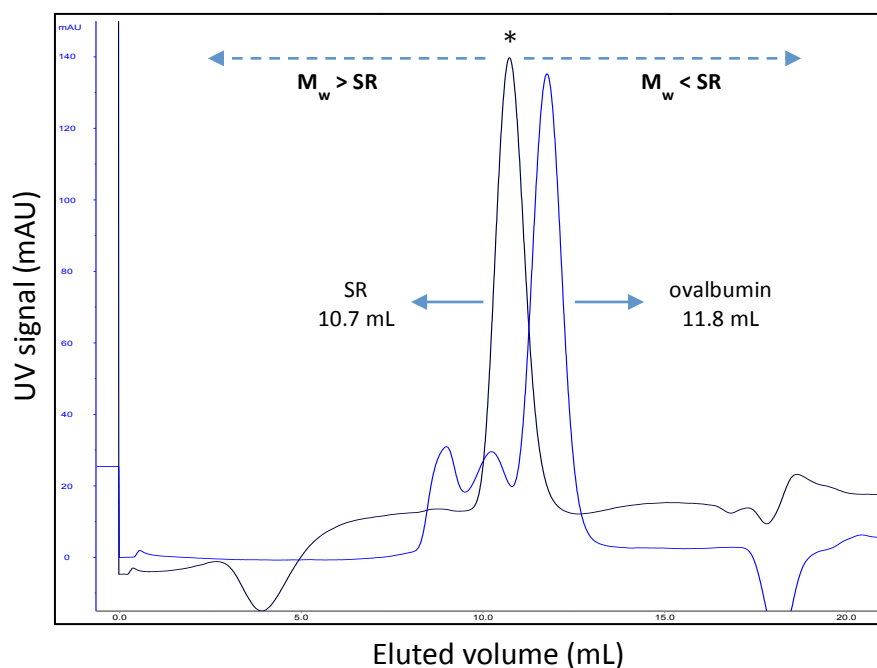


Figure 2.6. Analytical SEC with an ovalbumin marker to estimate molecular weight of purified SR.

Larger proteins elute from the SEC column first, so the order in which SR ($M_w = 37.4$ kDa monomer, 74.8 kDa dimer) and ovalbumin ($M_w = 46$ kDa) elute could be used to estimate the oligomeric species of SR. Both SR (black trace) and ovalbumin (blue trace) were loaded onto a Superdex 75 10/300 GL column and eluted at 10.7 mL and 11.8 mL, respectively. SR eluted from the column first, suggesting its molecular weight was greater than that of ovalbumin. Based on this observation, it was a reasonable supposition that purified SR was a dimer, because only the SR dimer, and not monomer, has a greater molecular weight than 46 kDa. However, this is only a qualitative estimate and should be supported by other methods.

Although one would expect all the protein to be denatured into the monomeric form from the effects of SDS and boiling on the samples, it is possible some dimer would still be present due to incomplete denaturation, protein aggregation at high temperatures, and the persistence of hydrophobic interactions between molecules in a dimer even as the temperature increases (Watt *et al.*, 2013).

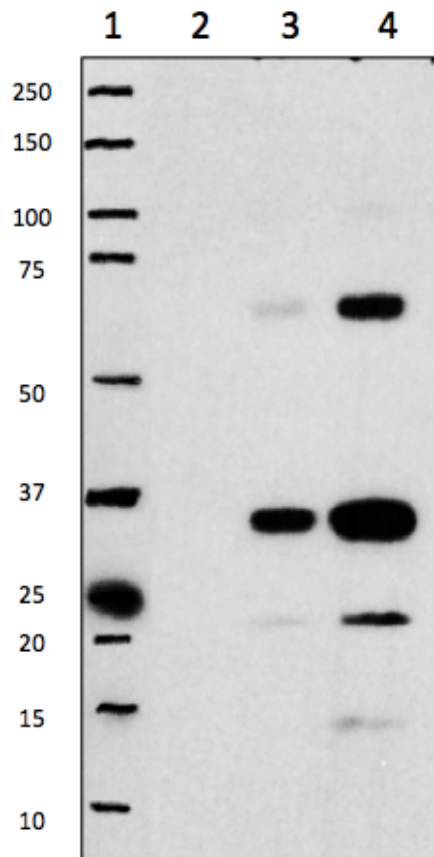


Figure 2.7. Human SR verified in the purified sample by chemiluminescence western blot.

SR was purified in-house and three concentrations of SR were used to perform a western blot: 10 ng (lane 2), 50 ng (lane 3) and 100 ng (lane 4) per well. Lane 1 contains the M_w marker (Precision Plus Protein Dual Color, Bio-Rad). The western blot was performed using anti-SR rabbit polyclonal primary antibody, and goat anti-rabbit secondary antibody conjugated to HRP (both from Santa Cruz Biotechnology). Bands in the region of 37 kDa and 75 kDa correspond to SR monomer (37.4 kDa) and dimer (74.7 kDa). Small low molecular weight bands in the 20–25 kDa region can be attributed to protein degradation.

2.4.7 SR sequence confirmed by mass spectrometry

Mass spectrometry represents an additional way of identifying unknown compounds in a sample, as well as the relative abundance of those compounds, so gives an indication of sample purity as well. Both the monomer and dimer bands were excised from an SDS-PAGE gel and analysed by mass spectrometry. The results showed that the samples consisted almost exclusively of human SR, as determined by the sequence homology between several unique peptides and the SR primary sequence. The unique peptides identified by mass spectrometry of purified SR covered 50% of the SR primary sequence, which gives confidence the purified protein was indeed SR.

A

```

1  MCAQYCISFA DVEKAHINIR DSIHLTPVLT SSILNQLTGR NLFFKCELFQ
51  KTGSFKIRGA LNAVRS LVPD ALERKPKAVV THSSGNHGQA LTYAAKLEGI
101 PAYIVVPQTA PDCKKLAIQA YGASIVYCEP SDESRENVAK RVTEETEGIM
151 VHPNQEPAVI AGQGTIALEV LNQVPLVDAL VVPVGGGGML AGIAITVKAL
201 KPSVKVYAAE PSNADDCYQS KLGKLPNL YPPETIADGV KSSIGLNTWP
251 IIRDLVDDIF TVTEDEIKCA TQLVWERMKL LIEPTAGGVV AAVLSQHFQT
301 VSPEVKNICI VLSGGNVDLT SSITWVKQAE RPASYQSVSV

```

B

Peptide region	M _w (expt)	M _w (calc)	Sequence
15 - 20	722.4	722.4	K.AHINIR.D
41 - 45	667.4	667.4	R.NLFFK.C
46 - 51	823.4	823.4	K.CELFQK.T
59 - 65	699.4	699.4	R.GALNAVR.S
66 - 74	998.5	998.5	R.SLVPDALER.K
78 - 96	1911.0	1911.0	K.AVVTHSSGNHGQALTYAAK.L
97 - 114	1970.0	1970.0	K.LEGIPAYIVVPQTAPDCK.K
116 - 135	2228.0	2228.0	K.LAIQAYGASIVYCEPSDES.R
116 - 140	2769.3	2769.3	K.LAIQAYGASIVYCEPSDESRENVAK.R
199 - 205	741.5	741.5	K.ALKPSVK.V
206 - 221	1816.8	1816.8	K.VYAAEPSNADDCYQSK.L
224 - 241	1958.0	1958.0	K.GKLPNLYPPETIADGVK.S
226 - 241	1756.9	1756.9	K.LMPNLYPPETIADGVK.S
242 - 253	1355.8	1355.8	K.SSIGLNTWPIIR.D
254 - 268	1750.8	1750.9	R.DLVDDIFTVTEDEIK.C
269 - 277	1161.6	1161.6	K.CATQLVWER.M

Figure 2.8. Peptide sequences from mass spectrometry analysis of purified SR.

(A) Identified peptides (red) from SR sample matched with SR sequence, giving 50% sequence coverage.

(B) Unique peptides identified with the region covered, expected molecular weight, calculated molecular weight, and sequence. Mass spectrometry analysis confirmed the purified protein contained almost exclusively human SR.

2.4.8 Summary of SR purifications

The results detailed in the preceding sections are a representative SR purification. Naturally, several purifications were required to meet the demands of this research. The table below shows a summary of the yield from each purification, and the purpose for which each batch was used.

Table 2.1. Summary of all SR purifications, individual yields, and purpose of each batch.

Batch	Concentration (mg/mL)	Volume (mL)	Total protein (mg)	Use
1-3 (pooled)	5.6	2.5	14	Purification optimisation
4	19.1	1	19.1	Assay optimisation, fragment screen, literature inhibitor studies
5	23.2	1.2	27.8	Thermal shift, mass spec, western blot, crystallography
6	27.7	1.1	30.5	MST, ITC, crystallography
7	13.6	1.2	16.3	MST, ITC, crystallography
8	16.5	1	16.5	ITC, crystallography

2.5 DISCUSSION

The SR production described in the current chapter was fundamental for this drug discovery strategy to generate the large amounts of protein required for biochemical and biophysical assays, fragment screening, and crystallography. To this end, the purification procedure was successfully optimised to reduce aggregation and maximise levels of soluble SR purified from each batch. Verification of the authenticity of the isolated protein was achieved through further analysis of the purified sample by mass spectrometry and western blot.

The relative simplicity of the SR expression and purification procedure can be largely attributed to the use of the Evotec plasmid containing the C2,6D mutations in the SR gene. Previous studies of recombinant SR purification reported high levels of SR located in bacterial inclusion bodies, caused in part by codon bias (Nagayoshi *et al.*, 2005). Likewise, the Evotec authors (Smith *et al.*, 2010) initially found that expression of wild-type SR yielded very low levels of soluble protein. By studying a homology model of the *S. pombe* SR structure, they identified the two N-terminal surface-exposed cysteines, Cys2 and Cys6 as candidates for influencing protein solubility. Mutation of the cysteines to aspartates did indeed improve protein expression and the levels of soluble enzyme, possibly by preventing the formation of erroneous disulphide bonds that could contribute to aggregation. The authors further stabilised the SR mutant with the addition of a C-terminal His-tag, yielding highly pure, stable, and homogenous protein that had comparable activity to wild-type SR when assessed in a biochemical assay. The availability of the optimised mutant SR plasmid here undoubtedly facilitated the work conducted in this chapter.

Although the expression construct was optimised to mitigate aggregation, there was still a challenge keeping SR solubilised when the purification was performed in-house. Aggregation of protein molecules into inclusion bodies during high-level expression of recombinant protein in *E. coli* and subsequent purification is a common problem (Williams *et al.*, 1982). Although care was taken to minimise inclusion bodies, they may

still occur if there is a high translational rate of protein expression. This leads to a high level of metabolic burden on the cells and a strain on the cellular quality control system of proteins, so partially-folded and misfolded proteins are more likely to aggregate (Carrió and Villaverde, 2005). It is possible that while the BL21 CodonPlus (DE3)-RIL competent cells minimise codon bias, they may actually contribute to the aggregation observed throughout the purification by increasing expression levels. Additionally, the *E. coli* bacterial environment may lack the apparatus required to correctly fold human proteins like hSR, such as eukaryotic chaperones and post-translational machinery (Carrió *et al.*, 2000).

It is therefore likely that inclusion bodies will form during the expression and purification process, but this can be mitigated by altering the conditions so that inclusion bodies are solubilised and then refolded to recover functionally active protein (Singh *et al.*, 2015). Typically, inclusion bodies can be solubilised by chaotropic agents such as MgCl_2 and reducing agents such as DTT, both of which are contained in the lysis, equilibration, and elution buffers at concentrations of 2mM and 5mM, respectively. The solubilised protein can then be refolded by removal or reduction of the solubilisation agents, which in this case occurs during elution from the SEC column in a refolding buffer containing DTT and half the concentration of MgCl_2 (1mM). It is during this process of refolding that the problem of aggregation commonly occurs, and indeed was seen in the initial purification experiments with SR. The addition of glycerol had such a profound effect on reducing protein aggregation because it is a folding enhancer, and works by inducing protein compaction, reducing protein flexibility, and stabilising partially-folded intermediates (Vagenende *et al.*, 2009). More specifically, it is thought that glycerol shifts proteins towards more compact formations by forming electrostatic interactions with the hydrophobic surface regions of the protein, causing hydration of the protein in the presence of glycerol and stabilising the refolding process (Vagenende *et al.*, 2009).

Negligible aggregation still occurred and was visualised by the small shoulder peak in the SEC UV trace, but further optimisation was not deemed necessary considering the yield and activity of SR were above that required for assays and crystallisation

experiments. All purifications following aggregation optimisation consistently yielded approximately 3 mg SR per litre of expression medium, sufficient to meet the demands of this project. The combined qualitative information provided by western blot and mass spectrometry has helped to confidently characterise the purified protein as one that comprises SR (in the case of western blot and mass spectrometry) and is free from impurities.

The purified SR obtained using the procedure outlined in this chapter was then used to optimise assays in the three key areas underpinning this thesis: biochemical assay development, biophysical methods, and crystallography. The next chapter focuses on optimisation of the biochemical assay for the characterisation of SR activity, particularly in relation to published assay parameters and in preparation for fragment screening.

3 RESULTS II: BIOCHEMICAL ASSAY DEVELOPMENT

3.1 INTRODUCTION

With the ultimate aim of this project being the identification of novel inhibitors of SR, a method of measuring SR activity needed to be developed to, firstly, characterise purified SR with respect to literature data, and secondly, develop an assay format suitable for screening large numbers of compounds against SR. The literature on SR was a valuable resource in this process because of the numerous different assay formats from which to draw inspiration.

A common published method was the use of separation techniques to quantify the relative amount of each serine isomer (L-serine and D-serine) such as capillary electrophoresis (CE; Koval *et al.*, 2006, Singh *et al.*, 2012) or high performance liquid chromatography (HPLC; Wolosker *et al.*, 1999a, Wolosker *et al.*, 1999b, Stríšovský *et al.*, 2003, Foltyn *et al.*, 2005). The other most frequently used method was the coupled enzyme assay, so called because it paired the racemisation reaction with a second reaction that degraded D-serine, and a third reaction quantified the resulting breakdown products. The final detection reaction could use lactate dehydrogenase (LDH) with spectrophotometric monitoring of decreasing NADH to detect pyruvate (Stríšovský *et al.*, 2003). Or, with the addition of DAO and horseradish peroxidase (HRP), the subsequent redox reaction that occurs with hydrogen peroxide could be quantified chromogenically (Cook *et al.*, 2002), with fluorescence (Smith *et al.*, 2010), or luminescence (Wolosker *et al.*, 1999b, Wang and Barger, 2011).

An important requirement for the assay format selected for this study was the potential to be modified for medium-throughput screening. This ruled out HPLC and mass spectrometry assays, which — although beneficial for directly determining the presence and/or concentration of isomers — are slow, low-throughput, and unable to screen thousands of molecules with follow-up IC₅₀ determinations in the 384-well

format required for fragment screening. In contrast, a biochemical assay enabled important kinetic parameters to be determined (such as Michaelis-Menten constant and IC_{50}), required little specialist equipment, and streamlined the process of screening fragment libraries by being optimisable for 384-well plates.

Accordingly, the literature on published SR assays was examined and the information is summarised in Appendix 10.2. The most appealing candidates were the fluorescence assay developed by Smith *et al.* and the chemiluminescence assay developed in the Wang and Barger paper and by Wolosker *et al.* The fluorescence assay was selected because the authors also utilised the mutant SR (C2,6D) construct so data obtained here would be directly comparable. Their fluorescence assay coupled the racemisation of L-serine to the degradation of D-serine product by DAO, and the resulting H_2O_2 was quantified by the HRP-catalysed oxidation of AmLite Red, a detection reagent that forms a fluorescent product after oxidation. The luminescence assay was also selected as a viable option because of its similarity to the fluorescence assay (AmLite substituted for luminol) and the well-established record of using chemiluminescence to quantify H_2O_2 production. To summarise, from the SR assays described extensively in the literature, coupled biochemical assays were deemed the most attractive method for measuring SR activity, and from those, fluorescence and luminescence were selected as potential detection techniques pending further investigation.

The assay ultimately used for measuring activity of SR was a coupled luminescence assay that indirectly quantified D-serine using luminol as a substrate (Fig. 3.1). SR converts L-serine to D-serine, and the produced D-serine was then degraded by D-amino acid oxidase (DAO) into α -keto acid (pyruvate), ammonia (NH_3) and hydrogen peroxide (H_2O_2). The H_2O_2 produced in the assay was quantified by the addition of horseradish peroxidase (HRP) and luminol. HRP catalysed the oxidation of luminol by H_2O_2 , producing a luminescent product that was measured in relative luminescence units (RLU) with a BMG PHERAstar plate reader. A schematic of the coupled assay is shown below.

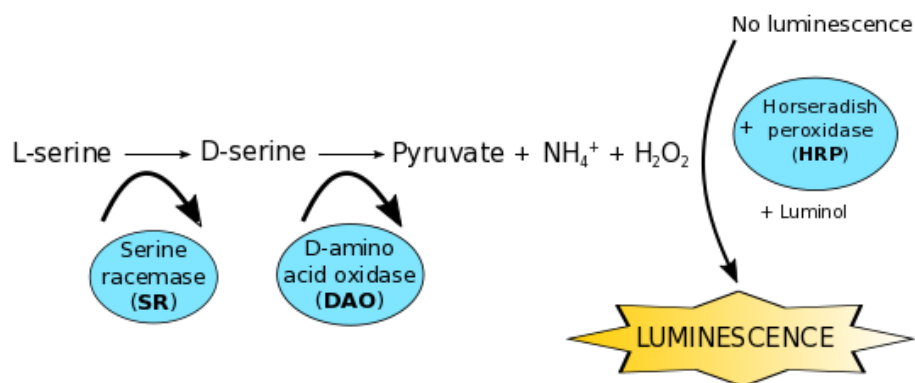


Figure 3.1. Principle of SR biochemical assay.

The literature inhibitor used as a tool compound was malonate (malonic acid), which has been well characterised as an inhibitor of SR (Stríšovský *et al.*, 2005), along with its derivatives (Vorlová *et al.*, 2015) and has also been crystallised in the SR active site (Smith *et al.*, 2010). Malonate is one of the most potent SR inhibitors to date, superseded only by L-erythro-3-hydroxyaspartate, which have reported K_i values of 0.077 mM and 0.049 mM, respectively (Stríšovský *et al.*, 2005). Malonate has not been developed further as an SR inhibitor due to its toxicity (Pubchem, 2017), and its non-specific competitive inhibition of other enzymes, such as succinate dehydrogenase of the respiratory electron transport chain (Gutman, 1978) and carbonic anhydrase (Innocenti *et al.*, 2009). Nevertheless, for assay development purposes, malonate was a suitable tool compound to use as a competitive inhibitor.

An additional important consideration is the dual functionality of SR — racemisation and β -elimination — and the effect it may have on determining the assay parameters. As well as isomerising serine, SR has the ability to catalyse the elimination of water from L-serine to form pyruvate and ammonia (De Miranda *et al.*, 2002). Both reactions occur in the same enzymatic site (Stríšovský *et al.*, 2005) and have comparable efficiencies (Jirásková-Vaníčková *et al.*, 2011). The β -elimination activity is thought to be related to the common ancestry of SR and serine dehydratase (Jirásková-Vaníčková *et al.*, 2011), another PLP-dependent enzyme that catalyses the elimination of L-serine to pyruvate.

Although SR β -elimination may have little physiological relevance in terms of energy contribution, since its rate of pyruvate production is less than 0.1% of pyruvate production from glucose (Dunlop and Neidle, 2005), it still has the potential to compete with racemisation activity. The assay employed throughout this chapter measures H_2O_2 as an indirect quantification of D-serine produced, and as H_2O_2 is not produced in the β -elimination reaction, this detection method can be considered specific to the racemisation reaction. The D-serine measured by DAO degradation and chemiluminescence technically only reflects the net amount, that is, the D-serine produced by racemisation minus the substrate consumed by elimination. With this in mind, a few other assumptions have to be made regarding the coupled assay: that H_2O_2 production occurs stoichiometrically with D-serine production; that all D-serine present was degraded by DAO; and that H_2O_2 levels were stable, being unaffected by extraneous sources.

This chapter contains the assay development process, from the initial discontinuance of Amplite Red in favour of luminol, to the optimisation of assay reagents and conditions, to the determination of kinetic parameters, and ultimately modification of the assay for medium-throughput screening. The latter step consisted of optimising the biochemical assay in 384-well plates, with the multiple addition steps being performed by automated liquid handlers (MultiDrop dispenser and FluidX Xpp-721). The automated SR assay represents a novel means of quantifying SR activity that has been uniquely adapted for a drug discovery setting.

3.2 MATERIALS

3.2.1 Reagents

Reagent	Supplier (product code)	Stock concentration
Serine racemase	Purified in-house	Various
L-serine	Sigma-Aldrich (S4500)	200mM
D-serine	Sigma-Aldrich (S4250)	10mM
Sodium malonate	Sigma-Aldrich (63409)	100mM or 1M
Malonic acid	Sigma-Aldrich (M1296)	100mM or 1M
Sodium benzoate	Sigma-Aldrich (B3420)	100mM
DMSO	Fisher Scientific (D4120/PB08)	100%

3.2.2 Buffers and assay solutions

Buffer	Compounds	Supplier (product code)	Concentration
Pre-treatment of L-serine solution	Tris-HCl pH 8.5	Sigma-Aldrich (154563)	100mM
	L-serine	Sigma-Aldrich (S4500)	200mM
	DAO	Sigma-Aldrich (A5222)	1.5U/mL
	Catalase	Sigma-Aldrich (C1345)	3U/ μ L
Tris mix buffer	Tris-HCl pH 8.5	Sigma-Aldrich (154563)	100mM
	Pluronic F-127	Sigma-Aldrich (P2443)	0.05%
	Magnesium chloride	Sigma-Aldrich (M2393)	1mM
	ATP	Acros Organics (102800100)	1mM
	PLP	Sigma-Aldrich (P9255)	10 μ M
Detection solution A	Tris-HCl pH 8.5	Sigma-Aldrich (154563)	100mM
	Pluronic F-127	Sigma-Aldrich (P2443)	0.05%
	EDTA	Alfa Aesar (A10713)	2mM
	HRP	Sigma (P8125)	0.5U/mL
	DAO	Sigma-Aldrich (A5222)	1U/mL
	Luminol	Sigma-Aldrich (A4683)	50 μ M
Detection solution B (counter screen)	Tris-HCl pH 8.5	Sigma-Aldrich (154563)	100mM
	Pluronic F-127	Sigma-Aldrich (P2443)	0.05%
	EDTA	Alfa Aesar (A10713)	2mM
	HRP	Sigma (P8125)	0.5U/mL
	Luminol	Sigma-Aldrich (A4683)	50 μ M
Amplite Red detection solution	CHES pH 8.5	Sigma-Aldrich (C2885)	100mM
	Pluronic F-127	Sigma-Aldrich (P2443)	0.05%
	DAO	Sigma-Aldrich (A5222)	1U/mL
	HRP	Sigma (P8125)	0.5U/mL
	Amplite Red	AAT Bioquest (11011)	1X

3.2.3 Reagent solutions

All solutions prepared in fresh Tris mix buffer

Purpose	Buffer	Concentration (μM)
SR solution I ¹	Tris mix buffer	0.4
SR solution II ²	Thermal shift buffer	1
L-serine solution I ¹	MST buffer	4000
L-serine solution II ²	ITC dialysis buffer	5000
D-serine solution	Tris mix buffer	10

¹ Solutions used when no fragment/compound is present

² Solutions used when fragment/compound is present (concentrations adjusted when there is a pre-incubation with inhibitor to keep final assay concentrations of enzyme and substrate the same)

3.2.4 Further materials, equipment and kits

Equipment	Supplier/manufacturer (product code)
Foil Plate Seals	SLS (PCR0620)
96-well v-bottom clear polypropylene plates	SLS (MIC9050)
Corning® 3574 384-well plates	Fisher Scientific (10382883)
NanoDrop 2000	ThermoFisher Scientific (n/a)
PERAstar FS plate reader	BMG (n/a)
Multidrop Combi™ reagent dispenser	Thermo Scientific (5840300)
Small tube metal tip dispensing cassette	Thermo Scientific (24073295)
Xpp-721 liquid handling robot	FluidX (n/a)
EZ-Load 96-well pipette tips 125 μL	Apricot Designs (125-096-EZ-NS)
EZ-Load 8-channel strip tips	Apricot Designs (125-008-EZ-NS)
Allegra X-30R centrifuge	Beckman Coulter (A99470)

3.3 METHODS

The following sections describe the methodology employed to develop a coupled biochemical assay using luminol as a detection substrate, and the adaptations made to optimise the assay to a 384-well format in preparation for medium-throughput screening.

3.3.1 General assay procedure

The 'front-end' racemisation reaction with 5 μL SR and 5 μL L-serine was performed in Tris mix buffer (100 mM Tris pH 8.5, 0.05% Pluronic F-127, 1 mM MgCl_2 , 1 mM ATP, 10 mM PLP) and incubated at RT for 20-30 min for single-point experiments and up to 3 h for time-dependency experiments. The 'back-end' chemiluminescence reaction was initiated after addition of 30 μL of Detection Solution A (100 mM Tris pH 8.5, 0.05% Pluronic F-127, 2 mM EDTA, 1 U/mL DAO, 0.5 U/mL HRP, 50 μM luminol) and incubated at RT for 5-10 min to allow non-specific luminol luminescence to decrease before the signal was read with a BMG PHERAstar plate reader. The gain of the PHERAstar was set to 3600, and the interval time was set to 0.5 s (initially) or 0.02 s (finally). All reactions were carried out in a Corning® 3574 384-well plate, and between each addition, the plate was centrifuged briefly at 500 rpm (Allegra X-30R) and sealed.

The above protocol was adapted slightly to test the effects of compounds (such as DMSO, malonate, or fragment molecules) on SR activity. In these cases, 4 μL SR was first incubated for 15 min at RT with 2 μL from a concentration series of compound or DMSO. After 15 min, 4 μL L-serine was added to start the racemisation reaction, and the remainder of the experiment proceeded as described in the above paragraph.

The inclusion of cofactors (PLP, ATP, Mg^{2+}) was based on guidance from previously established SR assays (refer to Appendix A). EDTA terminates the reaction by chelating the Mg^{2+} ions in the assay that are required for SR activity (De Miranda *et al.*, 2002),

and the cofactors ATP and Mg^{2+} have been demonstrated to significantly increase SR activity.

3.3.2 Pre-treatment of L-serine

L-serine required treatment to eliminate trace amounts of D-serine that contaminate virtually all commercial samples. Up to 200 mM L-serine was catabolised with 1.5 U/mL porcine DAO in conjunction with 3 U/ μL catalase in 100 mM Tris-HCl, pH 8.5. The mixture was incubated overnight at 37 °C with gentle shaking, then was heated at 95 °C for 10 min to inactivate the enzymes. After centrifugation at 13 000 rpm for 10 min, the supernatant was collected and stored at -20 °C. Successful removal of contaminating D-serine was verified by directly comparing pre-treated L-serine with untreated L-serine in the chemiluminescence reaction of the coupled assay.

3.3.3 Initial experiments with Amplite Red

Preliminary experiments were performed using Amplite Red™ (Stratech) as a detection reagent, before it was decided further assay development would be performed with luminol. The procedure of the Amplite Red assay was almost identical to that of the luminol assay, with the key distinction that H_2O_2 was quantified by the HRP-catalysed oxidation of Amplite Red, producing a fluorescent product (resorufin) measured in relative fluorescent units (RFU).

3.3.4 SR time course

Time course experiments enable the linear phase of the enzyme reaction to be observed. A 3 h time course was first performed to determine the reaction plateau. Reaction mixtures were prepared in 384-well plates in Tris mix buffer and contained five concentrations of SR (5 μL ; final concentrations 0.2, 0.3, 0.4, 0.5, 2 μM) and at each time interval (0–180 min) L-serine solution I was added (5 μL ; final substrate

concentration 2 mM). After the final addition of L-serine at 0 min, 30 μ L Detection Solution A was immediately added to all wells, and after a further 10 min incubation, the luminescence signal was measured with a BMG PHERAstar.

A 30 min time course was then performed to analyse the linear phase of the enzyme reaction in more detail. The assay procedure was the same as that described above, and tested two SR concentrations (0.2 and 0.4 μ M) every 2 min between 0–30 min.

3.3.5 Michaelis-Menten constant, K_m

The K_m measures the affinity of an enzyme for its substrate and is constant for an enzyme/substrate pair under a specific set of assay conditions. Determination of the K_m allows comparison of kinetic parameters between enzyme sources, such as in-house purification batches or literature data. A substrate concentration around or below the K_m should be used to prevent excess substrate overcoming the action of competitive inhibitors in IC_{50} experiments.

A 10-point 1:2 serial dilution of L-serine was prepared in Tris mix buffer. Reaction mixtures in 384-well plates containing SR solution I (5 μ L; final concentration 400 nM) and each of the ten concentrations of L-serine (5 μ L; final concentrations 0–50 mM) were incubated for 20 min at RT, after which 30 μ L Detection Solution A was dispensed into all wells. Following a further 10 min incubation, the luminescence signal was measured. Calculation of the K_m was performed using Graphpad Prism software.

3.3.6 Dimethyl sulfoxide tolerance

The purpose of a dimethyl sulfoxide (DMSO) tolerance test is to ensure that the enzyme being tested is not inhibited by DMSO at concentrations required for screening, because compounds and fragments are routinely solubilised with 100% DMSO. This applies to the fragment libraries used to identify novel inhibitors of SR in this study.

An 8-point 1:2 serial dilution of DMSO starting from 100% was prepared in water. The concentration series was then diluted 1:2 in Tris mix buffer to prepare the intermediate concentrations (0–50% DMSO).

Reaction mixtures in 384-well plates containing SR solution II (4 μ L; final concentration 400 nM) were incubated with each of the ten intermediate concentrations of DMSO (2 μ L; final concentrations 0–10%) for 15 min at RT. The SR reaction was started with the addition of L-serine solution II (4 μ L; final substrate concentration 2 mM) and the reaction was incubated for 20 min at RT. 30 μ L Detection Solution A was then dispensed to all wells, and after a further 10 min incubation the luminescence signal was measured.

3.3.7 Determination of IC₅₀

The IC₅₀ is the concentration of a compound that results in 50% inhibition of enzyme activity, and is important for assessing the potency of an inhibitor, as well as determining structure-activity relationship (SAR) measurements for a series of structurally-related compounds.

Inhibitor stocks were 100 mM (malonate, fragment libraries, literature compounds) or 10 mM (some literature compounds) in 100% DMSO. A 10-point 1:3 serial dilution was prepared in 100% DMSO from compound stocks of 100 mM or 10 mM DMSO. The concentration series was then diluted 1:4 in Tris mix buffer to prepare the intermediate dilution series (0–25 mM or 0–2.5 mM).

Reaction mixtures in 384-well plates containing SR solution II (4 μ L; final concentration 400 nM) were incubated with each of the ten intermediate concentrations of inhibitor (2 μ L; final concentrations 0–5 mM or 0–500 μ M) for 15 min at RT. The SR reaction was started with the addition of L-serine solution II (4 μ L; final substrate concentration 2 mM) and the reaction was incubated for 20 min at RT. 30 μ L Detection Solution A

was then dispensed to all wells, and after a further 10 min incubation the luminescence signal was measured.

Data were plotted as percentage inhibition using Graphpad Prism. IC₅₀ values were calculated and curves fitted using a variable slope model (four-parameter dose-response curve) according to the following equation:

$$y = Bottom + \frac{Top - Bottom}{1 + 10^{((LogIC_{50} - x) \times HillSlope)}}$$

Where *Hill Slope* refers to the steepness of the family of curves and *Top/Bottom* refers to plateaus in percentage inhibition.

3.3.8 Pre-screening plate tests

The purpose of the plate test experiments was to develop an assay suitable for medium-throughput screening, therefore in addition to optimising standard assay parameters, further optimisation steps were performed to account for any variability caused by introducing automation. Screening entire fragment libraries required the use of automated liquid handlers, namely a Multidrop Combi (with a small tube metal tip dispensing cassette) for dispensing SR, L-serine, and Detection Solution, and a FluidX Xpp-721 for transferring plates of compounds.

Before use, the dispensing head of the Multidrop Combi was primed with the assay solution to ensure there were no air bubbles in the tubes or blocked tips. After use, the head was successively cleaned with MilliQ H₂O, 0.05% Tween, 70% ethanol, and then MilliQ H₂O.

3.3.8.1 Plate test 1: Assay window

The purpose of the first plate test was to assess the assay window with automation and to identify whether there were any dispensing irregularities across the plate. It

was performed on a full 384-well plate, half (columns 1–12) containing no SR and half (columns 13–24) containing SR.

A 384-well plate was preloaded with Tris mix buffer (5 μ L) in columns 1–12 and SR solution I (5 μ L; final concentration 400 nM) in columns 13–24. L-serine solution I (5 μ L; final concentration 2 mM) was dispensed into all wells to start the reaction and the plate was incubated for 20 min at RT. 30 μ L Detection Solution A was then dispensed to all wells, and after a further 10 min incubation the luminescence signal was measured.

3.3.8.2 Plate test 2: Malonate IC₅₀

The purpose of the second plate test was to assess the reproducibility of IC₅₀ values obtained with automation across a 384-well plate, and to verify they were comparable to values obtained manually.

As with the manual IC₅₀ assay, the automated IC₅₀ assay required an initial dilution from stock in DMSO, followed by an intermediate dilution into assay buffer, then a final dilution into the assay plate. The stock and intermediate dilutions were performed in 96-well polypropylene plates (SLS) before being transferred to 384-well assay plates.

For the stock plate, a 1:3 serial dilution from 1 M malonate stock was prepared in 100% DMSO in all rows of a 96-well polypropylene plate (FluidX Xpp-721 liquid handler with EZ-Load 8-channel strip tips). The intermediate 96-well plate was preloaded with 78 μ L Tris mix buffer in all wells (Multidrop Combi) then 2 μ L from each well of the stock plate was transferred to the corresponding well in the intermediate plate (FluidX Xpp-721 with EZ-Load 96-well pipette tips) to produce the intermediate concentration series (0–25 mM).

The 384-well assay plate was manually preloaded with the positive (plus enzyme; 4 μ L SR solution II) and negative (no enzyme; 4 μ L Tris mix buffer) controls to columns 1, 2,

23, and 24 (see Fig. 3.2A for plate map). SR solution II (4 μ L; final concentration 400 nM) was dispensed to columns 3–22. The intermediate dilution series was then transferred from to the assay plate (2 μ L; final malonate concentrations 0–5 mM; FluidX-Xpp-721 with EZ-Load 96-well pipette tips) using a quadrant protocol (see Fig. 3.2B for quadrant layout). The plate was incubated for 15 min at RT.

L-serine solution II was dispensed to the entire plate to start the reaction (4 μ L; final concentration 2 mM; Multidrop Combi), then the plate was incubated for 20 min. After this time, 30 μ L Detection Solution A was dispensed to all wells, and after a further incubation the luminescence signal was measured. For optimisation purposes, the length of this final incubation was varied between 5–15 min, and the interval time (the length of time the reader collects a measurement from each well) of the PHERAstar was tested at 0.02, 0.1, and 0.5 s.

A

	1	2	3	4	5	6	7	8	9	10	11	12	13	14	15	16	17	18	19	20	21	22	23	24
A	No enzyme		1	2	1	2	1	2	1	2	1	2	1	2	1	2	1	2	1	2	1	2	Plus enzyme	
B			3	4	3	4	3	4	3	4	3	4	3	4	3	4	3	4	3	4	3	4		
C			5	6	5	6	5	6	5	6	5	6	5	6	5	6	5	6	5	6	5	6		
D			7	8	7	8	7	8	7	8	7	8	7	8	7	8	7	8	7	8	7	8		
E			9	10	9	10	9	10	9	10	9	10	9	10	9	10	9	10	9	10	9	10	No enzyme	
F			11	12	11	12	11	12	11	12	11	12	11	12	11	12	11	12	11	12	11	12		
G			13	14	13	14	13	14	13	14	13	14	13	14	13	14	13	14	13	14	13	14		
H			15	16	15	16	15	16	15	16	15	16	15	16	15	16	15	16	15	16	15	16		
I	Plus enzyme		9	10	9	10	9	10	9	10	9	10	9	10	9	10	9	10	9	10	9	10	No enzyme	
J			11	12	11	12	11	12	11	12	11	12	11	12	11	12	11	12	11	12	11	12		
K			13	14	13	14	13	14	13	14	13	14	13	14	13	14	13	14	13	14	13	14		
L			15	16	15	16	15	16	15	16	15	16	15	16	15	16	15	16	15	16	15	16		
M			9	10	9	10	9	10	9	10	9	10	9	10	9	10	9	10	9	10	9	10		
N			11	12	11	12	11	12	11	12	11	12	11	12	11	12	11	12	11	12	11	12		
O			13	14	13	14	13	14	13	14	13	14	13	14	13	14	13	14	13	14	13	14		
P			15	16	15	16	15	16	15	16	15	16	15	16	15	16	15	16	15	16	15	16		

B

	1	2	3	4	5	6	7	8	9	10	11	12	13	14	15	16	17	18	19	20	21	22	23	24
A	Q1	Q3	Q1	Q3	Q1	Q3	Q1	Q3	Q1	Q3	Q1	Q3	Q1	Q3	Q1	Q3	Q1	Q3	Q1	Q3	Q1	Q3	Q1	Q3
B	Q2	Q4	Q2	Q4	Q2	Q4	Q2	Q4	Q2	Q4	Q2	Q4	Q2	Q4	Q2	Q4	Q2	Q4	Q2	Q4	Q2	Q4	Q2	Q4
C	Q1	Q3	Q1	Q3	Q1	Q3	Q1	Q3	Q1	Q3	Q1	Q3	Q1	Q3	Q1	Q3	Q1	Q3	Q1	Q3	Q1	Q3	Q1	Q3
D	Q2	Q4	Q2	Q4	Q2	Q4	Q2	Q4	Q2	Q4	Q2	Q4	Q2	Q4	Q2	Q4	Q2	Q4	Q2	Q4	Q2	Q4	Q2	Q4
E	Q1	Q3	Q1	Q3	Q1	Q3	Q1	Q3	Q1	Q3	Q1	Q3	Q1	Q3	Q1	Q3	Q1	Q3	Q1	Q3	Q1	Q3	Q1	Q3
F	Q2	Q4	Q2	Q4	Q2	Q4	Q2	Q4	Q2	Q4	Q2	Q4	Q2	Q4	Q2	Q4	Q2	Q4	Q2	Q4	Q2	Q4	Q2	Q4
G	Q1	Q3	Q1	Q3	Q1	Q3	Q1	Q3	Q1	Q3	Q1	Q3	Q1	Q3	Q1	Q3	Q1	Q3	Q1	Q3	Q1	Q3	Q1	Q3
H	Q2	Q4	Q2	Q4	Q2	Q4	Q2	Q4	Q2	Q4	Q2	Q4	Q2	Q4	Q2	Q4	Q2	Q4	Q2	Q4	Q2	Q4	Q2	Q4
I	Q1	Q3	Q1	Q3	Q1	Q3	Q1	Q3	Q1	Q3	Q1	Q3	Q1	Q3	Q1	Q3	Q1	Q3	Q1	Q3	Q1	Q3	Q1	Q3
J	Q2	Q4	Q2	Q4	Q2	Q4	Q2	Q4	Q2	Q4	Q2	Q4	Q2	Q4	Q2	Q4	Q2	Q4	Q2	Q4	Q2	Q4	Q2	Q4
K	Q1	Q3	Q1	Q3	Q1	Q3	Q1	Q3	Q1	Q3	Q1	Q3	Q1	Q3	Q1	Q3	Q1	Q3	Q1	Q3	Q1	Q3	Q1	Q3
L	Q2	Q4	Q2	Q4	Q2	Q4	Q2	Q4	Q2	Q4	Q2	Q4	Q2	Q4	Q2	Q4	Q2	Q4	Q2	Q4	Q2	Q4	Q2	Q4
M	Q1	Q3	Q1	Q3	Q1	Q3	Q1	Q3	Q1	Q3	Q1	Q3	Q1	Q3	Q1	Q3	Q1	Q3	Q1	Q3	Q1	Q3	Q1	Q3
N	Q2	Q4	Q2	Q4	Q2	Q4	Q2	Q4	Q2	Q4	Q2	Q4	Q2	Q4	Q2	Q4	Q2	Q4	Q2	Q4	Q2	Q4	Q2	Q4
O	Q1	Q3	Q1	Q3	Q1	Q3	Q1	Q3	Q1	Q3	Q1	Q3	Q1	Q3	Q1	Q3	Q1	Q3	Q1	Q3	Q1	Q3	Q1	Q3
P	Q2	Q4	Q2	Q4	Q2	Q4	Q2	Q4	Q2	Q4	Q2	Q4	Q2	Q4	Q2	Q4	Q2	Q4	Q2	Q4	Q2	Q4	Q2	Q4

Figure 3.2. Plate maps for performing IC₅₀ experiments in a 384-well plate with automation.

(A) Plate map showing position of controls (columns 1, 2, 23, 24) and quadrant dilution series (columns 3-22). Pairs of numbers (1-2, 3-4, 5-6, etc.) are duplicates, and each pair across the plate contains a different inhibitor concentration in the 10-point 1:3 dilution series. Each row represents one concentration series, therefore eight inhibition curves are obtained from each plate. (B) Plate map showing quadrant protocol; each quadrant (Q1, Q2, Q3, Q4) reflects repeats from one well in the intermediate 96-well plate.

3.3.8.3 Plate test data analysis

Data from plate test 1 were assessed for the robustness of the assay window and variability of signal using the coefficient of variation (CV). The CV is a standardised measure of dispersion that describes the amount of variability relative to the mean. The % CV was calculated separately for the negative and positive controls using the formula (standard deviation ÷ mean) × 100. A % CV of ~10% was deemed sufficient.

Data from plate test 2 were assessed using the Z-prime (Z') factor, a method of assay quality control that shows the separation between the distributions of the positive and negative controls and indicates the likelihood of false positives or negatives (Zhang *et al.*, 1999). Plates were failed if they had a Z' of below 0.4. The formula used to calculate the Z' score is as follows:

$$Z' = 1 - \frac{3(\sigma_p + \sigma_n)}{(\mu_p - \mu_n)}$$

Where σ = standard deviation, μ = mean, subscript (p) = positive control, and subscript (n) = negative control.

The quadrant plate data was divided into 16 malonate inhibition curves with Q1 + Q2 and Q3 + Q4 forming duplicate wells. The raw data was converted to percentage inhibition and IC₅₀ values were calculated using GraphPad Prism. IC₅₀ values needed to be within a threefold range of those obtained manually to be considered valid.

3.4 RESULTS

3.4.1 Preliminary experiments with AmpLite Red

As discussed in the introduction of this chapter, an evaluation of the literature on SR assays yielded two viable assay detection systems that could feasibly be optimised for medium-throughput screening. The first attempted was a coupled fluorescence assay that used AmpLite Red as a detection substrate, it ultimately proved unreliable. The main difficulty was the fluorescence signal was often unstable and consequently not reproducible. Further, the background fluorescence signals could be unpredictable and often fluctuated between assays, particularly with different concentrations of DAO. It is possible the fluorescence reading was partially obscured by the bright yellow/orange colour of DAO, caused by its cofactor flavin adenine dinucleotide (FAD) which has its own excitation and emission spectra of 450 nm and 535 nm, respectively (Ramanujam, 2000). Those that used AmpLite Red in published SR assays did not report the same issues (Smith *et al.*, 2010, Nelson *et al.*, 2017). When there was no progress stabilising the fluorescence signal with AmpLite Red, the focus was shifted to luminol.

3.4.2 L-serine treatment removes contaminating D-serine

Commercial L-serine must be pre-treated to remove trace amounts of contaminating D-serine (refer to Methods 3.3.2). To confirm the efficacy of this step, 2 mM pre-treated L-serine and untreated L-serine were used as substrates in the chemiluminescence reaction of the coupled SR assay. As L-serine is not degraded by DAO to produce H₂O₂, little to no signal would indicate contaminating D-serine had been adequately removed. A single-point assay comparing 5 mM pre-treated and untreated L-serine was performed and the data (Fig. 3.3) illustrate that pre-treatment of commercial L-serine with DAO significantly reduced contaminating D-serine levels by approximately 95%.

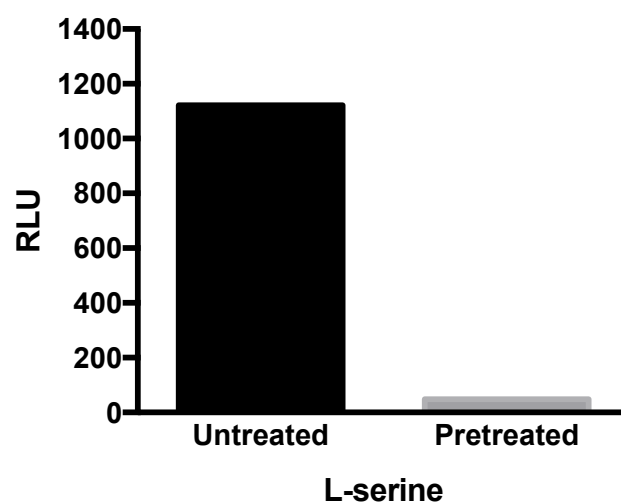


Figure 3.3. Pretreatment of commercial L-serine significantly reduces D-serine contamination.

L-serine was treated with 1.5 U/mL DAO and catalase and incubated at 37 °C overnight, then heated at 95 °C for 10 min to inactivate the enzymes. The solution was centrifuged at $14\,000 \times g$ for 10 min and the resulting supernatant was collected and compared with untreated L-serine (5 mM) in the chemiluminescence reaction with DAO, HRP and luminol. The data indicate that contaminating D-serine is reduced by approximately 95%. Data are the mean of three replicates.

3.4.3 D-serine standard curve

While raw signal values can be compared for optimisation purposes, it is more applicable to define data quantitatively in terms of specific enzyme activity based on the level of product produced. Hence, D-serine standard curves were obtained by measuring the RLU signals achieved with increasing concentrations of product (D-serine) in the chemiluminescence reaction with DAO, HRP, and luminol (Fig. 3.4). The standard curves were repeated for each of the different interval times tested within this chapter (0.5, 0.1, 0.02 s) because each elicited proportionally different RLU values. For subsequent assays, D-serine produced (x) was interpolated from RLU values (y) using GraphPad Prism, and from there, specific enzyme activity could be calculated from SR concentration and time length of the racemisation step (μmol D-serine produced per minute per μg of SR).

The plateaus observed in Fig. 3.4 may be representative of DAO saturation in the presence of high concentrations of D-serine, but product inhibition of DAO by H_2O_2 may also be a contributing factor because H_2O_2 has damaging oxidative properties and has been documented having a non-competitive inhibitory effect on DAO from *Rhodotorula gracilis* (de la Mata et al., 2000). The study also commented that DAO was resistant to inhibition up to concentrations of 5 mM H_2O_2 — so from the premise that H_2O_2 is being produced in a 1:1 stoichiometry with D-serine, the maximum levels of D-serine being produced remained in the low micromolar range. Therefore, the deleterious effect of H_2O_2 at these concentrations is likely to be negligible.

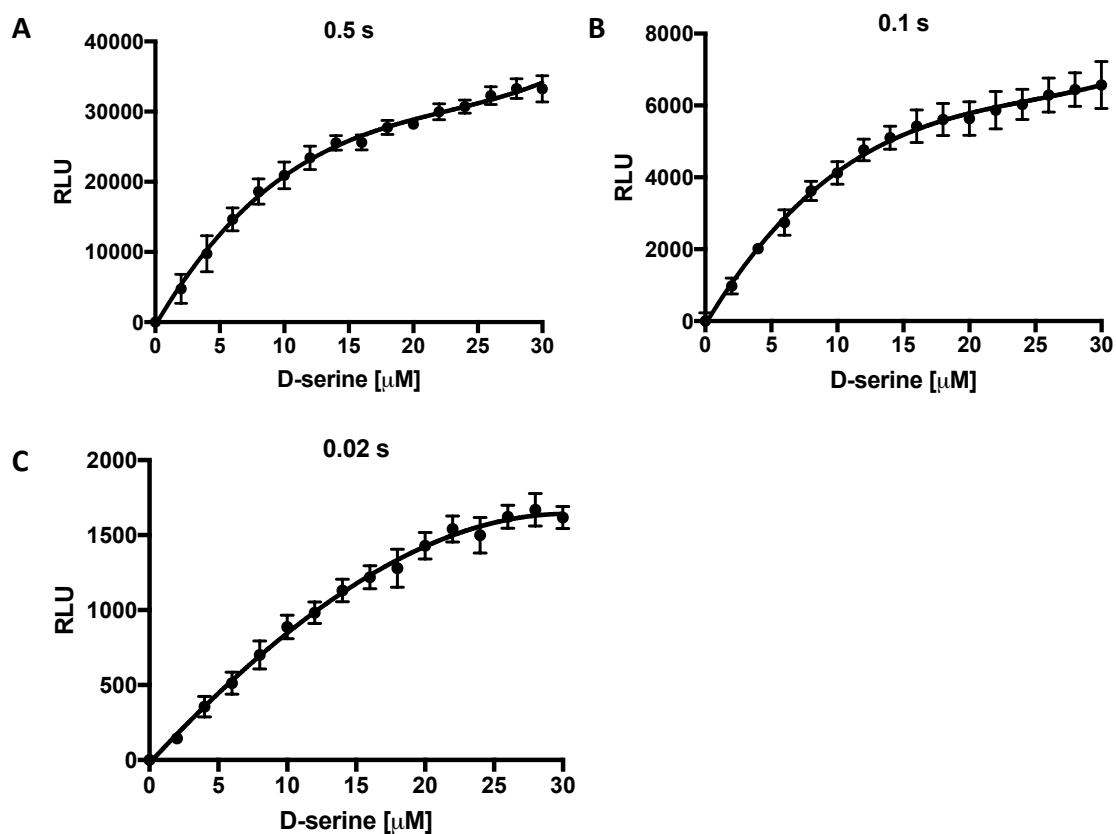


Figure 3.4. D-serine standard curves for determining the concentration of D-serine from the analytical signal, Relative Luminescence Units (RLU).

A concentration series of D-serine was prepared and degraded by DAO. The resulting H_2O_2 , which is produced in a 1:1 stoichiometry with D-serine, was quantified in a chemiluminescence reaction with HRP and luminol. The curves were repeated with interval times of 0.5 s (A), 0.1 s (B), and 0.02 s (C). Experiments were performed in triplicate; graphs are the means from three independent experiments ($n = 3$); error bars = SEM.

3.4.4 Effect of buffers on SR activity

A number of different buffers have been used for SR biochemical assays in the literature (see Appendix A for full list), including CHES pH 9 (Smith *et al.*, 2010), Tris pH 8 (Wolosker *et al.*, 1999b), HEPES pH 8 (Wang *et al.*, 2012), MOPS pH 8.1 (Cook *et al.*, 2002) and phosphate buffer pH 8 (Wang and Barger, 2011). Three buffers — Tris, CHES, and HEPES — were chosen for comparison, because Tris and CHES were employed in the respective luminescence and fluorescence assays that were the stimulus for this chapter, and HEPES had been routinely used in several published SR assays. The useful pH ranges are similarly basic for Tris (7.0–9.0) and CHES (8.6–10.0), while that for HEPES more closely reflects physiological pH (6.8–8.2). A principle feature of Tris buffer is that its pK_a declines approximately 0.03 units per degree Celsius rise in temperature (Vega *et al.*, 2002). In context, this means Tris pH 8.5 at 25 °C will have a pH of 8.22 at 37 °C (Sigma-Aldrich, 2017).

The activity of SR in the three buffers was compared in a 30 min single-point assay. The buffer pH was kept constant at 8.5 and buffer concentration at 100 mM to ensure the influence of the buffers alone was the only variable being measured. In the experiment, 500 nM SR was incubated with 2 mM L-serine for 30 min, both of which were prepared in either Tris, CHES, or HEPES, all supplemented with 0.05% (v/v) Pluronic F-127, 1 mM $MgCl_2$, 1 mM ATP, and 10 μ M PLP. The H_2O_2 produced in the assay was quantified by the addition of a detection solution containing 100 mM Tris, CHES, or HEPES, with 2 mM EDTA, 1 U/mL DAO, 0.5 U/mL HRP, and 50 μ M luminol. The results are presented in Fig. 3.5 as the raw luminescence values in the presence and absence of SR (Fig. 3.5A) and the assay window after background correction (Fig. 3.5B). The data clearly demonstrate that SR was most active in Tris buffer, which elicited the greatest activity signal and lowest background signal. The assay window with Tris was approximately fivefold that achieved with its closest contender, CHES. From these data, Tris was selected for further optimisation of the coupled assay.

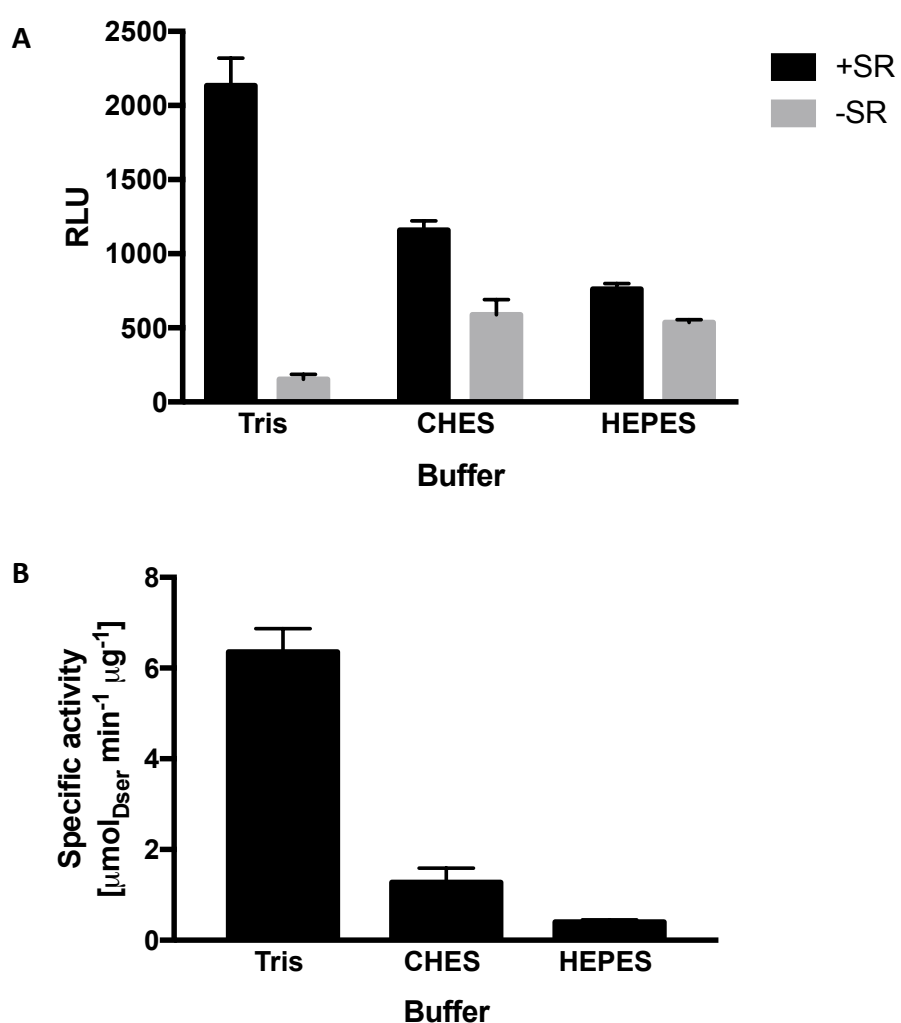


Figure 3.5. Comparison of SR activity in different buffer systems.

A 30 min single-point assay of SR activity was performed in 100 mM Tris pH 8.5, 100 mM CHES pH 8.5, and 100 mM HEPES pH 8.5, all supplemented with 0.05% Pluronic F-127, 1 mM ATP, and 10 μM PLP. Results shown are the raw luminescence values (**A**) and the assay window once background luminescence had been removed (**B**). The greatest assay window was achieved with Tris buffer, therefore all subsequent experiments were performed using Tris. Experiments were performed in triplicate; graphs are the means from three independent experiments ($n = 3$). Error bars = SEM, [SR] = 500 nM.

3.4.5 Influence of temperature and buffer pH and on SR activity

Common features in literature SR assays were used to determine which assay conditions were important to control. Two consistent features of practically all published SR assays is that the racemisation reaction was incubated at 37 °C, and that the assays were performed at pH 8–9. Both incubation temperature and buffer pH were investigated in this study to identify the conditions that were most favourable for SR activity. This was achieved by performing a 30 min single-point experiment with 500 nM SR and 2 mM L-serine at either RT or 37 °C, in 100 mM Tris mix buffer pH 7.5, 8.0, 8.5, 9.0, or 9.5.

The results (Fig. 3.6) indicate the pH sensitivity of SR was comparable between RT and 37 °C, demonstrating a typical pH dependence curve (Fig. 3.6B) that peaked at pH 8.5. Although SR activity was marginally increased at 37 °C compared to RT, this effect was minimal, and was accompanied by more variable data as represented by the larger margins of error at 37 °C (Fig. 3.6A). The signal variability could have been a plate effect resulting from inconsistent heat distribution across the plate, or caused by the proclivity of Tris buffer to fluctuate pH in different temperatures. This characteristic of Tris was another deterrent against implementing a 37 °C incubation temperature in this study.

Based on the data in Fig. 3.6, it was decided to perform subsequent incubations at RT. Previous studies may have implemented a 37 °C incubation temperature to increase L-serine turnover — for L-serine racemisation is an inherently slow process, with SR producing one molecule of D-serine in just over a second (Jirásková-Vaníčková *et al.*, 2011) — but this was not evident by a significantly different SR activity at 37 °C in Fig. 3.6. It is possible the higher incubation temperature functioned to keep SR stable over a longer time period. At the incubation times used here for most assays and screening (20 min), it was unlikely instability issues would be relevant. As many published SR assays often implemented incubation periods of an hour or more, they may have had more use for the stabilising effect of a 37 °C incubation temperature.

An additional consideration had to be made regarding the practicality of incorporating a 37 °C incubation step, when the objective was to optimise the assay for medium-throughput screening. All dispensing steps and the compound transfer steps were not possible to perform at 37 °C due to the nature of the equipment, and it was not practical to keep transferring plates to and from an incubator while screening multiple plates, or when adding substrate at each interval of a time course. Hence, to keep potential variability low, all assay steps were performed at room temperature.

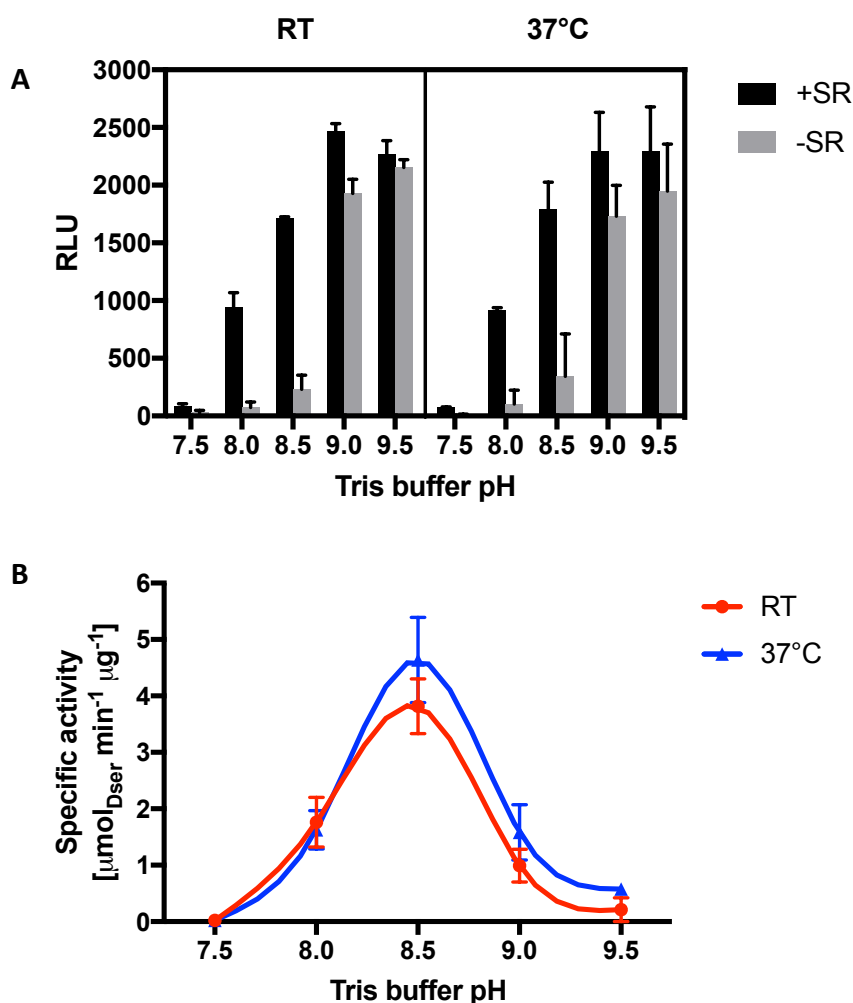


Figure 3.6. Influence of incubation temperature and buffer pH on SR activity.

A 30 min single-point assay of 500 nM SR activity was performed in 100 mM Tris buffer pH 7.5, 8.0, 8.5, 9.0, or 9.5, either at room temperature (RT) or 37 °C. Results shown are the raw luminescence values for each condition (A), and the assay windows once background luminescence had been removed (B). SR activity was largely similar for RT and 37 °C, with the greatest assay window achieved for both at pH 8.5. Experiments were performed in triplicate; graphs are the means from three independent experiments (n = 3); error bars = SEM.

3.4.6 DTT attenuates SR activity

A consistent feature of published SR assays is the inclusion of the thiol-reducing agent DTT (see Appendix), which has been generally accepted to increase the activity of SR when present during the purification process and in the reaction buffer. DTT is thought to cause this effect by elevating the levels of active SR dimer and preventing the formation of aggregates and tetramers via its reducing action at any of SR's eight cysteine residues (Wang and Barger, 2011). A DTT concentration-response assay was performed to evaluate any changes in SR activity in the presence of DTT. The experiment was a 20 min single-point assay and tested eight DTT concentrations between 0–5 mM to reflect the concentrations used in the literature. The results are presented in Fig. 3.7.

Interestingly, the data indicate that SR activity was considerably reduced in the presence of DTT, becoming effectively abolished at concentrations above 0.08 mM, while maintaining activity in the absence of DTT. It would be reasonable to link this discrepancy to the two cysteine-to-aspartate point mutations in the SR primary sequence. The mutations were introduced to improve SR solubility during purification and thus increase the recovery of active, dimeric SR (Smith *et al.*, 2010). It is possible the mutation of these exposed cysteine residues removed the previously described DTT-dependent activity increase by also preventing or breaking randomly-formed disulphide bonds that could cause aggregation. Although, this does not explain why extra DTT would then abolish activity.

In the current study, DTT was included during SEC purification to facilitate refolding and quaternary structure formation of SR, so it is unlikely SR stability is sensitive to DTT. Another possibility is that a different assay component is intolerant to DTT. For example, previous reports have found that DTT drastically decreases the stability of HRP (Chattopadhyay and Mazumdar, 2000). Further, detection of luminescence is dependent on the HRP-catalysed oxidation of luminol by the oxidising agent H_2O_2 , but high concentrations of DTT (approx. 1 mM) can react directly with the peroxide (Nelson and Parsonage, 2011), potentially depleting H_2O_2 produced in the assay. If this

were the case, it would be incongruous with other published SR assays involving a chemiluminescence reaction that did not observe the same effect with DTT (Wolosker *et al.*, 1999b). Regardless, SR was sufficiently active when DTT was absent, so optimisation continued without additional DTT in the reaction buffer.

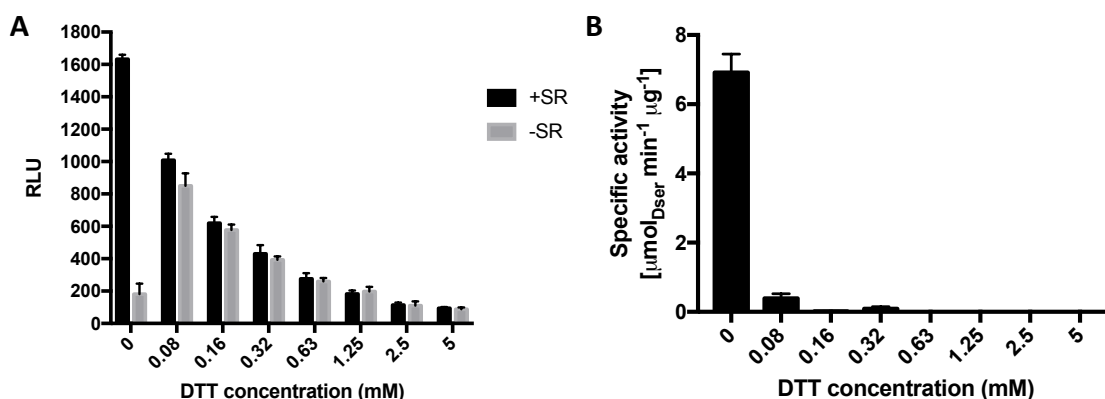


Figure 3.7. DTT attenuates the SR biochemical assay signal.

A 20 min single-point assay of 400 nM SR activity was performed in the presence of increasing concentrations of DTT up to 5 mM. Results shown are the raw luminescence values (A), and the specific activity calculated from the signal once corrected for background luminescence (B). The reporter signal was completely abolished above 0.08 mM. Experiments were performed in triplicate; data are from three independent experiments ($n = 3$); error bars = SEM.

3.4.7 Chemiluminescence reaction is in excess

It was of primary importance to optimise the chemiluminescence reaction reagents to ensure the rate of the racemisation reaction was not being limited by insufficient concentrations of other reagents. This was achieved by performing a 20 min single-point assay with 400 nM SR and 2 mM L-serine, and for the detection reaction a concentration series of either DAO (0–4 U/mL), HRP (0–4 U/mL), or luminol (0–100 μM) was added with the previously used concentrations of the other detection reagents. Fig. 3.8 shows concentration-response curves for DAO (A), HRP (B) and luminol (C).

Increasing concentrations of DAO and HRP both demonstrated a marked increase in signal that peaked and was followed by a gradual decline. The reason for the decrease in signal, rather than a plateau as might be expected, may be a consequence of the luminescence signal being quenched, or aggregation and/or precipitation of the enzymes at high concentrations. Concentrations around the peak were selected to avoid the quenching effect and to keep the detection reagents in excess: 1 U/mL DAO, 0.5 U/mL HRP, and 50 μ M luminol.

3.4.8 SR assay can be terminated by EDTA

A means of terminating the racemisation reaction was required to precisely control the lengths of incubation. Divalent cations such as Mg^{2+} , Mn^{2+} and Ca^{2+} are required to stabilise folding of SR and therefore chelators such as EDTA can completely inhibit SR activity (Cook *et al.*, 2002). Previous studies report the use of the inhibitory effect of EDTA for this purpose (Cook *et al.*, 2002, De Miranda *et al.*, 2002, Foltyn *et al.*, 2005). To verify the ability of EDTA to inhibit SR and stop the reaction, a 1 h time course (Fig. 3.9A) and L-serine Km (Fig. 3.9B) assays were performed in the presence of EDTA. The time course suggests 2 mM EDTA was more effective than 1 mM at stopping the reaction immediately, as indicated by some residual activity observed with 1 mM EDTA at 0 min but not 2 mM (Fig. 3.9A).

Enzyme activity was effectively abolished in the presence of EDTA (Fig. 3.9B), increasing the Km from 10.1 mM to a projected Km of > 200 mM. The luminescence signal appeared to be unaffected by the presence of EDTA. The substantial reduction in SR affinity for L-serine in the presence of EDTA (and thus, the absence of Mg^{2+}) reflects the obligatory requirement of divalent cations to sustain SR activity. It is thought that divalent cations potentiate the stimulatory effect of ATP (De Miranda *et al.*, 2002) and their binding to SR causes a conformational change in the tertiary structure that upregulates the catalytic activity of SR (Cook *et al.*, 2002).

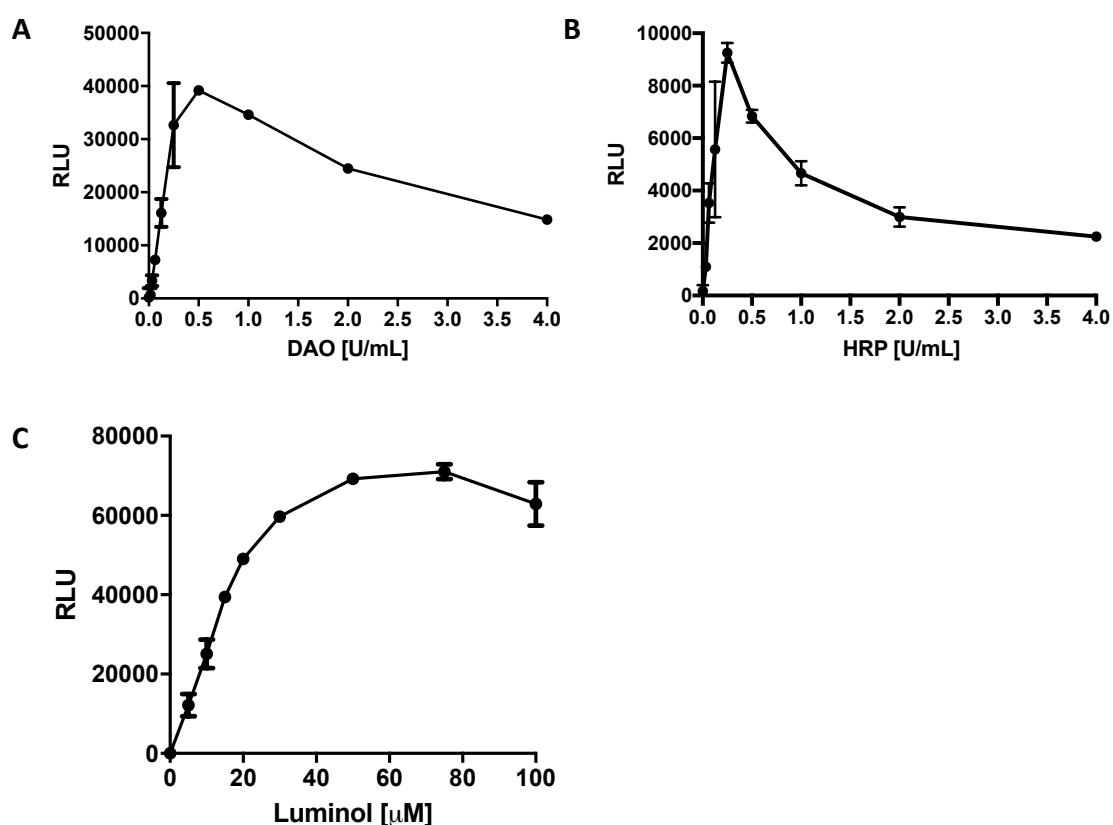


Figure 3.8. Concentration-response curves for DAO, HRP, and luminol to determine the concentrations at which they were in excess.

The racemisation of 5 mM L-serine to D-serine by 1 μ M SR is coupled to a chemiluminescence reaction that uses DAO, HRP and luminol to detect the D-serine produced, so these reagents must be non-limiting. Concentration-response curves for (A) DAO, (B) HRP, and (C) luminol were performed in the SR coupled assay, concentrations that elicited high signals were selected for subsequent experiments: 1 U/mL DAO, 0.5 U/mL HRP, and 50 μ M luminol. Experiments were performed in triplicate; data are the means from three (A and B) or two (C) experiments; error bars = SD.

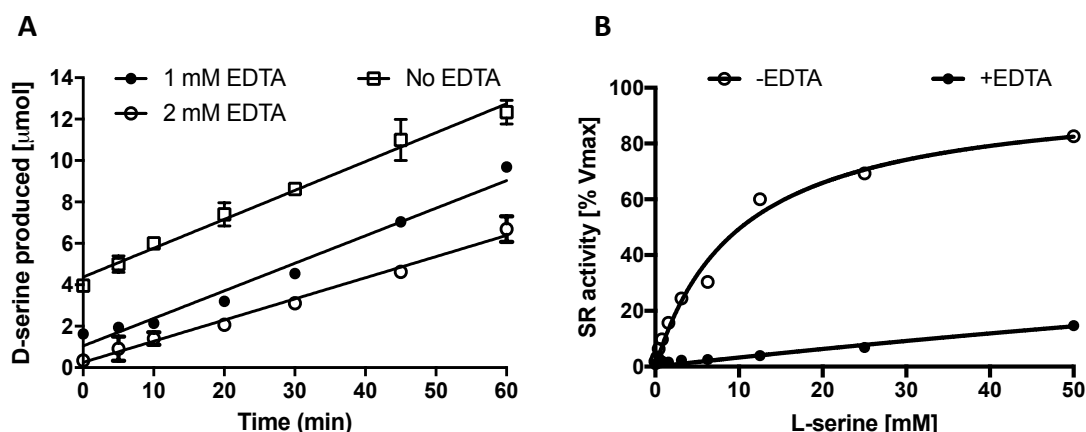


Figure 3.9. EDTA effectively inhibits SR to act as a reaction stop.

(A) A 1 h SR time course of L- to D-serine racemisation was performed, after which the reaction was stopped with either 1 mM or 2 mM EDTA and the D-serine produced was quantified by chemiluminescence reaction. EDTA inhibits SR racemisation by chelating Mg^{2+} required for structural stabilisation of SR. The increased background signal observed for 1 mM EDTA suggests there is some residual L-serine turnover with 1 mM EDTA after the reaction was stopped. (B) L-serine saturation curve performed in the presence of 2 mM EDTA increased the K_m from 10 mM to $>>200$ mM (projected), demonstrating the capability of EDTA to inhibit L-serine turnover by SR. Experiment performed in triplicate; gain = 0.5 s

3.4.9 Tris vs. phosphate buffer

It has been reported SR activity is increased in phosphate buffer in relation to Tris, which was attributed to a change in oligomer population as determined by gel-filtration chromatography. SR was found to be predominantly dimeric in phosphate buffer and monomeric in Tris buffer, and had higher activity in phosphate buffers potentially due to its similarity to physiological conditions (Wang and Barger, 2011). The profound effect prompted a comparison of Tris and phosphate buffer in a time course (Fig. 3.10), although the results illustrate the exact opposite effect. SR activity was much higher in Tris buffer compared to phosphate buffer, in disagreement with the Wang and Barger study. On the other hand, a later study also noted that phosphate did not elicit any relevant effect, and pyrophosphate actually abolished SR activity (Marchetti *et al.*, 2014), an effect that was attributed to chelation of Mg^{2+} by phosphate and pyrophosphate.

The discrepancy in effects between the published studies and Fig. 3.10 could be attributed to the different methodologies that were used and the influence they would have on oligomeric species formation. The Wang and Barger paper utilised a coupled chemiluminescence assay very similar to that used in the present study, with the additional inclusion of 0.2 mM DTT in the reaction buffer. The authors suggested DTT was a critical component in influencing the dominant oligomeric species of SR (and therefore, the activity they observed) by reducing the thiol group of critical cysteine residues and by breaking disulphide bonds that may impede correct folding. Moreover, they found that SR predominantly existed as the more active dimer when purified in phosphate buffer, and monomer when purified in Tris buffer. SR was purified in Tris buffer in the current study, and analytical SEC and crystallography indicated SR was mostly dimeric, not monomeric as described by Wang and Barger. A fundamental difference that may contribute to these contrasting results is that the assay of this study used mutant SR containing two cysteine point mutations. As cysteine residues play an important role in quaternary structure formation, it is probable the behaviour of mutant SR with respect to its oligomeric predisposition would not be comparable to the wild-type SR studied by Wang and Barger.

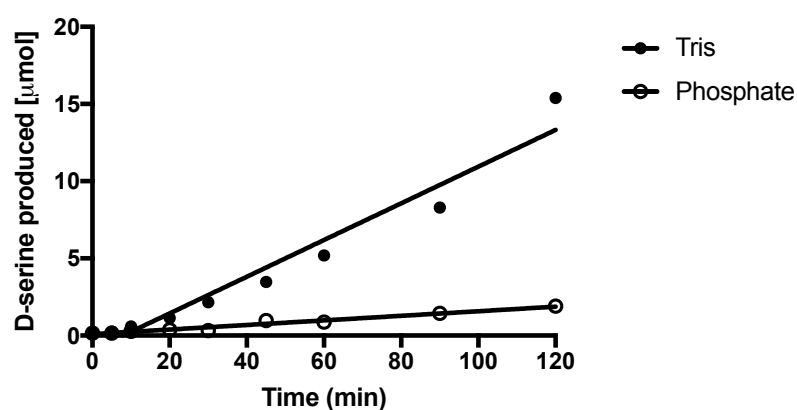


Figure 3.10. Influence of buffer components on SR activity.

A 2 h time course in the SR coupled assay was performed in Tris buffer (100 mM Tris-HCl pH 8.5) or phosphate buffer (100 mM sodium phosphate pH 8.5, 50 mM NaCl) supplemented with SR cofactors 1 mM Mg^{2+} , 1 mM ATP, and 10 μ M PLP. The data indicate that SR racemisation activity is greatly attenuated in phosphate buffer compared to Tris buffer. Experiments were performed in triplicate; $n = 2$.

3.4.10 Time-dependency experiment

Time course experiments were performed to identify the initial velocity region where less than 10% of the substrate had been converted to substrate. It is imperative reactions occur in this linear phase so the reaction is not limited by enzyme saturation, substrate depletion, or product inhibition. A 3 h time course of SR concentrations between 0.2–2 μM was performed (Fig. 3.11A) to determine the linear phase. Saturation occurred early with 2 μM SR whereas the other concentrations (0.2–0.5 μM) exhibited linear kinetics for a longer time period, suggesting it would be optimal to keep SR below 0.5 μM .

The position of the 2 μM plateau was used to estimate the point at which approximately 10% product had been formed. A 20 min time course was performed on two SR concentrations (200 nM and 400 nM) to analyse the linear phase in more detail (Fig. 3.11B). As it was desirable for SR activity to be as high as possible without sacrificing a practical initial velocity period, and because enzyme activity was negligible for up to 5 min with 200 nM SR, a concentration of 400 nM SR was selected for further experiments.

3.4.11 Determination of Michaelis-Menten constant, K_m

The initial velocity conditions established above were then used to generate a L-serine saturation curve to determine the K_m , according to the Michaelis-Menten kinetic model that defines the K_m as the substrate concentration at half the V_{max} . The L-serine K_m performed here (Fig. 3.12) was determined to be 10 mM for combined Batches 1–3, 9.2 mM for Batch 4, and 16 mM for Batch 5. All values were evidently in agreement, and also fell well within the range of reported L-serine K_m values of 10 mM (Wolosker *et al.*, 1999b) and 4.1 mM (Hoffman *et al.*, 2009b). The substrate concentration used must be around or below the K_m so that the velocity is sensitive to changes in substrate concentration, and relatedly, so that competitive inhibitors can be identified in IC_{50} experiments without being out-competed by excess substrate. The

K_m values obtained here were used as guidance when determining the optimum L-serine concentration.

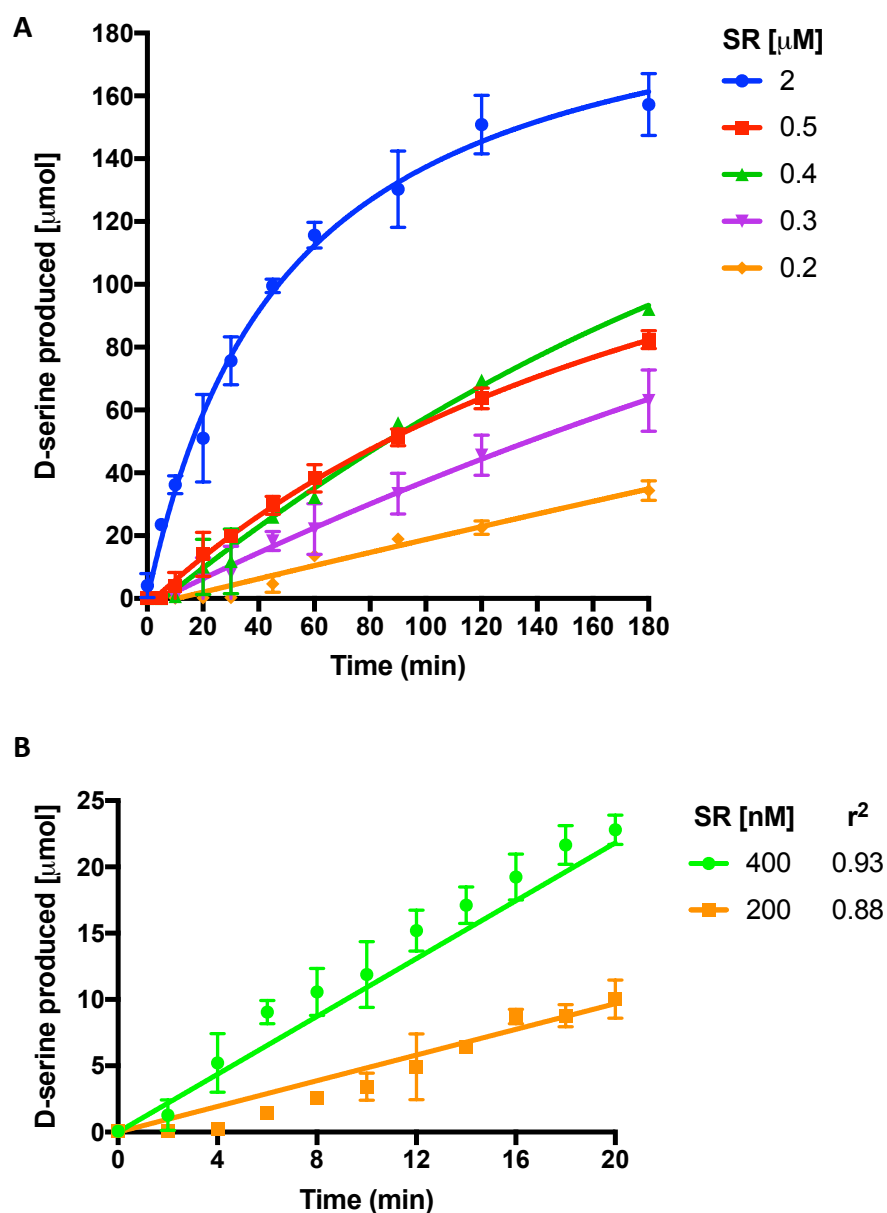


Figure 3.11. Time-dependency experiments with different SR concentrations.

D-serine produced by SR racemisation was quantified in **(A)** a 3 h timecourse, and **(B)** a 30 min time course. From the saturation level of 2 μM SR in **(A)**, the initial velocity region where $\sim 10\%$ substrate conversion occurred was estimated to be within 20 min. The time course in **(B)** focused on the initial velocity region, repeating two SR concentrations from **(A)**, and the reaction was found to be linear up to at least 20 min with 400 nM SR. Experiments were performed in triplicate; data are from three independent experiments ($n = 3$); error bars = SEM.

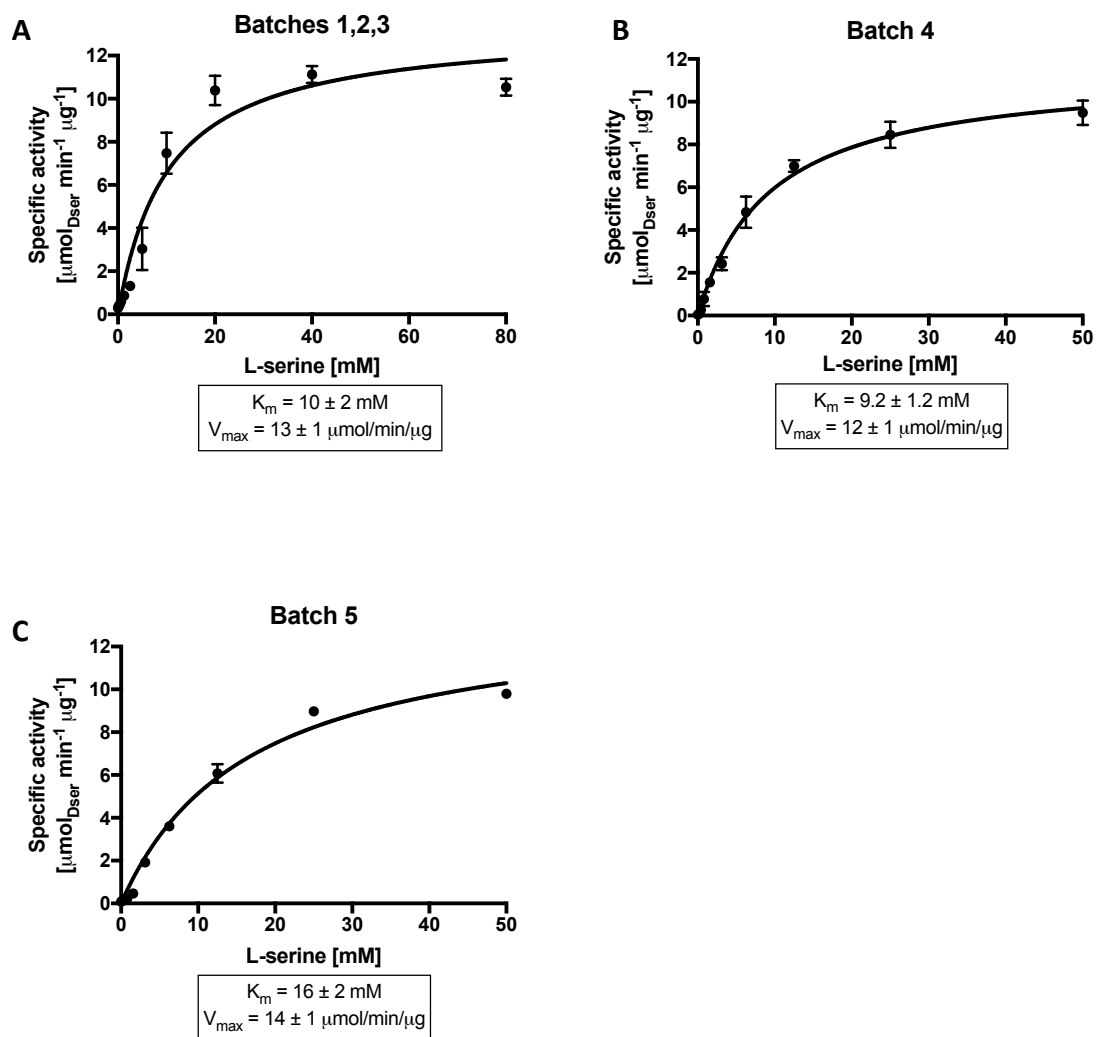


Figure 3.12. Michaelis-Menten plots of L-serine racemisation by SR.

An L-serine saturation curve was performed and Michaelis-Menten kinetics were used to calculate the K_m for (A) SR batches 1–3 (combined); (B) Batch 4; and (C) Batch 5. All K_m values (shown below each graph) were in agreement with each other, confirming reproducibility of the SR purification process. Experiments were performed in triplicate; data are from three independent experiments ($n = 3$); error bars = SEM.

3.4.12 SR tolerance to DMSO

Incubation of SR with increasing concentrations of DMSO revealed that SR was reasonably tolerant to DMSO, with a perceptible but minor reduction in enzyme activity occurring at concentrations from 2.5% DMSO. Importantly, SR activity was unaffected at DMSO concentrations required for single-point screening and biophysical validation methods (~1%). These data are shown in Fig. 3.13.

3.4.13 Determination of IC₅₀ values

IC₅₀ (inhibitor concentration which gives 50% inhibition) determination was carried out for the SR competitive inhibitor malonate at an enzyme concentration of 400 nM. IC₅₀ values were determined by plotting the percentage inhibition against log of inhibitor concentration. Because of its utility as a positive control when testing fragment screen hits and literature compounds, a great number of malonate IC₅₀ experiments have been performed throughout this study. A graph combining data from twelve independent experiments can be seen in Fig. 3.14A. The IC₅₀ of malonate determined from Fig. 3.14A was $63 \pm 5 \mu\text{M}$. This is in agreement with literature values of $67 \mu\text{M}$ (Vorlová *et al.*, 2015) and $25 \mu\text{M}$ (Katane *et al.*, 2013).

The competitive DAO inhibitor, benzoate (Mattevi *et al.*, 1996) was also assayed for its inhibitory potential because of its use as a control reference compound in the DAO counter screen (section 7.4.2). IC₅₀ determination was not performed for benzoate because the concentration of DAO in the chemiluminescence reaction was in excess and had not been optimised to be sensitive to substrate and inhibitor levels. Instead, the activity of DAO was tested with $10 \mu\text{M}$ D-serine in the presence of four concentrations of benzoate (10, 25, 100, $250 \mu\text{M}$). Fig. 3.14B shows inhibited DAO activity in relation to DAO activity with no inhibitor present. The percentage inhibition for $25 \mu\text{M}$ and $250 \mu\text{M}$ are satisfactory for use as 50% and 100% controls in the DAO counter screen following fragment screening.

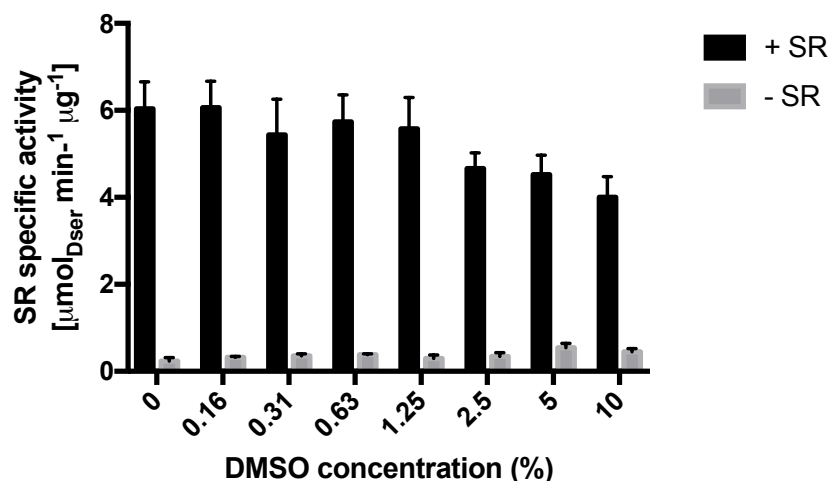


Figure 3.13. SR tolerance to dimethyl sulfoxide (DMSO).

SR was incubated with increasing concentrations of DMSO then the activity of SR was measured in the coupled enzyme assay. SR was found to be adequately tolerant to DMSO, including at concentrations required for fragment screening (~1%). Experiments were performed in triplicate; data are from three independent experiments ($n = 3$); error bars = SEM.

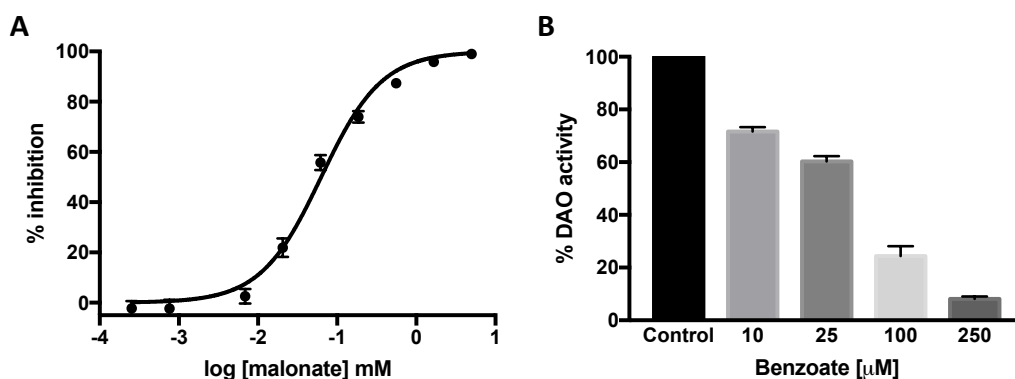


Figure 3.14. Inhibition of SR and DAO by control compounds.

(A) Inhibition of 400 nM SR by a concentration series of malonate between 0–5 mM; the IC_{50} of malonate was determined to be $63 \pm 5 \mu\text{M}$. (B) Inhibition of 1 U/mL DAO by benzoate in chemiluminescence reaction using 10 μM D-serine as a substrate; benzoate was able to sufficiently inhibit to levels required for fragment screen controls (50% and 100% inhibition). Bars represent percentage activity of DAO with benzoate in relation to a no-benzoate control. Experiments were performed in triplicate; data are from twelve (A) and three (B) independent experiments; error bars = SEM.

3.4.14 Optimisation of plate tests

The robustness of the automated SR assay was assessed by two plate tests. The first plate test studied the assay window between wells containing or omitting SR; the data from which were analysed by calculating the coefficient of variation (CV) and Z' scores of the positive and negative controls. These data are presented in Table 3.1.

Table 3.1. Percentage coefficient of variation (% CV) and Z' scores for positive (+ve) and negative (-ve) controls in plate test 1.

Interval time (s)	Read delay (min)	% CV (-ve)	% CV (+ve)	Z'
0.02	5	33.2	8.6	0.69
	10	35.5	9.0	0.67
0.1	5	19.4	9.9	0.57
	10	22.9	8.1	0.53
0.5	5	14.7	9.1	0.64
	10	19.4	8.1	0.68

After optimisation of the assay procedure, the luminescence signal was generally consistent across the plate with typically a 7–8-fold assay window. The Z' scores were above 0.5 for all interval times (the time taken by the reader to capture the luminescence signal of each well) and read delays (the time between adding Detection Solution and reading the plate). An acceptable % CV is considered to be around 10%, and the data for the positive controls of each condition tested all satisfied this criterion. The % CV was noticeably increased for the negative controls, increasing further as the interval time was reduced. Evaluation of the raw data and Z' scores suggested this effect was not a result of data variability, but instead can be attributed to the raw data values becoming smaller by ten- or twentyfold as the interval time was reduced. Low raw values mean the amount of variability relative to the mean is amplified, as small deviations result in a greater percentage deviation from the mean. Therefore, the % CV obtained here for the negative controls were not considered problematic.

The second plate test of malonate IC_{50} experiments was more difficult to optimise, because despite the experiments for plate test 1 resulting in satisfactory % CV and Z' scores, there was a great disparity between them and those for plate test 2. This observation was related to considerable variability in the signal measured in the positive control wells, specifically a decay in luminescence down the plate. Fig. 3.15A shows the luminescence signal of the malonate IC_{50} experiments with a 0.5 s interval time and 10 min read delay, and there is a clear spread of the top values that contributes to its extremely poor Z' of -0.4. Changing the read parameters of the PHERAstar to 0.1 s interval time with 10 min read delay (Fig. 3.15B), 0.1 s interval time with 5 min read delay (Fig. 3.15C), and 0.02 s interval time with 5 min read delay (Fig. 3.15D) successively improved the Z' to a final, far more satisfactory 0.55.

It was unclear why the control data for this plate test was so inconsistent. The main difference from plate test 1 was the introduction of the FluidX Xpp-721 liquid handler and manual pipetting of the control wells. Minor adjustments to the procedure (such as manually dispensing Detection Solution and ensuring thorough mixing) did not improve the Z' scores, and ultimately the signal decay was only mitigated by altering the reader parameters. As indicated by summary Table 3.2, the signal-to-noise ratio of the positive and negative controls was mostly unaffected by changing the parameters and remained around eightfold. The greatest variability occurred with the IC_{50} values of each plate (Table 3.2) which were much lower than those obtained manually. This effect was most pronounced for the read parameters in Fig. 3.15A, B, and C. The only protocol that generated IC_{50} values ($27 \pm 3 \mu\text{M}$) similar to those obtained manually ($63 \pm 5 \mu\text{M}$), as well as an acceptable Z' , was Fig. 3.15D. Both IC_{50} values do fall within a threefold range, although the discrepancy between the two values may be a result of SR stability being affected by automation. Hereafter, screening experiments were performed with a 0.02 s interval time and 5 min read delay.

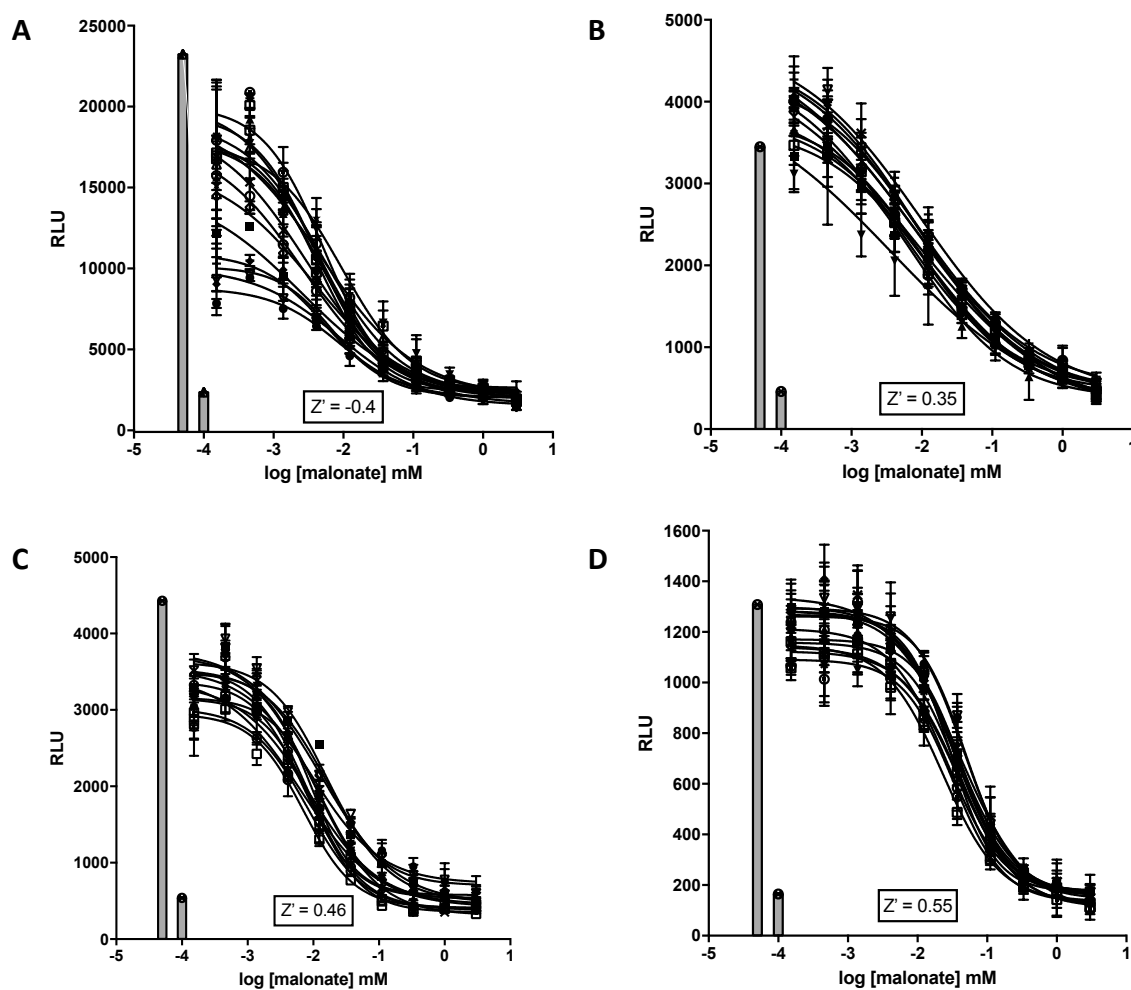


Figure 3.15. Effect of changing reader parameters on plate Z' scores.

Four independent plate tests of malonate inhibition curves were performed with (A) 0.5 s interval time and 10 min delay, (B) 0.1 s interval time and 10 min delay, (C) 0.1 s interval time and 5 min delay, and (D) 0.02 s interval time and 5 min delay. Z' scores were -0.4, 0.35, 0.46, and 0.55, respectively. Bars represent the maximum signal-to-noise ratio. Experiments were performed in duplicate; each graph shows 16 malonate inhibition curves performed in duplicate. Error bars = SD.

Table 3.2. Summary of plate test data from Figure 3.15.

The average IC_{50} values were calculated from 16 malonate inhibition curves generated per plate and were performed in duplicate. IC_{50} error = SEM.

Figure 3.15	Interval time (s)	Read delay (min)	Z'	Signal/noise	Average IC_{50} (μM)
A	0.5	10	-0.4	9.5	5.2 ± 0.5
B	0.1	10	0.35	7.5	19 ± 3
C	0.1	5	0.46	8.2	10 ± 1
D	0.02	5	0.55	7.9	27 ± 3

3.5 DISCUSSION

The purpose of this chapter was to develop and optimise a biochemical assay for quantifying SR activity that could be implemented for medium-throughput screening as part of a drug discovery strategy. The coupled assay is a classic method of measuring SR activity and there are many recent studies that have focused on this technique. It is versatile, relatively robust, and — as it has been demonstrated here — modifiable to be performed in a 384-well format. While the incorporation of a coupled assay in this study to measure SR activity must come with the caveat that it cannot be considered ‘gold-standard’ due to the multifunctional behaviour of SR, the determination of assay parameters that fall in line with published values certainly supports the technique as a method of SR characterisation. Moreover, the successful adaptation of the luminescence assay for use with automation fulfils the aims of this chapter and represents a novel means of screening SR that could have particular relevance for related drug discovery endeavours.

There were, however, limitations and challenges of the coupled assay. The multifaceted nature of the coupled assay meant there were multiple points at which the assay was susceptible to complications. For instance, as was discovered during optimisation with automation, the luminescence signal produced could be unstable and decline over time, possibly due to non-specific luminol luminescence. The apparent edge effect — that manifested as frequently failed plates (Z' below 0.4) — was mostly mitigated by reducing the interval time of the plate reader to 0.02 s, but it is possible the original problem was improperly identified.

The edge effect observed in the automated assay could potentially be attributed to the following factors. The activity of purified protein is difficult enough to maintain outside of their cellular environment, no matter what steps are taken to reproduce it. The manual assay certainly seemed robust, but it is possible that incorporating extra liquid handling equipment could have been the cause of the observed issues by introducing external sources of variability. More specifically, the process of dispensing through the

tubes of the Multidrop (in which enzymes and other reagents can get blocked or react with the plastic), dispensing with the tips of the liquid handler (which may accumulate contaminants over time), and the fans inside the liquid handling cabinet causing an uneven temperature distribution across the plate. Performing the assay at room temperature, far from the temperature of the physiological environment (37 °C) may have meant SR was more susceptible to destabilisation when there were deviations from the standard assay procedure.

It was taken for granted that all D-serine produced in the assay would be consumed by DAO in the incubation time given, but it has been documented that porcine kidney has a high K_m for D-serine (41 mM) therefore it is possible that the chemiluminescence reaction had not proceeded to completion. Although, this was unlikely to be a contributing factor at the low levels of D-serine being produced by SR and with DAO in excess. The greater challenge would be that multiple time points and incubation periods had to be incorporated in the coupled assay, which can be difficult when measuring enzyme kinetics that depend on accurately quantifying the rate at which product was produced.

Although D-serine calibration curves were used to calculate the specific activity of SR, and DAO is known to produce equimolar amounts of H_2O_2 from D-serine degradation (Pernot *et al.*, 2008), assumptions had to be made regarding the precise stoichiometry of H_2O_2 produced with D-serine, whether the production of H_2O_2 was linear, and the possibility of H_2O_2 fluctuations within the assay system. Nonetheless, the fact the assay data produced in this chapter, such as L-serine K_m and malonate IC_{50} , agree with data from analogous assays (Smith *et al.*, 2010), as well as different assay methods such as HPLC (Cook *et al.*, 2002), capillary electrophoresis (Singh *et al.*, 2012), and UV-absorbance assays (Nelson *et al.*, 2017), suggests the assay described here is reliable and capable of generating accurate data.

As with any technique, the SR coupled assay has its caveats, but these do not negate its overall utility. To begin to characterise purified SR with respect to published information, and to have a method for low- and medium-throughput screening of SR,

the coupled assay serves its original purpose and was demonstrably robust and reproducible. However, it is also important to employ additional orthogonal assays in conjunction with methods that indirectly quantify enzyme activity. To this end, three biophysical assay techniques — thermal shift, MST, and ITC — were optimised as methods to validate data obtained biochemically, and will be detailed in the next chapter. To summarise, the factors optimised during assay development are presented in the Table below.

Table 3.3. Summary of factors determined during optimisation of the SR coupled biochemical assay.

Parameter	Outcome
Detection system	Luminol preferred to AmpLite
Buffer system	Tris 100 mM
Buffer components	0.05% Pluronic F-127, 1 mM MgCl ₂ , 1mM ATP, 10 µM PLP
pH optimum	8.5
Incubation temperature	Room temperature
DTT inclusion	Not included, attenuates assay
Racemisation incubation period	20 min
Plate reader settings	Gain = 2500, interval time = 0.02 s
[SR]	400 nM
[L-serine]	2 mM
[EDTA]	2 mM
[DAO]	1 U/mL
[HRP]	0.5 U/mL
[Luminol]	50 µM

4 RESULTS III: BIOPHYSICAL METHODS

4.1 INTRODUCTION

The SR biochemical assay optimised in the previous chapter has proved very useful for characterising SR activity and stability, as well as providing the means of medium-throughput screening required for a fragment-based drug discovery approach. Complementary to biochemical assays, which assess enzyme activity, are the biophysical techniques that characterise binding events between proteins and ligands. Biophysical methods serve to confirm binding of hits with unknown mechanisms of action that are generated from biochemical screening; hits that could be demonstrating inhibition via off-target activity or protein destabilisation. The biophysical techniques outlined in this chapter — thermal shift, MST, and ITC — each have their own merit and generate different types of information that can contribute to the overall understanding of how inhibitors bind to SR. They are explained in detail in the following sections.

4.1.1 Thermal shift

Thermal shift quantifies the change in thermal denaturation temperature (or melting point) of a protein when exposed to different conditions — the obvious example being compound addition, but may also refer to something as simple as pH changes or as complex as protein mutations. Successful binding of the protein to a ligand can increase its thermal stability (Koshland, 1958), causing a curve shift to the right, while ligands that have a destabilising effect would cause a shift to the left. The thermal shift (also known as thermofluor) assay described in this chapter utilises the fluorescent dye SYPRO Orange (Lo *et al.*, 2004), which binds non-specifically to hydrophobic surfaces and is quenched by water. As the temperature is gradually increased, the protein unfolds and exposes more hydrophobic residues that bind the dye, expelling water and

increasing the fluorescence. Eventually the protein will start to aggregate and the dye will dissociate. By measuring the fluorescence at each temperature increment, curves can be plotted for both the protein and protein/ligand to assess its stability and find its melting temperature (T_m , the midpoint of the curve). Representative thermal denaturation data are presented in Fig. 4.1.

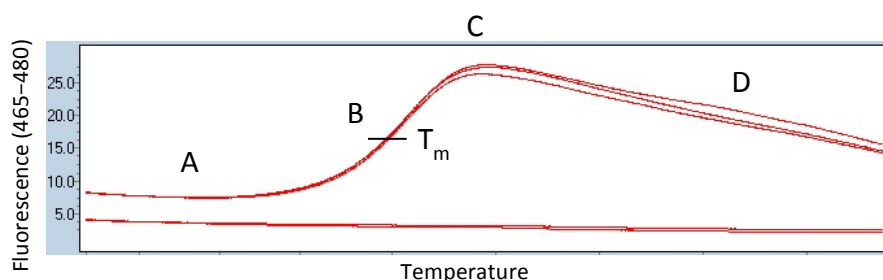


Figure 4.1. Example trace from a thermal shift experiment using a Roche LightCycler®.

(A) Protein melting as temperature increases; (B) dye binds to internal hydrophobic residues; (C) fluorescence peak; (D) protein aggregation and dye dissociation. Flat red line = negative (no protein) control. T_m = melting temperature.

The 96-well format of thermal shift assays made it suitable for screening small libraries of compounds and hit molecules to assess their effect on protein stability. Thermal shift is a limited biophysical approach because it cannot determine K_D or stoichiometry, it is target-dependent, and it does not always definitively indicate a binding event. For instance, results can be obscured by protein denaturation to fibrils (which interferes with the fluorescence emission), high background signal due to the fluorophore binding to the protein in its native state, or an insufficiently hydrophobic core (Grøftehaug *et al.*, 2015). The advantage of thermal shift over MST and ITC is the ability to infer whether compounds destabilise or bind to the protein of interest.

4.1.2 Microscale Thermophoresis (MST)

Microscale Thermophoresis (MST) is a technique used to analyse the interaction of biomolecules. The principle of the assay is based on inducing a microscopic

temperature gradient with an infrared laser, and the directed movement of molecules along that temperature gradient is quantified by covalently attached dyes, fluorescent fusion proteins or intrinsic tryptophan fluorescence. Changes in the hydration shell, charge, or size of the molecules, and the reciprocal fluorescence that is detected, can be indicative of a binding event, whether it be small molecules to proteins, complex protein-protein interactions, ligands to enzyme, or with other biomolecules such as liposomes and DNA (Jerabek-Willemsen *et al.*, 2011). A representative MST experiment is presented in Fig. 4.2.

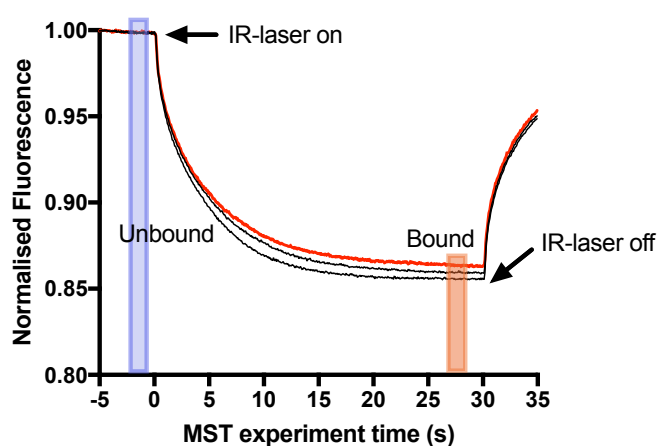


Figure 4.2. Example trace from an MST experiment using a NanoTemper Monolith NT.115.

The molecules begin by being homogeneously distributed and a constant 'initial fluorescence' is detected. When the infrared laser is activated, the 'T-jump' occurs, in response to the rapid change in fluorophore properties as the temperature quickly changes. The thermodiffusion of the fluorescently labelled molecules can be detected (for approximately 30 s), usually away from the heat source but occasionally towards it. Once the laser is deactivated there is a rapid mass diffusion of the molecules back into their previously occupied space. The change in thermophoresis is expressed as the change in normalised fluorescence, which is then used to calculate the F_{norm} , defined as $F_{\text{hot}}/F_{\text{cold}}$, where 'F' is the average fluorescence value at the orange ('hot') and blue ('cold') markers. Different F_{norm} values are achieved from the thermophoretic movement of the 'unbound' (black trace) and 'bound' (red trace) fluorescent molecule, which can then be plotted to obtain a binding curve.

The MST signal quantifies changes in normalised fluorescence, which is then used to calculate the F_{norm} (see Fig. 4.2). F_{norm} is defined as $F(\text{bound or 'hot'})/F(\text{unbound or 'cold'})$ where 'F' is the average fluorescence value at the bound and unbound states. All values are multiplied by a factor of 1000, giving a relative fluorescence change per

thousand. Differences in normalised fluorescence of the bound and unbound state will allow the fraction bound to be determined and thus the dissociation constant.

The sensitivity of MST means binding events can be detected without an increase in size or mass upon complex formation, making it advantageous over other fluorescence techniques such as thermal shift, which require large amounts of protein and are unable to analyse more than one type of interaction (Masi *et al.*, 2010). These features make MST an attractive technique for investigating binding between SR and fragment hit molecules, especially if the manner in which they bind is unknown, and they do not dramatically change the size of the complex or its hydration shell.

4.1.3 Isothermal Titration Calorimetry (ITC)

ITC is a highly sensitive technique used to study interactions between biomolecules by directly measuring the heat either released or absorbed during a biomolecular binding event, which it does upon gradual titration of the ligand into the sample cell containing protein. The instrument also has a water-containing reference cell, and it keeps these two cells at exactly the same temperature. If binding occurs upon each injection of ligand, heat changes are detected and measured to a sensitivity of a few millionths of a degree, and this continues until binding has reached equilibrium. The differential power (DP) is a measurement of the power differential between the reference and sample cells necessary to maintain their temperature difference at close to zero. A representative ITC experiment is shown in Fig. 4.3.

ITC does not rely on immobilisation and unlike MST, does not require labelling of the binding partners, meaning they are tested in their native state. ITC produces an impressive breadth of thermodynamic information such as the K_D , the reaction stoichiometry (n), enthalpy (ΔH), and entropy (ΔS), which can all be simultaneously measured in a single experiment. The capabilities of ITC means it is often considered the gold-standard for quantitative measurements of biomolecular interactions, and is therefore a powerful tool in drug discovery and lead optimisation processes.

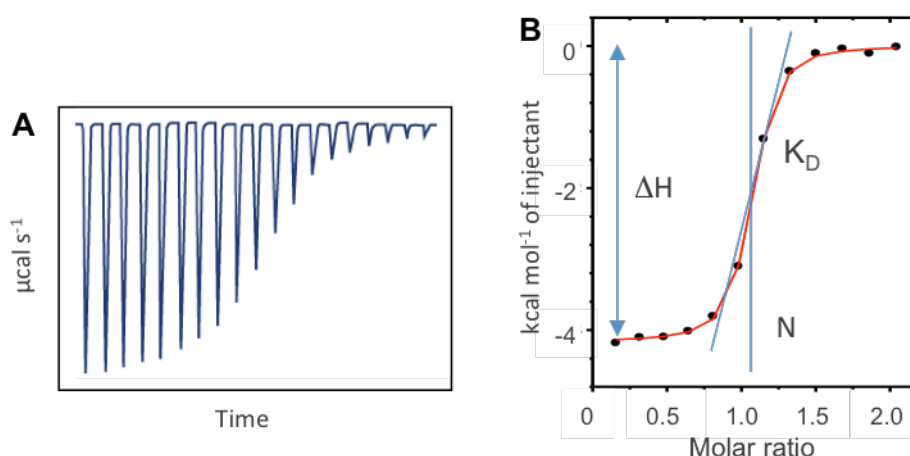


Figure 4.3. Fundamentals of an ITC experiment.

(A) With the first injection of low-concentration ligand in the syringe into the cell containing protein, all of the injected ligand becomes bound to the protein. The downward peak in the signal indicates that the reaction is exothermic, meaning the sample cell becomes warmer than the reference cell. The signal returns to its starting position as the temperature of the two cells returns to equal. This process is repeated, and with each injection the protein becomes more saturated with ligand as the molar ratio between the two increases, so less binding occurs and the heat changes start to decrease. Eventually the protein will become saturated and the ligand will be in excess, so only the heat of dilution peaks are observed. (B) The area of each peak is then integrated and plotted against the molar ratio of ligand to protein, from which the K_D , stoichiometry (N), and binding mechanism can be determined.

The purpose of this chapter was to optimise the three biophysical techniques described above, and authenticate their suitability for an SR drug discovery strategy using the tool inhibitor malonate. The ultimate aim was to use an integrated biophysical approach of thermal shift, MST, and ITC, to validate binding of the 61 hits identified from the biochemical fragment screen and to build a biophysical profile of any promising candidates for hit-to-lead development.

4.2 MATERIALS

4.2.1 Reagents

Reagent	Supplier (product code)	Stock concentration
Serine racemase	Purified in-house	Various
Sodium malonate	Sigma-Aldrich (63409)	100mM or 1M
Malonic acid	Sigma-Aldrich (M1296)	100mM or 1M

4.2.2 Buffers and solutions

Buffer	Compounds	Supplier (product code)	Concentration
Thermal shift buffer	CHES pH 8.5	Sigma-Aldrich (C2885)	100mM
	Magnesium chloride	Sigma-Aldrich (M2393)	1mM
	ATP	Acros Organics (102800100)	1mM
	PLP	Sigma-Aldrich (P9255)	10μM
MST buffer	Tris-HCl pH 8.5	Sigma-Aldrich (154563)	100mM
	Pluronic F-127	Sigma-Aldrich (P2443)	0.1%
	Magnesium chloride	Sigma-Aldrich (M2393)	1mM
	ATP	Acros Organics (102800100)	1mM
	PLP	Sigma-Aldrich (P9255)	10μM
MST denaturation solution	SDS	Sigma-Aldrich (L3771)	10%
	DTT	Fisher Scientific (BP172)	2mM
ITC dialysis buffer	Tris-HCl pH 8.5	Sigma-Aldrich (154563)	100mM
	Magnesium chloride	Sigma-Aldrich (M2393)	1mM
	ATP	Acros Organics (102800100)	1mM
	PLP	Sigma-Aldrich (P9255)	10μM
	DMSO	Fisher Scientific	0.5% or 1%, if required

4.2.3 Further materials, equipment and kits

Equipment	Supplier/manufacturer (product code)
SYPRO Orange 5000X	ThermoFisher Scientific (S6650)
LightCycler® 480 Multiwell plate 96	Roche (04729692001)
LightCycler® 480 sealing foil	Roche (04729757001)
LightCycler® 480	Roche (n/a)
Monolith™ Protein Labeling Kit RED-NHS (Amine Reactive)	NanoTemper (MO-L001)
Monolith™ NT.115 MST Premium Coated Capillaries	NanoTemper (MO-K005)
Monolith™ NT.115 MST Standard Treated Capillaries	NanoTemper (MO-K002)
Premium capillary tray for NT.115	NanoTemper (MO-T001)
Monolith™ NT.115	NanoTemper (n/a)
Slide-A-Lyzer Dialysis Cassettes 10K MWCO	ThermoFisher Scientific (66385)
Hamilton® syringe 1 mL	Sigma-Aldrich (20740-U)
MicroCal PEAQ-ITC	Malvern (n/a)
NanoDrop 2000	ThermoFisher Scientific (n/a)

4.3 METHODS

4.3.1 Thermal shift

Thermal shift assays quantify the changes in thermal denaturation temperature (melting point, T_m) between the complexed and uncomplexed protein under varying conditions, such as the presence of conformational stabilisers (Pantoliano *et al.*, 2001).

CHES buffer was used for thermal shift assays because Tris, the buffer used during biochemical assay development (Chapter 3), cannot maintain pH with changes in temperature. Pluronic F-127 was omitted because detergents interfere with fluorescence by causing saturation of the signal.

Thermal shift experiments were performed in LightCycler 480 96-well plates (Roche) in a reaction volume of 20 μ L per well. Apart from in the initial optimisation steps, in which the concentrations of SR and SYPRO Orange were varied, all experiments required (per well) a final protein concentration of 1 μ M SR and final dye concentration of 5x SYPRO Orange (ThermoFisher Scientific). Compounds were added to the reaction mixture at a concentration of 100 μ M and fragments at 1 mM. Plates were centrifuged for 1 min at 500 rpm and sealed before being equilibrated briefly on ice, then thermal denaturation analysis was performed using a Roche LightCycler® 480 System.

4.3.2 MST

Assay procedure. MST experiments are conducted in small glass capillaries containing a solution of the fluorescently labelled protein and the ligand to be tested, and 16 capillaries could be loaded onto one sample tray. An infrared laser (emission wavelength 1480 nm) is directed at the capillary to induce a microscopic temperature gradient between 2–6 °C, during which the fluorophores are excited and their emitted

fluorescence is collected and measured. Purified SR was labelled using the MonolithTM Protein Labeling Kit RED-NHS (Amine Reactive; NanoTemper Technologies). The dye carries a reactive NHS-ester group that modifies primary amines in the amino acids of the protein, such as lysine.

All solutions of SR, malonate, and fragment inhibitors were prepared in Tris mix buffer (as with the biochemical assay), supplemented with 0.1% Pluronic F-127 (as recommended by NanoTemper) to limit adhesion to the capillaries. Binding confirmation of fragment molecule hits was carried out by first single-point screening the fragments at a concentration of 1 mM, and those that gave a significant response in MST were analysed again at multiple concentrations to derive binding constants (K_D). For determination of the K_D , a 10-point 1:2 dilution series of test ligand was prepared in Tris mix buffer. Solutions of SR and ligand/inhibitor were combined in a 1:1 ratio to achieve final assay concentrations of 50 nM SR and 0–2 mM inhibitor. The positive control inhibitor, malonate, was included for single-point screening and K_D determination at a single concentration of 375 μ M. A negative control comprising Tris mix buffer and 1–2% DMSO was also included in each experiment.

Once SR and inhibitor were combined in 0.2 mL tubes (NanoTemper), the tubes were incubated for 10 min at RT then centrifuged at 13 000 rpm for 3 min. Samples were transferred into a capillary by inserting the capillary into a tube and letting it fill by capillary action. Each ligand was tested in duplicate. Once all capillaries had been inserted into the sample tray, it was loaded into the NanoTemper Monolith NT.115 machine and left to equilibrate for 5 min.

When reading the capillaries, the MST analysis settings were the default recommended by NanoTemper. The LED power was set to 35% and the MST power to 40%. A capillary scan was performed prior to each MST measurement (Fig. 4.4).

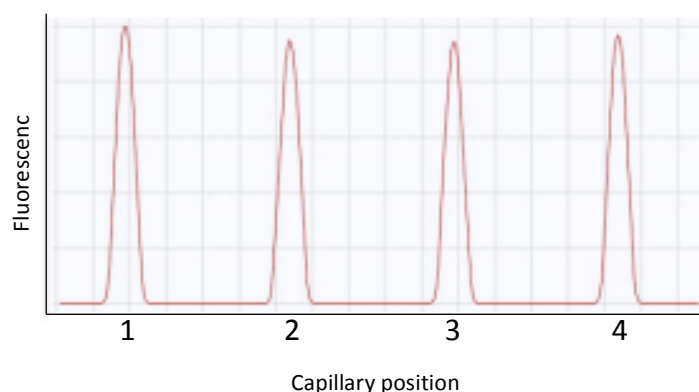


Figure 4.4. Example capillary scan from a NanoTemper Monolith NT.115.

Once the samples are placed on a tray and inserted into the instrument, a fluorescence scan is performed across the capillaries to accurately determine the position of the capillaries and assess the quality of the sample. The fluorescence from the capillary scan should be between 200–1200 counts, and the trace should show equal-sized symmetric peaks. Dips or shoulders in the peaks are indicative of adhesion of the sample to the capillaries, precipitation, or faulty technique (e.g. improper mixing).

Aggregation and denaturation controls. To rule out aggregation artefacts during K_D determination, each MST measurement was repeated on the original capillary set after a 45 min incubation period. An MST signal that was mostly unchanged suggested the inhibitors were not causing aggregation of SR. For the denaturation control, the SR and inhibitor mixtures were combined with denaturation solution (5% SDS + 1 mM DTT) and heated at 95 °C for 10 min. The tubes were then centrifuged at 13 000 rpm for 3 min, loaded into the capillaries, and the MST experiment was repeated. If upon denaturation the fluorescence of the samples was restored to an equal value across the dilution series, it indicated the changes observed were protein-dependent and could therefore be attributed to a binding event, rather than being caused by sample loss due to adsorption or precipitation. If fluorescence remained, it would not be possible to analyse the thermophoresis signal as it would be biased by different fluorescence intensities of the bound and unbound molecules.

Data interpretation. The initial fluorescence of each peak from the capillary scan should not vary by more than 10%; strong random variations suggest samples are not well mixed, dilutions are imprecise, or buffer conditions need to be optimised.

Moreover, adhesion to the capillaries is evident in the capillary scan by dips or shoulders in the peaks. Bumpy traces or increased noise in the thermophoresis signal indicates aggregation has occurred.

Data from the MST and Fnorm traces were exported as raw data and plotted using Graphpad Prism. K_D calculations were performed with NanoTemper MAO.Affinity Analysis software.

4.3.3 ITC

Dynamics of the ITC experiment. Obtaining a complete binding curve is heavily dependent on the stoichiometry of protein and ligand in relation to the K_D of the ligand, and their relationship is quantified by the equation $c = [\text{Protein}]/K_D$, where c is the product of the predicted affinity of the system and is used to determine the optimal protein concentration (Duff *et al.*, 2011). The c value of the system is considered very good when between 10–100, good between 5–500, fair between 1–5 and 500–1000, and not suitable when < 1 and > 1000 . Adjustments to either the protein or ligand concentration can be made based on the c value to drive the system towards or away from saturation. As a starting point, the concentration of the ligand should be 7–25-fold more concentrated than the K_D for the weakest ligand-binding site, so that saturation occurs in the first third to half of the titration.

Two types of ITC experiment were utilised in this study. The first, to determine the K_D of malonate, was simply a titration of malonate into the sample cell, which itself contained either buffer (for the heat of dilution control) or SR (for the binding experiment). The second, for assessing binding of the fragment hits, was a displacement experiment, which was incorporated to account for the very weak binding (≈ 1 mM) of the fragment molecules. These assays allow for interactions between weak binders and a target to be indirectly measured via their ability to displace a stronger binder. Displacement assays were performed by titrating malonate

(strong binder) into the sample cell, which contained either SR alone (for the control) or SR with fragment (weak binder, for the displacement experiment).

Dialysis. The heat sensing devices of the calorimeter are ultra sensitive to changes in heat and will detect heat of dilution as well as binding heats. For this reason, all solutions needed to be in the exact same buffer. Prior to an ITC experiment, up to 500 μ L SR stock was dialysed overnight in 1 L ITC dialysis buffer (Tris mix buffer, with no Pluronic F-127) using Slide-A-Lyzer dialysis cassettes with 10 kDa molecular weight cut-off (ThermoFisher Scientific). The SR concentration was measured by NanoDrop after dialysis to account for some protein loss and buffer equilibration. The dialysis buffer was also used to make all working solutions of SR and inhibitor.

Assay procedure. SR was tested at concentrations of either 50 μ M or 100 μ M. Concentrations were adapted during optimisation based on the fit of the curve and the c value. For malonate-only binding experiments, 0.5 mM or 1 mM malonate was prepared from 100 mM malonate stock in 100% DMSO. For displacement experiments, a mixture of 100 μ M SR and 1 mM fragment inhibitor was prepared for the cell sample, and a 1 mM solution of malonate for the syringe sample. The DMSO concentration of the cell and syringe samples had to be identical (usually 0.5% or 1% depending on ligand dilution).

ITC experiments were performed on a MicroCal PEAQ-ITC instrument (Malvern). The sample cell was loaded with 300 μ L SR solution (or SR + fragment mixture). For control experiments to check the heat of dilution, the sample cell was filled with dialysis buffer. Care was taken when loading the cell to avoid bubble formation; bubbles at the bottom of the cell could be released by gently knocking the sides of the cell with the Hamilton syringe. The injection syringe was then loaded with the malonate solution and lowered into the cell.

The experimental parameters were set at 13 injections, 25 °C. Before the injections begin, the calorimeter undergoes an equilibration phase where the differential power is adjusted to as close to 10 μ cal/s as possible. If the equilibrated DP deviated from this

by more than 2 $\mu\text{cal/s}$, the experiment was paused and the reference cell refilled. The first injection was always small ($\sim 2 \mu\text{L}$) to account for some mixing between the protein and ligand solutions in the injection syringe once it is inserted into the sample cell. This artefactual data was always discarded.

Data analysis. Data analysis was performed using the associated MicroCal ITC Analysis software. Experimental data was loaded and firstly the injection trace was checked for any signs of air bubbles or artefacts in the signal. These are characterised by spikes or peaks in the baseline where injections did not occur. The baseline was adjusted to account for aberrant peaks, and artefactual data was removed. If a heat of dilution control experiment was performed first, the adjusted data was subtracted from the binding experiment with SR and malonate.

Data fitting models were applied depending on the experiment performed: one-binding site (for K_D determination of malonate) or competitive binding (for analysis of fragment hits). In the case of the latter, parameters from the control experiment (such as malonate K_D , enthalpy, and n) were automatically entered. As the stoichiometry of malonate to SR is known to be 1:1 from crystallographic observations, the 'N' value was fixed to 1.

4.4 RESULTS

4.4.1 Thermal shift: protein and dye concentration

The thermal shift assay required few optimisation steps, namely determination of the protein and dye concentration, and a DMSO tolerance to account for the addition of compounds.

To find the optimum concentrations of SR and dye, an initial screen was performed with increasing concentrations of enzyme (0.16, 0.3125, 0.625, 1.25, 2.5, 5 μ M) and SYPRO Orange dye (2x, 5x, 10x, 20x). The thermal denaturation curves for the conditions tested with their corresponding melting temperatures are shown in Fig. 4.5.

The higher concentrations of SR (2.5 μ M and 5 μ M) appear to cause fluorescence quenching, or at least yield fluorescence signals that are beyond the scale of the graph at dye concentrations of 5x and 10x. For this reason, and based on the shape and size of the remaining curves, an enzyme concentration of between 0.625 μ M and 1.25 μ M was deemed sufficient. For convenience, a final SR concentration of 1 μ M was selected for subsequent thermal shift experiments. Although 2.5 μ M SR did not saturate the signal when in the presence of 2x dye, ideally the protein concentration would be kept low to reduce depletion of enzyme stocks. Increasing the concentration of dye appears to have a detrimental effect on the strength of the fluorescence signal, which is damped for all but the highest SR concentrations as the level of dye increases to 10x and 20x. Of the two remaining dye concentrations, 2x and 5x, a greater signal was achieved for 1.25 μ M in the presence of 5x dye, therefore this concentration was selected.

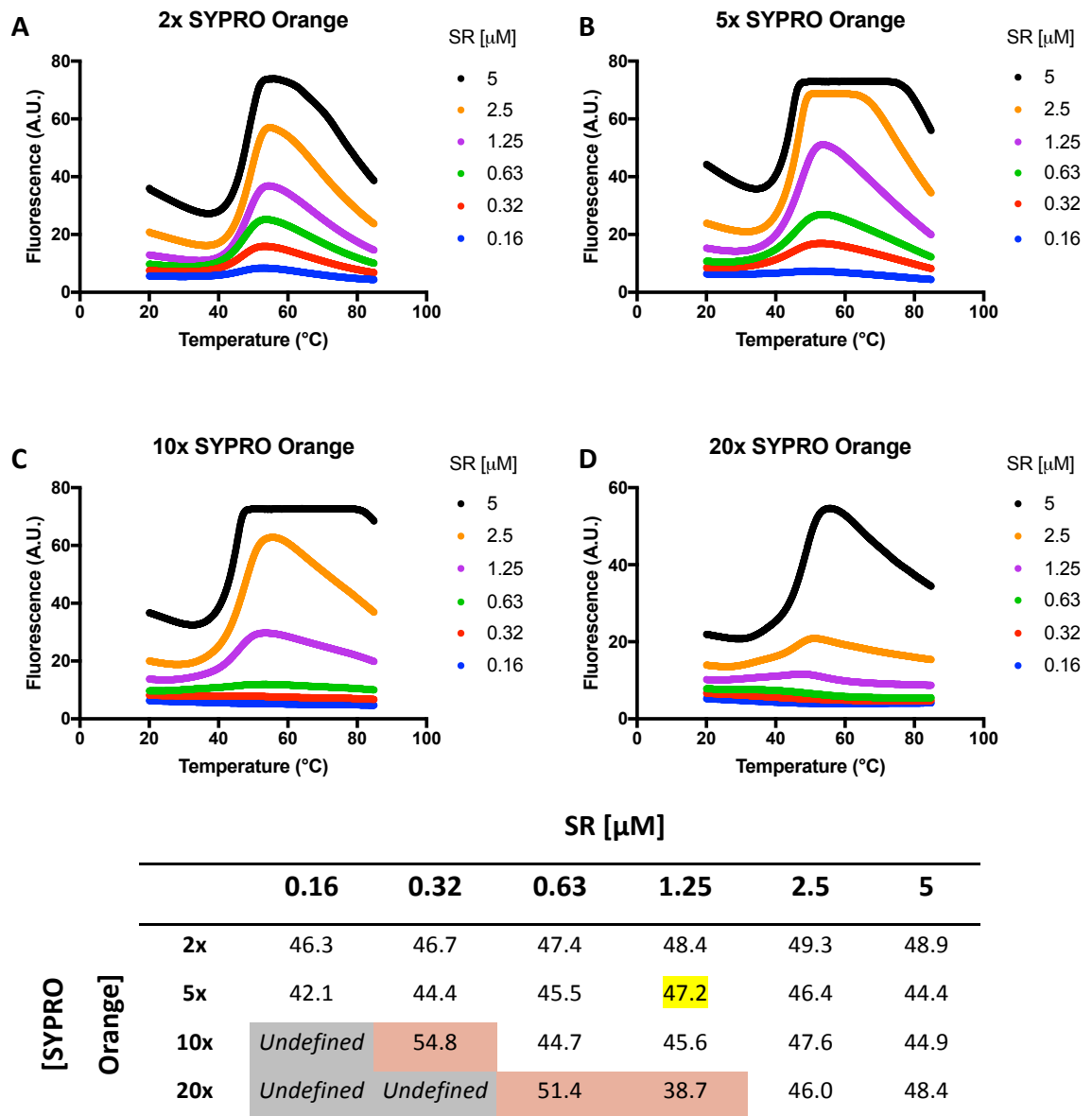


Figure 4.5. Optimisation of SR and dye concentrations for the thermal shift assay.

(A) Thermal denaturation curves of six concentrations of SR (0.16, 0.3125, 0.625, 1.25, 2.5, 5 μM) and four concentrations of SYPRO Orange dye (2x, 5x, 10x, 20x) to determine the optimal conditions for a fluorescence signal. Flattening of the peaks indicates signal saturation has occurred. Optimal fluorescence signals are obtained at 2x or 5x dye and 1–2 μM SR. For subsequent thermal shift assays, 5x dye and 1 μM SR were used. (B) Melting temperatures of SR in each of the conditions in (A). Orange boxes are artefactual data caused by excess dye inhibition. Optimal conditions are highlighted in yellow. Each datum is the mean of four replicates.

4.4.2 Thermal shift: DMSO tolerance

As with the biochemical assay, a DMSO tolerance assay was required to ensure the thermal shift assay was tolerant up to at least the DMSO concentration introduced by dissolved compounds (1%). Thermal denaturation analysis was performed on SR in the presence of increasing concentrations of DMSO (0–10%) and the denaturation curves are presented in Fig. 4.6 with the corresponding SR melting temperatures. Although the peak fluorescence signal was marginally increased for a few DMSO concentrations, the T_m values were consistent across the dilution series. As DMSO can improve the solubility of proteins, the variations in peak fluorescence may have been caused by DMSO increasing the solubility and therefore the level of available and active protein in the experiment.

4.4.3 Thermal shift: Malonate binding stabilises SR

Thermal denaturation analysis was performed on 1 μ M SR in the presence of 1 mM malonate and 1 mM L-serine to observe effects on protein stabilisation (Fig. 4.7). The T_m of SR alone was determined to be 47.4 ± 0.5 °C, with malonate 53.8 ± 0.4 °C, and with L-serine 44.6 ± 0.8 °C. These data give thermal shifts of +6.4 °C for malonate and -2.8 °C for L-serine. The positive thermal shift observed with malonate corresponds to stabilisation of the closed conformation of SR, which then requires a higher temperature to unfold the protein. The negative thermal shift with L-serine indicates increased instability, and may be a result of SR rapidly turning over L-serine (as opposed to L-serine simply binding in the active site, as with malonate) and therefore existing more frequently in an unstable intermediate state.

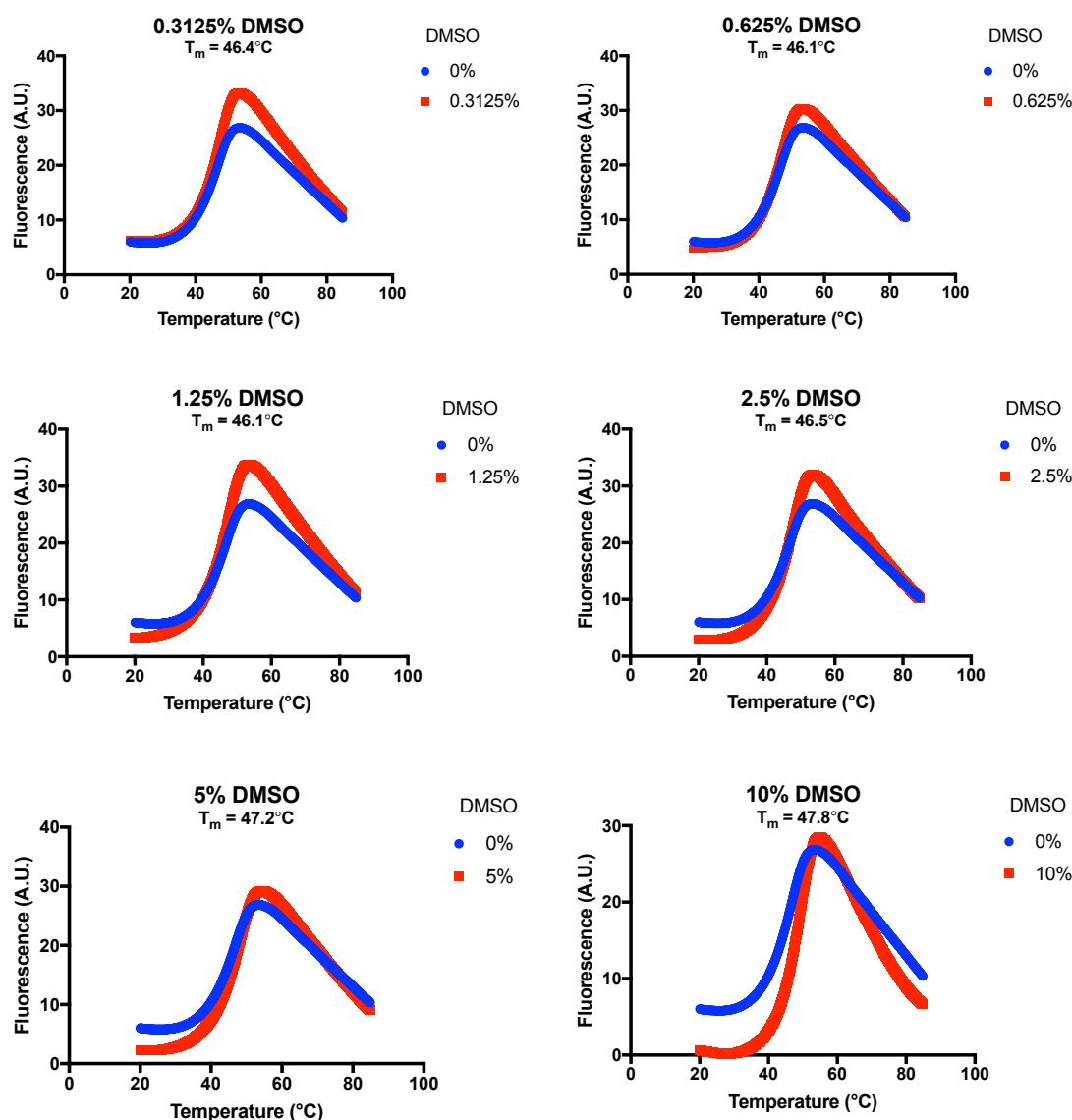


Figure 4.6. DMSO tolerance of SR in the thermal shift assay.

A dilution series of DMSO was prepared and included in the 20 μ L reaction mixture with 1 μ M SR and 5x SYPRO Orange dye. Select concentrations of DMSO (0.3125–2.5%) result in an increase in the peak fluorescence signal, but otherwise SR remains stable across the dilution series, as indicated by consistent T_m values. Experiments were performed in triplicate; data are from two independent experiments (n = 2).

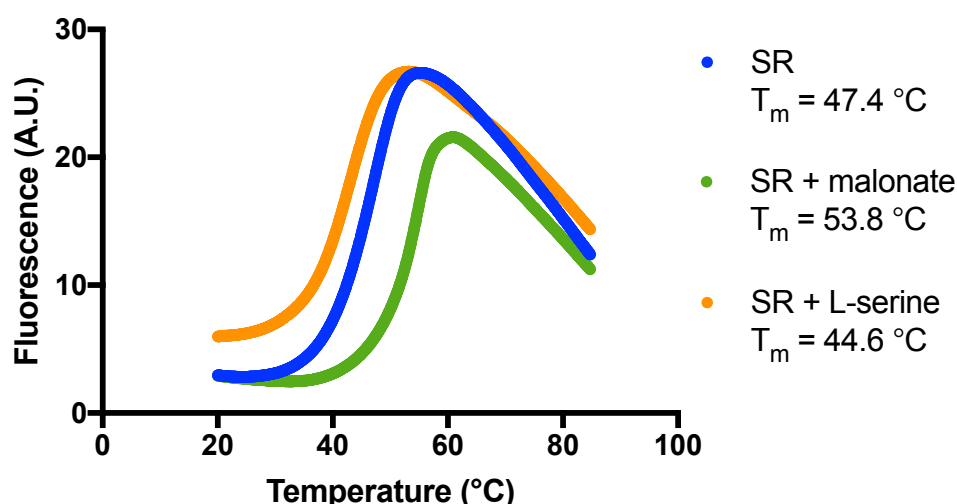


Figure 4.7. Thermal denaturation analysis of SR with malonate and L-serine.

Thermal denaturation analysis was performed on 1 μ M SR alone and in the presence of either 1 mM malonate or 1 mM L-serine. The T_m of SR in the presence of malonate increased from 47.4 ± 0.5 °C to 53.8 ± 0.4 °C, giving a thermal shift of $+6.4$ °C. In the presence of L-serine, the T_m of SR decreased to 44.6 ± 0.8 °C, giving a thermal shift of -2.8 °C. Experiments were performed in triplicate; data are from three independent experiments ($n = 3$).

4.4.4 MST: Influence of buffers and centrifugation

Initial optimisation steps involved performing scans of the capillaries and adjusting either the conditions inside the capillaries or the instrument settings to achieve a signal with an ideal size and quality for MST measurements. The fluorescence signal should be between 200–1200 counts and the shape of the peak should be a smooth peak with no shoulders or dips.

Protein has a tendency to aggregate within or stick to the capillary tubes in MST, so various buffers were examined for their ability to minimise this occurrence, as was the effect of centrifuging the protein sample prior to capillary loading. Capillary scans were performed with a total of eight conditions: four buffers, including the MST optimised buffer recommended by the supplier and the SR biochemical assay buffer; each either centrifuged or not centrifuged. The capillary scan trace with the corresponding buffer conditions is presented in Fig. 4.8.

Centrifuging the samples removes aggregated protein that can exacerbate surface adhesion, causing a subtle improvement in the shapes of the peaks between centrifuged and non-centrifuged samples. There was also clearly a higher fluorescence signal achieved with the SR buffer, which may be because of the presence of SR cofactors (PLP, ATP, Mg^{2+}) that stabilise folding, reducing aggregation and increasing the levels of free and active SR.

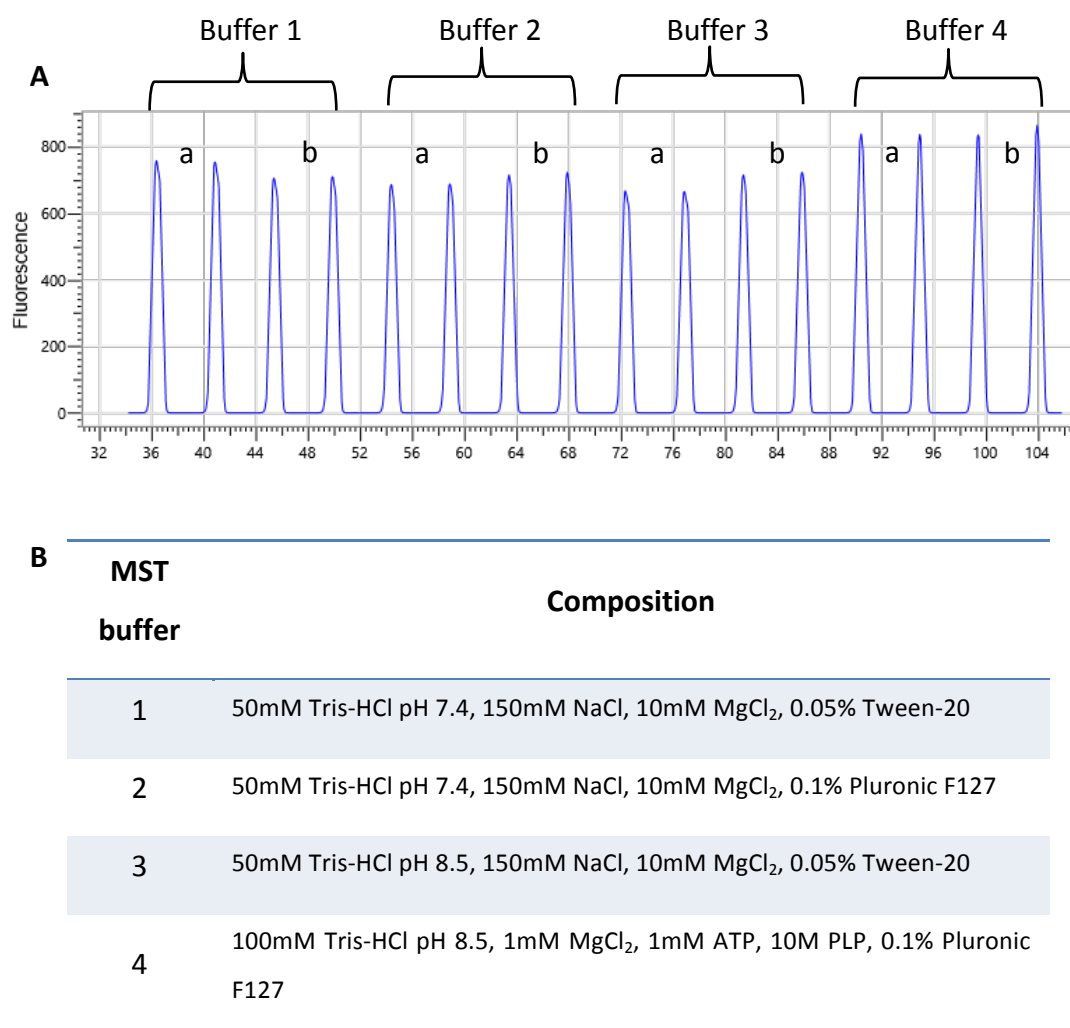


Figure 4.8. Capillary scan of four buffer conditions for MST assay optimisation.

The scan was performed using the NanoTemper Monolith NT.115 system (top trace) with SR in different buffer compositions (bottom table). Each buffer was tested with a protein sample that had either been centrifuged at 13 000 rpm for 5 min (**A**) or not centrifuged (**B**) prior to loading. Adhesion of protein to the capillary tubes is indicated by dips or shoulders in the peaks (e.g. as seen in Buffer 3a). Each condition was performed in duplicate, giving two peaks.

4.4.5 MST: Optimisation of software parameters

There are two variables within the software that require optimisation: the LED power and the MST power. The LED power is adjusted depending on the concentration of labelled molecule until the maximum fluorescence of the capillaries is between 200–1200 counts. The MST power is the power of the infrared laser that is used to induce the temperature gradient.

Initial experiments with SR and 1% DMSO at an LED power of 30% consistently gave a fluorescence signal within the optimum range at approximately 800 counts, so no further adjustments on this factor were deemed necessary. Following this, an MST experiment was performed with SR and 1% DMSO at three MST powers — 20%, 40%, and 60% (Fig. 4.9). The MST power selected was based on the data points that displayed the most consistency and a narrow assay window. The resulting data illustrated that 20% power produces a noisy signal (Fig 4.9A; blue trace), with a standard deviation of the fluorescence between capillaries of 2.9 (Fig. 4.9B; blue points). By comparison, the data for 40% and 60% were less variable, with respective standard deviations of 1.3 and 1.5 (Fig 4.9B; red and green points). The data for 40% were slightly tighter, so MST experiments were hereafter performed at 40% power.

4.4.6 MST: DMSO and malonate controls

The effect of the MST positive and negative controls (malonate and DMSO) on thermophoresis was examined using the previously established 40% MST power. The results (Fig. 4.10) suggest both controls could be consistently and reliably measured, and there was a clear F_{norm} shift of 12–15 counts when SR was present with 250 μM malonate. The size of this shift is in agreement with published values describing F_{norm} shifts up to 20 counts for MST analyses of protein-small molecule interactions (Jerabek-Willemsen *et al.*, 2011).

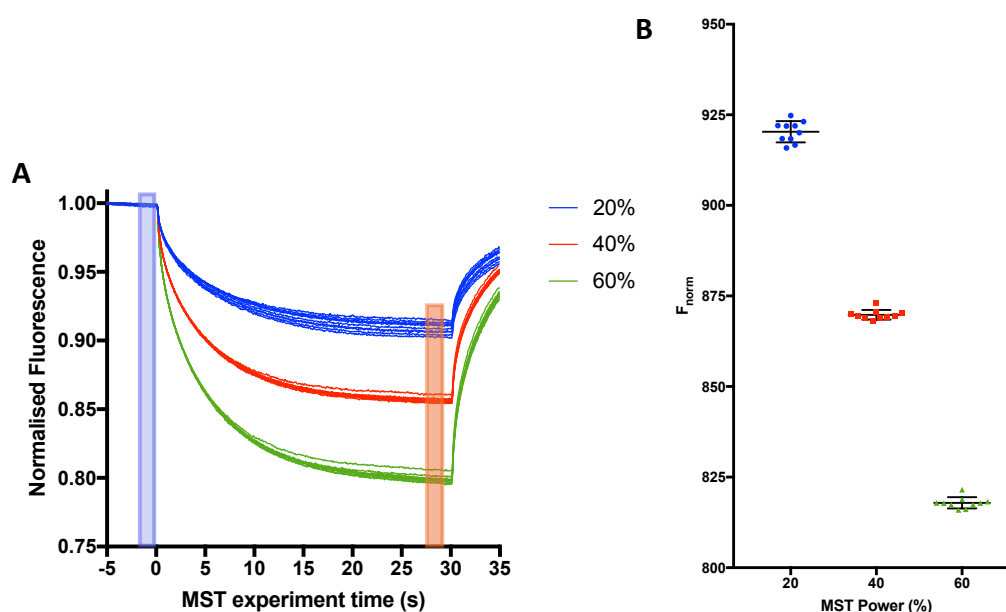


Figure 4.9. MST analysis of SR at 20%, 40%, and 60% power.

The data show MST traces of the change in normalized fluorescence over time (A) and single-point F_{norm} (B) at MST powers of 20%, 40%, or 60%. Ten capillaries containing 50 nM SR in MST buffer (100 mM Tris pH 8.5, 0.1% Pluronic F-127, 1 mM MgCl₂, 1 mM ATP, and 10 μ M PLP) were scanned using different MST powers in three independent experiments. Each trace (A) or data point (B) represents a replicate from one capillary. Black horizontal bars = mean; error bars = SD.

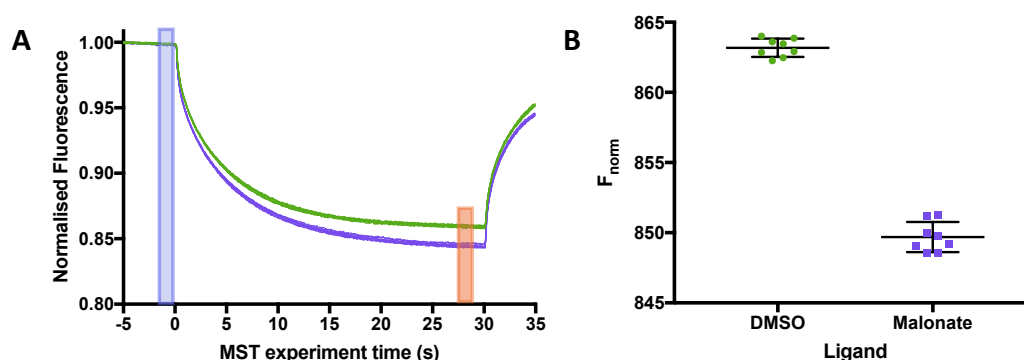


Figure 4.10. MST analysis of SR in the presence of DMSO and malonate.

An MST experiment was performed with SR in the presence of 1% DMSO (green; negative control) and 250 μ M orthosteric inhibitor malonate (purple; positive control). Each line on the change in F_{norm} over time (A) and calculated F_{norm} for the experiment (B) represents a measurement from an individual capillary. Binding is indicated by an upwards or downwards shift in fluorescence from the negative control. Data were collected using the Monolith NT.115 system. Black horizontal bars = mean; error bars = SD; LED power = 30%; MST power = 40%.

To ascertain the window between the positive and negative controls, and thus give an idea of the size of the shift expected with a binding event, all controls throughout the two screens were plotted in the order the trays were read (Fig. 4.11). With a few exceptions, there was generally a negative shift in the fluorescence upon the inclusion of malonate. The size of the shift itself was small, ranging from approximately 5–15 counts. Over time, there was a clear gradual decline in the fluorescence for both controls, which might be attributed to a decay in the integrity of the labelled SR samples over the several-week period that they were stored at -80°C .

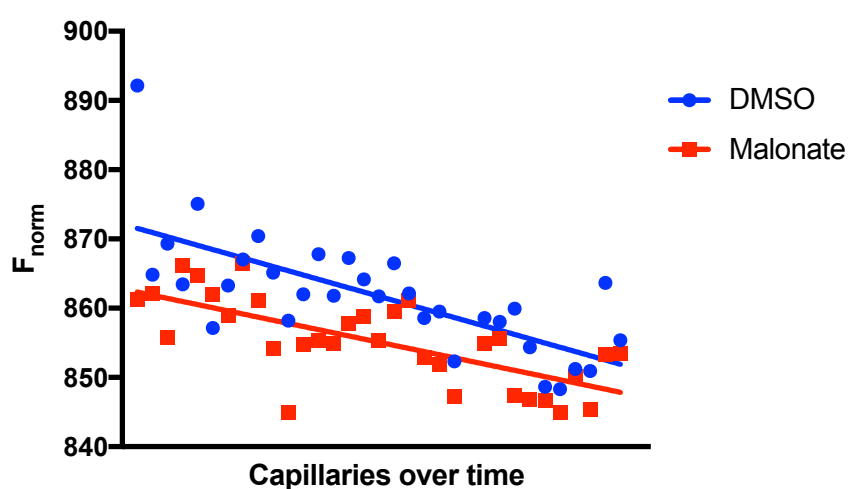


Figure 4.11. Normalised fluorescence of all controls from MST screen of potential SR inhibitors.

Hits identified from the SR fragment screen using the biochemical assay were analysed by MST to evaluate binding. The F_{norm} of the positive (red) and negative (blue) controls from this process as performed over a two-week period are plotted in the order the sample trays were read. Malonate is a confirmed binder to SR and causes a downward shift in the F_{norm} . Data plotted are each control in the order they were measured, so reflect the F_{norm} of the controls over a period of two weeks. The overall trend is illustrated by the red and blue trendlines, and shows that with time there is a gradual decline in the F_{norm} for both controls. This may be due to compromised integrity of labeled SR the longer it is kept stored at -80°C .

4.4.7 MST: K_D determination of malonate

A concentration-response curve of malonate was performed using MST to ascertain whether binding could be successfully observed and measured, ultimately to determine the K_D (the equilibrium dissociation constant used as a measure of affinity). The K_D experiment was a 12-point 1:2 dilution series starting from 500 μM . To avoid artefactual F_{norm} data that can occur when the ligand concentration is high, possibly caused by protein precipitation or aggregation in the capillary, a malonate concentration of 375 μM was used as a positive control throughout MST screening.

The malonate binding curve (Fig. 4.12) indicates F_{norm} shifted in a concentration-dependent manner, exhibiting negative thermodiffusion from the SR-malonate complex moving towards the heat source. The K_D of malonate was determined to be $28.2 \pm 10.3 \mu\text{M}$.

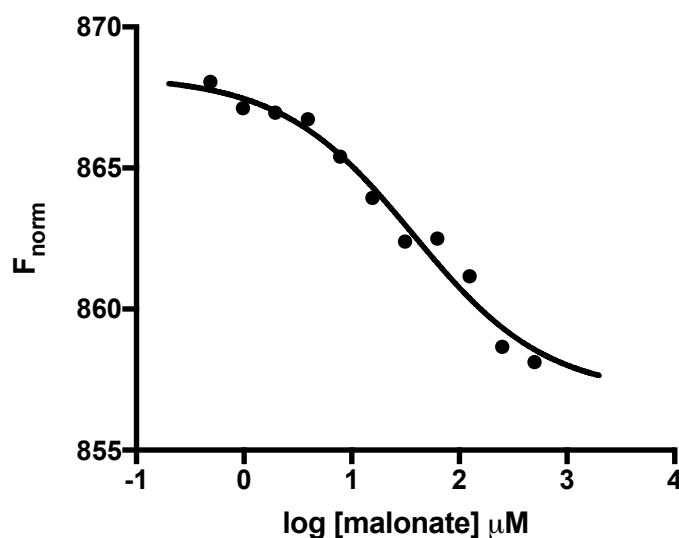


Figure 4.12. Binding affinity curve of malonate and SR.

MST analysis was performed on 50 nM SR and 0–2 mM malonate in MST-optimised Tris mix buffer (100mM Tris pH 8.5, 0.1% Pluronic F-127, 1 mM MgCl_2 , 1 mM ATP, 10 μM PLP). The K_D of malonate was calculated to be $28.2 \pm 10.3 \mu\text{M}$. Data are from one MST experiment.

4.4.8 ITC: K_D determination of malonate

An ITC experiment was first performed on malonate, a known binder. Initial concentrations of 100 μM SR and 1 mM malonate were selected from software predictions based on the c value calculated from the approximate K_D of the ligand of interest. The result was a partial exothermic binding curve (Fig. 4.13A) which, when extrapolated by the analysis software, calculated a K_D of 4.3 μM . Although this value is similar to the malonate K_D determined via MST, the calculation is highly likely to be error prone without a full binding curve. Only the top plateau and part of the slope was measured, which is indicative of the equilibrium being shifted heavily towards saturation and suggests the ligand concentration outweighs the enzyme concentration to the point where binding reaches saturation almost immediately.

The malonate concentration was then reduced by half in order to slow the rate at which the reaction reached saturation. The outcome was a complete binding curve (Fig. 4.13B) with a calculated malonate K_D of $8.5 \pm 1.7 \mu\text{M}$, which is within range of the K_D determined by MST (28.2 μM). ITC can additionally be used to calculate the stoichiometry of ligand to protein binding. It is known from the crystal structure of the SR-malonate complex that only one molecule of malonate binds per SR monomer, which is why it was not expected for the stoichiometry to be 0.5, i.e. 1 molecule of ligand binds per two protein molecules. There are two possible explanations. First, the protein sample contained a sizeable inactive portion from protein denaturation during purification, over time, or during the experiment. Indeed, if the N value is fixed to 1 and the cell concentration allowed to vary, the software determined the concentration of 'active' SR to be approximately 50 μM . Second, not every SR monomer bound a molecule of malonate. The stabilised closed conformation of one malonate-bound SR monomer could induce negative cooperativity of the other monomer, allosterically affecting its binding mode and reducing its ability to bind to another malonate.

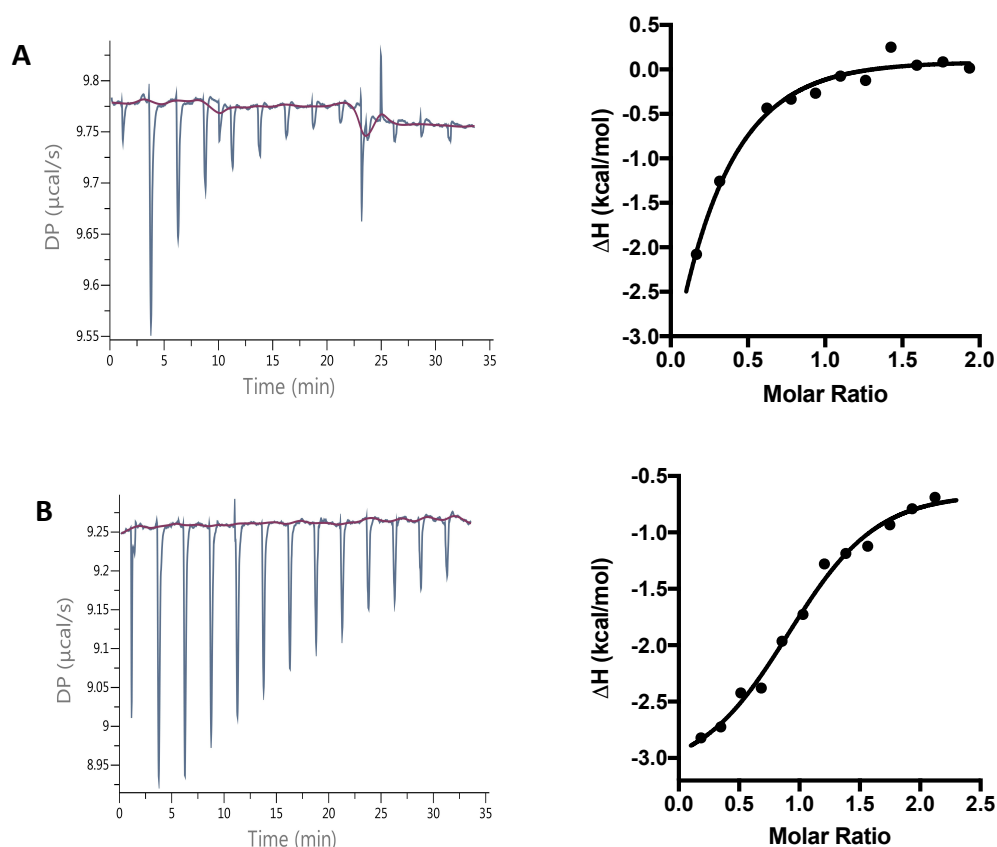


Figure 4.13. Binding affinity of malonate for SR determined by ITC.

(A) Initial ITC experiment with 100 μM SR and 1 mM malonate elicited a partial exothermic binding curve caused by SR becoming rapidly saturated by excess malonate. (B) Reducing the malonate concentration by half (500 μM) enabled a full binding curve to be achieved by slowing the equilibrium shift towards saturation. The K_D of malonate was calculated to be $8.5 \pm 1.7 \mu\text{M}$. Left figures show differential power (DP) of injection peaks obtained throughout the ITC experiment with the baseline in red. Right figures are the binding curves plotted from integration of the DP peaks.

4.5 DISCUSSION

Biophysical data are invaluable in drug discovery for elucidating the binding profile of potential hits. Biophysical techniques, such as the ones used here, help support biochemical data and build a case for promising candidates to be progressed to hit-to-lead development. This chapter has outlined the optimisation of all three methods (thermal shift, MST, and ITC) and has successfully demonstrated their utility from binding data obtained with the SR inhibitor malonate.

Each of the three techniques offers slightly different biophysical information. For instance, thermal denaturation analysis demonstrated a positive thermal shift when SR was stabilised in the malonate-bound conformation, and a negative thermal shift with its substrate, L-serine (Fig. 4.7). This suggests thermal denaturation is sensitive enough to detect binding events between SR and inhibitors (such as malonate) that cause a significant conformational shift — although it is unclear whether the same effect would be observed for inhibitors that do not cause a structural change. Moreover, that the assay could detect decreased SR stability in the presence of L-serine indicates it is possible to use thermal shift to distinguish between SR inhibition and destabilisation, which is important to ascertain for a potential hit lest it is actually a destabilising compound. The primary limitation with thermal denaturation is that it cannot be used to determine binding affinities, so in this sense it is useful for qualitative rather than quantitative assessments.

MST is a more powerful and sensitive technique, owing to its low protein consumption (especially compared to ITC), fast measurements, optimisation simplicity, and output of useful kinetic information down to the picomolar range. In this chapter, MST was used to obtain a binding curve for SR and malonate, as well as calculate a malonate K_D for SR (Fig. 4.13). This was a novel application for MST and represents the first time biophysical data has been obtained for SR and malonate using this technique. Further, the MST data obtained with malonate indicate it is possible to use MST as a means of characterising fragment hits, as malonate has features in common with those from

fragment libraries (e.g. $M_w < 300$ Da, $\text{ClogP} < 3$). The primary reason MST was not used as the sole biophysical method in this thesis is because of its potential to generate false positives. The fluorescent protein labelling that is required may cause non-specific binding, and a compound that is fluorescent or binds close to the fluorophore may generate artefactual data. To mitigate this issue, specific denaturation and fluorescence controls have been included during the screening process in Chapter 7. Even so, because there is still a possibility inhibitors could interact with the fluorophore, it is advantageous to implement a biophysical assay that tests proteins in their native state — such as ITC.

ITC, although protein-intensive, required little optimisation beyond altering ligand concentrations, and accordingly a complete binding curve was achieved with malonate (Fig. 4.13), giving a K_D of $8.3 \mu\text{M}$. While it was promising that malonate binding data could be achieved using ITC, an important caveat is that most fragment inhibitors will have affinities in the high micromolar to millimolar range, which may be beyond the detection limits of ITC. It was for this reason that ITC was used in conjunction with MST, which is more capable of detecting weak interactions.

The three biophysical methods discussed in this chapter have distinct capabilities that inform the screening cascade implemented in Chapter 7. Thermal shift has been used as an initial qualitative assessment of all the SR fragment hits to distinguish between destabilisers and inhibitors. The medium-throughput functionality of MST has been used to screen the hits progressed from biochemical screening and follow-up K_D determination. Finally, a small number of the most promising candidate inhibitors were assayed by ITC, to attempt to characterise their binding affinities to SR in its native state. Together, all the biophysical methods contribute to build a comprehensive profile of SR fragment hits viable for hit-to-lead development.

5 RESULTS IV: CRYSTALLOGRAPHY

5.1 INTRODUCTION

The crystallisation of proteins has historically been a considerable challenge, often requiring a multifaceted approach to a problem that cannot be solved empirically. In drug discovery, protein crystallisation and crystallography is invaluable for elucidating the structure of a target protein, confirming binding of hits, and developing SAR. Crystallography will typically be employed to investigate interactions between novel compounds and orthosteric/allosteric binding sites, which is then used as the rationale for structural optimisation of lead compounds.

5.1.1 Background to SR crystallisation

The crystal structure for human SR in complex with its orthosteric inhibitor malonate (Smith *et al.* 2010; PDB code 3L6B) provided the starting conditions used for crystallising inhibitor-bound SR in-house. The authors successfully crystallised hSR in 25% polyethylene glycol (PEG) 3350, 200 mM sodium malonate, and 50 mM MnCl_2 . During their crystallisation experiments, sodium malonate acted as a precipitant in the reservoir solution as well as binding to the active site to stabilise the closed conformation (McPherson, 2001). Therefore, these conditions were not suitable for crystallisation of the SR holoenzyme (unbound enzyme with cofactor present) because malonate binding to SR would still occur. The Smith group did purportedly crystallise the human SR holoenzyme in Bis-Tris, PEG 3350, and MgCl_2 (personal correspondence), so these components were used as the starting point for crystallising *holo* SR in-house.

When published conditions are not available, *de novo* crystallisation is frequently achieved with the use of commercially available sparse matrix screens. Commercial screens contain reservoir solutions that vary in numerous respects, including the type

of buffer, salt, and precipitant, their respective concentrations, and pH. Solutions that yield crystalline material can be optimised by systematically screening the protein, precipitant, and salt concentrations (and so on) to obtain better diffracting crystals.

5.1.2 Vapour diffusion: Sitting-drop vs. hanging-drop

Vapour diffusion is the predominant method to obtain crystals and involves sealing a drop containing protein and precipitant solutions in a chamber containing pure precipitant (the reservoir solution) in multi-well plates. Water vapour then diffuses out of the drop until the osmolarity between the drop and precipitant are equilibrated, resulting in a slow concentration of both solutions until protein nucleation and precipitation occurs.

The two types of vapour diffusion are sitting-drop and hanging-drop. In both techniques the reservoir is filled with precipitant, and equal volumes of precipitant and protein are present in the drop. In sitting-drop, the drop is put on a shelf next to the reservoir before the plate is sealed, and in hanging-drop the drop is put on a cover slide and suspended over the reservoir. The plates are then incubated at the desired temperature until crystal growth occurs.

5.1.3 Co-crystallisation vs. crystal soaking

Co-crystallisation is a method of obtaining crystals of a protein-ligand complex and is frequently employed when working with insoluble compounds or proteins prone to aggregation, as precipitated samples can be removed by centrifugation or filtration before use. Most commonly, the protein is pre-incubated with the ligand immediately prior to the crystallisation experiment, although an alternative method involves pre-coating crystallisation wells with ligand (Gelin *et al.*, 2015). The compound concentration during pre-incubation depends on the binding affinity, and in general should be at least three times the K_D (Müller, 2017). Co-crystallisation can be combined with sparse-matrix screening when first crystallising protein-ligand complexes, and as

such it can become quite labour- and resource-intensive if co-crystals for more than a small number of compounds are required. A co-crystallisation protocol for one protein-ligand complex cannot necessarily be applied to the same protein with a different compound, and that can be a limitation when studying large numbers of hit compounds, for example. Another typical challenge with co-crystallisation is reduced ligand occupancy, which can occur even with low-nanomolar affinity compounds (Müller, 2017). This outcome can be somewhat mitigated with the addition of further ligand to help shift the protein/ligand ratio towards the complexed protein (Mann *et al.*, 2016), or by an additional step where the crystal is soaked with ligand.

Crystal soaking is a relatively simple method that is beneficial where protein supply is limited and a soakable crystal form is readily available, and involves putting the crystals into 'stabilisation' buffers before immersing them in a concentrated ligand solution (Hassell *et al.*, 2007). The typical ligand concentration used for soaking is ten times the K_D to aim to achieve 90% ligand occupancy, and where the binding affinity is not known a concentration of 20–50 mM for fragments and 0.1–1 mM for higher molecular-weight compounds is usually tested (Müller, 2017). As it is common for several good-quality crystals to grow in the crystallisation drop once conditions have been optimised, all can be used for separate soaking experiments to maximise the production of co-crystals compared with the slower process of co-crystallisation. The primary caveat of crystal soaking is the requirement for a crystal form with an accessible binding site, which is soakable without the crystal lattice becoming disrupted by conformational changes and causing crystal degradation. In addition, conditions such as the ligand concentration, DMSO tolerance, and soaking time may have to be optimised, additives may be required to achieve effective ligand binding (Hassell *et al.*, 2007), and it has been reported that ligand-soaked crystals may change their diffraction properties or even their space group (Skarzynski and Thorpe, 2006). However, the potential to generate many co-crystals from one crystallisation protocol arguably makes crystal soaking a more powerful technique than co-crystallisation when screening numerous compounds.

5.1.4 Microseeding

Both co-crystallisation and soaking are frequently accompanied by the challenge of reproducing crystal growth. A crystal that formed one week may not grow in the same conditions the next, due to variations within the well (e.g. contaminants, precipitation, pH fluctuations), in the environment or solutions, or crystallographer technique. Additionally, the optimal conditions for crystal nucleation and crystal growth can differ substantially. Microseeding involves crushing crystals and suspending them in a slurry of reservoir solution to use as 'seeds' to promote crystal growth, which are added (as stock or dilutions thereof) to the protein sample prior to a crystallisation experiment. Seeds act as a template on which further molecules can assemble, as it is energetically more favourable to build upon an existing crystal plane than begin from a new nucleation point (Bergfors, 2003). With microseeding the quality of the initial crystal is irrelevant, meaning most crystalline material can be used as seeds. Microseeding can be used in conjunction with co-crystallisation and crystal soaking to remove the need for *de novo* nucleation and increase the number of drops in which crystals reproducibly grow; even more so when automation is used to seed into sparse-matrix screens (D'Arcy *et al.*, 2007).

The aim of this chapter was to crystallise purified SR in-house, in both the *holo* and malonate-bound form, using multiple techniques (sitting- and hanging-drop, microseeding) if necessary to achieve high-quality reproducible crystals. Both crystal structures are useful for comparing with SR-inhibitor complexes to investigate binding modes, conformational shifts, or lack thereof. It was particularly important to obtain a *holo* crystal structure because an unbound form of human SR does not currently exist in the PDB. This chapter details the successful crystallisation of the SR holoenzyme and malonate-bound form, and the development of a protocol for obtaining reproducible SR *holo* crystals to be used for hit confirmation via crystal soaking.

5.2 MATERIALS

5.2.1 Crystallisation reagents

Reagent	Supplier (product code)
PEG 3350	Sigma-Aldrich (202444)
Manganese chloride	Sigma-Aldrich (63535)
Magnesium chloride	Sigma-Aldrich (M2670)
Sodium malonate	Sigma-Aldrich (63409)
Bis-Tris	Sigma-Aldrich (B9754)
DTT	Fisher Scientific (BP172)

5.2.2 Buffers and solutions

Buffer	Compounds	Supplier (product code)	Concentration (mM)
SR SEC buffer (Buffer D)	Tris-HCl pH 8	Sigma-Aldrich (154563)	50
	Sodium chloride	Sigma-Aldrich (S7653)	100
	Glycerol	Fisher Scientific (BP229)	10%
	Magnesium chloride	Sigma-Aldrich (M8266)	1
	ATP	Acros Organics (102800100)	1
	PLP	Sigma-Aldrich (P9255)	0.05
	DTT	Fisher Scientific (BP172)	5

5.2.3 Commercial screens

Screen	Supplier (product code)
JCSG- <i>plus</i> TM	Molecular Dimensions (MD1-40)
MIDAS <i>plus</i> TM	Molecular Dimensions (MD1-107)
Morpheus [®]	Molecular Dimensions (MD1-47)
ProPlex TM	Molecular Dimensions (MD1-42)
ANGSTROM Additive Screen TM	Molecular Dimensions (MD1-100)

5.2.4 Other materials, equipment and kits

Equipment	Supplier/manufacturer (product code)
DMSO	Fisher Scientific
Glycerol	Fisher Scientific (BP229)
Ethylene glycol	Fisher Scientific (10695572)
Liquid nitrogen	n/a
MRC Maxi 48-well plates	Swissci (HR3-180)
MRC 2-drop 96-well plates	Swissci (HR3-107)
XRL TM 24-well hanging drop plates	Molecular Dimensions (MD3-11)
Siliconised 22mm round cover slips	Molecular Dimensions (MD4-04)
Seed Bead Kit	Hampton Research (HR2-320)
ClearVue TM Sealing Sheets	Molecular Dimensions (MDS-01S)
CryoLoop TM 10 and 20 micron	Hampton Research (HR4-991 & HR4-937)

Oryx4 protein crystallisation robot	Douglas Instruments
Crystal Phoenix	Art Robbins Instruments
Saturn 944+ CCD detector	Rigaku

5.3 METHODS

All plate maps (24-well, 48-well, and 96-well) were designed using the Hampton Research Make Tray online tool (https://hamptonresearch.com/make_tray.aspx).

5.3.1 Preparation of protein solution

SR stock was stored at -80 °C and diluted with SR SEC buffer to test concentrations ranging from 5–12 mg/mL. Additionally, 5 mM DTT was always included in the protein solution to prevent oxidation of free sulfhydryl residues (cysteines), since oxidation can lead to non-specific aggregation, sample heterogeneity, inactivity or denaturation of the sample.

For microseeding, the 100% seed stock was prepared using a Seed Bead Kit (Hampton Research) with the reservoir solution that produced the crystal, from which 1–10% dilutions were prepared and added to the protein solution. For co-crystallisation experiments, the protein solution was incubated with 5 mM or 10 mM ligand for 30 min at RT, then returned to ice for the remainder of the experiment. Protein solutions were kept on ice where possible and only removed when pipetting.

5.3.2 Sitting-drop vapour diffusion

Sitting drop trials were performed in MRC Maxi 48-well crystallisation plates (Swissci) or MRC 2-drop 96-well crystallisation plates (Swissci), either manually or using an Oryx4 protein crystallisation robot (Douglas Instruments). The reservoirs contained either 100 µL (48-well) or 50 µL (96-well) precipitant. 48-well plates were used because they allowed bigger drop sizes, and thus potentially bigger crystals, while 96-well plates enabled screening of a higher number of conditions. The dispensed protein drops had a volume of 1 µL if performed manually or 0.2–0.3 µL if automation was used. The protein-to-reservoir solution drop ratio was always 1:1.

A number of conditions were varied to optimise crystal growth, including: buffer pH, the precipitant, salt, and buffer concentrations, and incubation temperature (4/14/20 °C). Plates were sealed with ClearVue™ Sealing Sheets, placed in an incubator, and were checked periodically for crystal growth using a light microscope.

Commercial crystallisation screens were all performed in MRC 2-drop 96-well plates using a Crystal Phoenix (Art Robbins Instruments) with a 0.2 µL protein drop size.

5.3.3 Hanging-drop vapour diffusion

Hanging drop trials were performed manually in 24-well XRL™ plates (#MD3-11, Molecular Dimensions), which were prepared with 1 mL precipitant in the reservoirs. A 1 µL drop of protein solution was pipetted onto a siliconised cover slip (Molecular Dimensions) and 1 µL reservoir solution was pipetted on top of the drop. The cover slip was then placed drop-down on the top of each well and pressed firmly until the cover slip formed a complete seal with the grease around the rim. Hanging drop plates were incubated at 20 °C and checked periodically for crystal growth using a light microscope.

5.3.4 Crystal soaking

Crystals selected for soaking were picked and placed into a 1 µL drop of reservoir solution supplemented with successive concentrations of 10%, 20%, and 30% glycerol for cryoprotection. For fragment soaking, stock solutions of 100 mM in 100% DMSO were diluted to 10 mM in reservoir solution and 1 µL was added to the protein drop, giving a final DMSO concentration of 10% in the drop. Crystals were left to soak for 1 h at 4 °C prior to data collection.

5.3.5 Selection of crystals

Crystals selected for X-ray diffraction were assessed based on their morphology — the external appearance of crystals that covers crystal shape, the relative sizes of its faces, and its 3D periodicity. Crystal morphology is related to the lattice arrangement of the internal crystal structure, so the ideal crystal will have multiple faces from which diffraction data can be collected and will be larger or approximately equal sized to the diameter of the X-ray beam (70 μm for in-house diffractometer and 5–100 μm at Diamond Light Source).

5.3.6 Data collection and structure solution

Crystals were selected for X-ray analysis once they had grown to their maximum size (approximately seven days). The crystals were cryo-protected by successive soaking in reservoir solutions containing 10%, 20%, and 30% glycerol before cryo-cooling in liquid nitrogen. Crystals were first screened in-house at 100 K using a Rigaku 007HFM rotating anode X-ray generator and a Saturn 944+ CCD detector. If the initial diffraction images indicated poor resolution, the crystals were stored in liquid nitrogen and a dataset was collected at Diamond Light Source (beamline I03) using synchrotron radiation. The diffraction dataset collected was handled by our resident crystallographer Dr Mark Roe, for phase determination, structure solution, and refinement. Data collection statistics were obtained from Mark Roe and MolProbity statistics from the MolProbity web server (molprobity.biochem.duke.edu/index.php); statistics tables can be viewed in Appendix 10.5. For comparing superimposed structures, the root-mean-square deviation (RMSD) was calculated using Maestro (Shrödinger software suite) to determine the average distance between atoms. Figures visualising the protein structure were produced using Maestro.

5.4 RESULTS

5.4.1 Crystallisation with malonate

The first step was to attempt to replicate the crystallisation of SR in complex with malonate based on the conditions published by Smith *et al.* (25% PEG 3350, 200 mM sodium malonate, 50 mM MnCl_2). An initial protein concentration of 10 mg/mL was used as this is generally thought to be a good starting point (Newby *et al.*, 2009). All initial trials were performed using the sitting drop method due to its capacity to screen considerably more conditions than hanging drop.

The first 96-well matrix tested 12 concentrations of malonate (60–280 mM) and eight concentrations of MnCl_2 (0–64 mM) and kept the concentration of PEG 3350 constant (25%). The plate was incubated at 20 °C and checked for crystal growth each day. Many of the drops showed brown amorphous precipitation, suggesting that the protein concentration should be reduced. Some crystalline material grew where the malonate concentration was high and the MnCl_2 concentration was relatively low but these crystals were not large enough to collect a diffraction dataset.

Based on the concentrations that yielded the crystalline material, a 48-well matrix was then prepared that screened a narrower range of concentrations to pinpoint the optimum conditions for crystal growth. Eight concentrations of malonate (180–250 mM) and six concentrations of MnCl_2 (4–24 mM) were tested with 25% PEG 3350. The protein concentration was reduced to 5 mg/mL to keep the protein soluble and encourage singular crystals to grow. Crystals began to grow overnight in several drops, and within a week several optimised SR crystals formed (Fig. 5.1).

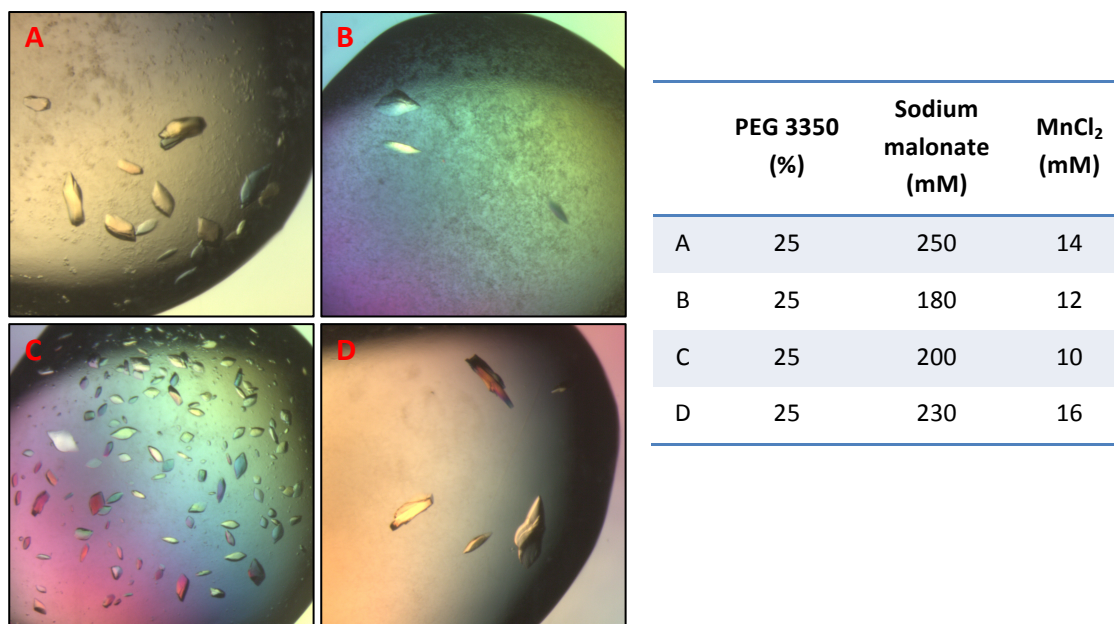


Figure 5.1. Crystallisation of human SR with the inhibitor malonate.

Conditions for each drop are given in the table. Crystallisation trials were performed with increasing concentrations of sodium malonate and manganese chloride, and a constant concentration of 25% PEG 3350. The protein drop contained 5 mg/mL SR. The plate was incubated at 20 °C and crystals grew to 50 µm within a week. A crystal from (D) was selected for X-ray diffraction.

5.4.2 Crystal structure of SR-malonate complex

A single crystal was picked from a drop containing 25% PEG 3350, 230 mM sodium malonate, and 16 mM MnCl_2 . After analysis by X-ray diffraction, the structure of the SR-malonate complex was determined to a resolution of 2.4 Å.

As expected, the crystal structure of hSR was revealed to be a dimer consisting of two SR molecules separated by a twofold crystallographic axis (Fig. 5.2A). Both monomers were generally well ordered, and almost all residues were well defined, with the exceptions of 1, 2, 69–75, and 322–340. The missing residues 69–75 belong to a solvent-exposed flexible loop region, the inherent mobility of which may have prevented stabilisation of this region into the crystal lattice.

As previously demonstrated by Smith et al. and corroborated here in Fig. 5.2B, each SR monomer comprises a large domain (teal) and small domain (purple) connected by a flexible loop region (orange) that allows the small domain to undergo a conformational shift upon ligand binding. The active site exists at the interface of the two domains.

The inhibitor malonate was shown to reside within the active site in close proximity to the catalytic cofactor PLP and the hydrogen donor Ser84. In addition, malonate comes into contact with several other residues within the active site (Fig. 5.2C), which may contribute to its occlusion of the active site and related competitive inhibition. PLP is covalently linked to the catalytic residue Lys56 via the formation of a Schiff base between the lysyl side chain of lysine and the carbonyl carbon of PLP. A manganese ion is associated with a surface-exposed region of the large domain, between helices 9 and 12.

Overall, the crystal structure of the SR-malonate complex solved here revealed highly similar findings to those of the Smith group, and demonstrated purified SR could be successfully and reliably crystallised in-house.

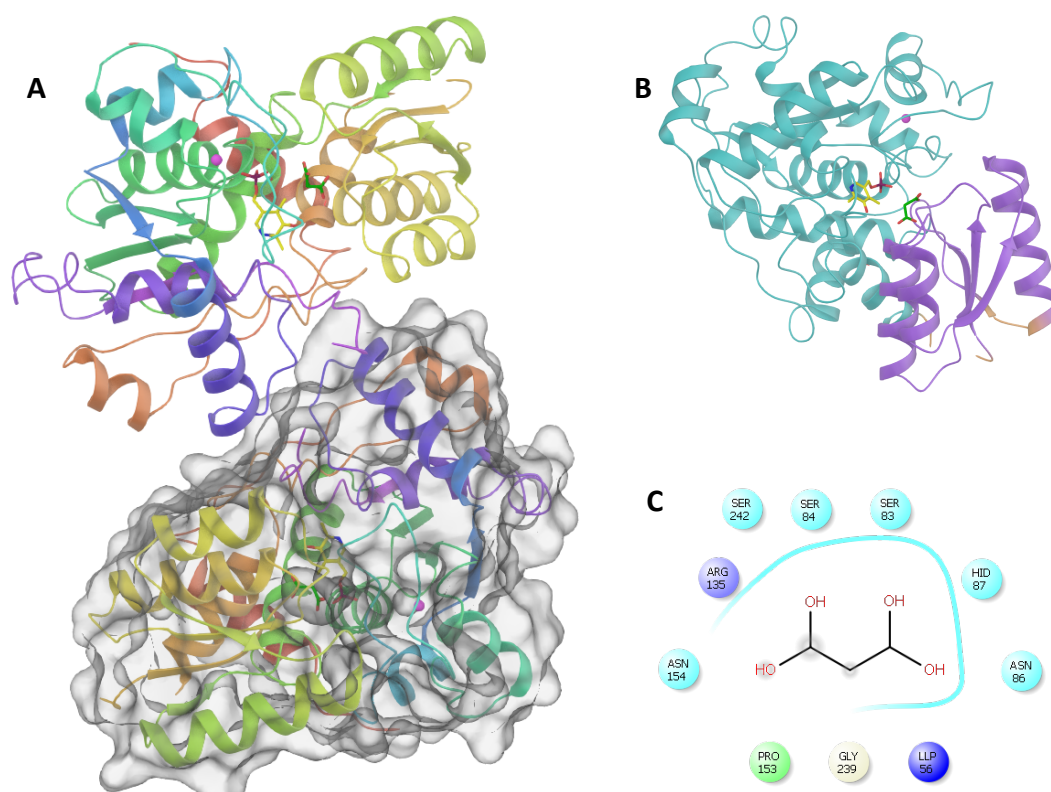


Figure 5.2. X-ray crystal structure of human SR in complex with its orthosteric inhibitor malonate.

The structure was determined to a resolution of 2.4 Å. **(A)** Secondary structure molecular scheme of SR dimer, with bottom monomer overlaid with protein surface visualisation. **(B)** SR monomer, showing the large (teal) and small (purple) domains linked by a flexible loop region (orange). In both **(A)** and **(B)**, malonate is represented by green carbon sticks, PLP (SR cofactor) by yellow carbon sticks, and Mn^{2+} by a pink sphere. **(C)** Malonate interaction pocket; malonate interacts with the active site in the cleft between the large and small domains, and is in close proximity to PLP, Ser84, Ser83, and His87, among others.

5.4.3 Crystallisation of the SR holoenzyme

SR was screened against two 48-well sparse matrix screens containing 100 mM Bis-Tris, PEG 3350, and MgCl_2 . Both screens tested six Bis-Tris pH (6.0–7.25) against either eight PEG 3350 concentrations (10–27.5%) or eight MgCl_2 concentrations (170–310 mM). Crystallisation experiments with *holo* SR used MgCl_2 rather than MnCl_2 based on observations by Evotec crystallographers that *holo* crystal formation favoured MgCl_2 (personal correspondence). An SR concentration of 5 mg/mL was used to prevent precipitation and drive single crystal formation. The crystals that grew were primarily needles (Fig. 5.3A–B, D–F) and a few single crystals (Fig. 5.3C).

The optimised crystals grew to 30 μm following a seven-day incubation at 20 °C in 100 mM Bis-Tris pH 6.5, across several concentrations of PEG 3350 (15–20%) and MgCl_2 (230–270 mM). The crystals selected for X-ray diffraction were picked from a drop containing 100 mM Bis-Tris pH 6.5, 15% PEG 3350, and 250 mM MgCl_2 , then cryo-protected using successive soaks in precipitant containing 10, 20, and 30% glycerol.

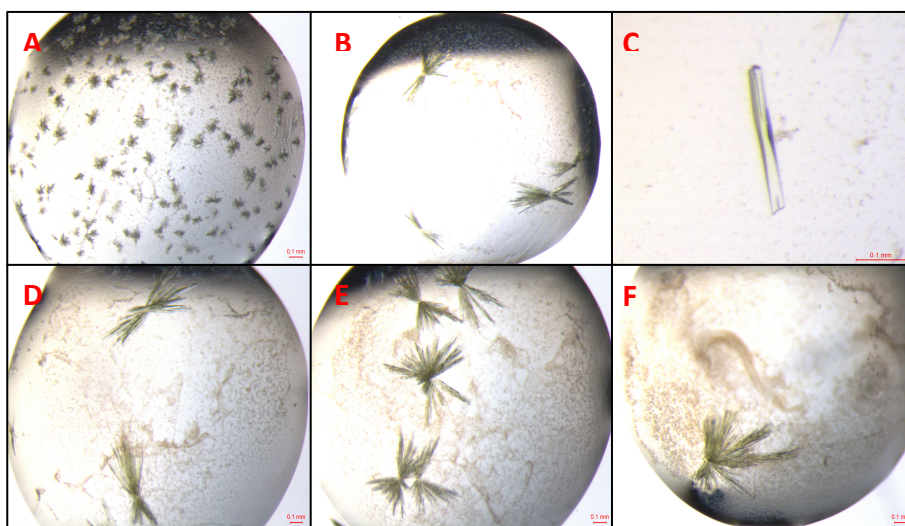


Figure 5.3. Crystallisation pH screen of the SR holoenzyme.

Sparse-matrix screens were performed with increasing concentrations of PEG 3350 and MgCl_2 in 100 mM Bis-Tris (A) pH 6.0; (B) pH 6.25; (C) pH 6.50; (D) pH 6.75; (E) pH 7.0; and (F) pH 7.25. The protein solution contained 5 mg/mL SR and 5 mM DTT. Protein was crystallised using sitting-drop, vapour diffusion and incubated at 20 °C. Crystal growth began overnight and grew to 30 μm within seven days.

5.4.4 Crystal structure of SR holoenzyme

A ligand-free SR crystal diffracted to 1.9 Å resolution using radiation generated in-house. The crystal structure of the SR holoenzyme (Fig. 5.4A) was organised in a similar arrangement to the SR-malonnate complex, comprising a large domain (teal), a small domain (purple) and a flexible loop region (orange). The PLP cofactor and Mg^{2+} occupied the same space as their counterparts in the SR-malonnate crystal structure. The ordering of residues appeared to be improved for the SR open conformation, and a few residues were not well defined: 1–3, 132–135, and 339–340. Aside from the residues at the protein C- and N-terminus, which are often lost during structure solution, the only other undefined residues (132–135) were at the top of helix 5 (refer to Fig. 1.5) in the small domain. In contrast to that for the SR-malonnate structure, the flexible loop region is complete and well defined in the SR holoenzyme structure. It is possible the absence of a ligand-induced conformational shift during crystallisation of the SR holoenzyme allowed the loop region to be stabilised into the crystal lattice.

The key difference between the two crystal structures is the organisation of the small domain. A superimposition of the unbound and malonnate-bound forms of SR (Fig. 5.4B) revealed the arrangement of the large domains was nearly identical whereas the orientation of the small domains deviated considerably. The small domain is positioned much closer to PLP in the malonnate-bound structure, and most notably helices 5 and 6 shift towards the large domain by 5.5 Å and 8 Å respectively, contributing to the overall ‘closed’ structure of the enzyme. After structural alignment of the SR holoenzyme and malonnate-bound enzyme, the RMSD increased considerably between the large domain (0.03) and the small domain (2.2), signifying large structural variation. The degree of conformational shift is reflective of the high mobility of the small domain, resulting from the flexibility allowed by the loop region.

Smith *et al.* made the same observations from a structural alignment of the rat holoenzyme and human malonnate complex; here, their observations have been verified by superimposing the human orthologues for both crystal structures.

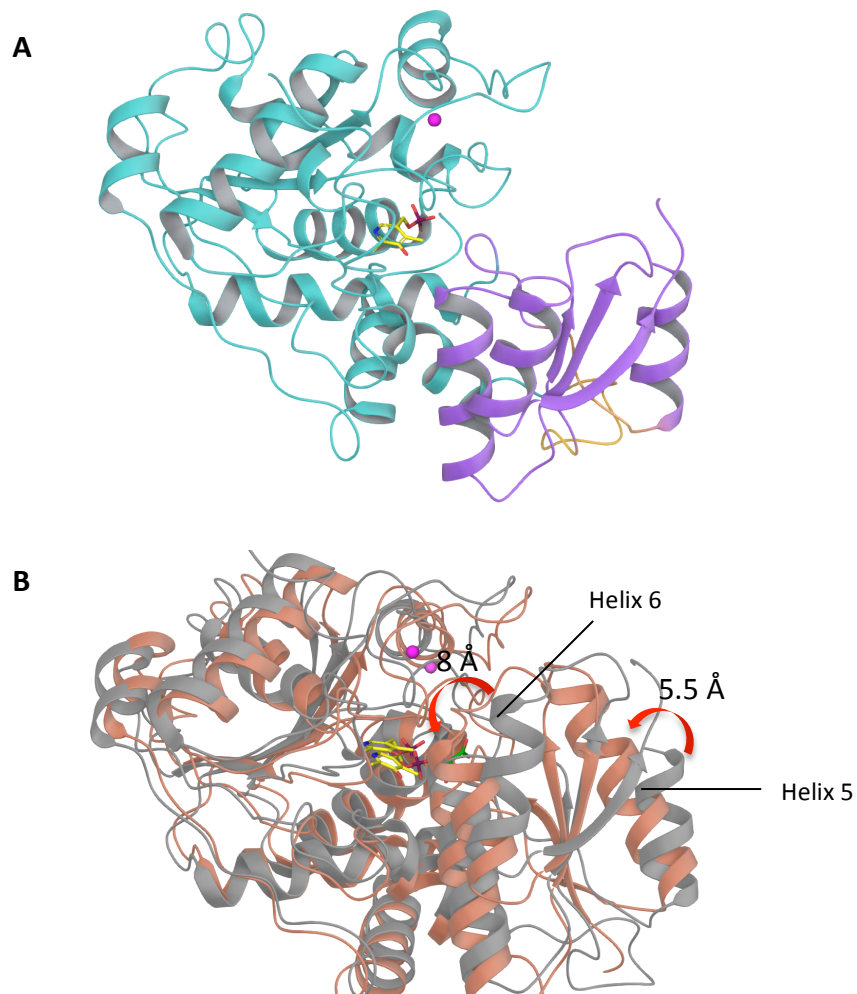


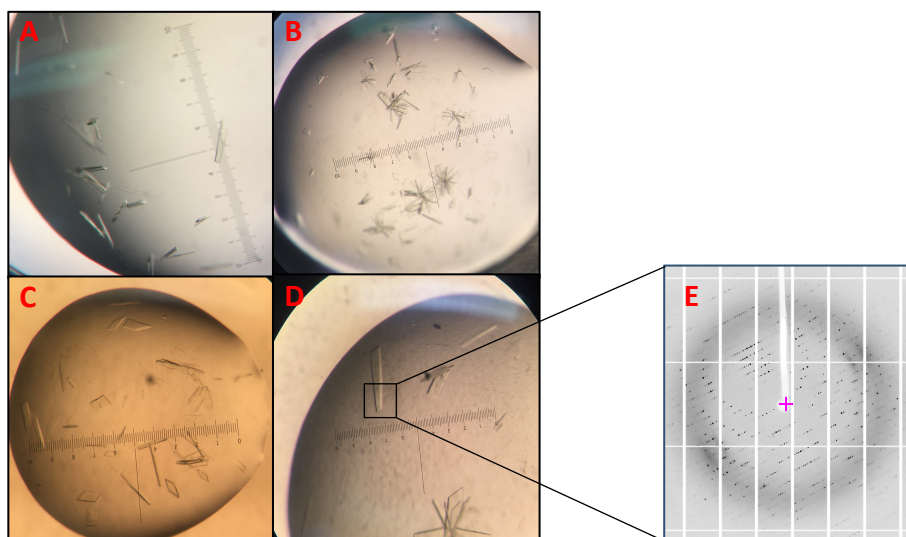
Figure 5.4. X-ray crystal structure of human SR holoenzyme and overlay with inhibitor-bound form.

The unbound SR crystal structure was determined to a resolution of 1.9 Å. **(A)** Holoenzyme monomer showing the large domain (teal), small domain (purple), flexible loop region (orange), PLP cofactor (yellow sticks), and magnesium ion (pink sphere). **(B)** Superimposition of SR holoenzyme ('open' conformation, grey) and malonate-bound ('closed' conformation, orange). The arrangement of the large domains is largely identical between the bound and unbound forms. There is a significant shift of the small domain towards PLP in the malonate-bound structure, shown here by the red arrows indicating a distance of 8 Å between the ends of helix 6, and 5.5 Å between the middles of helix 5.

5.4.5 Repetition of the SR *holo* crystal

Crystallisation was hindered by difficulties repeating growth of SR *holo* crystals, so microseeding was trialled to try to improve reproducibility. A crystal from the previous *holo* SR screen was used to create a 100% microseed stock, which was then added to the protein sample to give final concentrations of 0.1%, 1%, 5%, and 10% microseed with 5 mg/mL SR. The samples containing 5 mg/mL SR and the different concentrations of microseed were then screened against two 96-well sparse matrix screens containing either increasing concentrations of PEG 3350 (10–22.5%) and MgCl₂ (200–275 mM), or Bis-Tris (10–100 mM) and buffer pH (6.0–7.25), with either 0.1%, 1%, 5%, or 10% microseed in each quadrant. Images of the optimised crystals and their corresponding growth conditions are shown in Fig. 5.5A–D. Crystals grew prolifically in many conditions, and the optimum conditions for crystal growth with microseed were similar to those established previously: 100 mM Bis-Tris pH 6.5, 20% PEG 3350, and 250 mM MgCl₂. Although a full dataset was not collected, the initial diffraction pattern (Fig. 5.5E) indicated the crystals diffracted to a good resolution and lacked microscopic pathology.

In parallel to the microseeding experiments, SR was trialled in several commercial sparse-matrix screens to try to identify new crystallisation conditions that might lead to more reproducible *holo* crystals. Four screens were performed (JCSG*plus*[™], MIDAS*plus*[™], Morpheus[™], ProPlex[™]) with SR increased to 7.5 mg/mL to facilitate new crystal growth. Any resulting crystalline material was of a much poorer quality than that obtained in previous experiments, so the conditions from these commercial screens were not pursued further. A commercial additive screen (ANGSTROM) was then performed cooperatively with one of the *holo* crystal conditions that had previously yielded twinned crystals (100 mM Bis-Tris pH 6.5, 17% PEG 3350, 250 mM MgCl₂) to try to prevent twinning by slightly adjusting the growth environment. No crystal hits were observed.



	Bis-Tris pH 6.5 (mM)	PEG 3350 (%)	MgCl ₂ (mM)	Seed (%)
A	100	15	220	0.1
B	100	20	250	1
C	100	20	240	5
D	100	20	250	10

Figure 5.5. Optimisation of microseeding crystallisation with SR holoenzyme.

Conditions for each drop are given in the Table. 5 mg/mL SR was screened against increasing concentrations of PEG 3350 (10–22.5%) and MgCl₂ (200–275 mM) in conjunction with (A) 0.1%, (B) 1%, (C) 5%, and (D) 10% microseed. (E) The diffraction pattern from the optimised SR crystal that grew using microseeding, using radiation generated in-house.

5.4.6 Crystallisation of *holo* SR by hanging-drop vapour diffusion

The conditions optimised for growing SR *holo* crystals using sitting-drop vapour diffusion and microseeding were repeated using hanging-drop vapour diffusion to try to produce larger crystals that would be well suited for soaking.

Two 24-well matrix screens of PEG 3350 (15–25%) and MgCl_2 (220–280 mM) with either Bis-Tris pH 6.0 or 6.5 were screened against 5 mg/mL SR and 10% microseed by hanging-drop method. After two days of incubation at 20 °C, large SR crystals with good morphology began to form in 19–21% PEG 3350 and in all concentrations of MgCl_2 . Select crystals grew to 60 μm (Fig. 5.6A–B) and diffracted well upon preliminary analysis (Fig. 5.6C). Crystal formation using the hanging-drop method appeared to favour Bis-Tris pH 6.0 over pH 6.5, as was observed previously with sitting drop. From these studies, one condition (100 mM Bis-Tris pH 6.0, 20% PEG 3350, 250 mM MgCl_2 , 10% seed) was repeated across a 24-well plate to generate crystals in preparation for soaking.

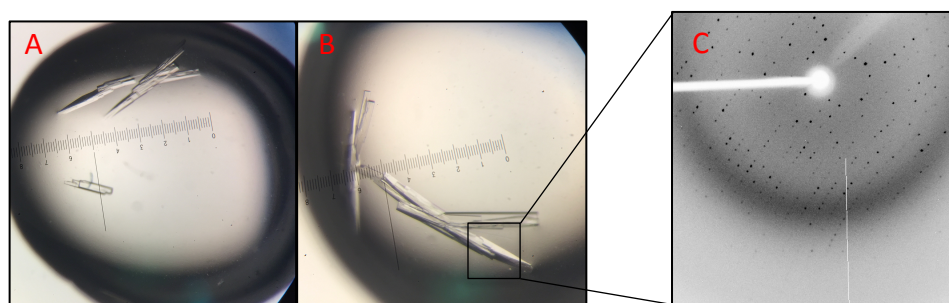


Figure 5.6. Crystallisation of SR holoenzyme by hanging drop-vapour diffusion.

A 24-well matrix screen of increasing concentrations of PEG 3350 (15–25%) and MgCl_2 (220–280 mM) was performed with 5 mg/mL SR and 10% microseed. Crystals shown formed in 100mM Bis-Tris pH 6.0, 240 mM MgCl_2 , and 19% (A) or 21% (B) PEG 3350. (C) Diffraction pattern from a 60 μm SR *holo* crystal produced by hanging-drop vapour diffusion.

5.5 DISCUSSION

In this chapter, purified SR was successfully crystallised both as the malonate-bound complex and as the unbound holoenzyme, and their structures were determined to respective resolutions of 2.4 Å and 1.9 Å. The in-house crystal structure of the SR-malonate complex corroborated the findings of Smith *et al.*: SR is a dimer, with each monomer comprising a large and small domain, the smaller of which undergoes a ligand-induced conformational shift when malonate is bound at the active site. The rearrangement of the small domain can primarily be attributed to a 5.5 Å shift by helix 5 and an 8 Å shift by helix 6 that serve to orientate the small domain towards the PLP cofactor, thereby placing the key catalytic residue Ser84 close to the active site. These distances are specific to the SR structural images obtained in-house but it is likely the range of motion of the small domain is larger and more continuous, owing to the flexibility of the hinge region that connects the large and small domains. Indeed, when Smith *et al.* aligned the structures of the human malonate-bound and yeast *holo* enzymes, they found that helix 6 was tilted away from the active site by almost 4.5 Å in the yeast *holo* structure.

The structure of the human SR holoenzyme described in this chapter is currently the first crystal structure of its type; in the PDB, the only crystal structure for human SR is the malonate-bound form (PDB code 3L6B) and is accompanied by the rat holoenzyme (PDB code 3HMK) and rat malonate-bound enzyme (PDB code 3L6C), as well as various non-mammalian orthologues (PDB codes 1V71, 1WTC, 2ZPU). For the purpose of structural studies of human SR, the rat holoenzyme is still useful because it shares 90% sequence identity with the human holoenzyme and thus both structures are virtually indistinguishable. However, now that the structure of human SR has been visualised, we are able to have a more complete understanding of human SR without relying on extrapolations from the rat orthologue.

It was imperative to develop a reproducible crystallisation protocol for the SR holoenzyme to enable soaking of hits generated through fragment screening, of which

there could be many. Although it is possible to perform soaking with co-crystals, the soaked ligand would only displace the co-crystallised ligand if it has an equal or greater affinity for the enzyme (Müller, 2017), which is highly unlikely with weakly-binding fragment inhibitors. To this end, the inclusion of 5 or 10% microseed improved the reproducibility of holoenzyme crystal growth, and when used in conjunction with hanging-drop vapour diffusion, produced many large crystals that diffracted well upon preliminary X-ray analysis. These crystals were also tolerant of up to 40% DMSO, indicating they are suitable for soaking with high-concentration ligands.

Overall, crystallisation of the SR holoenzyme and malonate-bound enzyme in this chapter showed, firstly, the homogeneity and purity of the target protein; secondly, a reproducible crystallisation protocol for soaking with the SR holoenzyme; and thirdly, structural insights into the binding mechanism of SR and its ligands that will have relevance when characterising the binding of SR fragment hits.

6 RESULTS V: ANALYSIS OF LITERATURE INHIBITORS

6.1 INTRODUCTION

The development of SR inhibitors is a relatively new field, with the first group of inhibitors derived from L-serine and L-serine-*O*-sulfate (LSOS) only being identified little more than a decade ago (Stríšovský *et al.*, 2005). This followed the observation that LSOS, from which SR generates pyruvate via its β -elimination activity, acts as an inhibitor of D-serine synthesis (Panizzutti *et al.*, 2001), and led to the discovery of several competitive SR inhibitors including malonate and L-erythro-3-hydroxyaspartate (Stríšovský *et al.*, 2005). Thereafter, a series of peptide inhibitors of SR was identified that had slow-binding kinetics and were structurally distinct from serine, but were still thought to be competitive inhibitors (Dixon *et al.*, 2006). Further studies described additional inhibitor families including hydroxamic acids (Hoffman *et al.*, 2009a), cyclopropane derivatives (Beato *et al.*, 2015), and more malonate-based inhibitors such as 2,2-dichloromalonate (Vorlová *et al.*, 2015).

A new series of peptide inhibitors was later characterised through *in silico* and pharmacological screening based on one of the dipeptide-like inhibitors identified by Dixon *et al.* (Mori *et al.*, 2014). Many of the compounds demonstrated SR inhibition that was comparable to or stronger than malonate ($IC_{50} = 1.31$ mM), with IC_{50} values in the high micromolar-to-low millimolar range. The same group developed derivatives of the peptide inhibitors, one of which showed significantly more potent inhibition and suppressed neuronal over-activation *in vivo* (Mori *et al.*, 2017). A more comprehensive discussion of these SR inhibitors can be found in section 1.7.7.

From a drug discovery perspective, these inhibitors are useful tools for aiding rational drug design, especially for an enzyme such as SR with limited druggability. A selection from the aforementioned literature inhibitors, as well as six pyrazole compounds identified by Evotec from an SR compound screen (40 in total) were either purchased

or synthesised and purified in-house for assessment in the biochemical and thermal shift assays. Many of these inhibitors have not had their activity confirmed by other laboratories, so the first objective was to try to reproduce their inhibitory effects in-house. Those that proved to be effective inhibitors in the biochemical assay and show a discernable T_m shift in the thermal denaturation assay could be promising starting points for structural optimisation, ultimately to create SR inhibitors with increased potency and improved physicochemical properties. The identification of novel and potent inhibitors using this method of studying existing inhibitors is often considered to have a higher chance of success compared to screening and analysing unknown compounds, due to the advantages of developing chemical properties from a well-characterised starting point. With a growing inventory of readily available SR inhibitors, this seemed like a reasonable approach with SR.

Forty SR inhibitors from the literature including malonate-derivatives, pyrazole-derivatives, amino acid derivatives, and peptides inhibitors were selected for characterisation in the SR biochemical assay (refer to Chapter 3) and thermal shift assay (refer to Chapter 4). The aim was to then collaborate with chemists in synthesising novel, potent derivatives with activities that could be verified in the biochemical assay. This chapter details the characterisation of these literature inhibitors, the findings that published inhibitory data could not be replicated in-house with the SR biochemical assay, and the eventual conclusion that none of those that had the most promising credentials or were structurally distinct from classical inhibitors such as malonate were suitable to drive medicinal chemistry efforts.

6.2 MATERIALS

6.2.1 SR inhibitors

Refer to Appendix 10.3 for SR literature inhibitors (numbered **1–40**) and their chemical structures. Compounds were purchased from Fluorchem, Sigma-Aldrich, and Alfa Aesar, or were synthesised in-house. Stock concentrations were 100 mM (**1–29, 33, 34**) or 10 mM (**30–32, 35–40**). All stock compounds were solubilised in 100% DMSO.

6.2.2 Buffers and solutions

Buffer	Compounds	Supplier (product code)	Concentration
Pre-treatment of L-serine solution	Tris-HCl pH 8.5	Sigma-Aldrich (154563)	100 mM
	L-serine	Sigma-Aldrich (S4500)	200 mM
	DAO	Sigma-Aldrich (A5222)	1.5 U/mL
	Catalase	Sigma-Aldrich (C1345)	3 U/ μ L
Tris mix buffer	Tris-HCl pH 8.5	Sigma-Aldrich (154563)	100 mM
	Pluronic F-127	Sigma-Aldrich (P2443)	0.05%
	Magnesium chloride	Sigma-Aldrich (M2393)	1 mM
	ATP	Acros Organics (102800100)	1 mM
	PLP	Sigma-Aldrich (P9255)	10 μ M
Detection solution A	Tris-HCl pH 8.5	Sigma-Aldrich (154563)	100 mM
	Pluronic F-127	Sigma-Aldrich (P2443)	0.05%
	EDTA	Alfa Aesar (A10713)	2 mM
	HRP	Sigma (P8125)	0.5 U/mL
	DAO	Sigma-Aldrich (A5222)	1 U/mL
	Luminol	Sigma-Aldrich (A4683)	50 μ M
Thermal shift buffer	CHES pH 8.5	Sigma-Aldrich (C2885)	100 mM
	Magnesium chloride	Sigma-Aldrich (M2393)	1 mM
	ATP	Acros Organics (102800100)	1 mM
	PLP	Sigma-Aldrich (P9255)	10 μ M

6.2.3 Reagent solutions

Purpose	Buffer	Concentration
SR solution II	Tris mix buffer	0.4 μ M
L-serine solution II	Tris mix buffer	5 mM

These solutions are used when fragment/compound is present (concentrations adjusted when there is a pre-incubation with inhibitor to keep final assay concentrations of enzyme and substrate the same)

6.2.4 Further materials, equipment and kits

Equipment	Supplier/manufacturer (product code)
SYPRO Orange 5000X	ThermoFisher Scientific (S6650)
LightCycler® 480 Multiwell plate 96	Roche (04729692001)
LightCycler® 480 sealing foil	Roche (04729757001)
LightCycler®	Roche (n/a)
DMSO	Fisher Scientific (D4120/PB08)
96-well v-bottom clear polypropylene plates	SLS (MIC9050)
Corning® 3574 384-well plates	Fisher Scientific (10382883)
Foil Plate Seals	SLS (PCR0620)
PERAstar FS plate reader	BMG (n/a)

6.3 METHODS

Analysis of literature inhibitors using the biochemical and thermal denaturation assays was performed as described in detail in Chapters 3 and 4, and are summarised briefly here.

6.3.1 Compound IC₅₀ determination

IC₅₀ values were measured according to the protocol in section 3.3.7. Each experiment consisted of a 10-point 1:3 serial dilution to give a final concentration series of 0–5 mM (fragments/malonate; 100 mM stock) or 0–500 μ M (compounds; 10 mM stock).

6.3.2 Thermal denaturation analysis

Reaction mixtures containing a final concentration of 1 μ M SR, 5x SYPRO Orange dye, and either 1 mM (fragments) or 100 μ M (compounds) were prepared up to a volume of 20 μ L per well in LightCycler Multiwell plates. Plates were centrifuged and sealed before being equilibrated briefly on ice, and thermal denaturation analysis was performed using a Roche LightCycler® 480. Thermal shifts were calculated by comparison with the T_m of the SR + 1% DMSO (no compound) control.

6.4 RESULTS

6.4.1 IC₅₀ values for literature compounds

Determination of IC₅₀ values of all literature inhibitors was performed manually in the coupled biochemical assay. Experiments were repeated at least twice, with at least one of the repeats using inhibitor that had been repurified in-house.

Surprisingly, almost all of the inhibitors exhibited no inhibition in the SR assay; those that did are displayed in Fig. 6.1. The most potent inhibitors with IC₅₀ values of below 1 mM were either malonate (**3**; 96 µM) or derivatives of malonate, namely dimethyl maleate (**4**; 180 µM), and hydroxymalonate (**6**; 66 µM). Another compound that showed inhibition but was far less potent was L(+)-tartaric acid (**1**; 2700 µM), although this agrees with published data describing the D-isomer as a much more potent inhibitor than the L-isomer (Stríšovský *et al.*, 2005). Two pyrazole-derivatives demonstrated reasonably good inhibition, specifically compounds **2** (480 µM) and **5** (1250 µM) and a third pyrazole **9** inhibited minimally (6800 µM). None of the peptides exhibited any noticeable inhibition, although interestingly the peptide precursor **28** did (580 µM).

Despite the inhibitors being well documented as having inhibitory activity against SR, it was not possible to repeat these effects in-house. Moreover, the fact that the positive control malonate inhibited SR completely and consistently, and that inhibition was observed for a compound from each key group (malonate derivatives, pyrazoles, peptides) suggests this discrepancy was not assay related. The comparatively high concentration of SR could be obscuring the inhibitory activity of some of the compounds; an SR concentration of 400 nM would limit the sensitivity to 200 nM, although, none of the inhibitors approached this lower limit anyway.

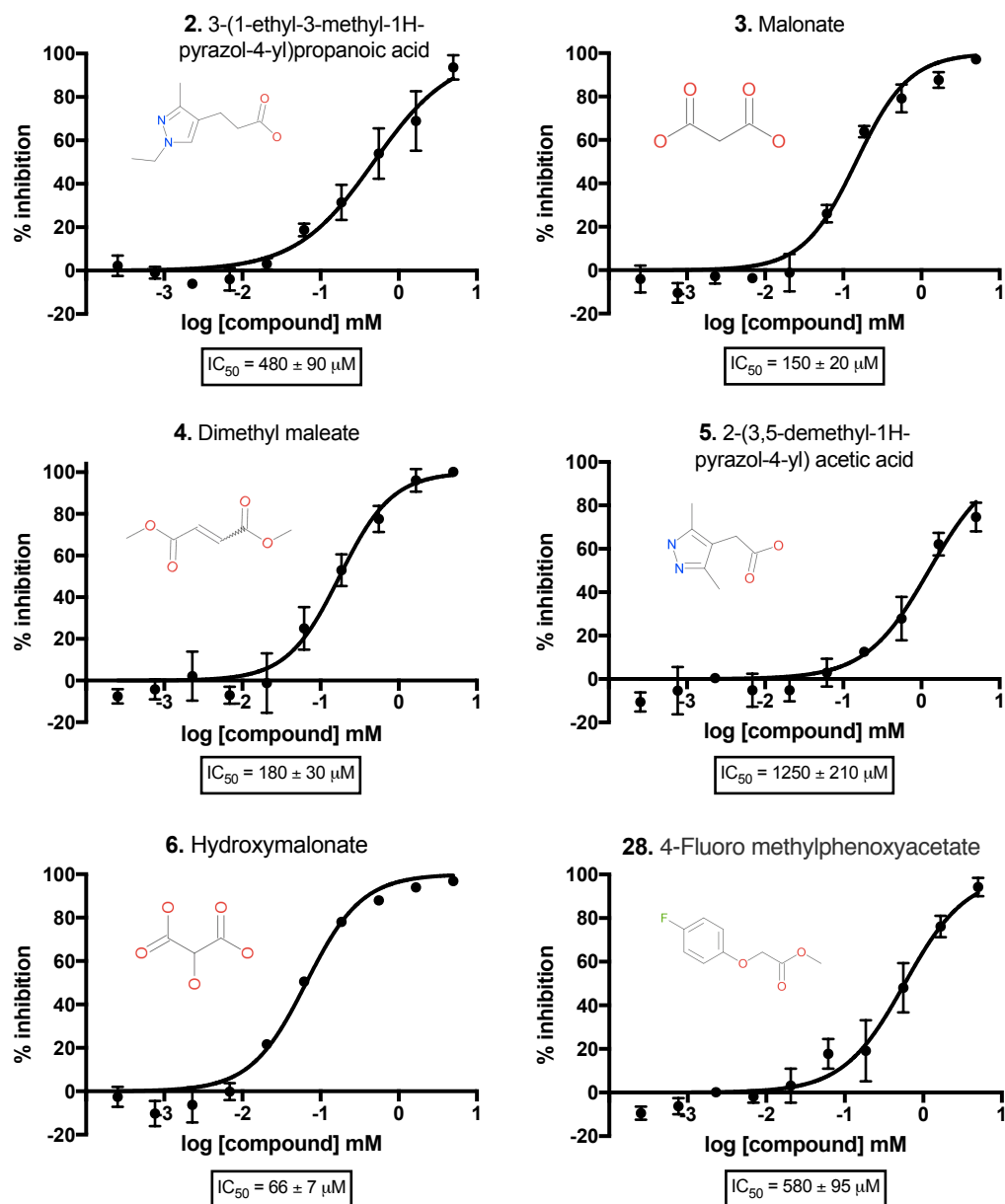


Figure 6.1. Inhibition curves for six SR literature inhibitors.

IC_{50} determination was performed in the coupled biochemical assay for 40 compounds described as SR inhibitors in the literature (Appendix 10.3). Those for which complete inhibition curves were obtained are shown above with their IC_{50} values below each graph, and consist of: malonate (**3**) and its derivatives dimethyl maleate (**4**) and hydroxymalonate (**6**); two pyrazole derivatives (**2** and **5**); and 4-fluoro methylphenoxyacetate (**28**). Assays were performed in triplicate and data shown are the mean of three experiments; error bars = SEM.

6.4.2 Thermal denaturation analysis of literature compounds

The thermal shifts of all literature compounds tested here are shown in Fig. 6.2. A thermal shift was defined as significant if it was equal or greater than the threshold determined by $3 \times \sigma$ (SR + DMSO controls). The standard deviation of the SR + DMSO controls across the thermal denaturation screening data was 0.82, giving $3\sigma = 2.5$. Therefore, shifts of 2.5 °C or greater were considered significant.

Many more of the inhibitors elicited a significant thermal shift than showed inhibition in the biochemical assay. Unsurprisingly, malonate (**3**) and its hydroxyl derivative (**6**) caused the greatest thermal shifts of 5–6 °C, and were the only compounds for which both good inhibition and thermal shift data were collected. After these, the largest thermal shifts were elicited by **10** (dimethyl malonate), and **21** (L-malic acid). It was interesting that D-malic acid (**20**) had a much lower thermal shift than L-malic acid, with DL-malic acid (**18**) falling in between, suggesting that the L-isomer has a higher binding affinity for SR; a conclusion supported by literature data (Stríšovský *et al.*, 2005). Ultimately, caution is advised when drawing conclusions about binding due to the lack of supporting IC₅₀ data.

One literature compound (**34**; small peptide) caused a significant negative thermal shift. As a negative thermal shift is associated with protein destabilisation, it is possible this compound is not an inhibitor but instead interacts with SR to cause denaturation. The small peptide compound **33** (and **34**, which elicited a moderate but statistically insignificant thermal shift) is distinct from the other peptides in the series by the presence of a free primary amine that has the potential to react with the carbonyl groups of residues within the SR structure. It is therefore possible the presence of the primary amine is the reason why this compound has a destabilising effect, whereas the other peptides that have side groups conjugated to the primary amine do not.

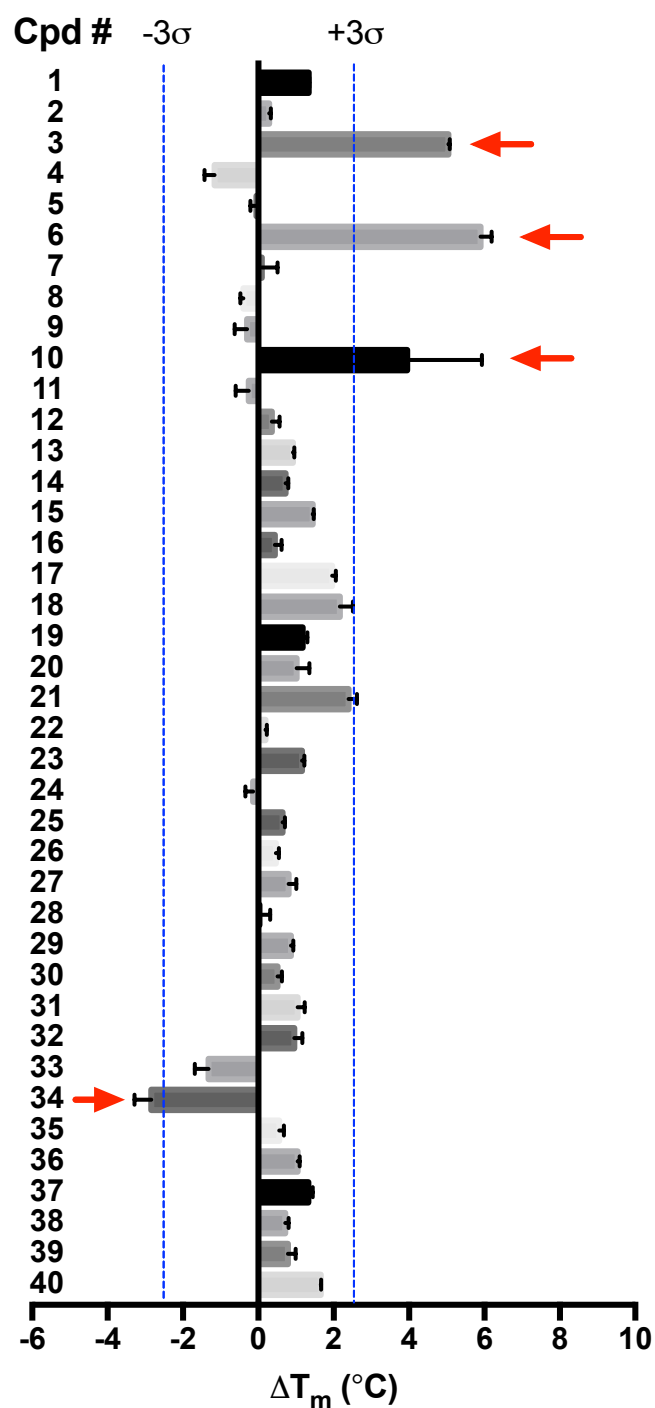


Figure 6.2. Thermal denaturation analysis of literature SR inhibitors.

The melting temperature (T_m) of 1 μ M SR in the presence of inhibitor (1mM for fragments, 100 μ M for compounds) was established and compared to SR + DMSO controls to find the thermal shift. The threshold for significant shifts (3σ) was determined to be 2.5 °C from the SR + DMSO controls. Red arrows indicate significant thermal shifts. Experiments were performed in triplicate; data are from three independent experiments ($n = 3$).

6.5 DISCUSSION

Out of 40 compounds described as SR inhibitors in the literature, IC₅₀ values could only be determined for six. This small group of compounds included the prototypic SR inhibitor malonate, two of its derivatives dimethyl maleate and hydroxymalonate, two pyrazole derivatives, and a peptide building block. In addition, two others, L(+)-tartaric acid and a pyrazole, elicited high IC₅₀ values (> 5 mM) beyond the range of usefulness for hit-to-lead development. None of the purported peptide inhibitors demonstrated any inhibitory effect in the SR assay.

The results from the peptide compounds were particularly disappointing because they were thought to represent a potent and structurally distinct class of SR inhibitors that could have signified a shift away from malonate-based inhibitors. These bulky hydrophobic peptides were described as having IC₅₀ values similar to malonate (Mori *et al.*, 2014) in distinct but conceptually analogous coupled assays to the one used here (Table 6.1). The authors of the first report on peptide SR inhibitors claimed the mode of inhibition was competitive based on double-reciprocal plots (Dixon *et al.*, 2006), but the Mori *et al.* report did not characterise enzyme kinetics to support this conclusion. It is possible the large, hydrophobic peptides compete for surface-exposed areas to inhibit allosterically. In the Mori study, the Dixon study, and the present study, both Mg²⁺ and ATP were present in excess (Table 6.1) and would be resistant to being outcompeted by an inhibitor, therefore it is unlikely the peptide compounds were interacting with the Mg-ATP site.

It could be that the stoichiometry between enzyme, substrate, and inhibitor had a significant influence on the level of inhibition observed. The study by Mori and colleagues used 1 µM hSR, 20 mM L-serine (unusually high, given the reported K_m of L-serine racemisation by SR is around 5 mM), and 1 mM peptide compound; whereas in this study, the concentrations used were 400 nM SR, 2 mM L-serine, and 500 µM maximum peptide concentration. That inhibition is not relieved with such a high concentration of substrate in the Mori study gives credence to the possibility of the

mode of inhibition being noncompetitive or uncompetitive. Alternatively, substrate inhibition could be occurring instead of or in conjunction with peptide inhibition due to the high levels of L-serine. Substrate inhibition occurs in about 20% of all known enzymes and is primarily caused by more than one substrate molecule binding to an active site meant for just one, usually by different parts of the substrate molecule binding to separate subsites.

Table 6.1. Comparison of assay parameters from the present study and two reports on SR peptide inhibitors.

Assay parameter	Dixon et al. 2006	Mori et al. 2014	Koulouris 2017
SR	Human	Human, 1 μ M	Human, 400 nM
Enzyme purity	?	80%	> 95%
[L-serine]	1.25 mM	20 mM	2 mM
[Compound]	2 mM	1 mM	1 mM
Buffer system	200 mM TEA-HCl	100 mM HEPES-NaOH pH 8.0	100 mM Tris pH 8.5
Cofactors	2.5 mM ATP, 5 mM Mg ²⁺ , 50 μ M PLP, 10 mM DTT	1 mM ATP, 1 mM Mg ²⁺ , 10 μ M PLP, 5 mM DTT	1 mM ATP, 1 mM Mg ²⁺ , 10 μ M PLP
Detection	NADH absorbance	Pyruvate degradation, absorbance	Chemiluminescence
Inhibitor incubation	40 min	?	15 min, RT
Substrate incubation	?	8 h, 37 °C	20 min, RT

The molecular docking studies performed by Mori and colleagues do build a compelling case for the peptide compounds as novel SR inhibitors. However, during biochemical analysis the same study also described an enzyme purity of 80% for human SR, which although adequate for assay purposes, does increase the risk of detecting contaminating enzyme activity when combined with the high concentrations of enzyme used in coupled assays. In consideration of these factors, it was expected the assay described in the present studies would be sufficiently sensitive to detect inhibition by the peptide compounds. That it did not could most likely be attributed to differences in assay format, or potentially the proposed slow-binding kinetics for the peptide inhibitors (Dixon *et al.*, 2006). Indeed, Dixon *et al.* incubated SR with

compound for 40 min to account for a slow binding mechanism, wherein the inhibitor initially binds in a loose complex with SR, followed by slow isomerisation to the final tighter complex. Further, they noted a slower loss of enzyme activity over time following an initial decrease, indicating slow dissociation of the inhibitor from the enzyme-inhibitor complex. The comparatively short incubation periods of the biochemical assay in the present study (Table 6.1) may have prevented observation of this slow inhibitory effect.

It is more difficult to explain why many of the analogues and derivatives of malonate, such as malic acid and succinic acid, did not exhibit inhibition. At least with the pyrazole and peptide compounds, one could argue that experimental discrepancies may be expected because the data had not been verified by other sources. Malonate derivatives and related carboxylic acids, on the other hand, have been well characterised in the literature for their inhibitory potential against SR. Succinic acid (**17**), L-malic acid (**21**), and dihydroxyfumaric acid (**7**) were all expected to demonstrate SR inhibition in the SR assay, especially as their structural similarity to malonate suggested they would be suitable for IC₅₀ determination using this method. Ultimately, most of the carboxylic acids only elicited thermal shifts that were insignificant, as well no measurable IC₅₀, which together suggests no inhibition was occurring despite published data to the contrary.

Although the results discussed in this chapter were unexpected, they do serve to highlight the lab-to-lab variability that exists even when performing very similar assays with almost identical reagents and compounds. From the 40 compounds investigated, no useful starting points were identified for the development of new SR tool inhibitors, which emphasises the need to explore other techniques in the search for novel modulators of SR activity. Ergo, the next chapter will focus on a fragment-based drug discovery approach to achieve such an aim.

7 RESULTS VI: FRAGMENT SCREEN AND HIT VALIDATION

7.1 INTRODUCTION

The development of new drugs targeting therapeutically relevant proteins is a particular challenge when there are few or no pre-existing chemical starting points. Screening of compound libraries has been a traditional approach in drug discovery, but is plagued by a high attrition rate of chemical compounds and a poor record of developing lead compounds (Kola and Landis, 2004). This has spurred the development of fragment-based drug discovery (FBDD) as an alternative approach to identify chemical leads by using as starting points fragments that have similar physical properties to successful drug molecules.

With respect to SR, there is still a distinct lack of potent and selective inhibitors that could function as chemical starting points for drug development. Previous efforts have focused either on compound screening or creating derivatives of pre-existing inhibitors with improved potency, but overall progress has been slow, and only very recently have inhibitors been developed that are structurally distinct from malonate and amino acid analogues (see section 1.7.7). To date, no studies have employed FBDD as an approach to develop novel SR inhibitors. FBDD may be particularly suited to SR because its crystal structure revealed that targeting its active site would require an inhibitor small enough to enter the tight cleft between the large and small domains. Fragment molecules such as those found in screening libraries may overcome this difficulty because they have a very low molecular mass (< 300 Mw) and can be structurally understood by X-ray crystallography and NMR (Rees *et al.*, 2004).

One of the major benefits of FBDD is that it requires significantly fewer fragment molecules to be screened and synthesised prior to generating new lead compounds, compared to the numbers of compounds needed for HTS. There are a number of reasons for this: firstly, fragments have a higher probability of binding to the target site

due to being smaller in both size and complexity (Hann *et al.*, 2001). Secondly, fragments are considered efficient binders because a higher percentage of their atoms are involved in binding despite themselves being weak binders (Schultes *et al.*, 2010). This characteristic is known as having a high 'ligand efficiency', which can be estimated using the free energy of binding ($-\Delta G$) and the number of non-hydrogen atoms of the ligand (Hopkins *et al.*, 2004). Thirdly, there is much more potential for inhibitory fragment molecules to undergo structural optimisation to produce lead compounds that are potent and also still have a low molecular weight (Erlanson *et al.*, 2016).

The characteristics of fragment molecules make FBDD a promising approach to finding novel chemical modulators of SR that have potential for structural optimisation and medicinal chemistry, and accordingly, FBDD has been employed as the primary approach in this thesis. The process of fragment screening and hit validation discussed herein employs the techniques optimised in the preceding chapters, and are all important components of a FBDD strategy. The use of multiple techniques — medium-throughput biochemical assay, three biophysical methods, and an optimised crystallisation protocol — enabled the development of a streamlined drug discovery process that covered fragment library screening, hit identification, and hit validation.

The fragment screen was performed in the biochemical assay with two fragment sets: the Maybridge Ro3 2500 Diversity Fragment Library (containing 2500 fragments) and the Life Chemicals 3D Fragment Library (containing 642 fragments). The Maybridge Ro3 library has been specifically engineered to improve Ro3 (rule of three) compliance, which is a set of parameters that ideal fragments should follow: $Mw < 300$, $ClogP < 3$, the number of hydrogen bond donors and acceptors each should be < 3 , and the number of rotatable bonds should be < 3 (Congreve *et al.*, 2003). The Maybridge library also contains computationally engineered structural diversity, useful levels of solubility in DMSO and buffer, and omits potentially problematic reactive groups to overall make it suited for generating hit matter in drug discovery (Maybridge, 2017). The Life Chemicals 3D library was developed based on the concept that higher three-dimensionality of molecules is a desirable feature of drug candidates and is thought to correlate with successful passage of molecules at various stages of clinical

development (Life Chemicals, 2017). Other key features of the Life Chemicals 3D library include $\text{ClogP} \leq 3$, at least one chiral centre, no more than one –cyano, –nitro, or bromine group, and ideally two points of functionalization. The Life Chemicals library has also removed undesirable functionalities, such as pan-assay interference compounds (PAINS) that manifest frequently as false positives and artefacts (Baell and Walters, 2014). Together, these two fragment libraries cover a broad range of structural diversity and beneficial features that are well suited to the generation of new hit matter for a drug target that is already lacking in biologically useful inhibitors.

The aim of this chapter was to use the techniques described in this thesis to perform a FBDD strategy with SR, by a) screening the two aforementioned fragment libraries using the biochemical assay optimised for medium-throughput screening, b) characterising binding of any hits using a combination of the three biophysical methods (thermal shift, MST, ITC) and deducing their K_D where possible, and c) confirming binding to SR with X-ray crystallography. As will be described in further detail hereafter, this process led to the elucidation of a novel SR inhibitor — 3-pyridin-4-yl benzoic acid (referred to as F01 in this chapter) — that not only showed activity and binding in the biochemical and biophysical assays, but most excitingly, was successfully crystallised bound to SR. The crystal structure of SR bound to this novel fragment inhibitor will be a valuable contribution to SR research and potentially enable rational design of novel drugs for the treatment of various CNS disorders. The SR screening cascade is shown in Fig. 7.1.

Note on nomenclature: individual fragments will be discussed as their assigned numbers preceded by 'F' to distinguish them from the compounds in Chapter 6 — e.g. F01, F39, etc.

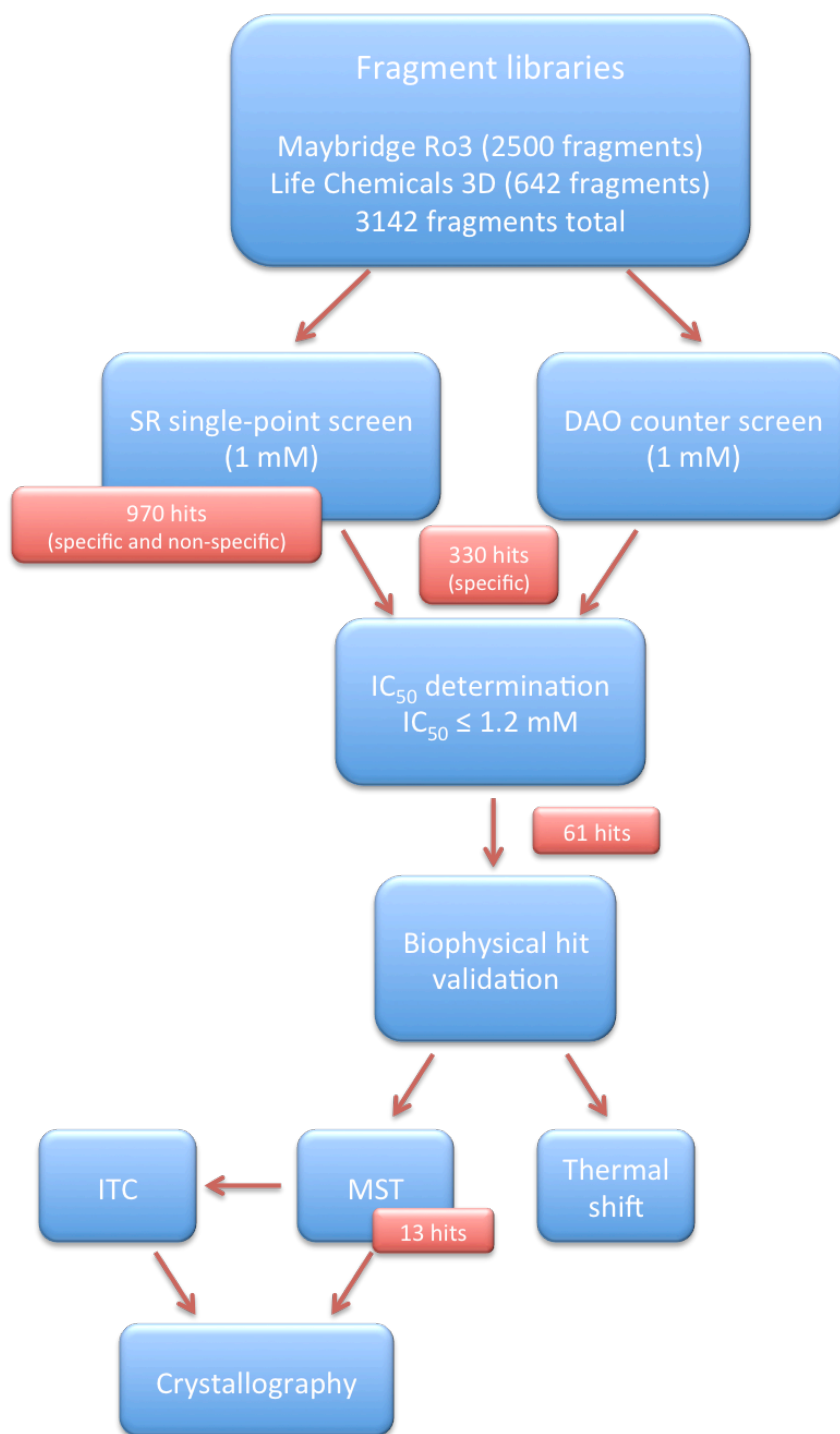


Figure 7.1. SR screening cascade.

Two fragment libraries (Maybridge Ro3 and Life Chemicals 3D) were screened at 1 mM in the SR assay, then in the DAO counter screen to eliminate non-specific hits. 330 SR-specific hits were advanced to IC₅₀ determination. The 61 most potent hits (IC₅₀ ≤ 1.2 mM) were advanced to biophysical hit validation. Thermal shift was inconclusive. 13 potential binders were identified from MST, and following ITC and crystallography trials, the X-ray crystal structure of SR-F01 was determined to 1.8 Å.

7.2 MATERIALS

7.2.1 Reagents

Reagent	Supplier (product code)	Stock concentration
Serine racemase	Purified in-house	Various
L-serine	Sigma-Aldrich (S4500)	200 mM
D-serine	Sigma-Aldrich (S4250)	10 mM
Sodium malonate	Sigma-Aldrich (63409)	100 mM or 1 M
Malonic acid	Sigma-Aldrich (M1296)	100 mM or 1 M
Benzoic acid	Sigma-Aldrich (B3420)	100 mM
DMSO	Fisher Scientific (D4120/PB08)	100%

7.2.2 Fragment libraries

Library	Source	Concentration (mM)		
		Stock	Single-point	Top IC ₅₀
Ro3 2500 Diversity Fragment Library	Maybridge	100	1	5
3D Fragment Library	Life Chemicals	100	1	5

7.2.3 Buffers and solutions

Buffer	Compounds	Supplier (product code)	Concentration
Tris mix buffer	Tris-HCl pH 8.5	Sigma-Aldrich (154563)	100 mM
	Pluronic F-127	Sigma-Aldrich (P2443)	0.05%
	Magnesium chloride	Sigma-Aldrich (M8266)	1 mM
	ATP	Acros Organics (102800100)	1 mM
	PLP	Sigma-Aldrich (P9255)	10 µM
Detection solution A	Tris-HCl pH 8.5	Sigma-Aldrich (154563)	100 mM
	Pluronic F-127	Sigma-Aldrich (P2443)	0.05%
	EDTA	Alfa Aesar (A10713)	2 mM
	HRP	Sigma (P8125)	0.5 U/mL
	DAO	Sigma-Aldrich (A5222)	1 U/mL
	Luminol	Sigma-Aldrich (A4683)	50 µM
Detection solution B (counter screen only)	Tris-HCl pH 8.5	Sigma-Aldrich (154563)	100 mM
	Pluronic F-127	Sigma-Aldrich (P2443)	0.05%
	EDTA	Alfa Aesar (A10713)	2 mM
	HRP	Sigma (P8125)	0.5 U/mL
	Luminol	Sigma-Aldrich (A4683)	50 µM
SR solution I ¹	Serine racemase	Purified in-house	400 nM
	Tris mix buffer	N/A	N/A
SR solution II ²	Serine racemase	Purified in-house	1 µM
	Tris mix buffer	N/A	N/A
L-serine solution I ¹	L-serine	Sigma-Aldrich (S4500)	4 mM
	Tris mix buffer	N/A	N/A
L-serine solution I ²	L-serine	Sigma-Aldrich (S4500)	5 mM
	Tris mix buffer	N/A	N/A
D-serine solution	D-serine	Sigma-Aldrich (S4500)	37.5 µM

	Tris mix buffer	N/A	N/A
--	-----------------	-----	-----

¹ Solutions used when no fragment/compound is present

² Solutions used when fragment/compound is present (concentrations adjusted when there is a pre-incubation with inhibitor to keep final assay concentrations of enzyme and substrate the same)

7.2.4 Further materials, equipment and kits

Equipment	Supplier/manufacturer (product code)
Tween-20	Sigma-Aldrich (P1379)
Ethanol	VWR (85651.320)
Foil Plate Seals	SLS (PCR0620)
96-well v-bottom clear polypropylene plates	SLS (MIC9050)
Corning® 3574 384-well plates	Fisher Scientific (10382883)
PERAstar FS plate reader	BMG (n/a)
Multidrop Combi™ reagent dispenser	Thermo Scientific (5840300)
Small tube metal tip dispensing cassette	Thermo Scientific (24073295)
Xpp-721 liquid handling robot	FluidX (n/a)
EZ-Load 96-well pipette tips 125 µL	Apricot Designs (125-096-EZ-NS)
EZ-Load 8-channel strip tips	Apricot Designs (125-008-EZ-NS)
Allegra X-30R centrifuge	Beckman Coulter (A99470)

7.3 METHODS

7.3.1 SR single-point fragment screen

The fragment screen was performed single-point, in duplicate, with 3142 fragments ($M_w < 300$) from two fragment libraries: the Maybridge Ro3 2500 Diversity Fragment Library, and the Life Chemicals 3D Fragment Library.

All automated dispensing steps were performed with a Multidrop Combi and compound addition steps with a FluidX Xpp-721 liquid handler. Before use, the dispensing cassette of the Multidrop Combi was primed with assay solution to ensure there were no air bubbles in the tubes or blocked tips. After use, the head was successively cleaned with MilliQ H₂O, 0.05% Tween, 70% ethanol, and then MilliQ H₂O. The plates were centrifuged briefly (Allegra X-30R) at 500 rpm after each addition and sealed with a foil plate seal during each incubation step.

Preparation of the stock and intermediate plates. The 96-well stock plates containing 100 mM fragment libraries solubilised in 100% DMSO were stored at -20 °C. Before use, the plates were thawed at RT and centrifuged briefly to settle insoluble particulates. The 96-well intermediate plate was preloaded with 38 μ L Tris mix buffer then manual additions were made for the 0% inhibition (2 μ L 100% DMSO; final concentration 1%), 50% inhibition (2 μ L 10 mM malonate in 100% DMSO; final concentration 100 μ M), and 100% inhibition (2 μ L 100 mM malonate in 100% DMSO; final concentration 1 mM) controls to columns 1 and 12 (Fig. 7.2A for plate map). Fragment stock was then transferred from the library stock plate to the corresponding wells of its intermediate plate (2 μ L; FluidX Xpp-721 with EZ-Load 96-well pipette tips). Four intermediate plates were required for one 384-well assay plate.

Assay procedure. The 384-well assay plate was preloaded with the positive (plus enzyme; 4 μ L SR solution II) and negative (no enzyme; 4 μ L Tris mix buffer) controls to

columns 1, 2, 23, and 24 (Fig. 7.2B for plate map). SR solution II was dispensed into columns 3-22 (4 μ L; final concentration 400 nM). Samples were then transferred from each of the four intermediate plates (2 μ L; final fragment concentration 1 mM; FluidX-Xpp-721 with EZ-Load 96-well pipette tips) to the 384-well assay plate using a quadrant layout (Fig. 3.2B), and the plate was incubated for 15 min at RT. L-serine solution II was dispensed to the entire plate to start the reaction (4 μ L; final concentration 2 mM; Multidrop Combi), and then the plate was incubated for 20 min. The H₂O₂ produced in the assay was quantified with the addition of 30 μ L Detection Solution A, and after a 5 min incubation the luminescence signal was measured.

A

	1	2	3	4	5	6	7	8	9	10	11	12
A	DMSO	Intermediate Fragment dilution										DMSO
B												
C												
D	100% malonate											50% malonate
E	50% malonate											100% malonate
F	DMSO											DMSO
G												
H												

B

	1	2	3	4	5	6	7	8	9	10	11	12	13	14	15	16	17	18	19	20	21	22	23	24
A	No enzyme (100% inhibition)	Samples																				Enzyme alone (0% inhibition)		
B																								
C																								
D																								
E																								
F																								
G	50%																					100%		
H	inhibition																					inhibition		
I	100%																					50%		
J	inhibition																					inhibition		
K	Enzyme alone (0% inhibition)																						No enzyme (100% inhibition)	
L																								
M																								
N																								
O																								
P																								

Figure 7.2. Plate maps for the SR fragment screen.

Shown are the plate maps for preparation of the intermediate plate (A) and 384-well assay plate (B). Inhibition controls contain malonate.

7.3.2 DAO counter screen

The DAO counter screen was designed to rule out fragments that appear to inhibit SR but could be non-specifically inhibiting other components of the SR assay, such as DAO or the chemiluminescence reaction. The general procedure of the DAO counter screen was the same as the SR fragment screen, but contained no SR, used D-serine as a substrate, and used the DAO inhibitor sodium benzoate as a control inhibitor.

Preparation of the stock and intermediate plates. The intermediate 96-well plate was prepared as in section 7.3.1 but with DAO controls for 0% inhibition (2 μ L 100% DMSO; final concentration 1%), 50% inhibition (2 μ L 2.5mM sodium benzoate; final concentration 25 μ M), and 100% inhibition (2 μ L 25mM sodium benzoate; final concentration 250 μ M).

Assay procedure. SR was omitted from the counter screen and instead 4 μ L Tris mix buffer was dispensed across the entire 384-well plate. The procedure was otherwise performed as in section 7.3.1, but instead of L-serine solution II, D-serine solution was dispensed into all wells of the 384-well plate (4 μ L; final concentration 15 μ M). The purpose of the D-serine solution was to mimic the product produced during the SR assay and to act as a substrate for DAO.

7.3.3 IC₅₀ determination of fragment screen hits

SR hits identified in the fragment and counter screen were selected for IC₅₀ determination. Experiments were repeated twice, in duplicate.

Preparation of stock and intermediate plates. Hits were cherry-picked from the fragment library stock plates to create new IC₅₀ stock plates. Each 100 mM fragment hit was used to perform one 10-point 1:3 serial dilution in 100% DMSO per row of a 96-well stock plate (FluidX Xpp-721 with EZ-Load 8-channel strip tips). The 96-well intermediate plates were preloaded with 9 μ L Tris mix buffer, then the stock dilution

series were transferred to the intermediate plates (3 μ L; FluidX Xpp-721 with EZ Load 96-well pipette tips). Two intermediate plates combined into one 384-well plate.

Assay procedure. The 384-well assay plate was manually preloaded with the positive (plus enzyme; 4 μ L SR solution II) and negative (no enzyme; 4 μ L Tris mix buffer) controls to columns 1, 2, 23, and 24. SR solution II was dispensed to columns 3-22 (4 μ L; final concentration 400 nM). Samples were transferred in duplicate from two intermediate plates to the 384-well assay plate (2 μ L; final concentrations 0–5 mM; FluidX-Xpp-721 with EZ-Load 96-well pipette tips) using a quadrant layout, and the plate was incubated for 15 min at RT. L-serine solution II was dispensed to all wells to start the reaction (4 μ L; final concentration 2 mM; Multidrop Combi) and the plate was incubated for 20 min. The H₂O₂ produced in the assay was quantified with the addition of 30 μ L Detection Solution A to all wells, and after a further 5 min incubation the luminescence signal was measured.

7.3.4 Fragment screen data analysis

Raw plate data from the fragment screen and counter screen was uploaded into and analysed using the Dotmatics Electronic Lab Notebook (ELN) server (<http://dotmatics.chem.sussex.ac.uk>) to calculate percentage inhibition. Plate data quality was assessed using the Z' score, as described in section 3.3.8.3. Plates were failed if they had a Z' score below 0.5. Plate data with a satisfactory Z' were then analysed using Dotmatics Vortex and GraphPad Prism software. Hits were defined as those exhibiting inhibition greater than $3 \times \sigma$ (positive controls) in the fragment screen, as well exhibiting 0% inhibition $\pm 3 \times \sigma$ (positive controls) in the counter screen. Thus, fragments were classified as hits if they demonstrated a significant percentage inhibition in the fragment screen, and little to no inhibition in the counter screen. Such hits were then selected for IC₅₀ determination. Those with an IC₅₀ of approximately 1.2 mM or less were subject to biophysical analysis to confirm binding.

7.4 RESULTS

The findings from fragment screening, DAO counter screening (to eliminate non-SR-specific hits) and IC_{50} determination are described in the following sections.

7.4.1 Initial SR screen yields >1000 hits

The fragment screen consisting of 3142 fragments was performed twice. During the screening process, the quality of the plate data was assessed by calculating the Z' for the plate controls; those that were below 0.5 were repeated. The Z' scores for each of the ten plates that comprised the screen are plotted in Fig. 7.3, for both repeats of the screen. All of the plate data taken through for fragment screen hit analysis had a Z' of 0.5 or above, signifying the controls were generally reliable throughout the screening process.

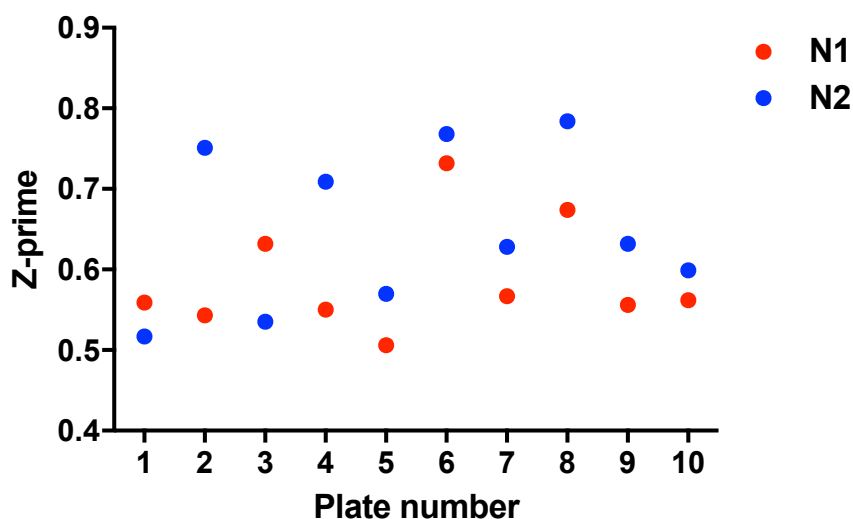


Figure 7.3. Z' scores of each plate from the SR fragment screen.

Each full screen of the fragment libraries required ten plates (numbered 1–10) and was repeated twice (N1 and N2). The Z' scores for all ten plates for both N1 and N2 are plotted on the graph. The Z' was calculated using the means and standard deviations of the positive and negative controls. A Z' of between 0.5 and 1 was considered to be a robust assay.

The percentage inhibition of all fragments from both screens is presented as a scatter plot in Fig. 7.4. The calculated r^2 value of 0.7 (GraphPad Prism) suggests there was a reasonably good correlation and reproducibility between the two screens. Several fragments appeared to inhibit greater than 100% as a result of the luminescence signal being reduced below the background (no enzyme) control, which may be caused by interference with DAO or the luminol redox reaction that respectively turn over basal levels of D-serine and H_2O_2 . Numerous outliers that demonstrated over threefold different inhibition data between screens were discounted from the ensuing hit selection procedure.

Initial 'hits' were defined as those that produced at least 40% inhibition in both assays. The threshold for significant inhibition was defined as $3 \times$ standard deviation of the positive (high enzyme) controls across the entire screen. Here, the standard deviation of all positive controls was calculated to be 13.2, giving an initial limit of $(3 \times 13.2) = 39.6\%$, which for simplicity was rounded to 40%. The number of hits that elicited 40% inhibition or greater in both screens was 1056.

It seemed pertinent, based on the substantially large number of hits, to then increase the stringency by raising the threshold to 50%. The outcome would be an improved likelihood of the fragments within the confidence interval being genuine hits, as well as reducing the initial hit number. A 50% significance threshold reduced the hit number to 970; equivalent to a hit rate of 30%. This hit rate was greater than that typically expected for a fragment screen (~10%), but it was probable many of these initial hits were false positives.

A histogram of the hits (Fig. 7.5), shows how the high hit rate resulted in a highly spread normal distribution. The fragments with 50% inhibitory activity or greater are shown in green after the vertical dashed line. At this stage, it was not possible to ascertain which fragments were inhibiting non-specifically.

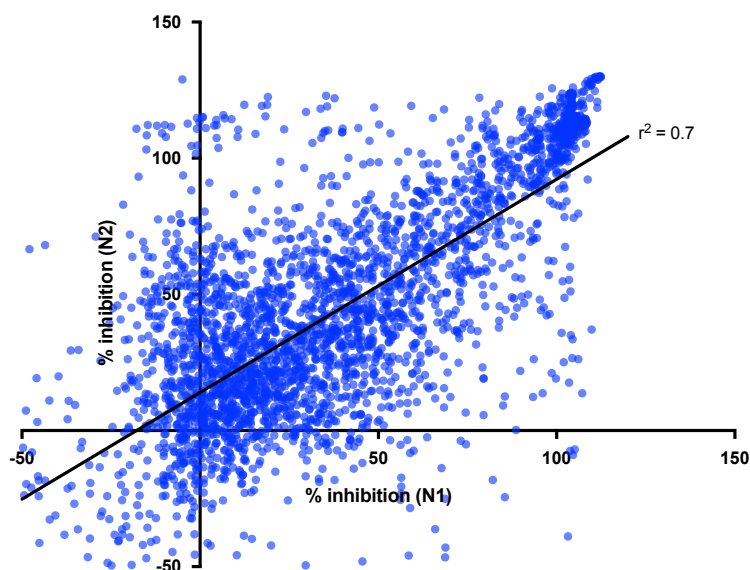


Figure 7.4. Percentage inhibition of SR activity by fragment molecules in the fragment screen.

Fragments from two libraries were screened twice at a concentration of 1 mM and the results from the first repeat (N1) are plotted against those from the second repeat (N2), giving an R^2 value of 0.7. Only fragments eliciting at least 50% inhibition in *both* screens were considered hits.

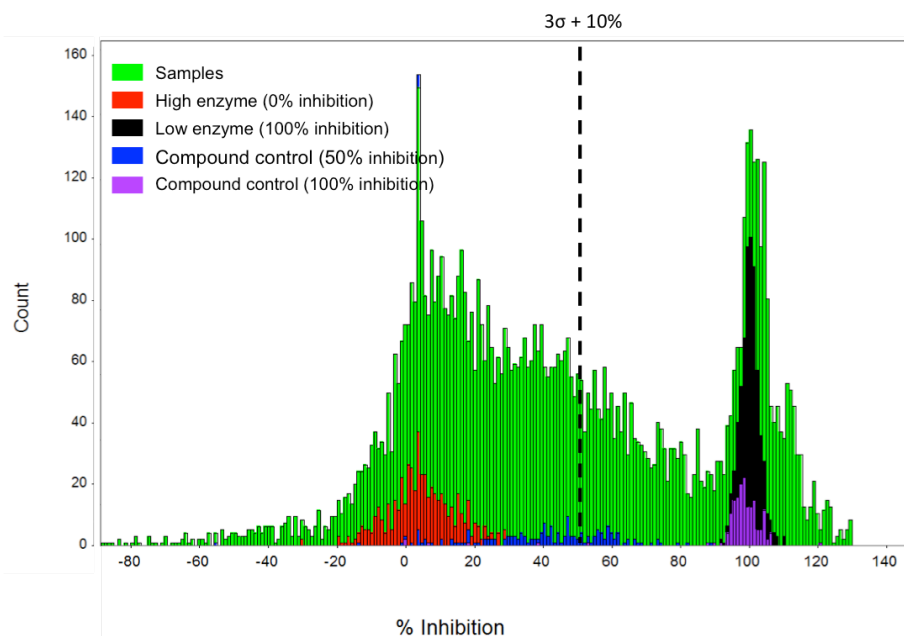


Figure 7.5. Histogram of fragment molecule activity in the SR fragment screen.

Fragments from two libraries (Maybridge Ro3 2500 and Life Chemicals 3D fragment libraries) were screened and the distribution of their percentage inhibition was plotted (green). The high (red) and low (black) enzyme controls were normally distributed around 0% and 100%, as expected. Malonate (SR inhibitor) was used as the compound control. The threshold for significant inhibition was defined as 50%, determined by $3 \times \sigma$ (positive controls) + 10% to increase stringency, resulting in 970 hits. $N = 2$.

7.4.2 DAO counter screen reduces hit number to 330

The purpose of the DAO counter-screen was to try to eliminate non-specific hits. By repeating the fragment screen without SR, and cross-referencing hits from the SR screen and the counter screen to eliminate those that inhibited the assay in the absence of SR, it was possible to produce a final list of specific SR hits (although unconfirmed binding). The counter screen was performed once, and the threshold for the counter screen was defined as previously: $3 \times \sigma$, where σ is the standard deviation of the positive (100% SR activity) controls across the entire screen. The threshold of the DAO counter screen was thus calculated to be 25% inhibition. Therefore, fragments that yielded an inhibitory effect of 50% or greater in the SR screen whilst also demonstrating inhibition of $0 \pm 25\%$ in the DAO counter-screen were considered hits specific to the racemisation reaction.

The scatter plot in Fig. 7.6A shows the average percentage inhibition of the 970 apparent inhibitors from the initial fragment screen against the percentage inhibition of those same fragments in the counter screen. All the fragments exhibited at least 50% inhibition in the SR screen, and highlighted in blue are those fragments that fell within the $0 \pm 25\%$ inhibition range in the DAO counter screen. Although there is not a discernable strong correlation between the SR screen and counter screen data, the cluster of data points upwards of 90% in both screens indicates much of the apparent SR inhibition was a result of non-specific activity against DAO or other components of the chemiluminescence reaction.

The corresponding histogram of the counter screen inhibition data is presented in Fig. 7.6B. As expected, the data appear to be largely normally distributed around 0% inhibition for SR specific hits, and around 100% inhibition for non-specific inhibitors. Those fragments that fell within the $0 \pm 25\%$ inhibition range are highlighted in blue; the total number of these hits was 330, bringing the hit rate down to a more congruous 10%.

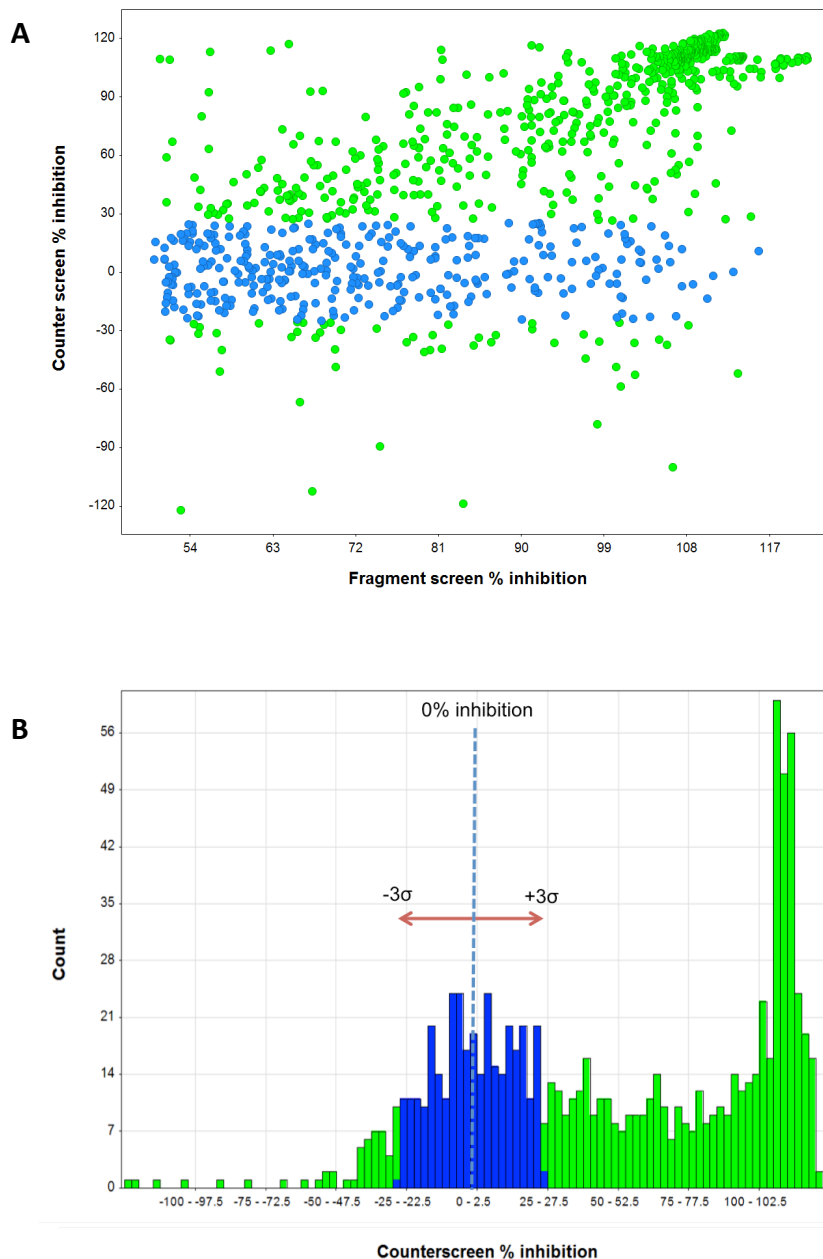


Figure 7.6. Inhibition data for fragment hits in the DAO counter screen.

(A) Scatter plot of the 970 fragments demonstrating at least 50% inhibition in the SR screen (averaged value from two repeats) against their percentage inhibition in the DAO counter screen. (B) Histogram showing the distribution of percentage inhibition data of the 970 fragment hits in the DAO counter screen. The fragments that fell within the $0 \pm 25\%$ inhibition range in the counter screen totalled 330 and are highlighted in blue in both (A) and (B).

The inhibitory activity of the 330 SR-specific hits remaining after elimination of non-specific hits in the counter screen was plotted again to determine the correlation between screen repeats (Fig. 7.7). The r^2 of the SR specific hits (0.3) was considerably lower than the correlation of all fragments in Fig. 7.4 (0.7), presumably because many of the inactive and non-specific fragments were respectively clustered around 0% and 100% inhibition, creating a more apparent trend. It is clear in both cases there was often a substantial amount of variability between repeats, and this effect is more pronounced with the smaller activity range of the SR-specific hits. The percentage inhibition values for F01 (Fig. 7.7; green circle) from each repeat of the fragment screen were in agreement with each other at 57% and 70% inhibition.

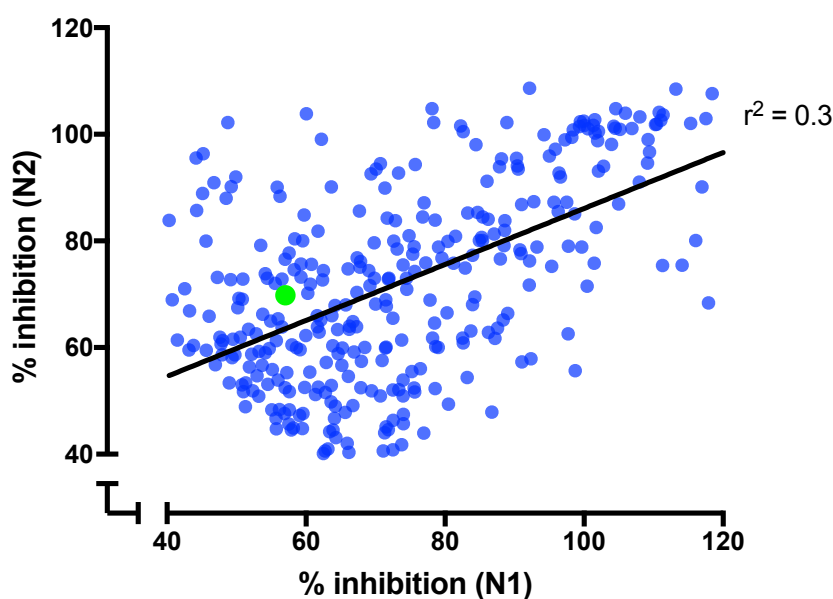


Figure 7.7. Correlation and distribution of SR-specific fragment hits.

(A) Scatter plot of percentage inhibition of the 330 fragment hits from each repeat of the screen. The correlation was found to have an r^2 value of 0.3. F01, the fragment with binding confirmed by X-ray crystallography, is highlighted in green.

7.4.3 IC₅₀ determination of the hits

The inhibitory potential of the 330 SR hits was characterised by determining their IC₅₀ values twice. Many of the hits inhibited moderately well but only at the highest concentrations, giving IC₅₀ values too high to be considered for the next stage of hit validation. The IC₅₀ values of the 330 inhibitors from both IC₅₀ screens are presented in Fig. 7.8A, and the r^2 was calculated to be 0.7. This is a reasonably good correlation, affected in part by the disparate IC₅₀ values observed between experimental repeats for several fragments. The variability was most likely a result of artefactual data, as malonate inhibition controls were in place to detect issues with the assay. F01, the crystallography confirmed SR inhibitor (highlighted in green in Fig. 7.8A), also had variable inhibition data (Fig. 7.8B) with IC₅₀ values of 1648 μ M and 532 μ M.

A majority of the 330 fragments were found to have IC₅₀ values greater than 1mM, despite the stipulation that only fragments eliciting 50% inhibition at 1mM were progressed from the fragment screen. This would mean, in theory, that the fragments should demonstrate an IC₅₀ of around 1 mM or below. That many did not could be reflective of the solubility issues exhibited by several fragments when diluted into buffer from DMSO, which would prevent accurate IC₅₀ determination.

The variability of the IC₅₀ data informed which fragments were selected for progression to biophysical hit validation. Initially, hits were selected if they had an average IC₅₀ up to 1 mM and if the two repeats were within a threefold range. Additional fragments were selected for follow-up if a) both repeats demonstrated a considerably low IC₅₀ value but were not within a threefold range, and b) only one of the determined IC₅₀ values was \leq 1 mM (giving an average IC₅₀ value above 1 mM). The latter stipulation applied to F01. A total of 61 fragments were progressed to biophysical hit validation; their structures and IC₅₀ values can be found in Appendix 10.4.

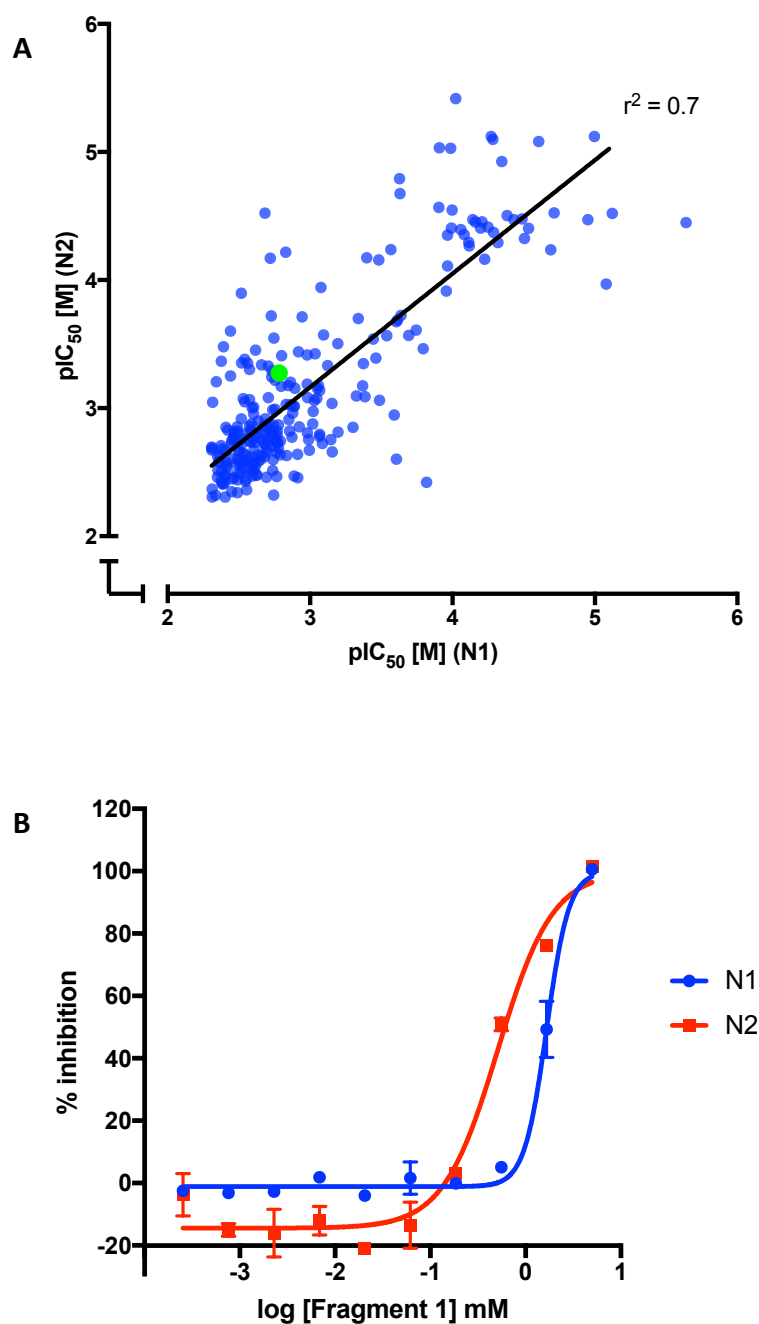


Figure 7.8. Inhibition data for SR-selective fragment hits.

(A) Plotted pIC_{50} values of the 330 fragment hits selective for SR. IC_{50} determination was performed twice on 330 hits identified from the SR fragment screen and DAO counter screen. The r^2 was calculated to be 0.7. 61 of the most potent fragments with an average IC_{50} value of approximately 1 mM or below were selected for biophysical hit validation. F01 is highlighted in green. (B) Inhibition curves for F01. The IC_{50} values were calculated to be 1648 μM (N1) and 532 μM (N2).

7.4.4 Biophysical hit validation

Thermal denaturation, MST, and ITC were utilised to investigate the binding potential of SR to fragment hits.

7.4.5 Thermal denaturation analysis of fragment hits

Following IC_{50} determination, all 61 fragments were subject to thermal denaturation analysis to determine their thermal shifts (Fig. 7.9). The positive control, malonate, produced positive thermal shifts associated with binding that agreed well with previous data (approx. 6 °C; section 4.4.3). A majority of the fragments (48; 79%) produced a negative T_m shift indicative of fragments destabilising SR in the unfolded state, or fragments aggregating and causing early destabilisation of the protein. In addition, some fragments have fluorescence properties that might interfere in the assay.

Significant T_m shifts are often determined qualitatively rather than statistically because there is frequently negligible variation in the control data, potentially resulting in a low threshold value that is inclusive of most of the test compounds. However, because malonate elicits a considerable thermal shift, the significance was determined empirically rather than using malonate data as a reference point. The threshold for significant T_m shift was therefore determined from $3 \times \sigma$, where σ was the standard deviation of the SR and DMSO (no inhibition) controls. This gave a value of 0.75 °C.

Thermal shift data for all 61 fragments in relation to this threshold is presented in Fig. 7.9. Only three fragments caused significant T_m shifts, as indicated by the red arrows: F02, F09, and F52. The remaining fragments either caused negligible shifts, or in the case of 37 fragments, caused a significant negative shift. As negative shifts are indicative of destabilisation, it is likely the 37 fragments were not classically inhibiting SR, but rather, inducing denaturation or aggregation.

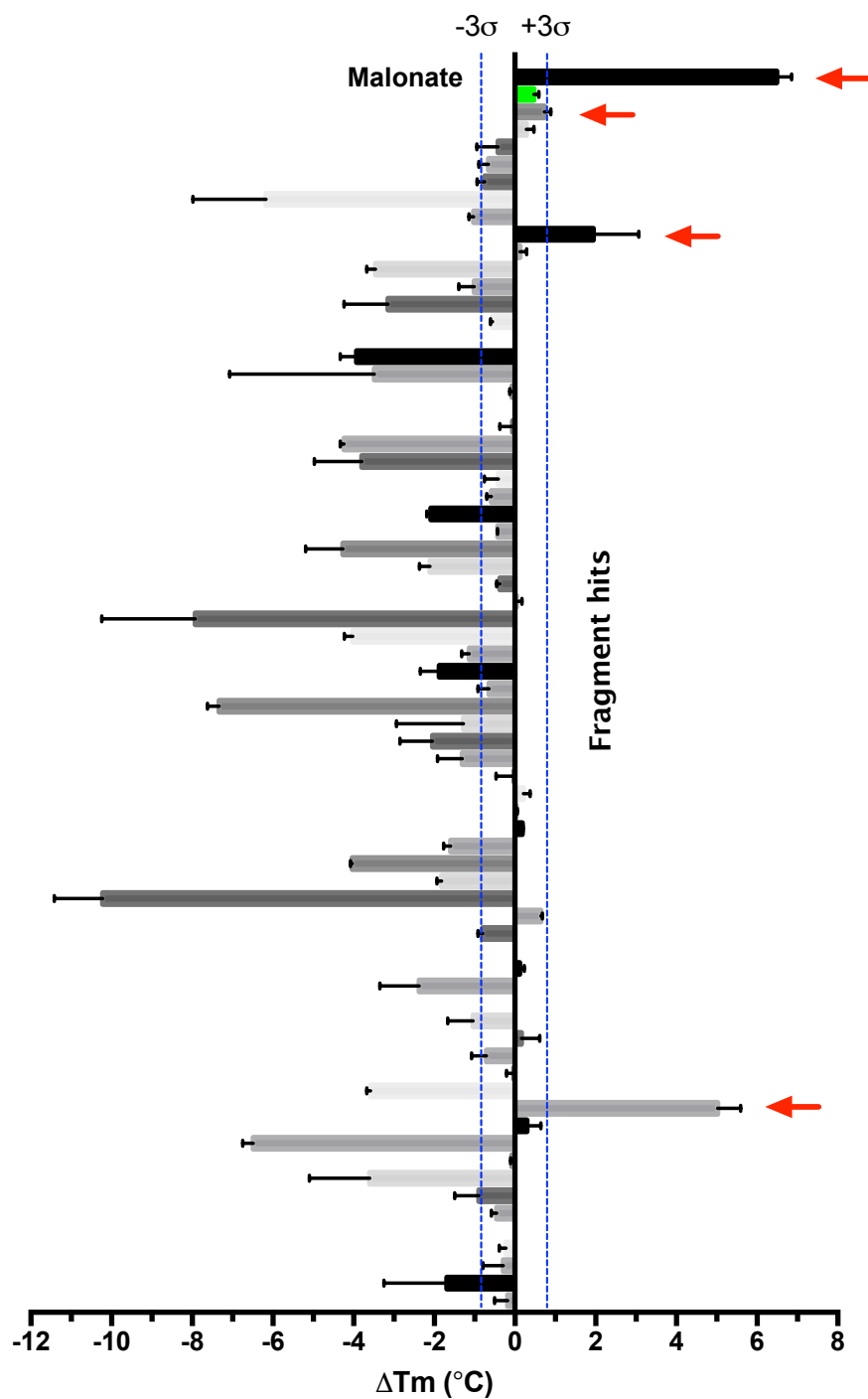


Figure 7.9. Melting temperature shifts for SR incubated with fragment molecule hits.

The melting temperatures (T_m) were determined in the thermal denaturation assay. The direction of the shift may indicate either stabilisation through binding (positive shift) or destabilisation (negative shift). The threshold for significant shifts was defined as $\geq 0.75^{\circ}\text{C}$, determined by $3 \times \sigma$ (SR + DMSO controls) and is indicated by the blue dashed line. Most fragments cause negative shifts; those that caused significant positive shifts are signaled by the red arrows. Error bars = SD, $n = 3$.

Fig. 7.10 shows the thermal denaturation curves of the three fragments that caused a significant positive shift. It is clear that for F52 in particular, and F09 to a lesser extent, the apparent T_m shifts were calculated as a result of abnormal thermal denaturation curves and may not be considered true T_m shifts in the same regard as malonate. Both F02 and F09 appeared to cause considerably elevated background fluorescence, even at the start of the experiment before SYPRO Orange was exposed, which may be responsible for their apparent significant T_m shifts.

Thermal shift assays are capable of detecting binding between low molecular-weight fragments and the target protein they stabilise (Kranz and Schalk-Hihi, 2011), but false negatives are a common problem, as fluorescence quenching by fragments can lead to a high rate of false negatives (Basse *et al.*, 2010). This may explain why F01, which is now known to bind to SR, produced an insignificant thermal shift (0.5 °C). Further, the fact no conformational change was observed in the crystal structure of the SR-F01 complex (section 7.4.12) suggests there was no thermal shift because F01 does not stabilise a closed conformation of SR, as malonate does.

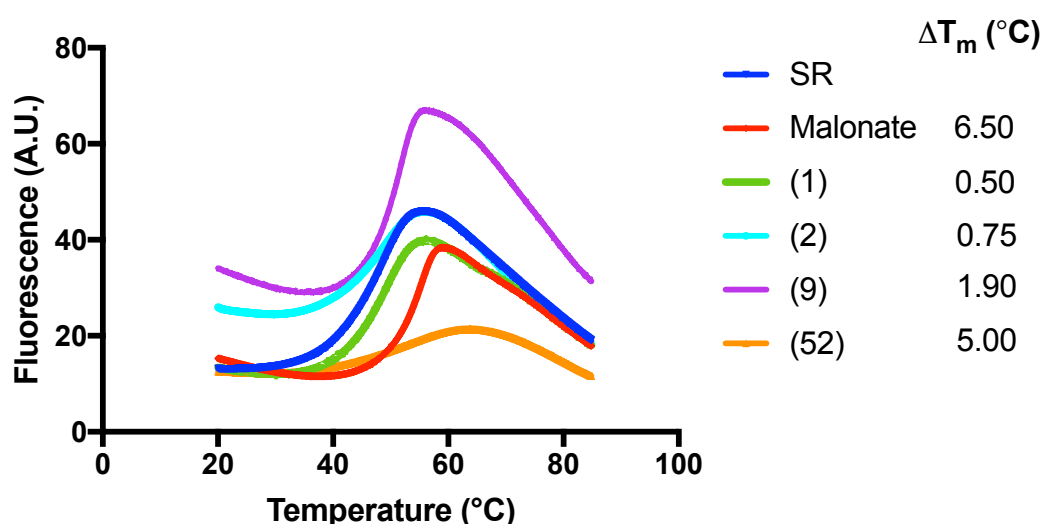


Figure 7.10. Thermal denaturation analysis and melting point shifts (ΔT_m) of SR with four fragment hits.

Thermal denaturation analysis was performed on 1 μ M SR with 61 fragment hits. Of those hits, three produced positive T_m shifts that were statistically significant: F02, F09, and F52. The T_m shift with F01 was not significant. Experiments were performed in triplicate; $n = 2$.

7.4.6 MST single-point analysis of 61 hits

Single-point MST analysis was performed on all 61 hits and repeated three times. The fragments were screened at 1 mM using the conditions previously established.

The average of the DMSO controls was calculated from each plate and used to determine the standard deviation for the entire screen. This resulted in three values, for each repeat of the screen (n), which were then multiplied by three to determine the degree F_{norm} shift that was significant. These values (17, 14, 15; rounded to two s.f.) were calculated independently for each repeat of the screen. The overall downward trend of F_{norm} observed over time (Fig. 4.11) meant even though internal control data for each screen were in agreement, the standard deviation of the DMSO controls across all screens was unusually high. Fragments that caused a significant F_{norm} shift were therefore identified individually from each screen.

When applying these parameters to each screen, eight fragments (F01, F04, F13, F16, F17, F28, F42, and F45) met the criteria for being defined as a hit, with a shift in either the positive or negative direction equal to or greater than the values defined above. A further five fragments (F22, F36, F39, F43, and F53) were approaching the threshold for significance, and ultimately were included in the final group of 13 fragments to increase the likelihood of obtaining a confirmed binder.

The F_{norm} shifts (ΔF_{norm}) of the 13 fragment hits can be seen in Fig. 7.11. Interestingly, all fragments displayed positive thermodiffusion (SR-fragment complex moved away from heat source) except F01, the confirmed binder, and malonate. The fact both F01 and malonate exhibited negative thermodiffusion suggests potential similarities between the two SR-inhibitor complexes. As all fragment molecules had comparable molecular weights, the observed negative thermodiffusion was probably not linked to particle size. Charge could be the common influence — as both F01 and malonate contain negative carboxylic acid groups — as could hydration shell entropy, because ligand binding displaces water molecules and causes shell reorientation, leading to increased entropy as water molecules become more disordered.

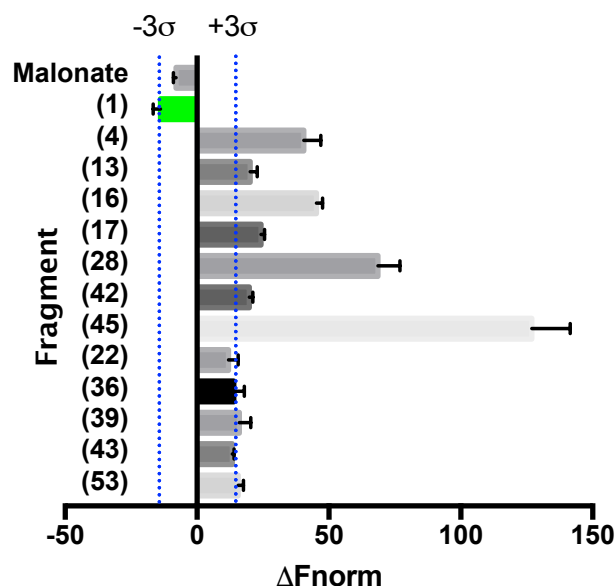


Figure 7.11. SR inhibitor malonate and 13 fragment hits demonstrating a significant F_{norm} shift in MST.

The binding of 1 mM fragment molecule to 50 nM SR was analysed by MST for all 61 fragment hits. The 13 fragments shown here demonstrated a significant F_{norm} shift in at least two of the three repeats. The threshold for significant inhibition was determined by $3 \times \sigma$ (SR + DMSO controls) and is indicated by the blue dashed line. Experiments were performed in duplicate; error bars = SEM, $n = 3$.

7.4.7 MST K_D determination of fragment hits

Further analysis consisted of performing a 10-point titration of each compound to determine their binding affinity via calculation of the dissociation constant (K_D). Not all of the 13 fragments were able to generate complete or even partial binding curves; those that did are displayed in Fig. 7.12 with their calculated K_D values.

A majority of the fragments (7; 54%) demonstrated moderate positive thermophoretic behaviour (Fig. 7.12A). Four of these fragments — F04, F13, F16, and F42 — do not approach a plateau at the top of the curve, which may be the cause of the poor K_D values obtained, or incalculable K_D value in the case of F04. Unfortunately, precipitation and insolubility issues observed for some fragments beyond the highest concentration of 2 mM hindered the complete elucidation of these curves, as adhesion became more prone to occur inside the capillary tubes (detected from the shape of the

peaks in the initial capillary scan). Fig. 7.12B shows the binding curve for the confirmed binder F01, which produced a reversed binding curve owing to its negative thermodiffusion. The approximate K_D of F01 was calculated to be 960 μ M.

The lack of plateau demonstrated by most of the fragments may have resulted in a K_D calculation more susceptible to errors, likely giving K_D values much higher than their true value despite extrapolation by the analysis software. With this in mind, some of the K_D values were still beyond the range of usefulness for further development and optimisation, even with allowances made for the inherent weak binding of fragments. A few fragments did show promising data, albeit not necessarily in all repeats, such as F01, F28, F45, F39 and F43 — all of which gave a K_D of around or less than 1 mM. Although none approached the K_D determined for malonate using MST (Fig. 4.12), the binding affinities suggest these fragments have the potential to be developed further into more potent hit compounds.

The MST signal amplitude of protein-small molecule interactions is typically small, up to 20 counts (Jerabek-Willemsen *et al.*, 2011), because the size or mass of the target protein is not altered considerably by fragment binding. By contrast, the large F_{norm} shifts produced by F28 and F45 of around 300 counts is incongruous with the data for the other fragments and suggests these fragments might be inherently fluorescent. Exceptionally strong fluorescence changes might also indicate aggregation of the bound or unbound state thus causing fluorescent material to be lost before MST analysis (Jerabek-Willemsen *et al.*, 2011). F28 and F45 might still bind to SR, but their intrinsic fluorescence may alter data obtained here, and accordingly, caution should be applied to further experiments in which they are studied.

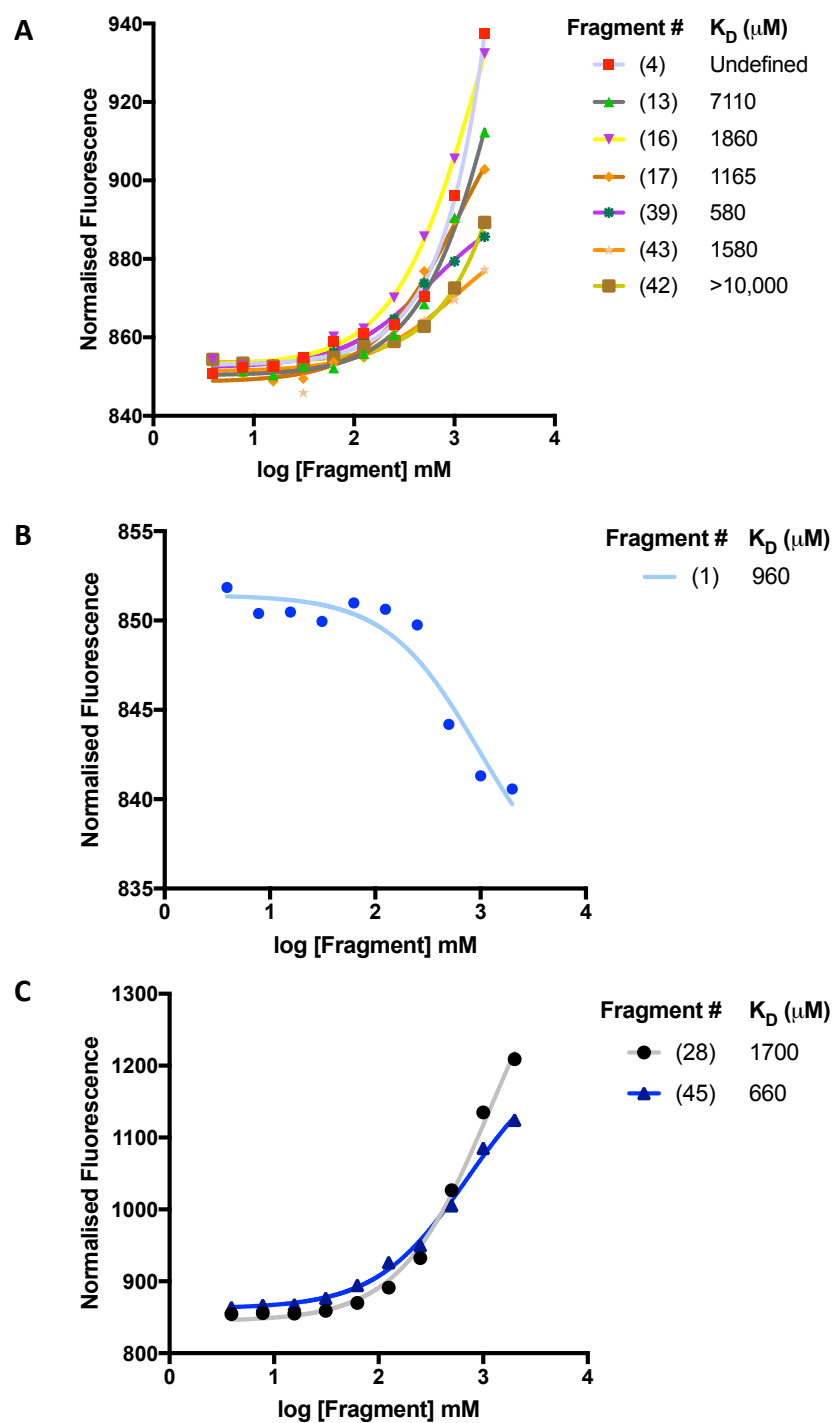


Figure 7.12. K_D determination of SR fragment hits by MST.

(A) 7 of the 13 fragments that elicited binding curves or partial curves and their calculated K_D values; (B) F01 exhibited negative thermodiffusion (towards heat source); (C) K_D curves for F28 and F45 exhibited F_{norm} shifts over threefold greater than others. Extrapolation of the curves and K_D determination were performed by MO. Affinity Analysis software (NanoTemper).

7.4.8 MST aggregation and fluorescence controls

An additional aggregation and fluorescence control was performed on each fragment binding curve, and an example reflective of the controls for the other fragments is given in Fig. 7.13. The aggregation control is a re-read of the plate after a 45 min incubation period to ensure the compound has not caused the protein to aggregate over time, giving a false positive. The curves displayed here retain their overall shape after 45 min, signifying that aggregation has not occurred. For the fluorescence control, all experiments indicate denaturation was successful based on the fluorescence of the samples being restored to an equal value across the dilution series. This suggests that the F_{norm} changes observed were protein-dependent and indicative of a binding event, because compound fluorescence is usually resistant to denaturation attempts.

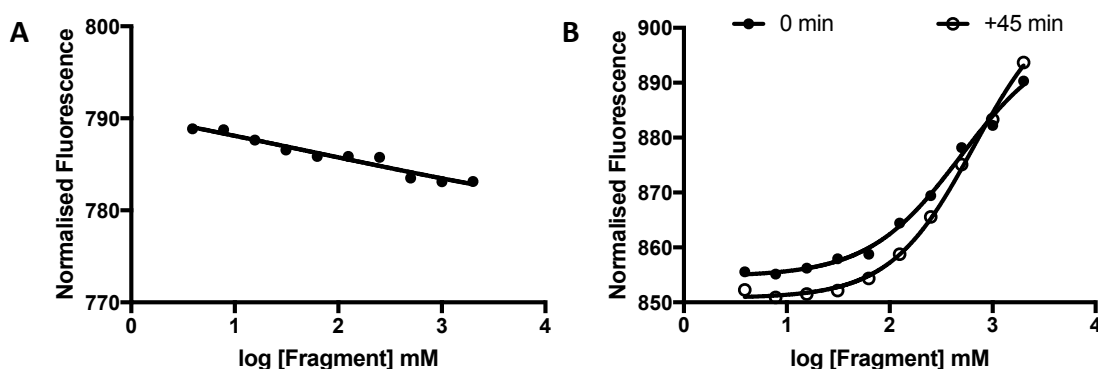


Figure 7.13. MST analysis of F39 and associated aggregation and fluorescence controls.

(A) Binding curve of SR and F39; data were collected immediately after sample preparation (closed circles) and again 45 min later (open circles). No distortion to the overall shape of the curve over time suggests the effect of the test fragment is not a result of causing SR aggregation. (B) Identical samples were denatured with the addition of 5% SDS and 1 mM DTT, followed by heating at 90 °C for 10 min, then analysed by MST. The fluorescence is restored to an equal value across the dilution series, indicating that the changes observed in (A) are protein dependent and therefore a binding event. Data shown are archetypal controls for all test fragments. $N = 2$.

7.4.9 ITC direct titration with fragments

ITC experiments were performed selectively due to experiments being limited by protein consumption. The three fragments with the lowest K_D as calculated by MST were selected for further analysis by ITC. While they were ostensibly the most promising candidates, it should be noted that their apparent potency (K_D values in the 500 μ M to 1000 μ M range) was still much lower than malonate. The three fragments and their K_D values were F01 (960 μ M), F39 (580 μ M) and F45 (660 μ M).

The MST K_D values are reasonably good for hit-to-lead molecules but there were initial complications when selecting relative concentrations of SR and ligand, which have to be adjusted depending on the K_D . The correct ratio of syringe (ligand) concentration to cell (protein) concentration is imperative to drive the equilibrium towards binding, and with weak binders a vastly greater (up to 100-fold) ligand concentration is needed to achieve a curve. To obtain a binding curve of a fragment with a K_D of 500 μ M, the ligand concentration needed to be approximately 80-fold the cell concentration. The challenge here was the difficulty maintaining ligand solubility, and high ligand concentrations increased the DMSO content by default, causing large obscuring DMSO peaks. Reducing the DMSO content (e.g. by dialysis) was not an option due to its function as a solvent. Furthermore, the binding curves that could be obtained by direct binding were unlikely to have the optimal sigmoidal shape necessary for analysis.

Following direct titration with F01, F39, and F45 (Fig. 7.14), the quantity of heat measured for each injection was roughly equal throughout the experiment. Due to the size of the peaks, it was not possible to ascertain whether the peaks were equal-sized because no binding had occurred and therefore there was no enthalpy change, or whether the large DMSO peaks were obscuring a binding curve. As analysing the fragments by direct titration did not appear viable, they were instead analysed by displacement binding experiments.

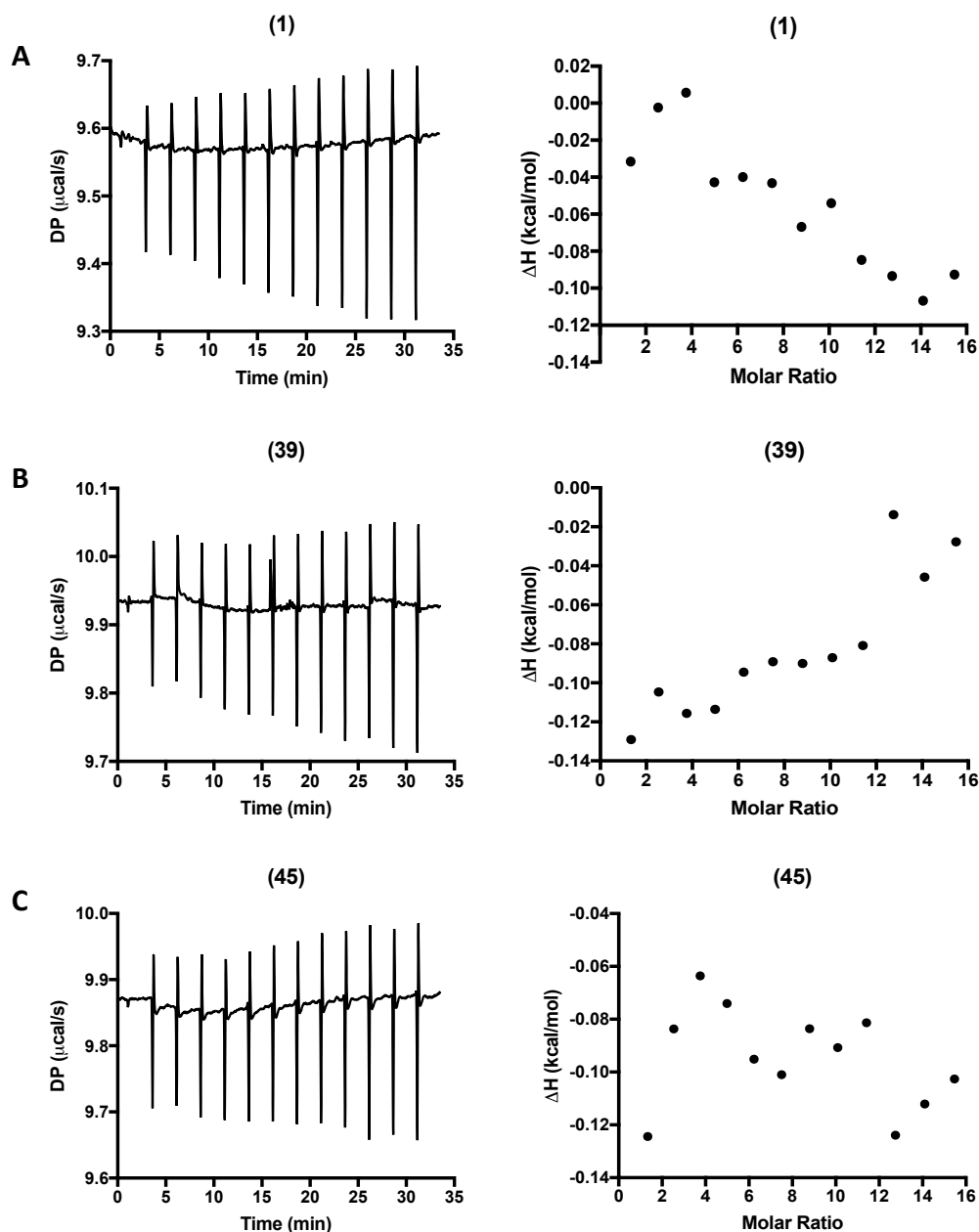


Figure 7.14. ITC analysis of SR and three inhibitory fragment hits by direct titration.

The experiment was performed with F01 (A), F39 (B) or F45 (C) and comprised 13 injections of 2 mM fragment into the sample cell containing 25 μM SR. The raw data peaks (left) were integrated to obtain the enthalpy change (ΔH) and were plotted against the molar ratio of inhibitor to SR in the sample cell (right). All isotherms exhibited large heat of dilution peaks that prevented binding curves of the inhibitors being established.

7.4.10 ITC displacement binding experiments

Weak binders can be analysed by performing a displacement (or competitive) binding assay, another type of ITC experiment. Here, two (or more) ligands that bind to the same target are analysed by measuring the displacement of the weak binder (in the cell with the protein) by the strong binder (titrated by the syringe). The competition of the two ligands will artificially lower the binding affinity of the strong binder and allow a broad thermodynamic profile of the weak binder to be established. This protocol is particularly relevant to drug discovery when evaluating several candidates that might bind to the same target with broadly different affinities, which may require comparison with a well-characterised reference ligand (malonate, in this case). The preface to the results discussed here is that malonate is not a particularly ‘strong’ binder by ITC standards — typically reference ligands are required to exhibit affinities in the high nanomolar range — and this may have affected the accuracy of calculations. A few assumptions have to be made prior to an ITC displacement experiment: binding reactions follow a 1:1 stoichiometry, both ligands bind to the same site of the protein, and the ligands do not interact with each other (Zhang and Zhang, 1998).

Four fragment hits with the best K_D values in the MST screen were chosen for analysis in ITC displacement binding experiments: F01, F17, F39, and F45. The experiment was performed with 100 μ M SR and 1 mM fragment (weak binder) in the cell, and 1 mM malonate (‘strong’ binder) in the injection syringe. Fig. 7.15 shows the binding curves of malonate and SR alone (blue) and malonate when SR was present in the cell with each fragment (red). The thermodynamic quantities of each experiment, in terms of Gibbs free energy (ΔG), enthalpy (ΔH) and entropy ($-T\Delta S$) are shown in Fig. 7.16, for both the strong binder and combined strong and weak binders. It is generally more applicable to discuss ΔG and ΔH values as these are the properties determined in an ITC experiment, whereas entropy ($-T\Delta S$) is calculated as the numerical difference between Gibbs free energy and enthalpy: $\Delta G = \Delta H - T\Delta S$.

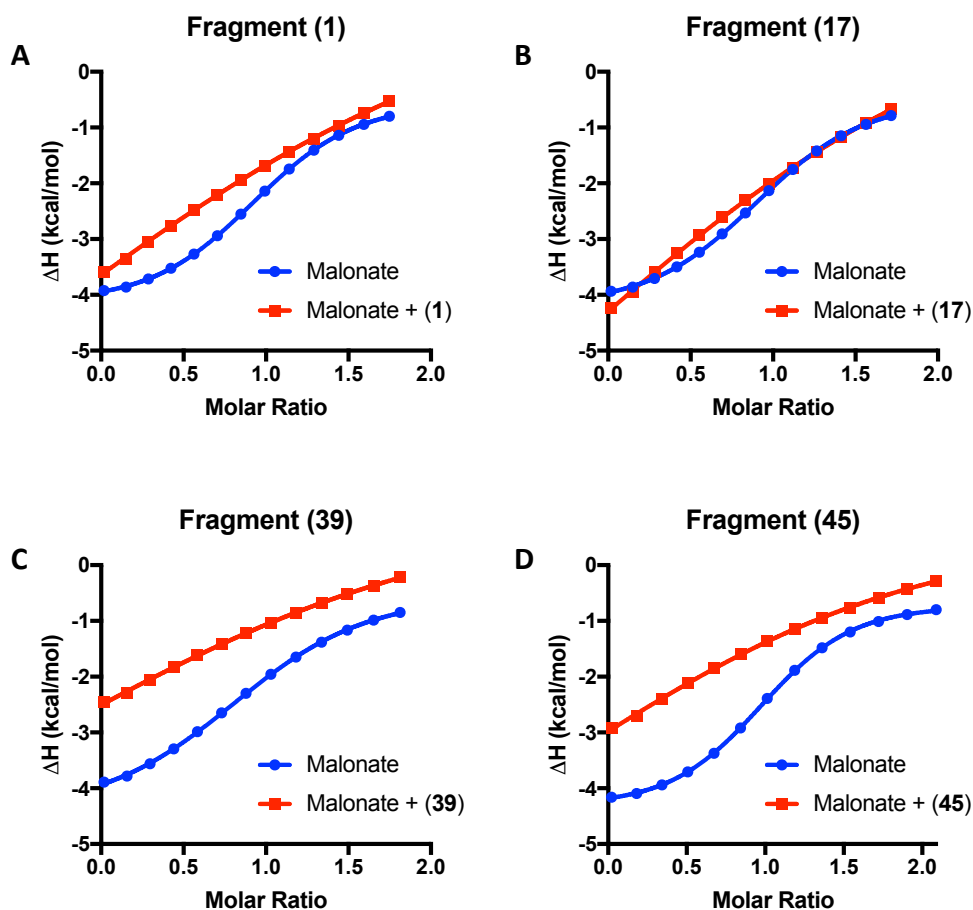


Figure 7.15. ITC displacement experiment of SR with malonate and fragment inhibitors.

The purpose of the displacement assay was to measure the interaction between SR and malonate in the absence (blue) and presence (red) of a fragment inhibitor. The experiment was performed with F01 (A), F17 (B), F39 (C), or F45 (D) and comprised 13 injections of 1 mM malonate into the sample cell containing 100 μ M SR and with or without 1 mM fragment inhibitor. The malonate concentration increases cumulatively with each injection until protein saturation is reached. The raw data peaks were integrated to obtain the above data and were plotted against the molar ratio of malonate to SR in the sample cell.

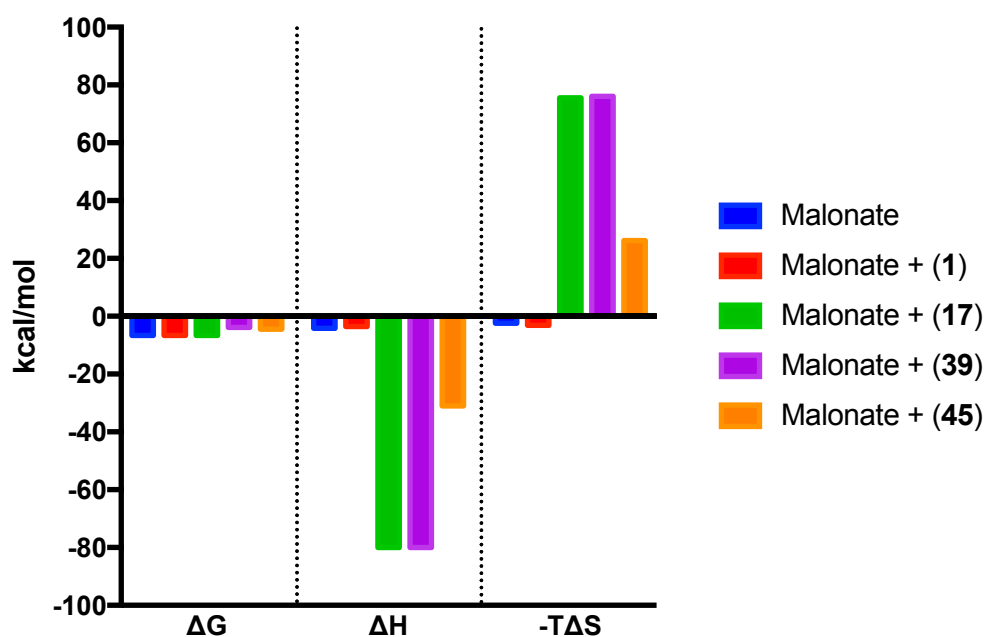


Figure 7.16. Thermodynamic parameters of SR-malonate binding in an ITC displacement experiment.

Values for the Gibbs free energy (ΔG), enthalpy (ΔH), and entropy ($-T\Delta S$) were derived from the titration of 100 μM SR with 1 mM malonate and 1 mM fragment inhibitors as coupling ligands.

Table 7.1. Thermodynamic parameters of SR-malonate binding in the absence and presence of fragment inhibitors.

ITC displacement binding experiments were performed with 100 μM SR, 1 mM malonate, and 1 mM fragment inhibitor to determine the malonate K_D , and reaction enthalpy (ΔH) and Gibbs free energy (ΔG).

	Malonate K_D		ΔH		ΔG	
	(μM)		(kcal/mol)		(kcal/mol)	
	-Ligand	+Ligand	-Ligand	+Ligand	-Ligand	+Ligand
F01	13	15	-4.04	-3.5	-6.67	-6.57
F17	15	638	-4.21	-80	-6.58	-4.36
F39	25	1380	-4.52	-80	-6.29	-3.9
F45	9	483	-3.96	-30.7	-6.9	-4.52

The malonate-only binding isotherms in Fig. 7.15 demonstrate typical exothermic binding modes with K_D constants of $13 \pm 1 \mu\text{M}$ (A), $15 \pm 2 \mu\text{M}$ (B), $25 \pm 5 \mu\text{M}$ (C), and $8.6 \pm 3 \mu\text{M}$ (D). The thermodynamic constants in Fig. 7.16 indicate SR binding to malonate was not dominantly enthalpic or entropic, but was instead favoured by both. It is immediately obvious the binding isotherms in Fig. 7.15 become less defined in the presence of the weak ligand than with malonate alone, suggesting there was some interference or displacement of malonate binding by the fragment inhibitors. This is reflected by the apparent K_D of malonate increasing by approximately 50-fold when in the presence of the fragment molecules (Table 7.1). The difference to the binding isotherms was not sufficient to empirically estimate the dissociation constants of the fragments. This may be because the fragments were not tested at concentrations required to saturate SR (typically tenfold the K_D), which in the case of these fragments would be between 5–10 mM. Unfortunately, it was not possible to approach saturating concentrations because as was discussed in section 7.4.9, even 2 mM fragment/2% DMSO elicited large heat of dilution peaks that prevented binding curves being defined.

Some inference can be made about the binding profile of the fragment inhibitors from the thermodynamic parameters in Fig. 7.16 and Table 7.1. For instance, the Gibbs free energy remains largely unchanged between fragments, but there are substantial variations in the component enthalpies and entropies. This is especially applicable to F17, F39, and F45, all of which displayed considerably greater negative enthalpies and positive entropies than malonate binding alone. A more negative enthalpy is typically associated with a molecular change leading to more and/or tighter van der Waals contacts and H-bonds between the ligand and enzyme, which may be indicative of the weak fragment contacts being displaced by malonate interactions in the active site. According to the phenomenon of enthalpy-entropy compensation, a more negative enthalpy would result in a compensatory reduction in entropy because protein flexibility is reduced when a ligand is bound — such as with the conformational change that occurs when SR binds to malonate. The opposite effect was observed with F17, F39, and F45, as all increased the entropy of the system, signifying increased disorder. A likely explanation is that malonate binding induced changes in the level of hydration

by displacing tightly bound water molecules in its binding pocket, consequently releasing more water molecules into the system and thereby increasing entropy (by increasing disorder).

F01, the inhibitor subsequently confirmed to bind to SR by X-ray crystallography, should theoretically compete with malonate because both ligands bind in the active site. However, the thermodynamic profile of F01 (Fig. 7.16) was not overly distinct from that of malonate, and it also did not appear to influence the K_D of malonate (Table 7.1). An explanation could be the experimental concentration of the fragment was not enough to saturate SR prior to malonate titration, therefore malonate binding would be largely unaffected by the presence of a fragment inhibitor because most binding pockets would be free. The altered binding isotherm of malonate in the presence of F01 (Fig. 7.15A) suggests that F01 does influence SR-malonate binding, but this is a qualitative assessment not supported by thermodynamic data.

ITC experiments enabled qualitative assessments on SR-fragment binding to be made based on the generated thermodynamic profiles, but challenges in manipulating concentrations to optimise the c -value, maintaining inhibitor solubility, and designing experiments around the incredibly weak binding affinities limited quantitative conclusions. Overall, the findings discussed here are not unequivocal and data from the displacements experiments are subject to interpretation. As ITC experiments yielded little information on which fragments to prioritise, crystallography studies encompassed all four fragments.

7.4.11 Co-crystallisation of fragment hits

In parallel to ITC studies, the four fragments (F01, F17, F39, F45) were subject to sitting-drop co-crystallisation trials. SR was incubated with saturating concentrations of each fragment (10 mM) prior to crystallisation in varying PEG 3350 and MgCl_2 concentrations around those determined for the SR *holo* crystal (section 5.4.3) in the pH range 6.0–7.25. Images of crystals from this initial screen are shown in Fig. 7.17. Crystallisation occurred with only two fragments (F01 and F39), but overall the crystals were too small for in-house X-ray analysis.

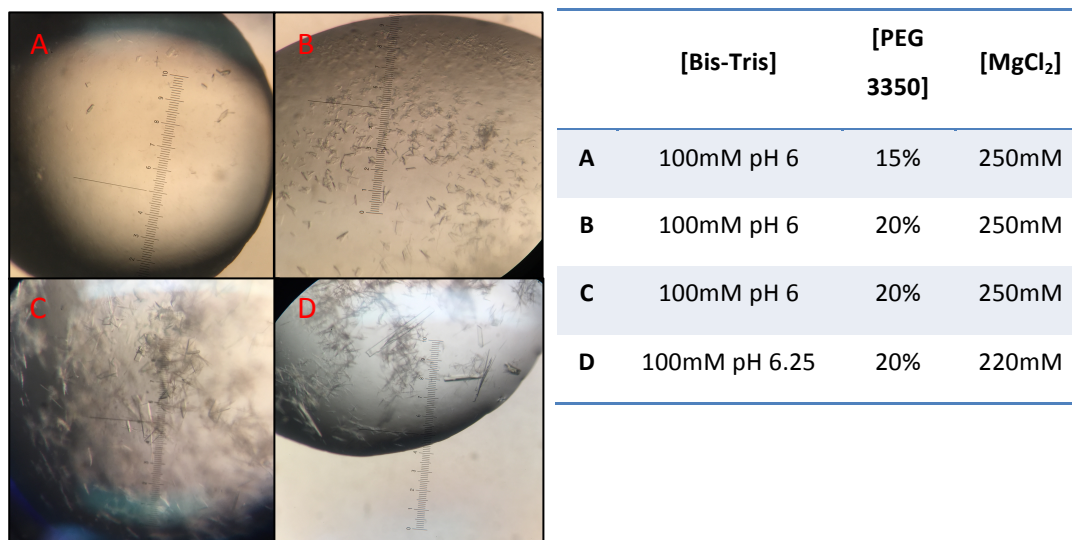


Figure 7.17. Co-crystallisation trials with SR and four inhibitory fragment hits.

An initial screen of Bis-Tris pH vs. PEG 3350, plus 250 mM MgCl_2 , was performed with F01, F17, F39, and F45. Each fragment was incubated with 7.5 mg/mL SR, 5% seed and 5 mM DTT at a concentration of 10 mM (approx. $10 \times K_D$) for 30 min RT prior to plating. Crystalline material and small crystals of SR grew with F01 (**A** and **B**) and F39 (**C** and **D**) in the conditions listed in the table.

An optimisation screen was then performed based on the observation crystal growth appeared to favour pH 6 buffer and up to 20% PEG 3350. Crystal growth began after one day for F01 and F39 but only precipitate and some protocrystalline material grew with F17 and F45. The co-crystals showed a much improved size and morphology with F01, but co-crystals with F39 remained too small ($< 20\ \mu\text{m}$) for diffraction (Fig. 7.18).

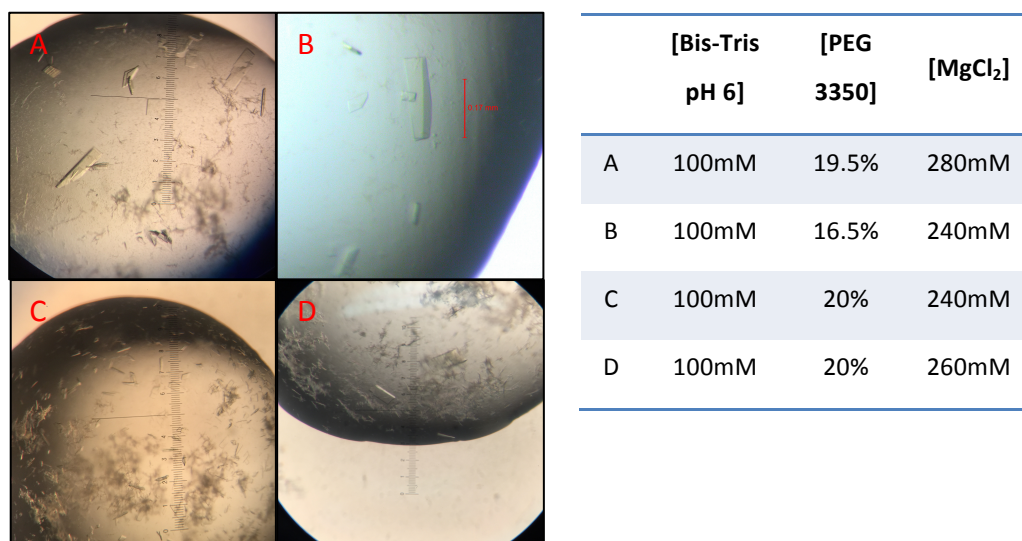


Figure 7.18. Optimisation of SR co-crystallisation with hits F01 and F39 in Bis-Tris pH 6.

A screen was performed with F01 (A–B) and F39 (C–D) in increasing concentrations of PEG 3350 and MgCl₂ in Bis-Tris pH 6. Each fragment was incubated with 7.5 mg/mL SR, 5% seed and 5 mM DTT at a concentration of 10 mM (F01) or 5 mM (F39) for 30 min RT prior to plating. Crystal growth began after one day in several conditions; examples of crystals with the best morphology are shown above with their corresponding growth conditions in the table.

Preliminary X-ray analysis of SR co-crystals with F01 and F39 was performed in-house. Despite macroscopic morphology appearing well suited for image collection, both crystals displayed prolific microscopic pathology (primarily twinning) upon diffraction. Extensive optimisation would have been required to resolve this problem, so focus was shifted from co-crystallisation to crystal soaking as a means to facilitate SR-inhibitor complex formation.

7.4.12 Crystal structure of SR complex with 3-pyridin-4-yl benzoic acid

Growth of SR holo crystals via hanging drop vapour diffusion and subsequent soaking with 10 mM of each F01, F16, F17, F28, and F39 was performed according to the protocol in section 5.3.3 and 5.3.4. After soaking, crystals were cryo-cooled and stored in liquid nitrogen. Datasets were collected using synchrotron radiation at Diamond Light Source (beamline I03). After structure solution, one fragment was found to have bound to SR — F01, 3-pyridin-4-yl benzoic acid. The crystal structure was refined to a resolution of 1.9 Å. The diffraction pattern of one SR-F01 crystal is shown in Fig. 7.19. Data collection statistics for the SR-inhibitor complex are presented in Appendix 10.5.3.

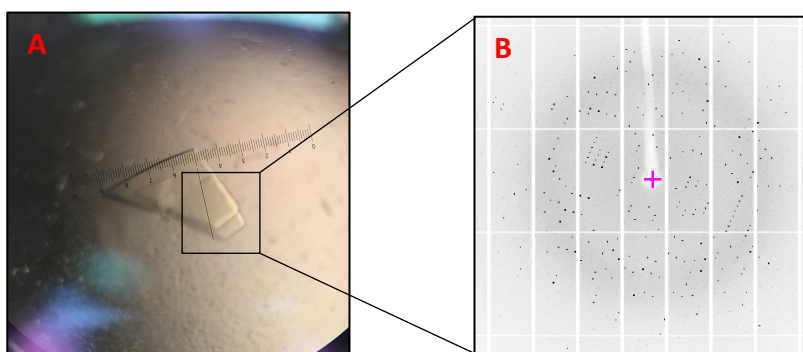


Figure 7.19. Crystallisation of SR and soaking with fragment inhibitors.

(A) Unbound SR was crystallised by hanging drop vapour diffusion then soaked with 10 mM F01. (B) Diffraction pattern from F01-soaked SR collected using synchrotron radiation. The crystal diffracted to a high resolution (1.8 Å) and did not exhibit any microscopic pathology.

The crystal structure of the SR-F01 complex (Fig. 7.20) reveals that F01 occupies the active site by forming a cation- π interaction with His82, two hydrogen bonds with Ser83 and Thr81, and an additional hydrogen bond with a structural water molecule (Fig. 7.20B and C). The His82 residue involved in the cation- π interaction has a protonated α -amino group (NH_3^+) and a partially protonated imidazole side chain, classifying it as a positively charged amino acid that can interact with the electron-rich π -system of the F01 benzene ring. Both Ser83 and Thr81 form hydrogen bonds by donating protons from their hydroxyl side chains to the negatively charged deprotonated carboxylic acid group of F01. The functionality of SR is known to depend on the critical role of Ser84, which donates a proton from its hydroxyl group to drive the transition state towards racemisation (Fig. 1.6). The positioning of F01 in close proximity to this catalytically important residue suggests it may inhibit SR by prohibiting the C α of L-serine from approaching and interacting with Ser84.

Ordinarily, when SR binds to its substrate, the small domain undergoes a major structural shift to place Ser84 in an ideal orientation for proton donation. This induced shift applies to both the substrate and orthosteric inhibitor malonate, and is true of other racemase orthologues such as yeast (Goto *et al.*, 2009) and rat (Smith *et al.*, 2010). Yet, an overlay of the SR holoenzyme, F01-bound and malonate-bound crystal structures (Fig. 7.20D) shows that a ligand-induced shift does not occur with the SR-F01 complex. There is a dramatic and obvious helical shift in the closed structure of the SR-malonate complex (see section 5.4.2), which prevents L-serine accessing the active site through the ensuing tight cleft between the large and small domains.

F01 is also an orthosteric inhibitor by virtue of its presence in the active site, but its mechanism of action seems distinct from that of malonate. Instead of inducing a conformational shift between the two domains, it appears F01 locks SR in its open conformation by occupying the active site to prevent substrate binding. Accordingly, both structures (Fig. 7.20D, grey and purple) have a highly similar conformation; after structural alignment, the calculated RMSD was 0.06 for the large domain, raising to 0.6 for the small domain (reflecting its inherent flexibility) and in contrast to 2.2 for the SR-malonate complex. That F01 does not induce a conformational shift is a useful quality

for medicinal chemistry as it may allow larger compound derivatives to penetrate the active site, ultimately improving specificity and potency by increasing the number of contacts with residues in the catalytic environment.

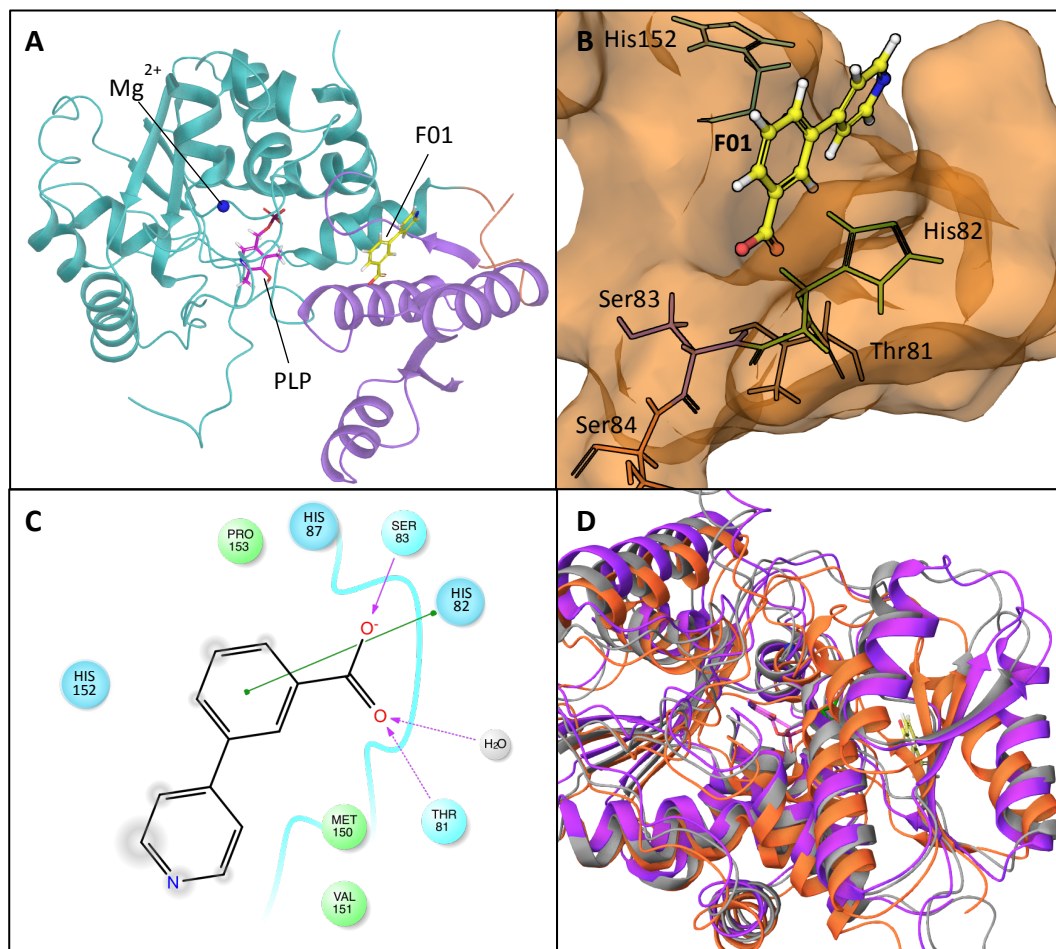


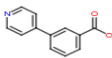
Figure 7.20. X-ray crystal structure of human SR bound to a novel fragment inhibitor, 3-pyridin-4-yl benzoic acid (F01).

(A) Secondary structure molecular image of SR monomer with F01 (yellow sticks) bound between the large (teal) and small (purple) domains. The PLP cofactor (pink sticks) and Mg^{2+} (blue sphere) are also present. (B) Surface binding pocket where F01 (yellow sticks) interacts with SR. Residues shown are His152, His82, Thr81, Ser83, and Ser84. (C) Ligand interaction diagram for F01. The inhibitor binds to SR via three hydrogen bonds (purple arrows) and cation- π stacking with neighbouring histidines (green lines). (D) Superimposition of SR holoenzyme (grey), SR-malonate complex (orange) and SR-F01 complex (purple). A ligand-induced conformational shift of the small domain occurs with the malonate complex, but not the F01 complex, which closely resembles the arrangement of the SR unbound crystal structure.

7.5 DISCUSSION

This chapter describes a drug discovery workflow that was successfully utilised to enable the identification of a novel fragment inhibitor of human SR. Through the optimisation and implementation of a medium-throughput biochemical assay, it was possible to screen a combined fragment library of approximately 3200 fragments in the search for viable hit matter. The SR fragment screen yielded 970 initial hits (30% hit rate) that demonstrated at least 50% inhibition, after which many false positives were eliminated via a DAO counter screen, reducing the hit rate to 330 (10% hit rate). The most potent fragments ($IC_{50} \leq 1$ mM) were retained following IC_{50} determination, further reducing the hit number to a final count of 61 (2% hit rate). The three biophysical techniques had varying degrees of usefulness; thermal shift experiments suggested most (79%) of the fragments destabilised SR, MST produced estimated binding affinities, and ITC could not confirm fragment binding to SR. Biophysical analysis of the novel SR inhibitor, F01 (3-pyridin-4-yl benzoic acid), revealed it caused a positive, albeit small T_m shift in the thermal shift assay (0.5 °C) and demonstrated a K_D of 960 μ M in the MST assay. Binding to SR was ultimately confirmed by X-ray crystallography, wherein F01 was shown to bind in the active site by forming hydrogen bonds with Ser-83 and Thr-81, as well as cation- π stacking with His-82.

Table 7.2. Summary profile of F01, the novel SR inhibitor and confirmed binder.

Name	Structure	Screen inhibition at 1 mM (%)		IC_{50} (μ M)		T_m shift (°C)	K_D (μ M)	Crystal resolution (Å)
3-pyridin-4-yl benzoic acid		57	70	1648	532	0.5	960	1.8

A comprehensive discussion of each fragment screening, biophysical methods, and crystallography as they apply to the 61 fragment hits will follow.

1. Fragment screen

Fragment screening is an effective technique that when applied to drug discovery can enable the generation of new hit matter for sites traditionally difficult to target with larger compounds. This especially applies to enzymes such as SR, which undergo a ligand-induced conformational change and may not be easily accessible to drug compounds. Our collaborators at Evotec have attempted SR compound screens with limited success likely for this reason (personal correspondence). There are currently drugs on the market that were developed using structure-based drug design, such as HIV protease inhibitors and the cancer drug imatinib (Hajduk and Greer, 2007), as well as several drugs derived from FBDD, such as the melanoma drug vemurafenib and leukaemia drug venetoclax (Erlanson *et al.*, 2016). These examples support the use of fragment screening as an alternate approach to generating lead compounds.

As was observed in the current study, fragment screening can result in a considerably higher (10–1000-fold) hit rate compared to conventional high-throughput compound screens. This occurs because fragment libraries cover substantially more chemical diversity space, due to fragments being much smaller than compounds and thus having far fewer potential molecular arrangements. Further, small fragments that form fewer interactions are able to bind to a greater number of sites, possibly on multiple proteins, leading to even higher hit rates.

Fragment screening does have its caveats: fragments are more likely to exhibit promiscuous binding; binding affinities are likely to be lower for fragments; and it can be more difficult to identify false positives and non-specific binders within a high hit number. The purpose of the DAO counter screen was to identify and extract non-specific inhibitors from the initial hit rate, by defining SR-specific hits as those producing $\geq 50\%$ inhibition in the SR screen and $0 \pm 25\%$ inhibition in the counter screen. While these stipulations removed many hits with moderate-to-substantial non-specific activity, it is possible that good SR inhibitors were removed indiscriminately for producing little over 25% inhibition in the counter screen. In this sense, the study would have benefited from a repeat of the counter screen to confirm which hits were

suitable for subsequent IC₅₀ determination and biophysical analysis. Nevertheless, the DAO counter screen assay was the most appropriate method for identifying non-specific inhibitors in this context and yielded a very reasonable SR-specific hit number of 330 (ultimately 61 following IC₅₀ determination) for further investigation.

Detailed characterisation of all 61 final hits was unfortunately beyond the scope of this project. As biophysical analysis was not necessarily predictive of success in crystallography, it would certainly be beneficial to revisit this group of 61 fragment hits and characterise them further with the aim to advance a greater variety of fragments through to crystallography trials. This process could incorporate, firstly, manual repetition of the counter screen assay for the hits to more reliably confirm their specificity, and secondly, experimentally confirming K_i values and ligand efficiency to better assess and rank the hits. An additional biophysical technique that could be of use is nuclear magnetic resonance (NMR), which is sensitive enough to detect weak binders and give information on the ligand-binding site, as well as provide the K_D by ligand titration (Lepre, 2011). Moreover, ligand-observed NMR experiments in the absence of protein can identify false positive and false negatives (Dalvit *et al.*, 2006)

To summarise, FBDD is a technique suitable for hit generation and hit-to-lead development for SR, as evidenced by the identification of a novel fragment inhibitor confirmed by X-ray crystallography. The final group of 61 hits can be considered a structurally diverse pool of SR fragment inhibitors that can be used as starting points for lead development pending further characterisation.

2. Biophysical methods

Thermal denaturation analysis of the 61 hits did not initially seem promising. Practically all fragments that caused a significant T_m shift did so in the negative direction, and those that did cause a positive shift exhibited atypical fluorescence curves. Negative shifts are usually indicative of protein destabilisation rather than inhibition, which does not lend confidence to the potential development of these fragments into lead molecules. Compounds that destabilise a protein usually lead to

more rapid protein degradation and ultimately protein depletion in a cellular context, which could trigger protein synthesis to replenish depleted enzyme pools. Such a response would clearly defeat the original purpose of inhibiting a protein for therapeutic benefit. An additional consideration is that destabilising compounds, by virtue of their generic denaturing effect, are unlikely to be specific to a particular protein, giving them limited capabilities from a drug discovery perspective.

There could be an alternative explanation to the negative thermal shifts observed. A recent study that screened fragments also from the Ro3 library against 7,8-diaminopelargonic synthase (BioA), a target for tuberculosis, found a number of the compounds demonstrating potent inhibition also caused a negative thermal shift (Dai, 2014). The researchers were able to identify the target of inhibition of one of their compounds as the PLP cofactor of BioA. Their compound, which contained a hydrazine, reacted with the aldehyde of PLP, and this mode of action was confirmed by crystallography. Although hydrazines were not identified as a common structural feature among the 61 hits in the current study, the Dai study highlights the possibility a proportion of them could be destabilising SR via PLP. If so, there could be potential to structurally optimise these fragments to improve their specificity for SR over other PLP-containing enzymes. It is, however, more likely that thermal shift assays are largely unsuitable for a FBDD strategy with SR. Although the control inhibitor malonate did produce a sizeable positive shift, this may not be possible for fragments that bind allosterically or do not otherwise stabilise the closed conformation of SR — as is the case with F01.

MST provided more biophysical information than thermal shift, enabling calculation of K_D values for the 13 fragments out of 61 that demonstrated a significant F_{norm} shift. Unfortunately, these values were only an estimate because the failure to obtain complete binding curves would have significantly increased the margin of error. Although estimations are not as desirable as definitive calculations, they do still have practical applications in prioritising which inhibitors to advance.

However, there is a possibility the MST results obtained herein could be due in part to protein destabilisation. MST measures effects arising from changes in macromolecular shape, size, charge and hydration shell. Therefore, one could reasonably assume the apparent binding data collected from MST could be a result of protein destabilisation or denaturation, which would be expected to alter the shape and hydration shell of SR. Given the thermal shift data, this is a very real possibility. A report that used MST to study denaturation states in the core protein of human hepatitis B virus (HBV) found the intermediate and denatured protein forms did indeed exhibit MST traces similar to those in this study — an upwards shift in relative fluorescence (Alexander *et al.*, 2013). By contrast, MST studies on protein stability found unfolding of bovine carbonic anhydrase II (BCAII) elicited an atypical thermophoresis signal with a peak rather than the typical gradual decline (Jerabek-Willemsen *et al.*, 2011). The findings were attributed to a globular intermediate state, and can be likened to the unusual MST traces of fragments 45 and others, that produced an increase in relative fluorescence above baseline.

3. Crystallography

Co-crystallisation, the initial approach used to crystallise SR with the fragment hits, had limited success in that crystals grew, but were either too small for X-ray analysis or diffracted poorly upon preliminary analysis. In the context of studies such as this, co-crystallisation is probably not a suitable technique to process large numbers of inhibitors because several different crystallisation environments may require optimisation. Certainly, the small crystals obtained through co-crystallisation studies here could be viable starting points for the production of high quality crystals. An improved approach might be to perform co-crystallisation trials with commercial sparse-matrix screens for *de novo* crystal generation. Crystallisation of the SR-F01 complex was instead achieved by soaking the inhibitor into SR *holo* crystals. The crystal soaking technique may have been successful because F01 stabilised SR in the open conformation and did not induce a structural shift, which can cause proteins to disintegrate.

Other structural studies have characterised SR similarly. When the crystal structure of SR from *S. pombe* (which shares 35% sequence similarity with hSR) was solved in complex with AMP-PCP, an ATP analogue, it was found that binding of AMP-PCP stabilised the structure of SR but did not induce a subunit conformational change (as observed with malonate) or a significant change in subunit or side chain orientation (Goto *et al.*, 2009). Upon soaking of the AMP-PCP-complexed crystals with L-serine, the conformation of SR changed from the open form to the closed form. The stabilisation of the closed structure was thought to be due to reorganisation of the hydrogen bond network between PLP and ATP to adjust the active site structure, and also due to the position of ATP in between the two domains, which made it ideally situated to affect the mode of open-closed conformational change. Using this information, it could be possible to stabilise SR in an open conformation by crystallising it with ATP (or an ATP analogue) and then soaking with inhibitors. If any inhibitors induce a conformational change, the presence of ATP may encourage successful binding of ligands by stabilising the complex and maintaining crystal integrity, thereby facilitating structure solution.

To conclude, the MTS-optimised biochemical assay and fragment screening process have proven effective at generating a sufficient number of hits for further development, with proof-of-concept achieved by X-ray crystallography of the SR-F01 complex. The three biophysical methods did contribute to the characterisation of the fragment hits, but most assessments were qualitative, and even the binding affinities determined by MST are likely to be error-prone. The successful solution of a protein crystal structure bound to a fragment inhibitor following a crystal soaking protocol emphasises that a shift to a structure-based approach to SR hit identification may be the future of SR drug discovery.

8 CONCLUSIONS AND FUTURE WORK

There is little doubt that the inhibition of SR remains an attractive therapeutic approach to indirectly modulate NMDAR function in disorders associated with glutamatergic hyperfunction. The current deficit of safe pharmacological modulators of NMDAR activity makes the development of compounds with an improved safety profile an even greater imperative. The accomplishment of the aim of this thesis through identification a novel, structurally validated SR inhibitor supports the capability of SR to be a credible drug target, and has the potential to significantly contribute to SR SAR studies and drug development.

As seen in the X-ray crystal structure of the SR-F01 complex, the fragment inhibitor binds in the active site at a position distinct from that of malonate, inhibiting SR possibly by acting as a 'door wedge' that prevents the ligand-induced conformational shift necessary for activity. That it does not bind in the same position as malonate enables approaches to develop SR inhibitors with improved potency and specificity by 1) growing the fragment to search for interactions using the co-crystal structure, and 2) linking two adjacent fragments in the active site via the carboxylic acid group of F01. It would certainly be interesting to attempt to tether F01 to malonate or a malonate-like inhibitor to determine whether the new chimeric compound could overcome the lack of specificity and related toxicity associated with malonate alone, especially as malonate and its derivatives comprise the majority of the most potent SR inhibitors. Given that it has been notoriously difficult to identify SR inhibitors structurally unique from amino acid-like compounds, having the possibility to revisit and fully exploit these compounds would be of real benefit.

Even more compelling about the identification of F01 is the presence of two of its isomers, F02 (4-(pyridin-4-yl)benzoic acid) and F09 (3-(pyridin-3-yl)benzoic acid) in the final list of 61 hits (Appendix 10.4). The two isomers had respective IC_{50} values of 536 μ M and 126 μ M and both produced statistically significant thermal shifts. However, both were perhaps unduly eliminated from the characterisation process during MST analysis despite demonstrating greater F_{norm} shifts than malonate,

highlighting potential flaws in adhering to a purely statistical selection procedure for methods wherein the generated data may not be proportional to the binding intensity. Nonetheless, the presence of F01, F02, and F09 in the final hit list could be demonstrative of a distinct series for which more comprehensive SAR could be determined using analogues containing a pyridine or imidazole scaffold. A developed SAR picture would certainly aid rational drug design and open avenues for fragment tethering, either to a reported inhibitor or another of the 61 hits. To this end, it would be advisable to obtain crystal structures of SR in complex with other fragment hits. .

There are surprisingly few structural and docking studies of SR and its inhibitors in the literature. Understanding the interactions between inhibitors and surrounding residues can advance development of lead compounds into viable drug-like molecules and enable structural optimisation. The field of SR inhibitor discovery would greatly benefit from more crystallographic studies, and it is clear this is the direction in which the field should develop.

Fortuitously, a recently developed technique transcends the historic bottleneck between hit identification and crystallography, enabling an approach for structure-based drug discovery. The implementation in 2015 of an open-access capability at Diamond Light Source in Oxford now allows an X-ray screening experiment of approximately 1000 fragments to be conducted as a highly streamlined process in less than a week. This process, called X-Chem screening, covers soaking, harvesting, automatic data collection, and data analysis. For a target such as SR, which has demonstrated here and elsewhere the ability to form soaking-resistant crystals, X-Chem would be a perfect method for identifying hits with confirmed binding, bypassing the rigmarole of a biochemical fragment screen and the ambiguity presented by other biophysical methods. X-Chem fragment screening might also lead to identification of novel allosteric as well as orthosteric modulators, the binding sites of which can be immediately visualised to facilitate structure-based drug design.

To this end, I have recently applied for and subsequently been awarded an MRC Confidence-in-Concept grant for the express purpose of performing an X-Chem

fragment screen with SR. A proposal for SR has already been submitted to Diamond Light Source and has been provisionally accepted pending final optimisation for X-Chem automation. It is anticipated that this process will lead to the discovery of novel hit molecules generated from the X-Chem fragment screen, which can then be tested in biophysical assays (MST and ITC) as well as the SR biochemical assay to determine inhibitory activity. These orthogonal assays can be used to prioritise follow-up analogue screening and the development of preliminary SAR such that an exploratory plan for lead optimisation can be formulated.

If the above process leads to the development of a novel selective and potent SR inhibitor, it would be interesting to then measure its functional effects on NMDARs. This could encompass the use of SR-overexpressing cell lines to determine changes to SR activity in a cell lysate assay using a similar DAO degradation and chemiluminescence detection method as the SR biochemical assay. Moreover, electrophysiological techniques (such as patch-clamp) could be employed to investigate if inhibiting the production of D-serine with an SR inhibitor alters the ionic current through an NMDAR. The ultimate objective would be to test the SR inhibitor *in vivo* to assess its safety profile, pharmacodynamics, target engagement, brain penetrance, and to understand the physiological impact of inhibiting SR with respect to homeostatic mechanisms that may further influence levels of D-serine.

9 BIBLIOGRAPHY

Aan Het Rot, M., Collins, K.A., Murrough, J.W., Perez, A.M., Reich, D.L., Charney, D.S. & Mathew, S.J. (2010) Safety and efficacy of repeated-dose intravenous ketamine for treatment-resistant depression. *Biol Psychiatry*, Vol. 67 (2) 139-45.

Aarsland, D., Ballard, C., Walker, Z., Bostrom, F., Alves, G., Kossakowski, K., Leroi, I., Pozo-Rodriguez, F., Minthon, L. & Londos, E. (2009) Memantine in patients with Parkinson's disease dementia or dementia with Lewy bodies: a double-blind, placebo-controlled, multicentre trial. *Lancet Neurol*, Vol. 8 (7) 613-8.

Abramov, E., Dolev, I., Fogel, H., Ciccotosto, G.D., Ruff, E. & Slutsky, I. (2009) Amyloid-beta as a positive endogenous regulator of release probability at hippocampal synapses. *Nat Neurosci*, Vol. 12 (12) 1567-76.

Adage, T., Trillat, A.C., Quattropiani, A., Perrin, D., Cavarec, L., Shaw, J., Guerassimenko, O., Giachetti, C., Gréco, B., Chumakov, I., Halazy, S., Roach, A. & Zaratin, P. (2008) In vitro and in vivo pharmacological profile of AS057278, a selective d-amino acid oxidase inhibitor with potential anti-psychotic properties. *Eur Neuropsychopharmacol*, Vol. 18 (3) 200-14.

Alberdi, E., Sanchez-Gomez, M.V., Cavaliere, F., Perez-Samartin, A., Zugaza, J.L., Trullas, R., Domercq, M. & Matute, C. (2010) Amyloid beta oligomers induce Ca²⁺ dysregulation and neuronal death through activation of ionotropic glutamate receptors. *Cell Calcium*, Vol. 47 (3) 264-72.

Alexander, C.G., Jürgens, M.C., Shepherd, D.A., Freund, S.M., Ashcroft, A.E. & Ferguson, N. (2013) Thermodynamic origins of protein folding, allostery, and capsid formation in the human hepatitis B virus core protein. *Proc Natl Acad Sci U S A*, Vol. 110 (30) E2782-91.

Allen Institute for Brain Science *Allen Institute for Brain Science*. [online] <http://www.brain-map.org/>

Alt, A., Weiss, B., Ogden, A.M., Knauss, J.L., Oler, J., Ho, K., Large, T.H. & Bleakman, D. (2004) Pharmacological characterization of glutamatergic agonists and antagonists at recombinant human homomeric and heteromeric kainate receptors in vitro. *Neuropharmacology*, Vol. 46 (6) 793-806.

Altamura, C.A., Mauri, M.C., Ferrara, A., Moro, A.R., D'andrea, G. & Zamberlan, F. (1993) Plasma and platelet excitatory amino acids in psychiatric disorders. *Am J Psychiatry*, Vol. 150 (11) 1731-3.

Amr, Y.M. (2010) Multi-day low dose ketamine infusion as adjuvant to oral gabapentin in spinal cord injury related chronic pain: a prospective, randomized, double blind trial. *Pain Physician*, Vol. 13 (3) 245-9.

Antonov, S.M. & Johnson, J.W. (1999) Permeant ion regulation of N-methyl-D-aspartate receptor channel block by Mg(2+). *Proc Natl Acad Sci U S A*, Vol. 96 (25) 14571-6.

Areosa, S.A., Sherriff, F. & Mcshane, R. (2005) Memantine for dementia. *Cochrane Database Syst Rev*, (3) CD003154.

Armstrong, N., Sun, Y., Chen, G.Q. & Gouaux, E. (1998) Structure of a glutamate-receptor ligand-binding core in complex with kainate. *Nature*, Vol. 395 (6705) 913-7.

Arriza, J.L., Fairman, W.A., Wadiche, J.I., Murdoch, G.H., Kavanaugh, M.P. & Amara, S.G. (1994) Functional comparisons of three glutamate transporter subtypes cloned from human motor cortex. *J Neurosci*, Vol. 14 (9) 5559-69.

Auer, D.P., Pütz, B., Kraft, E., Lipinski, B., Schill, J. & Holsboer, F. (2000) Reduced glutamate in the anterior cingulate cortex in depression: an in vivo proton magnetic resonance spectroscopy study. *Biol Psychiatry*, Vol. 47 (4) 305-13.

Ayala, G.X. & Tapia, R. (2005) Late N-methyl-D-aspartate receptor blockade rescues hippocampal neurons from excitotoxic stress and death after 4-aminopyridine-induced epilepsy. *Eur J Neurosci*, Vol. 22 (12) 3067-76.

Baell, J. & Walters, M.A. (2014) Chemistry: Chemical con artists foil drug discovery. *Nature*, Vol. 513 (7519) 481-3.

Baird, J.P., Turgeon, S., Wallman, A. & Hulick, V. (2008) Behavioral processes mediating phencyclidine-induced decreases in voluntary sucrose consumption. *Pharmacol Biochem Behav*, Vol. 88 (3) 272-9.

Balu, D.T. & Coyle, J.T. (2014) Chronic D-serine reverses arc expression and partially rescues dendritic abnormalities in a mouse model of NMDA receptor hypofunction. *Neurochem Int*, Vol. 75 76-8.

Balu, D.T., Li, Y., Puhl, M.D., Benneyworth, M.A., Basu, A.C., Takagi, S., Bolshakov, V.Y. & Coyle, J.T. (2013) Multiple risk pathways for schizophrenia converge in serine racemase knockout mice, a mouse model of NMDA receptor hypofunction. *Proc Natl Acad Sci U S A*, Vol. 110 (26) E2400-9.

Bare, T.M., Brown, D.G., Horchler, C.L., Murphy, M., Urbanek, R.A., Alford, V., Barlaam, C., Dyroff, M.C., Empfield, J.B., Forst, J.M., Herzog, K.J., Keith, R.A., Kirschner, A.S., Lee, C.M., Lewis, J., McLaren, F.M., Neilson, K.L., Steelman, G.B., Trivedi, S., Vacek, E.P. & Xiao, W. (2007) Pyridazinoquinolinetrienes as NMDA glycine-site antagonists with oral antinociceptive activity in a model of neuropathic pain. *J Med Chem*, Vol. 50 (13) 3113-31.

Baron, R., Binder, A. & Wasner, G. (2010) Neuropathic pain: diagnosis, pathophysiological mechanisms, and treatment. *Lancet Neurol*, Vol. 9 (8) 807-19.

Bartlett, G.R. (1948) The inhibition of d-amino acid oxidase by benzoic acid and various monosubstituted benzoic acid derivatives. *J Am Chem Soc*, Vol. 70 (3) 1010.

Bartlett, R.D., Esslinger, C.S., Thompson, C.M. & Bridges, R.J. (1998) Substituted quinolines as inhibitors of L-glutamate transport into synaptic vesicles. *Neuropharmacology*, Vol. 37 (7) 839-46.

Bass, N.J., Datta, S.R., Mcquillin, A., Puri, V., Choudhury, K., Thirumalai, S., Lawrence, J., Queded, D., Pimm, J., Curtis, D. & Gurling, H.M. (2009) Evidence for the association of the DAOA (G72) gene with schizophrenia and bipolar disorder but not for the association of the DAO gene with schizophrenia. *Behav Brain Funct*, Vol. 5 28.

Basse, N., Kaar, J.L., Settanni, G., Joerger, A.C., Rutherford, T.J. & Fersht, A.R. (2010) Toward the rational design of p53-stabilizing drugs: probing the surface of the oncogenic Y220C mutant. *Chem Biol*, Vol. 17 (1) 46-56.

Basu, A.C., Tsai, G.E., Ma, C.L., Ehmsen, J.T., Mustafa, A.K., Han, L., Jiang, Z.I., Benneyworth, M.A., Froimowitz, M.P., Lange, N., Snyder, S.H., Bergeron, R. & Coyle, J.T. (2009) Targeted disruption of serine racemase affects glutamatergic neurotransmission and behavior. *Mol Psychiatry*, Vol. 14 (7) 719-27.

Beato, C., Pecchini, C., Cocconcelli, C., Campanini, B., Marchetti, M., Pieroni, M., Mozzarelli, A. & Costantino, G. (2015) Cyclopropane derivatives as potential human serine racemase inhibitors: unveiling novel insights into a difficult target. *J Enzyme Inhib Med Chem*, 1-8.

Bedingfield, J.S., Jane, D.E., Kemp, M.C., Toms, N.J. & Roberts, P.J. (1996) Novel potent selective phenylglycine antagonists of metabotropic glutamate receptors. *Eur J Pharmacol*, Vol. 309 (1) 71-8.

- Bendikov, I., Nadri, C., Amar, S., Panizzutti, R., De Miranda, J., Wolosker, H. & Agam, G. (2007) A CSF and postmortem brain study of D-serine metabolic parameters in schizophrenia. *Schizophr Res*, Vol. 90 (1-3) 41-51.
- Beneyto, M. & Meador-Woodruff, J.H. (2006) Lamina-specific abnormalities of AMPA receptor trafficking and signaling molecule transcripts in the prefrontal cortex in schizophrenia. *Synapse*, Vol. 60 (8) 585-98.
- Benneyworth, M.A., Basu, A.C. & Coyle, J.T. (2011) Discordant behavioral effects of psychotomimetic drugs in mice with altered NMDA receptor function. *Psychopharmacology (Berl)*, Vol. 213 (1) 143-53.
- Benneyworth, M.A. & Coyle, J.T. (2012) Altered acquisition and extinction of amphetamine-paired context conditioning in genetic mouse models of altered NMDA receptor function. *Neuropsychopharmacology*, Vol. 37 (11) 2496-504.
- Benneyworth, M.A., Li, Y., Basu, A.C., Bolshakov, V.Y. & Coyle, J.T. (2012) Cell selective conditional null mutations of serine racemase demonstrate a predominate localization in cortical glutamatergic neurons. *Cell Mol Neurobiol*, Vol. 32 (4) 613-24.
- Bergfors, T. (2003) Seeds to crystals. *J Struct Biol*, Vol. 142 (1) 66-76.
- Berman, R.M., Cappiello, A., Anand, A., Oren, D.A., Heninger, G.R., Charney, D.S. & Krystal, J.H. (2000) Antidepressant effects of ketamine in depressed patients. *Biol Psychiatry*, Vol. 47 (4) 351-4.
- Bernard, R., Kerman, I.A., Thompson, R.C., Jones, E.G., Bunney, W.E., Barchas, J.D., Schatzberg, A.F., Myers, R.M., Akil, H. & Watson, S.J. (2011) Altered expression of glutamate signaling, growth factor, and glia genes in the locus coeruleus of patients with major depression. *Mol Psychiatry*, Vol. 16 (6) 634-46.
- Bertram, L. & Tanzi, R.E. (2008) Thirty years of Alzheimer's disease genetics: the implications of systematic meta-analyses. *Nat Rev Neurosci*, Vol. 9 (10) 768-78.
- Bhave, G., Nadin, B.M., Brasier, D.J., Glauner, K.S., Shah, R.D., Heinemann, S.F., Karim, F. & Gereau, R.W. (2003) Membrane topology of a metabotropic glutamate receptor. *J Biol Chem*, Vol. 278 (32) 30294-301.
- Billard, J.M. & Rouaud, E. (2007) Deficit of NMDA receptor activation in CA1 hippocampal area of aged rats is rescued by D-cycloserine. *Eur J Neurosci*, Vol. 25 (8) 2260-8.
- Birch, P.J., Grossman, C.J. & Hayes, A.G. (1988) Kynurenic acid antagonises responses to NMDA via an action at the strychnine-insensitive glycine receptor. *Eur J Pharmacol*, Vol. 154 (1) 85-7.
- Bjerrum, E.J., Kristensen, A.S., Pickering, D.S., Greenwood, J.R., Nielsen, B., Liljefors, T., Schousboe, A., Brauner-Osborne, H. & Madsen, U. (2003) Design, synthesis, and pharmacology of a highly subtype-selective GluR1/2 agonist, (RS)-2-amino-3-(4-chloro-3-hydroxy-5-isoxazolyl)propionic acid (Cl-HIBO). *J Med Chem*, Vol. 46 (11) 2246-9.
- Bliss, T.V. & Cooke, S.F. (2011) Long-term potentiation and long-term depression: a clinical perspective. *Clinics (Sao Paulo)*, Vol. 66 (Suppl 1) 3-17.
- Blot, K., Bai, J. & Otani, S. (2013) The effect of non-competitive NMDA receptor antagonist MK-801 on neuronal activity in rodent prefrontal cortex: an animal model for cognitive symptoms of schizophrenia. *J Physiol Paris*, Vol. 107 (6) 448-51.
- Boppana, K., Dubey, P.K., Jagarlapudi, S.A., Vadivelan, S. & Rambabu, G. (2009) Knowledge based identification of MAO-B selective inhibitors using pharmacophore and structure based virtual screening models. *Eur J Med Chem*, Vol. 44 (9) 3584-90.

- Bornhorst, J.A. & Falke, J.J. (2000) Purification of Proteins Using Polyhistidine Affinity Tags. *Methods Enzymol*, Vol. 326 245-54.
- Brandon, N.J. & Sawa, A. (2011) Linking neurodevelopmental and synaptic theories of mental illness through DISC1. *Nat Rev Neurosci*, Vol. 12 (12) 707-22.
- Breier, A., Malhotra, A.K., Pinals, D.A., Weisenfeld, N.I. & Pickar, D. (1997) Association of ketamine-induced psychosis with focal activation of the prefrontal cortex in healthy volunteers. *Am J Psychiatry*, Vol. 154 (6) 805-11.
- Bridges, T.M., Williams, R. & Lindsley, C.W. (2008) Design of potent GlyT1 inhibitors: in vitro and in vivo profiles. *Curr Opin Mol Ther*, Vol. 10 (6) 591-601.
- Brown, G.K., Ten Have, T., Henriques, G.R., Xie, S.X., Hollander, J.E. & Beck, A.T. (2005) Cognitive therapy for the prevention of suicide attempts: a randomized controlled trial. *JAMA*, Vol. 294 (5) 563-70.
- Bruno, S., Margiotta, M., Marchesani, F., Paredi, G., Orlandi, V., Faggiano, S., Ronda, L., Campanini, B. & Mozzarelli, A. (2017) Magnesium and calcium ions differentially affect human serine racemase activity and modulate its quaternary equilibrium toward a tetrameric form. *Biochim Biophys Acta*, Vol. 1865 (4) 381-387.
- Buchanan, R.W., Javitt, D.C., Marder, S.R., Schooler, N.R., Gold, J.M., McMahon, R.P., Heresco-Levy, U. & Carpenter, W.T. (2007) The Cognitive and Negative Symptoms in Schizophrenia Trial (CONSIST): the efficacy of glutamatergic agents for negative symptoms and cognitive impairments. *Am J Psychiatry*, Vol. 164 (10) 1593-602.
- Bugarski-Kirola, D., Wang, A., Abi-Saab, D. & Blättler, T. (2014) A phase II/III trial of bitopertin monotherapy compared with placebo in patients with an acute exacerbation of schizophrenia - results from the CandleLyte study. *Eur Neuropsychopharmacol*, Vol. 24 (7) 1024-36.
- Burgdorf, J., Kroes, R.A., Weiss, C., Oh, M.M., Disterhoft, J.F., Brudzynski, S.M., Panksepp, J. & Moskal, J.R. (2011a) Positive emotional learning is regulated in the medial prefrontal cortex by GluN2B-containing NMDA receptors. *Neuroscience*, Vol. 192 515-23.
- Burgdorf, J., Zhang, X.L., Nicholson, K.L., Balster, R.L., Leander, J.D., Stanton, P.K., Gross, A.L., Kroes, R.A. & Moskal, J.R. (2013) GLYX-13, a NMDA receptor glycine-site functional partial agonist, induces antidepressant-like effects without ketamine-like side effects. *Neuropsychopharmacology*, Vol. 38 (5) 729-42.
- Burgdorf, J., Zhang, X.L., Weiss, C., Gross, A., Boikess, S.R., Kroes, R.A., Khan, M.A., Burch, R.M., Rex, C.S., Disterhoft, J.F., Stanton, P.K. & Moskal, J.R. (2015) The long-lasting antidepressant effects of rapastinel (GLYX-13) are associated with a metaplasticity process in the medial prefrontal cortex and hippocampus. *Neuroscience*, Vol. 308 202-11.
- Burgdorf, J., Zhang, X.L., Weiss, C., Matthews, E., Disterhoft, J.F., Stanton, P.K. & Moskal, J.R. (2011b) The N-methyl-D-aspartate receptor modulator GLYX-13 enhances learning and memory, in young adult and learning impaired aging rats. *Neurobiol Aging*, Vol. 32 (4) 698-706.
- Burns, A. & Iliffe, S. (2009) Alzheimer's disease. *BMJ*, Vol. 338 b158.
- Burton, A.W., Lee, D.H., Saab, C. & Chung, J.M. (1999) Preemptive intrathecal ketamine injection produces a long-lasting decrease in neuropathic pain behaviors in a rat model. *Reg Anesth Pain Med*, Vol. 24 (3) 208-13.
- Carrigan, C.N., Bartlett, R.D., Esslinger, C.S., Cybulski, K.A., Tongcharoensirikul, P., Bridges, R.J. & Thompson, C.M. (2002) Synthesis and in vitro pharmacology of substituted quinoline-2,4-dicarboxylic acids as inhibitors of vesicular glutamate transport. *J Med Chem*, Vol. 45 (11) 2260-76.

- Carrió, M.M., Cubarsi, R. & Villaverde, A. (2000) Fine architecture of bacterial inclusion bodies. *FEBS Lett*, Vol. 471 (1) 7-11.
- Carrió, M.M. & Villaverde, A. (2005) Localization of chaperones DnaK and GroEL in bacterial inclusion bodies. *J Bacteriol*, Vol. 187 (10) 3599-601.
- Cartmell, J., Monn, J.A. & Schoepp, D.D. (1999) The metabotropic glutamate 2/3 receptor agonists LY354740 and LY379268 selectively attenuate phencyclidine versus d-amphetamine motor behaviors in rats. *J Pharmacol Exp Ther*, Vol. 291 (1) 161-70.
- Castanotto, D. & Rossi, J.J. (2009) The promises and pitfalls of RNA-interference-based therapeutics. *Nature*, Vol. 457 (7228) 426-33.
- Chaki, S., Shimazaki, T., Karasawa, J., Aoki, T., Kaku, A., Iijima, M., Kambe, D., Yamamoto, S., Kawakita, Y., Shibata, T., Abe, K., Okubo, T., Sekiguchi, Y. & Okuyama, S. (2015) Efficacy of a glycine transporter 1 inhibitor TASP0315003 in animal models of cognitive dysfunction and negative symptoms of schizophrenia. *Psychopharmacology (Berl)*, Vol. 232 (15) 2849-61.
- Chattopadhyay, K. & Mazumdar, S. (2000) Structural and conformational stability of horseradish peroxidase: effect of temperature and pH. *Biochemistry*, Vol. 39 (1) 263-70.
- Chen, L., Muhlhauser, M. & Yang, C.R. (2003) Glycine transporter-1 blockade potentiates NMDA-mediated responses in rat prefrontal cortical neurons in vitro and in vivo. *J Neurophysiol*, Vol. 89 (2) 691-703.
- Chen, P.E., Geballe, M.T., Katz, E., Erreger, K., Livesey, M.R., O'toole, K.K., Le, P., Lee, C.J., Snyder, J.P., Traynelis, S.F. & Wyllie, D.J. (2008) Modulation of glycine potency in rat recombinant NMDA receptors containing chimeric NR2A/2D subunits expressed in *Xenopus laevis* oocytes. *J Physiol*, Vol. 586 (1) 227-45.
- Chenard, B.L., Bordner, J., Butler, T.W., Chambers, L.K., Collins, M.A., De Costa, D.L., Ducat, M.F., Dumont, M.L., Fox, C.B. & Mena, E.E. (1995) (1S,2S)-1-(4-hydroxyphenyl)-2-(4-hydroxy-4-phenylpiperidino)-1-propanol: a potent new neuroprotectant which blocks N-methyl-D-aspartate responses. *J Med Chem*, Vol. 38 (16) 3138-45.
- Chizh, B.A. & Headley, P.M. (2005) NMDA antagonists and neuropathic pain--multiple drug targets and multiple uses. *Curr Pharm Des*, Vol. 11 (23) 2977-94.
- Choudary, P.V., Molnar, M., Evans, S.J., Tomita, H., Li, J.Z., Vawter, M.P., Myers, R.M., Bunney, W.E., Akil, H., Watson, S.J. & Jones, E.G. (2005) Altered cortical glutamatergic and GABAergic signal transmission with glial involvement in depression. *Proc Natl Acad Sci U S A*, Vol. 102 (43) 15653-8.
- Christen, P. & Mehta, P.K. (2001) From cofactor to enzymes. The molecular evolution of pyridoxal-5'-phosphate-dependent enzymes. *Chem Rec*, Vol. 1 (6) 436-47.
- Christoph, T., Reissmüller, E., Schiene, K., Englberger, W. & Chizh, B.A. (2005) Antiallodynic effects of NMDA glycine(B) antagonists in neuropathic pain: possible peripheral mechanisms. *Brain Res*, Vol. 1048 (1-2) 218-27.
- Christoph, T., Schiene, K., Englberger, W., Parsons, C.G. & Chizh, B.A. (2006) The antiallodynic effect of NMDA antagonists in neuropathic pain outlasts the duration of the in vivo NMDA antagonism. *Neuropharmacology*, Vol. 51 (1) 12-7.
- Chun, W. & Johnson, G.V. (2007) The role of tau phosphorylation and cleavage in neuronal cell death. *Front Biosci*, Vol. 12 733-56.

- Clugnet, M.C. & Ledoux, J.E. (1990) Synaptic plasticity in fear conditioning circuits: induction of LTP in the lateral nucleus of the amygdala by stimulation of the medial geniculate body. *J Neurosci*, Vol. 10 (8) 2818-24.
- Congreve, M., Carr, R., Murray, C. & Jhoti, H. (2003) A 'rule of three' for fragment-based lead discovery? *Drug Discov Today*, Vol. 8 (19) 876-7.
- Conn, P.J., Lindsley, C.W. & Jones, C.K. (2009) Activation of metabotropic glutamate receptors as a novel approach for the treatment of schizophrenia. *Trends Pharmacol Sci*, Vol. 30 (1) 25-31.
- Cook, S.P., Galve-Roperh, I., Martínez Del Pozo, A. & Rodríguez-Crespo, I. (2002) Direct calcium binding results in activation of brain serine racemase. *J Biol Chem*, Vol. 277 (31) 27782-92.
- Cooper, D.C., (2008) *Introduction to Neuroscience I*.
- Coquelle, T., Christensen, J.K., Banke, T.G., Madsen, U., Schousboe, A. & Pickering, D.S. (2000) Agonist discrimination between AMPA receptor subtypes. *Neuroreport*, Vol. 11 (12) 2643-8.
- Correll, G.E., Maleki, J., Gracely, E.J., Muir, J.J. & Harbut, R.E. (2004) Subanesthetic ketamine infusion therapy: a retrospective analysis of a novel therapeutic approach to complex regional pain syndrome. *Pain Med*, Vol. 5 (3) 263-75.
- Corrigan, J.J. (1969) D-amino acids in animals. *Science*, Vol. 164 (3876) 142-9.
- Corvin, A., Mcghee, K.A., Murphy, K., Donohoe, G., Nangle, J.M., Schwaiger, S., Kenny, N., Clarke, S., Meagher, D., Quinn, J., Scully, P., Baldwin, P., Browne, D., Walsh, C., Waddington, J.L., Morris, D.W. & Gill, M. (2007) Evidence for association and epistasis at the DAOA/G30 and D-amino acid oxidase loci in an Irish schizophrenia sample. *Am J Med Genet B Neuropsychiatr Genet*, Vol. 144B (7) 949-53.
- Costigan, M., Scholz, J. & Woolf, C.J. (2009) Neuropathic pain: a maladaptive response of the nervous system to damage. *Annu Rev Neurosci*, Vol. 32 1-32.
- Coyle, J.T. & Tsai, G. (2004) The NMDA receptor glycine modulatory site: a therapeutic target for improving cognition and reducing negative symptoms in schizophrenia. *Psychopharmacology (Berl)*, Vol. 174 (1) 32-8.
- Cubelos, B., Gimenez, C. & Zafra, F. (2005) Localization of the GLYT1 glycine transporter at glutamatergic synapses in the rat brain. *Cereb Cortex*, Vol. 15 (4) 448-59.
- D'arcy, A., Villard, F. & Marsh, M. (2007) An automated microseed matrix-screening method for protein crystallization. *Acta Crystallogr D Biol Crystallogr*, Vol. 63 (Pt 4) 550-4.
- Dalvit, C., Caronni, D., Mongelli, N., Veronesi, M. & Vulpetti, A. (2006) NMR-based quality control approach for the identification of false positives and false negatives in high throughput screening. *Curr Drug Discov Technol*, Vol. 3 (2) 115-24.
- Danbolt, N.C. (2001) Glutamate uptake. *Prog Neurobiol*, Vol. 65 (1) 1-105.
- Danysz, W., Parsons, C.G., Mobius, H.J., Stoffler, A. & Quack, G. (2000) Neuroprotective and symptomatological action of memantine relevant for Alzheimer's disease--a unified glutamatergic hypothesis on the mechanism of action. *Neurotox Res*, Vol. 2 (2-3) 85-97.
- Davies, J., Evans, R.H., Francis, A.A., Jones, A.W. & Watkins, J.C. (1981) Antagonism of excitatory amino acid-induced and synaptic excitation of spinal neurones by cis-2,3-piperidine dicarboxylate. *J Neurochem*, Vol. 36 (3) 1305-7.

Dd, D.D. & Marek, G.J. (2002) Preclinical pharmacology of mGlu2/3 receptor agonists: novel agents for schizophrenia? *Curr Drug Targets CNS Neurol Disord*, Vol. 1 (2) 215-25.

De La Mata, I., Ramon, F., Obregon, V.V., Castillon, M.P. & Acebal, C. (2000) Effect of hydrogen peroxide on d-amino acid oxidase from *Rhodotorula gracilis*. *Enzyme Microb Technol*, Vol. 27 (3-5) 234-239.

De Miranda, J., Panizzutti, R., Foltyn, V.N. & Wolosker, H. (2002) Cofactors of serine racemase that physiologically stimulate the synthesis of the N-methyl-D-aspartate (NMDA) receptor coagonist D-serine. *Proc Natl Acad Sci U S A*, Vol. 99 (22) 14542-7.

De Miranda, J., Santoro, A., Engelender, S. & Wolosker, H. (2000) Human serine racemase: molecular cloning, genomic organization and functional analysis. *Gene*, Vol. 256 (1-2) 183-8.

Dellafiora, L., Marchetti, M., Spyraakis, F., Orlandi, V., Campanini, B., Cruciani, G., Cozzini, P. & Mozzarelli, A. (2015) Expanding the chemical space of human serine racemase inhibitors. *Bioorg Med Chem Lett*, Vol. 25 (19) 4297-303.

Demain, A.L. & Vaishnav, P. (2009) Production of recombinant proteins by microbes and higher organisms. *Biotechnol Adv*, Vol. 27 (3) 297-306.

Depoortère, R., Dargazanli, G., Estenne-Bouhtou, G., Coste, A., Lanneau, C., Desvignes, C., Poncelet, M., Heaulme, M., Santucci, V., Decobert, M., Cudennec, A., Voltz, C., Boulay, D., Terranova, J.P., Stemmelin, J., Roger, P., Marabout, B., Sevrin, M., Vigé, X., Biton, B., Steinberg, R., Françon, D., Alonso, R., Avenet, P., Oury-Donat, F., Perrault, G., Griebel, G., George, P., Soubrié, P. & Scatton, B. (2005) Neurochemical, electrophysiological and pharmacological profiles of the selective inhibitor of the glycine transporter-1 SSR504734, a potential new type of antipsychotic. *Neuropsychopharmacology*, Vol. 30 (11) 1963-85.

Desagher, S., Glowinski, J. & Prémont, J. (1997) Pyruvate protects neurons against hydrogen peroxide-induced toxicity. *J Neurosci*, Vol. 17 (23) 9060-7.

Devito, L.M., Balu, D.T., Kanter, B.R., Lykken, C., Basu, A.C., Coyle, J.T. & Eichenbaum, H. (2011) Serine racemase deletion disrupts memory for order and alters cortical dendritic morphology. *Genes Brain Behav*, Vol. 10 (2) 210-22.

Diazgranados, N., Ibrahim, L.A., Brutsche, N.E., Ameli, R., Henter, I.D., Luckenbaugh, D.A., Machado-Vieira, R. & Zarate, C.A. (2010) Rapid resolution of suicidal ideation after a single infusion of an N-methyl-D-aspartate antagonist in patients with treatment-resistant major depressive disorder. *J Clin Psychiatry*, Vol. 71 (12) 1605-11.

Dixon, S.M., Li, P., Liu, R., Wolosker, H., Lam, K.S., Kurth, M.J. & Toney, M.D. (2006) Slow-binding human serine racemase inhibitors from high-throughput screening of combinatorial libraries. *J Med Chem*, Vol. 49 (8) 2388-97.

Domino, E.F. (2010) Taming the ketamine tiger. 1965. *Anesthesiology*, Vol. 113 (3) 678-84.

Doody, R., Wirth, Y., Schmitt, F. & Möbius, H.J. (2004) Specific functional effects of memantine treatment in patients with moderate to severe Alzheimer's disease. *Dement Geriatr Cogn Disord*, Vol. 18 (2) 227-32.

Downing, A.M., Kinon, B.J., Millen, B.A., Zhang, L., Liu, L., Morozova, M.A., Brenner, R., Rayle, T.J., Nisenbaum, L., Zhao, F. & Gomez, J.C. (2014) A Double-Blind, Placebo-Controlled Comparator Study of LY2140023 monohydrate in patients with schizophrenia. *BMC Psychiatry*, Vol. 14 351.

Dravid, S.M., Burger, P.B., Prakash, A., Geballe, M.T., Yadav, R., Le, P., Vellano, K., Snyder, J.P. & Traynelis, S.F. (2010) Structural determinants of D-cycloserine efficacy at the NR1/NR2C NMDA receptors. *J Neurosci*, Vol. 30 (7) 2741-54.

- Duff, M.R., Grubbs, J. & Howell, E.E. (2011) Isothermal titration calorimetry for measuring macromolecule-ligand affinity. *J Vis Exp*, (55).
- Dumin, E., Bendikov, I., Foltyn, V.N., Misumi, Y., Ikehara, Y., Kartvelishvily, E. & Wolosker, H. (2006) Modulation of D-serine levels via ubiquitin-dependent proteasomal degradation of serine racemase. *J Biol Chem*, Vol. 281 (29) 20291-302.
- Dun, Y., Duplantier, J., Roon, P., Martin, P.M., Ganapathy, V. & Smith, S.B. (2008) Serine racemase expression and D-serine content are developmentally regulated in neuronal ganglion cells of the retina. *J Neurochem*, Vol. 104 (4) 970-8.
- Dunlop, D.S. & Neidle, A. (1997) The origin and turnover of D-serine in brain. *Biochem Biophys Res Commun*, Vol. 235 (1) 26-30.
- Dunlop, D.S. & Neidle, A. (2005) Regulation of serine racemase activity by amino acids. *Brain Res Mol Brain Res*, Vol. 133 (2) 208-14.
- Duplantier, A.J., Becker, S.L., Bohanon, M.J., Borzilleri, K.A., Chrunyk, B.A., Downs, J.T., Hu, L.Y., El-Kattan, A., James, L.C., Liu, S., Lu, J., Maklad, N., Mansour, M.N., Mente, S., Piotrowski, M.A., Sakya, S.M., Sheehan, S., Steyn, S.J., Strick, C.A., Williams, V.A. & Zhang, L. (2009) Discovery, SAR, and pharmacokinetics of a novel 3-hydroxyquinolin-2(1H)-one series of potent D-amino acid oxidase (DAAO) inhibitors. *J Med Chem*, Vol. 52 (11) 3576-85.
- Dyker, A.G. & Lees, K.R. (1999) Remacemide hydrochloride: a double-blind, placebo-controlled, safety and tolerability study in patients with acute ischemic stroke. *Stroke*, Vol. 30 (9) 1796-801.
- Ehmsen, J.T., Ma, T.M., Sason, H., Rosenberg, D., Ogo, T., Furuya, S., Snyder, S.H. & Wolosker, H. (2013) D-serine in glia and neurons derives from 3-phosphoglycerate dehydrogenase. *J Neurosci*, Vol. 33 (30) 12464-9.
- Eliasof, S., Mcilvain, H.B., Petroski, R.E., Foster, A.C. & Dunlop, J. (2001) Pharmacological characterization of threo-3-methylglutamic acid with excitatory amino acid transporters in native and recombinant systems. *J Neurochem*, Vol. 77 (2) 550-7.
- Ellison, G. (1995) The N-methyl-D-aspartate antagonists phencyclidine, ketamine and dizocilpine as both behavioral and anatomical models of the dementias. *Brain Res Brain Res Rev*, Vol. 20 (2) 250-67.
- Erlanson, D.A., Fesik, S.W., Hubbard, R.E., Jahnke, W. & Jhoti, H. (2016) Twenty years on: the impact of fragments on drug discovery. *Nat Rev Drug Discov*, Vol. 15 (9) 605-19.
- Esposito, Z., Belli, L., Toniolo, S., Sancesario, G., Bianconi, C. & Martorana, A. (2013) Amyloid beta, glutamate, excitotoxicity in Alzheimer's disease: are we on the right track? *CNS Neurosci Ther*, Vol. 19 (8) 549-55.
- Eulenburg, V., Armsen, W., Betz, H. & Gomeza, J. (2005) Glycine transporters: essential regulators of neurotransmission. *Trends Biochem Sci*, Vol. 30 (6) 325-33.
- Fairman, W.A., Vandenberg, R.J., Arriza, J.L., Kavanaugh, M.P. & Amara, S.G. (1995) An excitatory amino-acid transporter with properties of a ligand-gated chloride channel. *Nature*, Vol. 375 (6532) 599-603.
- Fava, M. (2003) Diagnosis and definition of treatment-resistant depression. *Biol Psychiatry*, Vol. 53 (8) 649-59.
- Fell, M.J., Svensson, K.A., Johnson, B.G. & Schoepp, D.D. (2008) Evidence for the role of metabotropic glutamate (mGlu)2 not mGlu3 receptors in the preclinical antipsychotic pharmacology of the mGlu2/3 receptor agonist (-)-(1R,4S,5S,6S)-4-amino-2-sulfonylbicyclo[3.1.0]hexane-4,6-dicarboxylic acid (LY404039). *J Pharmacol Exp Ther*, Vol. 326 (1) 209-17.

- Ferraris, D., Duvall, B., Ko, Y.S., Thomas, A.G., Rojas, C., Majer, P., Hashimoto, K. & Tsukamoto, T. (2008) Synthesis and biological evaluation of D-amino acid oxidase inhibitors. *J Med Chem*, Vol. 51 (12) 3357-9.
- Foltyn, V.N., Bendikov, I., De Miranda, J., Panizzutti, R., Dumin, E., Shleper, M., Li, P., Toney, M.D., Kartvelishvili, E. & Wolosker, H. (2005) Serine racemase modulates intracellular D-serine levels through an alpha,beta-elimination activity. *J Biol Chem*, Vol. 280 (3) 1754-63.
- Fujii, K., Maeda, K., Hikida, T., Mustafa, A.K., Balkissoon, R., Xia, J., Yamada, T., Ozeki, Y., Kawahara, R., Okawa, M., Haganir, R.L., Ujike, H., Snyder, S.H. & Sawa, A. (2006) Serine racemase binds to PICK1: potential relevance to schizophrenia. *Mol Psychiatry*, Vol. 11 (2) 150-7.
- Furukawa, H. (2012) Structure and function of glutamate receptor amino terminal domains. *J Physiol*, Vol. 590 (Pt 1) 63-72.
- Furukawa, H. & Gouaux, E. (2003) Mechanisms of activation, inhibition and specificity: crystal structures of the NMDA receptor NR1 ligand-binding core. *EMBO J*, Vol. 22 (12) 2873-85.
- Furuta, A., Martin, L.J., Lin, C.L., Dykes-Hoberg, M. & Rothstein, J.D. (1997) Cellular and synaptic localization of the neuronal glutamate transporters excitatory amino acid transporter 3 and 4. *Neuroscience*, Vol. 81 (4) 1031-42.
- Gashaw, I., Ellinghaus, P., Sommer, A. & Asadullah, K. (2012) What makes a good drug target? *Drug Discov Today*, Vol. 17 Suppl S24-30.
- Gasparini, F., Inderbitzin, W., Francotte, E., Lecis, G., Richert, P., Dragic, Z., Kuhn, R. & Flor, P.J. (2000) (+)-4-phosphonophenylglycine (PPG) a new group III selective metabotropic glutamate receptor agonist. *Bioorg Med Chem Lett*, Vol. 10 (11) 1241-4.
- Gasparini, F., Lingenhoehl, K., Stoehr, N., Flor, P.J., Heinrich, M., Vranesic, I., Biollaz, M., Allgeier, H., Heckendorn, R., Urwyler, S., Varney, M.A., Johnson, E.C., Hess, S.D., Rao, S.P., Sacca, A.I., Santori, E.M., Velicelebi, G. & Kuhn, R. (1999) 2-Methyl-6-(phenylethynyl)-pyridine (MPEP), a potent, selective and systemically active mGlu5 receptor antagonist. *Neuropharmacology*, Vol. 38 (10) 1493-503.
- Ge Healthcare Life Sciences (2017) *Superdex Size Exclusion Media*. [online] <http://www.gelifesciences.com/> [accessed 07-07-17].
- Gegelashvili, G. & Schousboe, A. (1998) Cellular distribution and kinetic properties of high-affinity glutamate transporters. *Brain Res Bull*, Vol. 45 (3) 233-8.
- Gelin, M., Delfosse, V., Allemand, F., Hoh, F., Sallaz-Damaz, Y., Pirocchi, M., Bourguet, W., Ferrer, J.L., Labesse, G. & Guichou, J.F. (2015) Combining 'dry' co-crystallization and in situ diffraction to facilitate ligand screening by X-ray crystallography. *Acta Crystallogr D Biol Crystallogr*, Vol. 71 (Pt 8) 1777-87.
- Gilron, I. & Dickenson, A.H. (2014) Emerging drugs for neuropathic pain. *Expert Opin Emerg Drugs*, Vol. 19 (3) 329-41.
- Goda, Y. & Stevens, C.F. (1994) Two components of transmitter release at a central synapse. *Proc Natl Acad Sci U S A*, Vol. 91 (26) 12942-6.
- Goedert, M., Spillantini, M.G. & Crowther, R.A. (1991) Tau proteins and neurofibrillary degeneration. *Brain Pathol*, Vol. 1 (4) 279-86.
- Goel, A.P., Maher, D.P. & Cohen, S.P. (2017) Ketamine: miracle drug or latest fad? *Pain Manag*.
- Goff, D.C. (2014) Bitopertin: the good news and bad news. *JAMA Psychiatry*, Vol. 71 (6) 621-2.

- Goff, D.C., Tsai, G., Levitt, J., Amico, E., Manoach, D., Schoenfeld, D.A., Hayden, D.L., Mccarley, R. & Coyle, J.T. (1999) A placebo-controlled trial of D-cycloserine added to conventional neuroleptics in patients with schizophrenia. *Arch Gen Psychiatry*, Vol. 56 (1) 21-7.
- Goltsov, A.Y., Loseva, J.G., Andreeva, T.V., Grigorenko, A.P., Abramova, L.I., Kaleda, V.G., Orlova, V.A., Moliaka, Y.K. & Rogaev, E.I. (2006) Polymorphism in the 5'-promoter region of serine racemase gene in schizophrenia. *Mol Psychiatry*, Vol. 11 (4) 325-6.
- Goto, M., Yamauchi, T., Kamiya, N., Miyahara, I., Yoshimura, T., Mihara, H., Kurihara, T., Hirotsu, K. & Esaki, N. (2009) Crystal structure of a homolog of mammalian serine racemase from *Schizosaccharomyces pombe*. *J Biol Chem*, Vol. 284 (38) 25944-52.
- Grøftehaug, M.K., Hajizadeh, N.R., Swann, M.J. & Pohl, E. (2015) Protein-ligand interactions investigated by thermal shift assays (TSA) and dual polarization interferometry (DPI). *Acta Crystallogr D Biol Crystallogr*, Vol. 71 (Pt 1) 36-44.
- Gutman, M. (1978) Modulation of mitochondrial succinate dehydrogenase activity, mechanism and function. *Mol Cell Biochem*, Vol. 20 (1) 41-60.
- Hajduk, P.J. & Greer, J. (2007) A decade of fragment-based drug design: strategic advances and lessons learned. *Nat Rev Drug Discov*, Vol. 6 (3) 211-9.
- Hamase, K., Konno, R., Morikawa, A. & Zaitsev, K. (2005) Sensitive determination of D-amino acids in mammals and the effect of D-amino-acid oxidase activity on their amounts. *Biol Pharm Bull*, Vol. 28 (9) 1578-84.
- Hann, M.M., Leach, A.R. & Harper, G. (2001) Molecular complexity and its impact on the probability of finding leads for drug discovery. *J Chem Inf Comput Sci*, Vol. 41 (3) 856-64.
- Harada, K., Nakato, K., Yarimizu, J., Yamazaki, M., Morita, M., Takahashi, S., Aota, M., Saita, K., Doihara, H., Sato, Y., Yamaji, T., Ni, K. & Matsuoka, N. (2012) A novel glycine transporter-1 (GlyT1) inhibitor, ASP2535 (4-[3-isopropyl-5-(6-phenyl-3-pyridyl)-4H-1,2,4-triazol-4-yl]-2,1,3-benzoxadiazole), improves cognition in animal models of cognitive impairment in schizophrenia and Alzheimer's disease. *Eur J Pharmacol*, Vol. 685 (1-3) 59-69.
- Hardy, J. & Allsop, D. (1991) Amyloid deposition as the central event in the aetiology of Alzheimer's disease. *Trends Pharmacol Sci*, Vol. 12 (10) 383-8.
- Harty, M., Nagar, M., Atkinson, L., Legay, C.M., Derksen, D.J. & Bearne, S.L. (2014) Inhibition of serine and proline racemases by substrate-product analogues. *Bioorg Med Chem Lett*, Vol. 24 (1) 390-3.
- Harvey, R.J. & Napper, R.M. (1991) Quantitative studies on the mammalian cerebellum. *Prog Neurobiol*, Vol. 36 (6) 437-63.
- Harvey, R.J. & Yee, B.K. (2013) Glycine transporters as novel therapeutic targets in schizophrenia, alcohol dependence and pain. *Nat Rev Drug Discov*, Vol. 12 (11) 866-85.
- Hashimoto, A., Nishikawa, T., Hayashi, T., Fujii, N., Harada, K., Oka, T. & Takahashi, K. (1992) The presence of free D-serine in rat brain. *FEBS Lett*, Vol. 296 (1) 33-6.
- Hashimoto, A., Nishikawa, T., Konno, R., Niwa, A., Yasumura, Y., Oka, T. & Takahashi, K. (1993) Free D-serine, D-aspartate and D-alanine in central nervous system and serum in mutant mice lacking D-amino acid oxidase. *Neurosci Lett*, Vol. 152 (1-2) 33-6.
- Hashimoto, K., Fukushima, T., Shimizu, E., Komatsu, N., Watanabe, H., Shinoda, N., Nakazato, M., Kumakiri, C., Okada, S., Hasegawa, H., Imai, K. & Iyo, M. (2003) Decreased serum levels of D-serine in

patients with schizophrenia: evidence in support of the N-methyl-D-aspartate receptor hypofunction hypothesis of schizophrenia. *Arch Gen Psychiatry*, Vol. 60 (6) 572-6.

Hashimoto, K., Fukushima, T., Shimizu, E., Okada, S., Komatsu, N., Okamura, N., Koike, K., Koizumi, H., Kumakiri, C., Imai, K. & Iyo, M. (2004) Possible role of D-serine in the pathophysiology of Alzheimer's disease. *Prog Neuropsychopharmacol Biol Psychiatry*, Vol. 28 (2) 385-8.

Hashimoto, K., Sawa, A. & Iyo, M. (2007) Increased levels of glutamate in brains from patients with mood disorders. *Biol Psychiatry*, Vol. 62 (11) 1310-6.

Hasler, G., Van Der Veen, J.W., Tumonis, T., Meyers, N., Shen, J. & Drevets, W.C. (2007) Reduced prefrontal glutamate/glutamine and gamma-aminobutyric acid levels in major depression determined using proton magnetic resonance spectroscopy. *Arch Gen Psychiatry*, Vol. 64 (2) 193-200.

Hassell, A.M., An, G., Bledsoe, R.K., Bynum, J.M., Carter, H.L., Deng, S.J., Gampe, R.T., Grisard, T.E., Madauss, K.P., Nolte, R.T., Rocque, W.J., Wang, L., Weaver, K.L., Williams, S.P., Wisely, G.B., Xu, R. & Shewchuk, L.M. (2007) Crystallization of protein-ligand complexes. *Acta Crystallogr D Biol Crystallogr*, Vol. 63 (Pt 1) 72-9.

Hayashi, T. (1952) A physiological study of epileptic seizures following cortical stimulation in animals and its application to human clinics. *Jpn J Physiol*, Vol. 3 (1) 46-64.

Hebert, L.E., Scherr, P.A., Bienias, J.L., Bennett, D.A. & Evans, D.A. (2003) Alzheimer disease in the US population: prevalence estimates using the 2000 census. *Arch Neurol*, Vol. 60 (8) 1119-22.

Helton, D.R., Tizzano, J.P., Monn, J.A., Schoepp, D.D. & Kallman, M.J. (1998) Anxiolytic and side-effect profile of LY354740: a potent, highly selective, orally active agonist for group II metabotropic glutamate receptors. *J Pharmacol Exp Ther*, Vol. 284 (2) 651-60.

Heresco-Levy, U. & Javitt, D.C. (2004) Comparative effects of glycine and D-cycloserine on persistent negative symptoms in schizophrenia: a retrospective analysis. *Schizophr Res*, Vol. 66 (2-3) 89-96.

Heresco-Levy, U., Javitt, D.C., Ermilov, M., Mordel, C., Silipo, G. & Lichtenstein, M. (1999) Efficacy of high-dose glycine in the treatment of enduring negative symptoms of schizophrenia. *Arch Gen Psychiatry*, Vol. 56 (1) 29-36.

Hinoi, E., Ogita, K., Takeuchi, Y., Ohashi, H., Maruyama, T. & Yoneda, Y. (2001) Characterization with [3H]quisqualate of group I metabotropic glutamate receptor subtype in rat central and peripheral excitable tissues. *Neurochem Int*, Vol. 38 (3) 277-85.

Hochuli, E., Dobeli, H. & Schacher, A. (1987) New metal chelate adsorbent selective for proteins and peptides containing neighbouring histidine residues. *J Chromatogr*, Vol. 411 177-84.

Hoffman, H.E., Jirásková, J., Cígler, P., Sanda, M., Schraml, J. & Konvalinka, J. (2009a) Hydroxamic acids as a novel family of serine racemase inhibitors: mechanistic analysis reveals different modes of interaction with the pyridoxal-5'-phosphate cofactor. *J Med Chem*, Vol. 52 (19) 6032-41.

Hoffman, H.E., Jirásková, J., Ingr, M., Zvelebil, M. & Konvalinka, J. (2009b) Recombinant human serine racemase: enzymologic characterization and comparison with its mouse ortholog. *Protein Expr Purif*, Vol. 63 (1) 62-7.

Holmseth, S., Scott, H.A., Real, K., Lehre, K.P., Leergaard, T.B., Bjaalie, J.G. & Danbolt, N.C. (2009) The concentrations and distributions of three C-terminal variants of the GLT1 (EAAT2; slc1a2) glutamate transporter protein in rat brain tissue suggest differential regulation. *Neuroscience*, Vol. 162 (4) 1055-71.

Homayoun, H. & Moghaddam, B. (2007) NMDA receptor hypofunction produces opposite effects on prefrontal cortex interneurons and pyramidal neurons. *J Neurosci*, Vol. 27 (43) 11496-500.

- Hong, P., Koza, S. & Bouvier, E.S. (2012) Size-Exclusion Chromatography for the Analysis of Protein Biotherapeutics and their Aggregates. *J Liq Chromatogr Relat Technol*, Vol. 35 (20) 2923-2950.
- Hons, J., Zirko, R., Ulrychova, M., Cermakova, E. & Libiger, J. (2008) D-serine serum levels in patients with schizophrenia: relation to psychopathology and comparison to healthy subjects. *Neuro Endocrinol Lett*, Vol. 29 (4) 485-92.
- Hood, W.F., Compton, R.P. & Monahan, J.B. (1989) D-cycloserine: a ligand for the N-methyl-D-aspartate coupled glycine receptor has partial agonist characteristics. *Neurosci Lett*, Vol. 98 (1) 91-5.
- Hopkins, A.L., Groom, C.R. & Alex, A. (2004) Ligand efficiency: a useful metric for lead selection. *Drug Discov Today* 845845 England, 430-1.
- Horak, M. & Wenthold, R.J. (2009) Different roles of C-terminal cassettes in the trafficking of full-length NR1 subunits to the cell surface. *J Biol Chem*, Vol. 284 (15) 9683-91.
- Horio, M., Fujita, Y., Ishima, T., Iyo, M., Ferraris, D., Tsukamoto, T. & Hashimoto, K. (2009) Effects of D-Amino Acid Oxidase Inhibitor on the Extracellular D-Alanine Levels and the Efficacy of D-Alanine on Dizocilpine-Induced Prepulse Inhibition Deficits in Mice. *The Open Clinical Chemistry Journal*, Vol. 2 (1).
- Horio, M., Kohno, M., Fujita, Y., Ishima, T., Inoue, R., Mori, H. & Hashimoto, K. (2012) Role of serine racemase in behavioral sensitization in mice after repeated administration of methamphetamine. *PLoS One*, Vol. 7 (4) e35494.
- Hota, D., Bansal, V. & Pattanaik, S. (2007) Evaluation of ketamine, nimodipine, gabapentin and imipramine in partial sciatic nerve transection model of neuropathic pain in rat: an experimental study. *Methods Find Exp Clin Pharmacol*, Vol. 29 (7) 443-6.
- Howes, O., Mccutcheon, R. & Stone, J. (2015) Glutamate and dopamine in schizophrenia: an update for the 21st century. *J Psychopharmacol*, Vol. 29 (2) 97-115.
- Hsieh, H., Boehm, J., Sato, C., Iwatsubo, T., Tomita, T., Sisodia, S. & Malinow, R. (2006) AMPAR removal underlies Abeta-induced synaptic depression and dendritic spine loss. *Neuron*, Vol. 52 (5) 831-43.
- Hsieh, M.H., Gu, S.L., Ho, S.C., Pawlak, C.R., Lin, C.L., Ho, Y.J., Lai, T.J. & Wu, F.Y. (2012) Effects of MK-801 on recognition and neurodegeneration in an MPTP-induced Parkinson's rat model. *Behav Brain Res*, Vol. 229 (1) 41-7.
- Huang, C., Li, H.T., Shi, Y.S., Han, J.S. & Wan, Y. (2004a) Ketamine potentiates the effect of electroacupuncture on mechanical allodynia in a rat model of neuropathic pain. *Neurosci Lett*, Vol. 368 (3) 327-31.
- Huang, C.C., Wei, I.H., Huang, C.L., Chen, K.T., Tsai, M.H., Tsai, P., Tun, R., Huang, K.H., Chang, Y.C., Lane, H.Y. & Tsai, G.E. (2013) Inhibition of glycine transporter-I as a novel mechanism for the treatment of depression. *Biol Psychiatry*, Vol. 74 (10) 734-41.
- Huang, Y.H., Dykes-Hoberg, M., Tanaka, K., Rothstein, J.D. & Bergles, D.E. (2004b) Climbing fiber activation of EAAT4 transporters and kainate receptors in cerebellar Purkinje cells. *J Neurosci*, Vol. 24 (1) 103-11.
- Huge, V., Lauchart, M., Magerl, W., Schelling, G., Beyer, A., Thieme, D. & Azad, S.C. (2010) Effects of low-dose intranasal (S)-ketamine in patients with neuropathic pain. *Eur J Pain*, Vol. 14 (4) 387-94.
- Hughes, J.P., Rees, S., Kalindjian, S.B. & Philpott, K.L. (2011) Principles of early drug discovery. *Br J Pharmacol*, Vol. 162 (6) 1239-49.

- Innocenti, A., Hall, R.A., Schlicker, C., Mühlischlegel, F.A. & Supuran, C.T. (2009) Carbonic anhydrase inhibitors. Inhibition of the beta-class enzymes from the fungal pathogens *Candida albicans* and *Cryptococcus neoformans* with aliphatic and aromatic carboxylates. *Bioorg Med Chem*, Vol. 17 (7) 2654-7.
- Inoue, R., Hashimoto, K., Harai, T. & Mori, H. (2008) NMDA- and beta-amyloid1-42-induced neurotoxicity is attenuated in serine racemase knock-out mice. *J Neurosci*, Vol. 28 (53) 14486-91.
- Isaac, J.T., Nicoll, R.A. & Malenka, R.C. (1995) Evidence for silent synapses: implications for the expression of LTP. *Neuron*, Vol. 15 (2) 427-34.
- Ishida, M., Saitoh, T., Shimamoto, K., Ohfune, Y. & Shinozaki, H. (1993) A novel metabotropic glutamate receptor agonist: marked depression of monosynaptic excitation in the newborn rat isolated spinal cord. *Br J Pharmacol*, Vol. 109 (4) 1169-77.
- Iwama, H., Takahashi, K., Kure, S., Hayashi, F., Narisawa, K., Tada, K., Mizoguchi, M., Takashima, S., Tomita, U. & Nishikawa, T. (1997) Depletion of cerebral D-serine in non-ketotic hyperglycinemia: possible involvement of glycine cleavage system in control of endogenous D-serine. *Biochem Biophys Res Commun*, Vol. 231 (3) 793-6.
- Iwata, H., Takasusuki, T., Yamaguchi, S. & Hori, Y. (2007) NMDA receptor 2B subunit-mediated synaptic transmission in the superficial dorsal horn of peripheral nerve-injured neuropathic mice. *Brain Res*, Vol. 1135 (1) 92-101.
- Izumi, H., Ishimoto, T., Yamamoto, H. & Mori, H. (2017) Application of hairless mouse strain to bioluminescence imaging of Arc expression in mouse brain. *BMC Neurosci*, Vol. 18 (1) 18.
- Jabaudon, D., Shimamoto, K., Yasuda-Kamatani, Y., Scanziani, M., Gähwiler, B.H. & Gerber, U. (1999) Inhibition of uptake unmasks rapid extracellular turnover of glutamate of nonvesicular origin. *Proc Natl Acad Sci U S A*, Vol. 96 (15) 8733-8.
- Jackson, D.L., Graff, C.B., Richardson, J.D. & Hargreaves, K.M. (1995) Glutamate participates in the peripheral modulation of thermal hyperalgesia in rats. *Eur J Pharmacol*, Vol. 284 (3) 321-5.
- Jane, D.E., Thomas, N.K., Tse, H.W. & Watkins, J.C. (1996) Potent antagonists at the L-AP4- and (1S,3S)-ACPD-sensitive presynaptic metabotropic glutamate receptors in the neonatal rat spinal cord. *Neuropharmacology*, Vol. 35 (8) 1029-35.
- Jansonius, J.N. (1998) Structure, evolution and action of vitamin B6-dependent enzymes. *Curr Opin Struct Biol*, Vol. 8 (6) 759-69.
- Janssen (2017) *A Study of Intranasal Esketamine Plus an Oral Antidepressant for Relapse Prevention in Adult Participants With Treatment-resistant Depression | Global Trial Finder*. [online] <http://globaltrialfinder.janssen.com/trial/CR107128-1> [accessed 20-03-17]
- Javitt, D.C. (2006) Is the glycine site half saturated or half unsaturated? Effects of glutamatergic drugs in schizophrenia patients. *Curr Opin Psychiatry*, Vol. 19 (2) 151-7.
- Javitt, D.C. (2007) Glutamate and schizophrenia: phencyclidine, N-methyl-D-aspartate receptors, and dopamine-glutamate interactions. *Int Rev Neurobiol*, Vol. 78 69-108.
- Javitt, D.C. (2008) Glycine transport inhibitors and the treatment of schizophrenia. *Biol Psychiatry*, Vol. 63 (1) 6-8.
- Javitt, D.C., Sershen, H., Hashim, A. & Lajtha, A. (1997) Reversal of phencyclidine-induced hyperactivity by glycine and the glycine uptake inhibitor glycyldodecylamide. *Neuropsychopharmacology*, Vol. 17 (3) 202-4.

- Javitt, D.C., Zylberman, I., Zukin, S.R., Heresco-Levy, U. & Lindenmayer, J.P. (1994) Amelioration of negative symptoms in schizophrenia by glycine. *Am J Psychiatry*, Vol. 151 (8) 1234-6.
- Jensen, T.S., Baron, R., Haanpää, M., Kalso, E., Loeser, J.D., Rice, A.S. & Treede, R.D. (2011) A new definition of neuropathic pain. *Pain*, Vol. 152 (10) 2204-5.
- Jerabek-Willemsen, M., Wienken, C.J., Braun, D., Baaske, P. & Duhr, S. (2011) Molecular interaction studies using microscale thermophoresis. *Assay Drug Dev Technol*, Vol. 9 (4) 342-53.
- Jirásková-Vaničková, J., Ettrich, R., Vorlová, B., Hoffman, H.E., Lepšík, M., Jansa, P. & Konvalinka, J. (2011) Inhibition of human serine racemase, an emerging target for medicinal chemistry. *Curr Drug Targets*, Vol. 12 (7) 1037-55.
- Johansen, T.H., Drejer, J., Watjen, F. & Nielsen, E.O. (1993) A novel non-NMDA receptor antagonist shows selective displacement of low-affinity [3H]kainate binding. *Eur J Pharmacol*, Vol. 246 (3) 195-204.
- Johnson, M.P., Muhlhauser, M.A., Nisenbaum, E.S., Simmons, R.M., Forster, B.M., Knopp, K.L., Yang, L., Morrow, D., Li, D.L., Kennedy, J.D., Swanson, S. & Monn, J.A. (2017) Broad spectrum efficacy with LY2969822, an oral prodrug of metabotropic glutamate 2/3 receptor agonist LY2934747, in rodent pain models. *Br J Pharmacol*, Vol. 174 (9) 822-835.
- Jursky, F. & Nelson, N. (1995) Localization of glycine neurotransmitter transporter (GLYT2) reveals correlation with the distribution of glycine receptor. *J Neurochem*, Vol. 64 (3) 1026-33.
- Jönsson, E.G., Saetre, P., Vares, M., Andreou, D., Larsson, K., Timm, S., Rasmussen, H.B., Djurovic, S., Melle, I., Andreassen, O.A., Agartz, I., Werge, T., Hall, H. & Terenius, L. (2009) DTNBP1, NRG1, DAOA, DAO and GRM3 polymorphisms and schizophrenia: an association study. *Neuropsychobiology*, Vol. 59 (3) 142-50.
- Kakegawa, W., Miyoshi, Y., Hamase, K., Matsuda, S., Matsuda, K., Kohda, K., Emi, K., Motohashi, J., Konno, R., Zaitzu, K. & Yuzaki, M. (2011) D-serine regulates cerebellar LTD and motor coordination through the delta2 glutamate receptor. *Nat Neurosci*, Vol. 14 (5) 603-11.
- Kalsi, S.S., Wood, D.M. & Dargan, P.I. (2011) The epidemiology and patterns of acute and chronic toxicity associated with recreational ketamine use. *Emerg Health Threats J*, Vol. 4 7107.
- Kane, J.F. (1995) Effects of rare codon clusters on high-level expression of heterologous proteins in *Escherichia coli*. *Curr Opin Biotechnol*, Vol. 6 (5) 494-500.
- Kang, T.C., Kim, D.S., Kwak, S.E., Kim, J.E., Kim, D.W., Kang, J.H., Won, M.H., Kwon, O.S. & Choi, S.Y. (2005) Valproic acid reduces enhanced vesicular glutamate transporter immunoreactivities in the dentate gyrus of the seizure prone gerbil. *Neuropharmacology*, Vol. 49 (6) 912-21.
- Karakas, E. & Furukawa, H. (2014) Crystal structure of a heterotetrameric NMDA receptor ion channel. *Science*, Vol. 344 (6187) 992-7.
- Karakas, E., Regan, M.C. & Furukawa, H. (2015) Emerging structural insights into the function of ionotropic glutamate receptors. *Trends Biochem Sci*, Vol. 40 (6) 328-337.
- Kartvelishvili, E., Shleper, M., Balan, L., Dumin, E. & Wolosker, H. (2006) Neuron-derived D-serine release provides a novel means to activate N-methyl-D-aspartate receptors. *J Biol Chem*, Vol. 281 (20) 14151-62.
- Katane, M., Osaka, N., Matsuda, S., Maeda, K., Kawata, T., Saitoh, Y., Sekine, M., Furuchi, T., Doi, I., Hirono, S. & Homma, H. (2013) Identification of novel D-amino acid oxidase inhibitors by in silico screening and their functional characterization in vitro. *J Med Chem*, Vol. 56 (5) 1894-907.

- Katona, C.L. & Katona, C.P. (2014) New generation multi-modal antidepressants: focus on vortioxetine for major depressive disorder. *Neuropsychiatr Dis Treat*, Vol. 10 349-54.
- Kellner, C.H., Fink, M., Knapp, R., Petrides, G., Husain, M., Rummans, T., Mueller, M., Bernstein, H., Rasmussen, K., O'connor, K., Smith, G., Rush, A.J., Biggs, M., McClintock, S., Bailine, S. & Malur, C. (2005) Relief of expressed suicidal intent by ECT: a consortium for research in ECT study. *Am J Psychiatry*, Vol. 162 (5) 977-82.
- Kew, J.N. & Kemp, J.A. (1998) An allosteric interaction between the NMDA receptor polyamine and ifenprodil sites in rat cultured cortical neurones. *J Physiol*, Vol. 512 (Pt 1) 17-28.
- Kew, J.N. & Kemp, J.A. (2005) Ionotropic and metabotropic glutamate receptor structure and pharmacology. *Psychopharmacology (Berl)*, Vol. 179 (1) 4-29.
- Kidd, F.L. & Isaac, J.T. (1999) Developmental and activity-dependent regulation of kainate receptors at thalamocortical synapses. *Nature*, Vol. 400 (6744) 569-73.
- Kieburz, K., Feigin, A., McDermott, M., Como, P., Abwender, D., Zimmerman, C., Hickey, C., Orme, C., Claude, K., Sotack, J., Greenamyre, J.T., Dunn, C. & Shoulson, I. (1996) A controlled trial of remacemide hydrochloride in Huntington's disease. *Mov Disord*, Vol. 11 (3) 273-7.
- Kiefer, R.T., Rohr, P., Ploppa, A., Dieterich, H.J., Grothusen, J., Koffler, S., Altemeyer, K.H., Unertl, K. & Schwartzman, R.J. (2008) Efficacy of ketamine in anesthetic dosage for the treatment of refractory complex regional pain syndrome: an open-label phase II study. *Pain Med*, Vol. 9 (8) 1173-201.
- Kim, J.S., Schmid-Burgk, W., Claus, D. & Kornhuber, H.H. (1982) Increased serum glutamate in depressed patients. *Arch Psychiatr Nervenkr (1970)*, Vol. 232 (4) 299-304.
- Kim, P.M., Aizawa, H., Kim, P.S., Huang, A.S., Wickramasinghe, S.R., Kashani, A.H., Barrow, R.K., Haganir, R.L., Ghosh, A. & Snyder, S.H. (2005) Serine racemase: activation by glutamate neurotransmission via glutamate receptor interacting protein and mediation of neuronal migration. *Proc Natl Acad Sci U S A*, Vol. 102 (6) 2105-10.
- Kim, S., Cho, H., Lee, D. & Webster, M.J. (2012) Association between SNPs and gene expression in multiple regions of the human brain. *Transl Psychiatry*, Vol. 2 e113.
- Kinon, B.J., Zhang, L., Millen, B.A., Osuntokun, O.O., Williams, J.E., Kollack-Walker, S., Jackson, K., Kryzhanovskaya, L. & Jarkova, N. (2011) A multicenter, inpatient, phase 2, double-blind, placebo-controlled dose-ranging study of LY2140023 monohydrate in patients with DSM-IV schizophrenia. *J Clin Psychopharmacol*, Vol. 31 (3) 349-55.
- Kitzinger, H. & Arnold, D.G. (1949) A preliminary study of the effects of glutamic acid on catatonic schizophrenics. *Rorschach Res Exch J Proj Tech*, Vol. 13 (2) 210-8.
- Kleckner, N.W. & Dingledine, R. (1988) Requirement for glycine in activation of NMDA-receptors expressed in *Xenopus* oocytes. *Science*, Vol. 241 (4867) 835-7.
- Klodzinska, A., Chojnacka-Wojcik, E., Palucha, A., Branski, P., Popik, P. & Pilc, A. (1999) Potential anti-anxiety, anti-addictive effects of LY 354740, a selective group II glutamate metabotropic receptors agonist in animal models. *Neuropharmacology*, Vol. 38 (12) 1831-9.
- Kocaeli, H., Korfali, E., Ozturk, H., Kahveci, N. & Yilmazlar, S. (2005) MK-801 improves neurological and histological outcomes after spinal cord ischemia induced by transient aortic cross-clipping in rats. *Surg Neurol*, Vol. 64 Suppl 2 S22-6; discussion S27.

- Kohara, A., Toya, T., Tamura, S., Watabiki, T., Nagakura, Y., Shitaka, Y., Hayashibe, S., Kawabata, S. & Okada, M. (2005) Radioligand binding properties and pharmacological characterization of 6-amino-N-cyclohexyl-N,3-dimethylthiazolo[3,2-a]benzimidazole-2-carboxamide (YM-298198), a high-affinity, selective, and noncompetitive antagonist of metabotropic glutamate receptor type 1. *J Pharmacol Exp Ther*, Vol. 315 (1) 163-9.
- Kola, I. & Landis, J. (2004) Can the pharmaceutical industry reduce attrition rates? *Nat Rev Drug Discov* 820820 England, 711-5.
- Konno, R., Okamura, T., Kasai, N., Summer, K.H. & Niwa, A. (2009) Mutant rat strain lacking D-amino-acid oxidase. *Amino Acids*, Vol. 37 (2) 367-75.
- Koshland, D.E. (1958) Application of a Theory of Enzyme Specificity to Protein Synthesis. *Proc Natl Acad Sci U S A*, Vol. 44 (2) 98-104.
- Kotermanski, S.E., Johnson, J.W. & Thiels, E. (2013) Comparison of behavioral effects of the NMDA receptor channel blockers memantine and ketamine in rats. *Pharmacol Biochem Behav*, Vol. 109 67-76.
- Koval, D., Jirásková, J., Strískovský, K., Konvalinka, J. & Kasicka, V. (2006) Capillary electrophoresis method for determination of D-serine and its application for monitoring of serine racemase activity. *Electrophoresis*, Vol. 27 (13) 2558-66.
- Kranz, J.K. & Schalk-Hihi, C. (2011) Protein thermal shifts to identify low molecular weight fragments. *Methods Enzymol*, Vol. 493 277-98.
- Krystal, J.H., Karper, L.P., Seibyl, J.P., Freeman, G.K., Delaney, R., Bremner, J.D., Heninger, G.R., Bowers, M.B. & Charney, D.S. (1994) Subanesthetic effects of the noncompetitive NMDA antagonist, ketamine, in humans. Psychotomimetic, perceptual, cognitive, and neuroendocrine responses. *Arch Gen Psychiatry*, Vol. 51 (3) 199-214.
- Kuner, T., Seeburg, P.H. & Guy, H.R. (2003) A common architecture for K⁺ channels and ionotropic glutamate receptors? *Trends Neurosci*, Vol. 26 (1) 27-32.
- Kurtz, M.M., Moberg, P.J., Gur, R.C. & Gur, R.E. (2001) Approaches to cognitive remediation of neuropsychological deficits in schizophrenia: a review and meta-analysis. *Neuropsychol Rev*, Vol. 11 (4) 197-210.
- Labrie, V., Fukumura, R., Rastogi, A., Fick, L.J., Wang, W., Boutros, P.C., Kennedy, J.L., Semeralul, M.O., Lee, F.H., Baker, G.B., Belsham, D.D., Barger, S.W., Gondo, Y., Wong, A.H. & Roder, J.C. (2009) Serine racemase is associated with schizophrenia susceptibility in humans and in a mouse model. *Hum Mol Genet*, Vol. 18 (17) 3227-43.
- Laemmli, U.K. (1970) Cleavage of structural proteins during the assembly of the head of bacteriophage T4. *Nature*, Vol. 227 (5259) 680-5.
- Lahti, A.C., Weiler, M.A., Tamara Michaelidis, B.A., Parwani, A. & Tamminga, C.A. (2001) Effects of ketamine in normal and schizophrenic volunteers. *Neuropsychopharmacology*, Vol. 25 (4) 455-67.
- Lambert, M.P., Barlow, A.K., Chromy, B.A., Edwards, C., Freed, R., Liosatos, M., Morgan, T.E., Rozovsky, I., Trommer, B., Viola, K.L., Wals, P., Zhang, C., Finch, C.E., Krafft, G.A. & Klein, W.L. (1998) Diffusible, nonfibrillar ligands derived from Abeta1-42 are potent central nervous system neurotoxins. *Proc Natl Acad Sci U S A*, Vol. 95 (11) 6448-53.
- Lane, H.Y., Chang, Y.C., Liu, Y.C., Chiu, C.C. & Tsai, G.E. (2005) Sarcosine or D-serine add-on treatment for acute exacerbation of schizophrenia: a randomized, double-blind, placebo-controlled study. *Arch Gen Psychiatry*, Vol. 62 (11) 1196-204.

- Lane, H.Y., Lin, C.H., Green, M.F., Hellemann, G., Huang, C.C., Chen, P.W., Tun, R., Chang, Y.C. & Tsai, G.E. (2013) Add-on treatment of benzoate for schizophrenia: a randomized, double-blind, placebo-controlled trial of D-amino acid oxidase inhibitor. *JAMA Psychiatry*, Vol. 70 (12) 1267-75.
- Lane, H.Y., Liu, Y.C., Huang, C.L., Chang, Y.C., Liao, C.H., Perng, C.H. & Tsai, G.E. (2008) Sarcosine (N-methylglycine) treatment for acute schizophrenia: a randomized, double-blind study. *Biol Psychiatry*, Vol. 63 (1) 9-12.
- Laurido, C., Hernández, A., Pelissier, T. & Constandil, L. (2012) Antinociceptive effect of rat D-serine racemase inhibitors, L-serine-O-sulfate, and L-erythro-3-hydroxyaspartate in an arthritic pain model. *ScientificWorldJournal*, Vol. 2012 279147.
- Lavreysen, H., Wouters, R., Bischoff, F., Nobrega Pereira, S., Langlois, X., Blokland, S., Somers, M., Dillen, L. & Lesage, A.S. (2004) JNJ16259685, a highly potent, selective and systemically active mGlu1 receptor antagonist. *Neuropharmacology*, Vol. 47 (7) 961-72.
- Lechner, S.M. (2006) Glutamate-based therapeutic approaches: inhibitors of glycine transport. *Curr Opin Pharmacol*, Vol. 6 (1) 75-81.
- Lee, C.H., Lü, W., Michel, J.C., Goehring, A., Du, J., Song, X. & Gouaux, E. (2014) NMDA receptor structures reveal subunit arrangement and pore architecture. *Nature*, Vol. 511 (7508) 191-7.
- Lein, E.S., Hawrylycz, M.J., Ao, N., Ayres, M., Bensinger, A., Bernard, A., Boe, A.F., Boguski, M.S., Brockway, K.S., Byrnes, E.J., Chen, L., Chen, T.M., Chin, M.C., Chong, J., Crook, B.E., Czaplinska, A., Dang, C.N., Datta, S., Dee, N.R., Desaki, A.L., Desta, T., Diep, E., Dolbeare, T.A., Donelan, M.J., Dong, H.W., Dougherty, J.G., Duncan, B.J., Ebbert, A.J., Eichele, G., Estin, L.K., Faber, C., Facer, B.A., Fields, R., Fischer, S.R., Fliss, T.P., Frensley, C., Gates, S.N., Glattfelder, K.J., Halverson, K.R., Hart, M.R., Hohmann, J.G., Howell, M.P., Jeung, D.P., Johnson, R.A., Karr, P.T., Kawal, R., Kidney, J.M., Knapik, R.H., Kuan, C.L., Lake, J.H., Laramée, A.R., Larsen, K.D., Lau, C., Lemon, T.A., Liang, A.J., Liu, Y., Luong, L.T., Michaels, J., Morgan, J.J., Morgan, R.J., Mortrud, M.T., Mosqueda, N.F., Ng, L.L., Ng, R., Orta, G.J., Overly, C.C., Pak, T.H., Parry, S.E., Pathak, S.D., Pearson, O.C., Puchalski, R.B., Riley, Z.L., Rockett, H.R., Rowland, S.A., Royall, J.J., Ruiz, M.J., Sarno, N.R., Schaffnit, K., Shapovalova, N.V., Sivisay, T., Slaughterbeck, C.R., Smith, S.C., Smith, K.A., Smith, B.I., Sodt, A.J., Stewart, N.N., Stumpff, K.R., Sunkin, S.M., Sutram, M., Tam, A., Teemer, C.D., Thaller, C., Thompson, C.L., Varnam, L.R., Visel, A., Whitlock, R.M., Wohnoutka, P.E., Wolkey, C.K., Wong, V.Y., Wood, M., et al. (2007) Genome-wide atlas of gene expression in the adult mouse brain. *Nature*, Vol. 445 (7124) 168-76.
- Lepre, C.A. (2011) Practical aspects of NMR-based fragment screening. *Methods Enzymol*, Vol. 493 219-39.
- Lester, R.A., Clements, J.D., Westbrook, G.L. & Jahr, C.E. (1990) Channel kinetics determine the time course of NMDA receptor-mediated synaptic currents. *Nature*, Vol. 346 (6284) 565-7.
- Leung, A., Wallace, M.S., Ridgeway, B. & Yaksh, T. (2001) Concentration-effect relationship of intravenous alfentanil and ketamine on peripheral neurosensory thresholds, allodynia and hyperalgesia of neuropathic pain. *Pain*, Vol. 91 (1-2) 177-87.
- Levy, L.M., Warr, O. & Attwell, D. (1998) Stoichiometry of the glial glutamate transporter GLT-1 expressed inducibly in a Chinese hamster ovary cell line selected for low endogenous Na⁺-dependent glutamate uptake. *J Neurosci*, Vol. 18 (23) 9620-8.
- Li, S., Hong, S., Shepardson, N.E., Walsh, D.M., Shankar, G.M. & Selkoe, D. (2009) Soluble oligomers of amyloid Beta protein facilitate hippocampal long-term depression by disrupting neuronal glutamate uptake. *Neuron*, Vol. 62 (6) 788-801.

- Li, X., Li, J., Gardner, E.L. & Xi, Z.X. (2010) Activation of mGluR7s inhibits cocaine-induced reinstatement of drug-seeking behavior by a nucleus accumbens glutamate-mGluR2/3 mechanism in rats. *J Neurochem*, Vol. 114 (5) 1368-80.
- Liao, D., Hessler, N.A. & Malinow, R. (1995) Activation of postsynaptically silent synapses during pairing-induced LTP in CA1 region of hippocampal slice. *Nature*, Vol. 375 (6530) 400-4.
- Life Chemicals (2017) *Fragment Libraries*. [online] <http://www.lifechemicals.com/services/fragments> [accessed 12-08-17].
- Lin, C.H., Chen, P.K., Chang, Y.C., Chuo, L.J., Chen, Y.S., Tsai, G.E. & Lane, H.Y. (2014) Benzoate, a D-amino acid oxidase inhibitor, for the treatment of early-phase Alzheimer disease: a randomized, double-blind, placebo-controlled trial. *Biol Psychiatry*, Vol. 75 (9) 678-85.
- Lin, C.Y., Liang, S.Y., Chang, Y.C., Ting, S.Y., Kao, C.L., Wu, Y.H., Tsai, G.E. & Lane, H.Y. (2015) Adjunctive sarcosine plus benzoate improved cognitive function in chronic schizophrenia patients with constant clinical symptoms: A randomised, double-blind, placebo-controlled trial. *World J Biol Psychiatry*, 1-12.
- Lipton, S.A. (2004) Paradigm shift in NMDA receptor antagonist drug development: molecular mechanism of uncompetitive inhibition by memantine in the treatment of Alzheimer's disease and other neurologic disorders. *J Alzheimers Dis*, Vol. 6 (6 Suppl) S61-74.
- Lisman, J.E., Coyle, J.T., Green, R.W., Javitt, D.C., Benes, F.M., Heckers, S. & Grace, A.A. (2008) Circuit-based framework for understanding neurotransmitter and risk gene interactions in schizophrenia. *Trends Neurosci*, Vol. 31 (5) 234-42.
- Liu, J., Chang, L., Roselli, F., Almeida, O.F., Gao, X., Wang, X., Yew, D.T. & Wu, Y. (2010) Amyloid-beta induces caspase-dependent loss of PSD-95 and synaptophysin through NMDA receptors. *J Alzheimers Dis*, Vol. 22 (2) 541-56.
- Lo, M.C., Aulabaugh, A., Jin, G., Cowling, R., Bard, J., Malamas, M. & Ellestad, G. (2004) Evaluation of fluorescence-based thermal shift assays for hit identification in drug discovery. *Anal Biochem*, Vol. 332 (1) 153-9.
- Lomo, T. (1971) Potentiation of monosynaptic EPSPs in the perforant path-dentate granule cell synapse. *Exp Brain Res*, Vol. 12 (1) 46-63.
- Lorrain, D.S., Baccei, C.S., Bristow, L.J., Anderson, J.J. & Varney, M.A. (2003) Effects of ketamine and N-methyl-D-aspartate on glutamate and dopamine release in the rat prefrontal cortex: modulation by a group II selective metabotropic glutamate receptor agonist LY379268. *Neuroscience*, Vol. 117 (3) 697-706.
- Luykx, J.J., Bakker, S.C., Visser, W.F., Verhoeven-Duif, N., Buizer-Voskamp, J.E., Den Heijer, J.M., Boks, M.P., Sul, J.H., Eskin, E., Ori, A.P., Cantor, R.M., Vorstman, J., Strengman, E., Deyoung, J., Kappen, T.H., Pariama, E., Van Dongen, E.P., Borgdorff, P., Bruins, P., De Koning, T.J., Kahn, R.S. & Ophoff, R.A. (2015) Genome-wide association study of NMDA receptor coagonists in human cerebrospinal fluid and plasma. *Mol Psychiatry*, Vol. 20 (12) 1557-64.
- Lynch, D.R. & Gallagher, M.J. (1996) Inhibition of N-methyl-D-aspartate receptors by haloperidol: developmental and pharmacological characterization in native and recombinant receptors. *J Pharmacol Exp Ther*, Vol. 279 (1) 154-61.
- Lüscher, C. & Frerking, M. (2001) Restless AMPA receptors: implications for synaptic transmission and plasticity. *Trends Neurosci*, Vol. 24 (11) 665-70.
- Lüscher, C. & Malenka, R.C. (2012) NMDA receptor-dependent long-term potentiation and long-term depression (LTP/LTD). *Cold Spring Harb Perspect Biol*, Vol. 4 (6).

- Lüscher, C., Xia, H., Beattie, E.C., Carroll, R.C., Von Zastrow, M., Malenka, R.C. & Nicoll, R.A. (1999) Role of AMPA receptor cycling in synaptic transmission and plasticity. *Neuron*, Vol. 24 (3) 649-58.
- Ma, D., Tian, H. & Zou, G. (1999) Asymmetric Strecker-Type Reaction of alpha-Aryl Ketones. Synthesis of (S)-alphaM4CPG, (S)-MPPG, (S)-AIDA, and (S)-APICA, the Antagonists of Metabotropic Glutamate Receptors. *J Org Chem*, Vol. 64 (1) 120-125.
- Ma, T.M., Abazyan, S., Abazyan, B., Nomura, J., Yang, C., Seshadri, S., Sawa, A., Snyder, S.H. & Pletnikov, M.V. (2013) Pathogenic disruption of DISC1-serine racemase binding elicits schizophrenia-like behavior via D-serine depletion. *Mol Psychiatry*, Vol. 18 (5) 557-67.
- Maccaferri, G. & Dingledine, R. (2002) Control of feedforward dendritic inhibition by NMDA receptor-dependent spike timing in hippocampal interneurons. *J Neurosci*, Vol. 22 (13) 5462-72.
- Madeira, C., Freitas, M.E., Vargas-Lopes, C., Wolosker, H. & Panizzutti, R. (2008) Increased brain D-amino acid oxidase (DAAO) activity in schizophrenia. *Schizophr Res*, Vol. 101 (1-3) 76-83.
- Madeira, C., Lourenco, M.V., Vargas-Lopes, C., Suemoto, C.K., Brandão, C.O., Reis, T., Leite, R.E., Laks, J., Jacob-Filho, W., Pasqualucci, C.A., Grinberg, L.T., Ferreira, S.T. & Panizzutti, R. (2015) d-serine levels in Alzheimer's disease: implications for novel biomarker development. *Transl Psychiatry*, Vol. 5 e561.
- Maekawa, M., Wakamatsu, S., Huse, N., Konno, R. & Hori, Y. (2012) Functional roles of endogenous D-serine in the chronic pain-induced plasticity of NMDAR-mediated synaptic transmission in the central amygdala of mice. *Neurosci Lett*, Vol. 520 (1) 57-61.
- Maes, M., Verkerk, R., Vandoolaeghe, E., Lin, A. & Scharpé, S. (1998) Serum levels of excitatory amino acids, serine, glycine, histidine, threonine, taurine, alanine and arginine in treatment-resistant depression: modulation by treatment with antidepressants and prediction of clinical responsivity. *Acta Psychiatr Scand*, Vol. 97 (4) 302-8.
- Maj, J., Rogoz, Z. & Skuza, G. (1992) The effects of combined treatment with MK-801 and antidepressant drugs in the forced swimming test in rats. *Pol J Pharmacol Pharm*, Vol. 44 (3) 217-26.
- Malenka, R.C. (1994) Synaptic plasticity in the hippocampus: LTP and LTD. *Cell*, Vol. 78 (4) 535-8.
- Mann, P.A., Muller, A., Wolff, K.A., Fischmann, T., Wang, H., Reed, P., Hou, Y., Li, W., Muller, C.E., Xiao, J., Murgolo, N., Sher, X., Mayhood, T., Sheth, P.R., Mirza, A., Labroli, M., Xiao, L., McCoy, M., Gill, C.J., Pinho, M.G., Schneider, T. & Roemer, T. (2016) Chemical Genetic Analysis and Functional Characterization of Staphylococcal Wall Teichoic Acid 2-Epimerases Reveals Unconventional Antibiotic Drug Targets. *PLoS Pathog*, Vol. 12 (5) e1005585.
- Marchand, F., Perretti, M. & McMahon, S.B. (2005) Role of the immune system in chronic pain. *Nat Rev Neurosci*, Vol. 6 (7) 521-32.
- Marchetti, M., Bruno, S., Campanini, B., Bettati, S., Peracchi, A. & Mozzarelli, A. (2014) Regulation of human serine racemase activity and dynamics by halides, ATP and malonate. *Amino Acids*.
- Martin-Facklam, M., Pizzagalli, F., Zhou, Y., Ostrowitzki, S., Rayment, V., Brašić, J.R., Parkar, N., Umbricht, D., Dannals, R.F., Goldwater, R. & Wong, D.F. (2013) Glycine Transporter Type 1 Occupancy by Bitopertin: a Positron Emission Tomography Study in Healthy Volunteers. *Neuropsychopharmacology*, Vol. 38 (3) 504-12.
- Masi, A., Cicchi, R., Carloni, A., Pavone, F.S. & Arcangeli, A. (2010) Optical methods in the study of protein-protein interactions. *Adv Exp Med Biol*, Vol. 674 33-42.

Massey, P.V. & Bashir, Z.I. (2007) Long-term depression: multiple forms and implications for brain function. *Trends Neurosci*, Vol. 30 (4) 176-84.

Matsui, T., Sekiguchi, M., Hashimoto, A., Tomita, U., Nishikawa, T. & Wada, K. (1995) Functional comparison of D-serine and glycine in rodents: the effect on cloned NMDA receptors and the extracellular concentration. *J Neurochem*, Vol. 65 (1) 454-8.

Mattevi, A., Vanoni, M.A., Todone, F., Rizzi, M., Teplyakov, A., Coda, A., Bolognesi, M. & Curti, B. (1996) Crystal structure of D-amino acid oxidase: a case of active site mirror-image convergent evolution with flavocytochrome b2. *Proc Natl Acad Sci U S A*, Vol. 93 (15) 7496-501.

Mauri, M.C., Ferrara, A., Boscati, L., Bravin, S., Zamberlan, F., Alecci, M. & Invernizzi, G. (1998) Plasma and platelet amino acid concentrations in patients affected by major depression and under fluvoxamine treatment. *Neuropsychobiology*, Vol. 37 (3) 124-9.

Maybridge (2017) *Maybridge Screening Libraries*. [online]
http://www.maybridge.com/portal/alias__Rainbow/lang__en/tabID__190/DesktopDefault.aspx
 [accessed 15-08-17].

Mcbain, C.J., Kleckner, N.W., Wyrick, S. & Dingledine, R. (1989) Structural requirements for activation of the glycine coagonist site of N-methyl-D-aspartate receptors expressed in *Xenopus* oocytes. *Mol Pharmacol*, Vol. 36 (4) 556-65.

McInnes, C. (2007) Virtual screening strategies in drug discovery. *Curr Opin Chem Biol*, Vol. 11 (5) 494-502.

Mcnamara, D., Smith, E.C., Calligaro, D.O., O'malley, P.J., Mcquaid, L.A. & Dingledine, R. (1990) 5,7-Dichlorokynurenic acid, a potent and selective competitive antagonist of the glycine site on NMDA receptors. *Neurosci Lett*, Vol. 120 (1) 17-20.

Mcpherson, A. (2001) A comparison of salts for the crystallization of macromolecules. *Protein Sci*, Vol. 10 (2) 418-22.

Meldrum, B.S. (2000) Glutamate as a neurotransmitter in the brain: review of physiology and pathology. *J Nutr*, Vol. 130 (4S Suppl) 1007S-15S.

Messer, M., Haller, I.V., Larson, P., Pattison-Crisostomo, J. & Gessert, C.E. (2010) The use of a series of ketamine infusions in two patients with treatment-resistant depression. *J Neuropsychiatry Clin Neurosci*, Vol. 22 (4) 442-4.

Mezler, M., Geneste, H., Gault, L. & Marek, G.J. (2010) LY-2140023, a prodrug of the group II metabotropic glutamate receptor agonist LY-404039 for the potential treatment of schizophrenia. *Curr Opin Investig Drugs*, Vol. 11 (7) 833-45.

Michael, N., Erfurth, A., Ohrmann, P., Arolt, V., Heindel, W. & Pfleiderer, B. (2003) Neurotrophic effects of electroconvulsive therapy: a proton magnetic resonance study of the left amygdalar region in patients with treatment-resistant depression. *Neuropsychopharmacology*, Vol. 28 (4) 720-5.

Michellini, E., Cevenini, L., Mezzanotte, L., Coppa, A. & Roda, A. (2010) Cell-based assays: fuelling drug discovery. *Anal Bioanal Chem*, Vol. 398 (1) 227-38.

Millar, J.K., Wilson-Annan, J.C., Anderson, S., Christie, S., Taylor, M.S., Semple, C.A., Devon, R.S., St Clair, D.M., Muir, W.J., Blackwood, D.H. & Porteous, D.J. (2000) Disruption of two novel genes by a translocation co-segregating with schizophrenia. *Hum Mol Genet*, Vol. 9 (9) 1415-23.

- Mitani, H., Shirayama, Y., Yamada, T., Maeda, K., Ashby, C.R. & Kawahara, R. (2006) Correlation between plasma levels of glutamate, alanine and serine with severity of depression. *Prog Neuropsychopharmacol Biol Psychiatry*, Vol. 30 (6) 1155-8.
- Miya, K., Inoue, R., Takata, Y., Abe, M., Natsume, R., Sakimura, K., Hongou, K., Miyawaki, T. & Mori, H. (2008) Serine racemase is predominantly localized in neurons in mouse brain. *J Comp Neurol*, Vol. 510 (6) 641-54.
- Miyoshi, Y., Hamase, K., Okamura, T., Konno, R., Kasai, N., Tojo, Y. & Zaitzu, K. (2011) Simultaneous two-dimensional HPLC determination of free D-serine and D-alanine in the brain and periphery of mutant rats lacking D-amino-acid oxidase. *J Chromatogr B Analyt Technol Biomed Life Sci*, Vol. 879 (29) 3184-9.
- Miyoshi, Y., Konno, R., Sasabe, J., Ueno, K., Tojo, Y., Mita, M., Aiso, S. & Hamase, K. (2012) Alteration of intrinsic amounts of D-serine in the mice lacking serine racemase and D-amino acid oxidase. *Amino Acids*, Vol. 43 (5) 1919-31.
- Moechars, D., Weston, M.C., Leo, S., Callaerts-Vegh, Z., Goris, I., Daneels, G., Buist, A., Cik, M., Van Der Spek, P., Kass, S., Meert, T., D'hooge, R., Rosenmund, C. & Hampson, R.M. (2006) Vesicular glutamate transporter VGLUT2 expression levels control quantal size and neuropathic pain. *J Neurosci*, Vol. 26 (46) 12055-66.
- Moghaddam, B. (2003) Bringing order to the glutamate chaos in schizophrenia. *Neuron*, Vol. 40 (5) 881-4.
- Moghaddam, B. (2004) Targeting metabotropic glutamate receptors for treatment of the cognitive symptoms of schizophrenia. *Psychopharmacology (Berl)*, Vol. 174 (1) 39-44.
- Moghaddam, B., Adams, B., Verma, A. & Daly, D. (1997) Activation of glutamatergic neurotransmission by ketamine: a novel step in the pathway from NMDA receptor blockade to dopaminergic and cognitive disruptions associated with the prefrontal cortex. *J Neurosci*, Vol. 17 (8) 2921-7.
- Moghaddam, B. & Adams, B.W. (1998) Reversal of phencyclidine effects by a group II metabotropic glutamate receptor agonist in rats. *Science*, Vol. 281 (5381) 1349-52.
- Monaghan, D.T. & Cotman, C.W. (1982) The distribution of [3H]kainic acid binding sites in rat CNS as determined by autoradiography. *Brain Res*, Vol. 252 (1) 91-100.
- Monn, J.A., Valli, M.J., Massey, S.M., Wright, R.A., Salhoff, C.R., Johnson, B.G., Howe, T., Alt, C.A., Rhodes, G.A., Robey, R.L., Griffey, K.R., Tizzano, J.P., Kallman, M.J., Helton, D.R. & Schoepp, D.D. (1997) Design, synthesis, and pharmacological characterization of (+)-2-aminobicyclo[3.1.0]hexane-2,6-dicarboxylic acid (LY354740): a potent, selective, and orally active group 2 metabotropic glutamate receptor agonist possessing anticonvulsant and anxiolytic properties. *J Med Chem*, Vol. 40 (4) 528-37.
- Mony, L., Kew, J.N., Gunthorpe, M.J. & Paoletti, P. (2009) Allosteric modulators of NR2B-containing NMDA receptors: molecular mechanisms and therapeutic potential. *Br J Pharmacol*, Vol. 157 (8) 1301-17.
- Moon, J.Y., Choi, S.R., Roh, D.H., Yoon, S.Y., Kwon, S.G., Choi, H.S., Kang, S.Y., Han, H.J., Kim, H.W., Beitz, A.J., Oh, S.B. & Lee, J.H. (2015) Spinal sigma-1 receptor activation increases the production of D-serine in astrocytes which contributes to the development of mechanical allodynia in a mouse model of neuropathic pain. *Pharmacol Res*, Vol. 100 353-64.
- Mori, H., Wada, R., Li, J., Ishimoto, T., Mizuguchi, M., Obita, T., Gouda, H., Hirono, S. & Toyooka, N. (2014) In silico and pharmacological screenings identify novel serine racemase inhibitors. *Bioorg Med Chem Lett*, Vol. 24 (16) 3732-5.

Mori, H., Wada, R., Takahara, S., Horino, Y., Izumi, H., Ishimoto, T., Yoshida, T., Mizuguchi, M., Obita, T., Gouda, H., Hirono, S. & Toyooka, N. (2017) A novel serine racemase inhibitor suppresses neuronal over-activation in vivo. *Bioorg Med Chem*, Vol. 25 (14) 3736-3745.

Morikawa, A., Hamase, K., Inoue, T., Konno, R., Niwa, A. & Zaitsu, K. (2001) Determination of free D-aspartic acid, D-serine and D-alanine in the brain of mutant mice lacking D-amino acid oxidase activity. *J Chromatogr B Biomed Sci Appl*, Vol. 757 (1) 119-25.

Morita, Y., Ujike, H., Tanaka, Y., Otani, K., Kishimoto, M., Morio, A., Kotaka, T., Okahisa, Y., Matsushita, M., Morikawa, A., Hamase, K., Zaitsu, K. & Kuroda, S. (2007) A genetic variant of the serine racemase gene is associated with schizophrenia. *Biol Psychiatry*, Vol. 61 (10) 1200-3.

Moskal, J.R., Burch, R., Burgdorf, J.S., Kroes, R.A., Stanton, P.K., Disterhoft, J.F. & Leander, J.D. (2014) GLYX-13, an NMDA receptor glycine site functional partial agonist enhances cognition and produces antidepressant effects without the psychotomimetic side effects of NMDA receptor antagonists. *Expert Opin Investig Drugs*, Vol. 23 (2) 243-54.

Moskal, J.R., Kuo, A.G., Weiss, C., Wood, P.L., O'connor Hanson, A., Kelso, S., Harris, R.B. & Disterhoft, J.F. (2005) GLYX-13: a monoclonal antibody-derived peptide that acts as an N-methyl-D-aspartate receptor modulator. *Neuropharmacology*, Vol. 49 (7) 1077-87.

Mothet, J.P., Parent, A.T., Wolosker, H., Brady, R.O., Linden, D.J., Ferris, C.D., Rogawski, M.A. & Snyder, S.H. (2000) D-serine is an endogenous ligand for the glycine site of the N-methyl-D-aspartate receptor. *Proc Natl Acad Sci U S A*, Vol. 97 (9) 4926-31.

Muir, K.W. & Lees, K.R. (1995) Clinical experience with excitatory amino acid antagonist drugs. *Stroke*, Vol. 26 (3) 503-13.

Mukhin, A.G., Ivanova, S.A., Knoblach, S.M. & Faden, A.I. (1997) New in vitro model of traumatic neuronal injury: evaluation of secondary injury and glutamate receptor-mediated neurotoxicity. *J Neurotrauma*, Vol. 14 (9) 651-63.

Murrough, J.W., Iosifescu, D.V., Chang, L.C., Al Jurdi, R.K., Green, C.E., Perez, A.M., Iqbal, S., Pillemer, S., Foulkes, A., Shah, A., Charney, D.S. & Mathew, S.J. (2013) Antidepressant efficacy of ketamine in treatment-resistant major depression: a two-site randomized controlled trial. *Am J Psychiatry*, Vol. 170 (10) 1134-42.

Mustafa, A.K., Ahmad, A.S., Zeynalov, E., Gazi, S.K., Sikka, G., Ehmsen, J.T., Barrow, R.K., Coyle, J.T., Snyder, S.H. & Doré, S. (2010) Serine racemase deletion protects against cerebral ischemia and excitotoxicity. *J Neurosci*, Vol. 30 (4) 1413-6.

Mustafa, A.K., Kumar, M., Selvakumar, B., Ho, G.P., Ehmsen, J.T., Barrow, R.K., Amzel, L.M. & Snyder, S.H. (2007) Nitric oxide S-nitrosylates serine racemase, mediating feedback inhibition of D-serine formation. *Proc Natl Acad Sci U S A*, Vol. 104 (8) 2950-5.

Mustafa, A.K., Van Rossum, D.B., Patterson, R.L., Maag, D., Ehmsen, J.T., Gazi, S.K., Chakraborty, A., Barrow, R.K., Amzel, L.M. & Snyder, S.H. (2009) Glutamatergic regulation of serine racemase via reversal of PIP2 inhibition. *Proc Natl Acad Sci U S A*, Vol. 106 (8) 2921-6.

Möbius, H.J. & Stöffler, A. (2003) Memantine in vascular dementia. *Int Psychogeriatr*, Vol. 15 Suppl 1 207-13.

Möykkynen, T., Coleman, S.K., Semenov, A. & Keinänen, K. (2014) The N-terminal domain modulates α -amino-3-hydroxy-5-methyl-4-isoxazolepropionic acid (AMPA) receptor desensitization. *J Biol Chem*, Vol. 289 (19) 13197-205.

- Müller, I. (2017) Guidelines for the successful generation of protein–ligand complex crystals. *Acta Crystallogr D Struct Biol* 841841, 79-92.
- Nagata, Y., Horiike, K. & Maeda, T. (1994) Distribution of free D-serine in vertebrate brains. *Brain Res*, Vol. 634 (2) 291-5.
- Nagayoshi, C., Ishibashi, M., Kita, Y., Matsuoka, M., Nishimoto, I. & Tokunaga, M. (2005) Expression, refolding and characterization of human brain serine racemase in *Escherichia coli* with N-terminal His-tag. *Protein Pept Lett*, Vol. 12 (5) 487-90.
- Nakanishi, S. (1992) Molecular diversity of glutamate receptors and implications for brain function. *Science*, Vol. 258 (5082) 597-603.
- Nash, J.E., Fox, S.H., Henry, B., Hill, M.P., Peggs, D., McGuire, S., Maneuf, Y., Hille, C., Brotchie, J.M. & Crossman, A.R. (2000) Antiparkinsonian actions of ifenprodil in the MPTP-lesioned marmoset model of Parkinson's disease. *Exp Neurol*, Vol. 165 (1) 136-42.
- Nash, J.E., Hill, M.P. & Brotchie, J.M. (1999) Antiparkinsonian actions of blockade of NR2B-containing NMDA receptors in the reserpine-treated rat. *Exp Neurol*, Vol. 155 (1) 42-8.
- Neale, S.A., Copeland, C.S. & Salt, T.E. (2014) Effect of VGLUT inhibitors on glutamatergic synaptic transmission in the rodent hippocampus and prefrontal cortex. *Neurochem Int*, Vol. 73 159-65.
- Neill, D. (1995) Alzheimer's disease: maladaptive synaptoplasticity hypothesis. *Neurodegeneration*, Vol. 4 (2) 217-32.
- Neill, J.C., Barnes, S., Cook, S., Grayson, B., Idris, N.F., Mclean, S.L., Snigdha, S., Rajagopal, L. & Harte, M.K. (2010) Animal models of cognitive dysfunction and negative symptoms of schizophrenia: focus on NMDA receptor antagonism. *Pharmacol Ther*, Vol. 128 (3) 419-32.
- Neill, J.C., Harte, M.K., Haddad, P.M., Lydall, E.S. & Dwyer, D.M. (2014) Acute and chronic effects of NMDA receptor antagonists in rodents, relevance to negative symptoms of schizophrenia: a translational link to humans. *Eur Neuropsychopharmacol*, Vol. 24 (5) 822-35.
- Nelson, D.L., Applegate, G.A., Beio, M.L., Graham, D.L. & Berkowitz, D.B. (2017) Human serine racemase structure/activity relationship studies provide mechanistic insight and point to position 84 as a hot spot for β -elimination function.
- Nelson, K.A., Park, K.M., Robinovitz, E., Tsigos, C. & Max, M.B. (1997) High-dose oral dextromethorphan versus placebo in painful diabetic neuropathy and postherpetic neuralgia. *Neurology*, Vol. 48 (5) 1212-8.
- Nelson, K.J. & Parsonage, D. (2011) Measurement of Peroxiredoxin Activity. *Curr Protoc Toxicol*, Vol. 0 7 Unit7 10.
- Newby, Z.E., O'connell, J.D., Gruswitz, F., Hays, F.A., Harries, W.E., Harwood, I.M., Ho, J.D., Lee, J.K., Savage, D.F., Miercke, L.J. & Stroud, R.M. (2009) A general protocol for the crystallization of membrane proteins for X-ray structural investigation. *Nat Protoc*, Vol. 4 (5) 619-37.
- Niesters, M., Martini, C. & Dahan, A. (2014) Ketamine for chronic pain: risks and benefits. *Br J Clin Pharmacol*, Vol. 77 (2) 357-67.
- Niswender, C.M. & Conn, P.J. (2010) Metabotropic glutamate receptors: physiology, pharmacology, and disease. *Annu Rev Pharmacol Toxicol*, Vol. 50 295-322.
- Noda, Y., Yamada, K., Furukawa, H. & Nabeshima, T. (1995) Enhancement of immobility in a forced swimming test by subacute or repeated treatment with phencyclidine a new model of schizophrenia,

British Journal of Pharmacology Volume 116, Issue 5. *British Journal of Pharmacology*, Vol. 116 (5) 2531-2537.

Noppers, I.M., Niesters, M., Aarts, L.P., Bauer, M.C., Drewes, A.M., Dahan, A. & Sarton, E.Y. (2011) Drug-induced liver injury following a repeated course of ketamine treatment for chronic pain in CRPS type 1 patients: a report of 3 cases. *Pain*, Vol. 152 (9) 2173-8.

Ogita, K., Hirata, K., Bole, D.G., Yoshida, S., Tamura, Y., Leckenby, A.M. & Ueda, T. (2001) Inhibition of vesicular glutamate storage and exocytotic release by Rose Bengal. *J Neurochem*, Vol. 77 (1) 34-42.

Ohnishi, M., Saito, M., Wakabayashi, S., Ishizuka, M., Nishimura, K., Nagata, Y. & Kasai, S. (2008) Purification and characterization of serine racemase from a hyperthermophilic archaeon, *Pyrobaculum islandicum*. *J Bacteriol*, Vol. 190 (4) 1359-65.

Ohnuma, T., Shibata, N., Maeshima, H., Baba, H., Hatano, T., Hanzawa, R. & Arai, H. (2009) Association analysis of glycine- and serine-related genes in a Japanese population of patients with schizophrenia. *Prog Neuropsychopharmacol Biol Psychiatry*, Vol. 33 (3) 511-8.

Olney, J.W., Labruyere, J. & Price, M.T. (1989) Pathological changes induced in cerebrocortical neurons by phencyclidine and related drugs. *Science*, Vol. 244 (4910) 1360-2.

Onur, O.A., Schlaepfer, T.E., Kukulja, J., Bauer, A., Jeung, H., Patin, A., Otte, D.M., Shah, N.J., Maier, W., Kendrick, K.M., Fink, G.R. & Hurlmann, R. (2010) The N-methyl-D-aspartate receptor co-agonist D-cycloserine facilitates declarative learning and hippocampal activity in humans. *Biol Psychiatry*, Vol. 67 (12) 1205-11.

Otto, M.W., Basden, S.L., Mchugh, R.K., Kantak, K.M., Deckersbach, T., Cather, C., Goff, D.C., Hofmann, S.G., Berry, A.C. & Smits, J.A. (2009) Effects of D-cycloserine administration on weekly nonemotional memory tasks in healthy participants. *Psychother Psychosom*, Vol. 78 (1) 49-54.

Otto, M.W., Kredlow, M.A., Smits, J.A., Hofmann, S.G., Tolin, D.F., De Kleine, R.A., Van Minnen, A., Evins, A.E. & Pollack, M.H. (2015) Enhancement of Psychosocial Treatment With d-Cycloserine: Models, Moderators, and Future Directions. *Biol Psychiatry*.

Ozkan, E.D. & Ueda, T. (1998) Glutamate transport and storage in synaptic vesicles. *Jpn J Pharmacol*, Vol. 77 (1) 1-10.

O'donovan, S.M., Sullivan, C.R. & Mccullumsmith, R.E. (2017) The role of glutamate transporters in the pathophysiology of neuropsychiatric disorders. *NPJ Schizophr* 835835.

Palmer, I. & Wingfield, P.T. (2004) Preparation and extraction of insoluble (inclusion-body) proteins from *Escherichia coli*. *Curr Protoc Protein Sci*, Vol. Chapter 6 Unit 6.3.

Panatier, A., Theodosis, D.T., Mothet, J.P., Touquet, B., Pollegioni, L., Poulain, D.A. & Oliet, S.H. (2006) Glia-derived D-serine controls NMDA receptor activity and synaptic memory. *Cell*, Vol. 125 (4) 775-84.

Panizzutti, R., De Miranda, J., Ribeiro, C.S., Engelender, S. & Wolosker, H. (2001) A new strategy to decrease N-methyl-D-aspartate (NMDA) receptor coactivation: inhibition of D-serine synthesis by converting serine racemase into an eliminase. *Proc Natl Acad Sci U S A*, Vol. 98 (9) 5294-9.

Pantoliano, M.W., Petrella, E.C., Kwasnoski, J.D., Lobanov, V.S., Myslik, J., Graf, E., Carver, T., Asel, E., Springer, B.A., Lane, P. & Salemme, F.R. (2001) High-density miniaturized thermal shift assays as a general strategy for drug discovery. *J Biomol Screen*, Vol. 6 (6) 429-40.

Paoletti, P., Bellone, C. & Zhou, Q. (2013) NMDA receptor subunit diversity: impact on receptor properties, synaptic plasticity and disease. *Nat Rev Neurosci*, Vol. 14 (6) 383-400.

- Papouin, T., Ladépêche, L., Ruel, J., Sacchi, S., Labasque, M., Hanini, M., Groc, L., Pollegioni, L., Mothet, J.P. & Oliet, S.H. (2012) Synaptic and extrasynaptic NMDA receptors are gated by different endogenous coagonists. *Cell*, Vol. 150 (3) 633-46.
- Papp, M. & Moryl, E. (1993) New evidence for the antidepressant activity of MK-801, a non-competitive antagonist of NMDA receptors. *Pol J Pharmacol*, Vol. 45 (5-6) 549-53.
- Paquette, M.A., Anderson, A.M., Lewis, J.R., Meshul, C.K., Johnson, S.W. & Paul Berger, S. (2010) MK-801 inhibits L-DOPA-induced abnormal involuntary movements only at doses that worsen parkinsonism. *Neuropharmacology*, Vol. 58 (7) 1002-8.
- Patel, S.A., Nagy, J.O., Bolstad, E.D., Gerdes, J.M. & Thompson, C.M. (2007) Tetrapeptide inhibitors of the glutamate vesicular transporter (VGLUT). *Bioorg Med Chem Lett*, Vol. 17 (18) 5125-8.
- Paternain, A.V., Vicente, A., Nielsen, E.O. & Lerma, J. (1996) Comparative antagonism of kainate-activated kainate and AMPA receptors in hippocampal neurons. *Eur J Neurosci*, Vol. 8 (10) 2129-36.
- Paul, I.A. & Skolnick, P. (2003) Glutamate and depression: clinical and preclinical studies. *Ann N Y Acad Sci*, Vol. 1003 250-72.
- Perin-Dureau, F., Rachline, J., Neyton, J. & Paoletti, P. (2002) Mapping the binding site of the neuroprotectant ifenprodil on NMDA receptors. *J Neurosci*, Vol. 22 (14) 5955-65.
- Pernot, P., Mothet, J.P., Schuvailo, O., Soldatkin, A., Pollegioni, L., Pilone, M., Adeline, M.T., Cespuaglio, R. & Marinesco, S. (2008) Characterization of a yeast D-amino acid oxidase microbiosensor for D-serine detection in the central nervous system. *Anal Chem*, Vol. 80 (5) 1589-97.
- Petr, G.T., Sun, Y., Frederick, N.M., Zhou, Y., Dhamne, S.C., Hameed, M.Q., Miranda, C., Bedoya, E.A., Fischer, K.D., Armsen, W., Wang, J., Danbolt, N.C., Rotenberg, A., Aoki, C.J. & Rosenberg, P.A. (2015) Conditional deletion of the glutamate transporter GLT-1 reveals that astrocytic GLT-1 protects against fatal epilepsy while neuronal GLT-1 contributes significantly to glutamate uptake into synaptosomes. *J Neurosci*, Vol. 35 (13) 5187-201.
- Petrenko, A.B., Yamakura, T., Baba, H. & Shimoji, K. (2003) The role of N-methyl-D-aspartate (NMDA) receptors in pain: a review. *Anesth Analg*, Vol. 97 (4) 1108-16.
- Phillips, R.S. (2015) Chemistry and diversity of pyridoxal-5'-phosphate dependent enzymes. *Biochim Biophys Acta*, Vol. 1854 (9) 1167-74.
- Poels, E.M., Kegeles, L.S., Kantrowitz, J.T., Javitt, D.C., Lieberman, J.A., Abi-Dargham, A. & Girgis, R.R. (2014) Glutamatergic abnormalities in schizophrenia: a review of proton MRS findings. *Schizophr Res*, Vol. 152 (2-3) 325-32.
- Pomarol-Clotet, E., Honey, G.D., Murray, G.K., Corlett, P.R., Absalom, A.R., Lee, M., Mckenna, P.J., Bullmore, E.T. & Fletcher, P.C. (2006) Psychological effects of ketamine in healthy volunteers. Phenomenological study. *Br J Psychiatry*, Vol. 189 173-9.
- Porath, J. (1992) Immobilized metal ion affinity chromatography. *Protein Expr Purif*, Vol. 3 (4) 263-81.
- Pow, D.V. & Barnett, N.L. (2000) Developmental expression of excitatory amino acid transporter 5: a photoreceptor and bipolar cell glutamate transporter in rat retina. *Neurosci Lett*, Vol. 280 (1) 21-4.
- Preskorn, S.H., Baker, B., Kolluri, S., Menniti, F.S., Krams, M. & Landen, J.W. (2008) An innovative design to establish proof of concept of the antidepressant effects of the NR2B subunit selective N-methyl-D-aspartate antagonist, CP-101,606, in patients with treatment-refractory major depressive disorder. *J Clin Psychopharmacol*, Vol. 28 (6) 631-7.

Price, R.B., Iosifescu, D.V., Murrough, J.W., Chang, L.C., Al Jurdi, R.K., Iqbal, S.Z., Soleimani, L., Charney, D.S., Foulkes, A.L. & Mathew, S.J. (2014) Effects of ketamine on explicit and implicit suicidal cognition: a randomized controlled trial in treatment-resistant depression. *Depress Anxiety*, Vol. 31 (4) 335-43.

Prorok, M. & Castellino, F.J. (2007) The molecular basis of conantokin antagonism of NMDA receptor function. *Curr Drug Targets*, Vol. 8 (5) 633-42.

Pubchem (2017) malonic acid | C3H4O4 - PubChem.

Pud, D., Eisenberg, E., Spitzer, A., Adler, R., Fried, G. & Yarnitsky, D. (1998) The NMDA receptor antagonist amantadine reduces surgical neuropathic pain in cancer patients: a double blind, randomized, placebo controlled trial. *Pain*, Vol. 75 (2-3) 349-54.

Purves, D., Augustine, G.J., Fitzpatrick, D., Katz, L.C., Lamantia, A.-S., Mcnamara, J.O. & Williams, S.M. (2001) *Neuroscience*. 2nd ed. Sunderland (MA): Sinauer Associates.

Puzzo, D., Privitera, L., Fa', M., Staniszewski, A., Hashimoto, G., Aziz, F., Sakurai, M., Ribe, E.M., Troy, C.M., Mercken, M., Jung, S.S., Palmeri, A. & Arancio, O. (2011) Endogenous amyloid- β is necessary for hippocampal synaptic plasticity and memory. *Ann Neurol*, Vol. 69 (5) 819-30.

Qian, A. & Johnson, J.W. (2002) Channel gating of NMDA receptors. *Physiol Behav*, Vol. 77 (4-5) 577-82.

Qu, X.X., Cai, J., Li, M.J., Chi, Y.N., Liao, F.F., Liu, F.Y., Wan, Y., Han, J.S. & Xing, G.G. (2009) Role of the spinal cord NR2B-containing NMDA receptors in the development of neuropathic pain. *Exp Neurol*, Vol. 215 (2) 298-307.

Quartaroli, M., Carignani, C., Dal Forno, G., Mugnaini, M., Ugolini, A., Arban, R., Bettelini, L., Maraia, G., Belardetti, F., Reggiani, A., Trist, D.G., Ratti, E., Di Fabio, R. & Corsi, M. (1999) Potent antihyperalgesic activity without tolerance produced by glycine site antagonist of N-methyl-D-aspartate receptor GV196771A. *J Pharmacol Exp Ther*, Vol. 290 (1) 158-69.

Quiroga, C., Chaparro, R.E., Karlinski, R., Erasso, D., Gordon, M., Morgan, D., Bosco, G., Rubini, A., Parmagnani, A., Paoli, A., Mangar, D. & Camporesi, E.M. (2014) Effects of repetitive exposure to anesthetics and analgesics in the Tg2576 mouse Alzheimer's model. *Neurotox Res*, Vol. 26 (4) 414-21.

Ramanujam, N. (2000) Fluorescence spectroscopy of neoplastic and non-neoplastic tissues. *Neoplasia*, Vol. 2 (1-2) 89-117.

Rammes, G., Hasenjaeger, A., Sroka-Saidi, K., Deussing, J.M. & Parsons, C.G. (2011) Therapeutic significance of NR2B-containing NMDA receptors and mGluR5 metabotropic glutamate receptors in mediating the synaptotoxic effects of beta-amyloid oligomers on long-term potentiation (LTP) in murine hippocampal slices. *Neuropharmacology*, Vol. 60 (6) 982-90.

Ray, B., Banerjee, P.K., Greig, N.H. & Lahiri, D.K. (2010) Memantine treatment decreases levels of secreted Alzheimer's amyloid precursor protein (APP) and amyloid beta (A β) peptide in the human neuroblastoma cells. *Neurosci Lett*, Vol. 470 (1) 1-5.

Rees, D.C., Congreve, M., Murray, C.W. & Carr, R. (2004) Fragment-based lead discovery. *Nat Rev Drug Discov*, Vol. 3 (8) 660-72.

Reimer, R.J. & Edwards, R.H. (2004) Organic anion transport is the primary function of the SLC17/type I phosphate transporter family. *Pflugers Arch*, Vol. 447 (5) 629-35.

Ricker, R.D. & Sandoval, L.A. (1996) Fast, reproducible size-exclusion chromatography of biological macromolecules. *J Chromatogr A*, Vol. 743 (1) 43-50.

- Riou, M., Stroebel, D., Edwardson, J.M. & Paoletti, P. (2012) An alternating GluN1-2-1-2 subunit arrangement in mature NMDA receptors. *PLoS One*, Vol. 7 (4) e35134.
- Rodríguez-Moreno, A. & Lerma, J. (1998) Kainate receptor modulation of GABA release involves a metabotropic function. *Neuron*, Vol. 20 (6) 1211-8.
- Rogawski, M.A. & Hanada, T. (2013) Preclinical pharmacology of perampanel, a selective non-competitive AMPA receptor antagonist. *Acta Neurol Scand Suppl*, (197) 19-24.
- Rogawski, M.A. & Wenk, G.L. (2003) The neuropharmacological basis for the use of memantine in the treatment of Alzheimer's disease. *CNS Drug Rev*, Vol. 9 (3) 275-308.
- Rorick-Kehn, L.M., Johnson, B.G., Knitowski, K.M., Salhoff, C.R., Witkin, J.M., Perry, K.W., Griffey, K.I., Tizzano, J.P., Monn, J.A., McKinzie, D.L. & Schoepp, D.D. (2007) In vivo pharmacological characterization of the structurally novel, potent, selective mGlu2/3 receptor agonist LY404039 in animal models of psychiatric disorders. *Psychopharmacology (Berl)*, Vol. 193 (1) 121-36.
- Rosenberg, D., Kartvelishvili, E., Shleper, M., Klinker, C.M., Bowser, M.T. & Wolosker, H. (2010) Neuronal release of D-serine: a physiological pathway controlling extracellular D-serine concentration. *FASEB J*, Vol. 24 (8) 2951-61.
- Rosenzweig-Lipson, S., Beyer, C.E., Hughes, Z.A., Khawaja, X., Rajarao, S.J., Malberg, J.E., Rahman, Z., Ring, R.H. & Schechter, L.E. (2007) Differentiating antidepressants of the future: efficacy and safety. *Pharmacol Ther*, Vol. 113 (1) 134-53.
- Roseth, S., Fykse, E.M. & Fonnum, F. (1998) Uptake of L-glutamate into synaptic vesicles: competitive inhibition by dyes with biphenyl and amino- and sulphonic acid-substituted naphthyl groups. *Biochem Pharmacol*, Vol. 56 (9) 1243-9.
- Rostas, J.A., Brent, V.A., Voss, K., Errington, M.L., Bliss, T.V. & Gurd, J.W. (1996) Enhanced tyrosine phosphorylation of the 2B subunit of the N-methyl-D-aspartate receptor in long-term potentiation. *Proc Natl Acad Sci U S A*, Vol. 93 (19) 10452-6.
- Rotaru, D.C., Yoshino, H., Lewis, D.A., Ermentrout, G.B. & Gonzalez-Burgos, G. (2011) Glutamate receptor subtypes mediating synaptic activation of prefrontal cortex neurons: relevance for schizophrenia. *J Neurosci*, Vol. 31 (1) 142-56.
- Rouaud, E. & Billard, J.M. (2003) D-cycloserine facilitates synaptic plasticity but impairs glutamatergic neurotransmission in rat hippocampal slices. *Br J Pharmacol*, Vol. 140 (6) 1051-6.
- Roussos, P., Giakoumaki, S.G., Adamaki, E., Georgakopoulos, A., Anastasios, G., Robakis, N.K., Nikos, R.K. & Bitsios, P. (2011) The association of schizophrenia risk D-amino acid oxidase polymorphisms with sensorimotor gating, working memory and personality in healthy males. *Neuropsychopharmacology*, Vol. 36 (8) 1677-88.
- Sabatini, B.L. & Regehr, W.G. (1996) Timing of neurotransmission at fast synapses in the mammalian brain. *Nature*, Vol. 384 (6605) 170-2.
- Saha, S., Chant, D., Welham, J. & Mcgrath, J. (2005) A systematic review of the prevalence of schizophrenia. *PLoS Med*, Vol. 2 (5) e141.
- Salussolia, C.L., Prodromou, M.L., Borker, P. & Wollmuth, L.P. (2011) Arrangement of subunits in functional NMDA receptors. *J Neurosci*, Vol. 31 (31) 11295-304.
- Sanacora, G., Gueorgieva, R., Epperson, C.N., Wu, Y.T., Appel, M., Rothman, D.L., Krystal, J.H. & Mason, G.F. (2004) Subtype-specific alterations of gamma-aminobutyric acid and glutamate in patients with major depression. *Arch Gen Psychiatry*, Vol. 61 (7) 705-13.

- Sarton, E., Teppema, L.J., Olievier, C., Nieuwenhuijs, D., Matthes, H.W., Kieffer, B.L. & Dahan, A. (2001) The involvement of the mu-opioid receptor in ketamine-induced respiratory depression and antinociception. *Anesth Analg*, Vol. 93 (6) 1495-500, table of contents.
- Sasabe, J., Chiba, T., Yamada, M., Okamoto, K., Nishimoto, I., Matsuoka, M. & Aiso, S. (2007) D-serine is a key determinant of glutamate toxicity in amyotrophic lateral sclerosis. *EMBO J*, Vol. 26 (18) 4149-59.
- Sasabe, J., Suzuki, M., Imanishi, N. & Aiso, S. (2014) Activity of D-amino acid oxidase is widespread in the human central nervous system. *Front Synaptic Neurosci*, Vol. 6 14.
- Schallier, A., Massie, A., Loyens, E., Moechars, D., Drinkenburg, W., Michotte, Y. & Smolders, I. (2009) vGLUT2 heterozygous mice show more susceptibility to clonic seizures induced by pentylentetrazol. *Neurochem Int*, Vol. 55 (1-3) 41-4.
- Schell, M.J., Brady, R.O., Molliver, M.E. & Snyder, S.H. (1997) D-serine as a neuromodulator: regional and developmental localizations in rat brain glia resemble NMDA receptors. *J Neurosci*, Vol. 17 (5) 1604-15.
- Schell, M.J., Molliver, M.E. & Snyder, S.H. (1995) D-serine, an endogenous synaptic modulator: localization to astrocytes and glutamate-stimulated release. *Proc Natl Acad Sci U S A*, Vol. 92 (9) 3948-52.
- Schizophrenia Working Group of the Psychiatric Genomics Consortium (2014) Biological insights from 108 schizophrenia-associated genetic loci. *Nature*, Vol. 511 (7510) 421-7.
- Schmitt, J., Hess, H. & Stunnenberg, H.G. (1993) Affinity purification of histidine-tagged proteins. *Mol Biol Rep*, Vol. 18 (3) 223-30.
- Schoemaker, J.H., Jansen, W.T., Schipper, J. & Szegedi, A. (2014) The selective glycine uptake inhibitor org 25935 as an adjunctive treatment to atypical antipsychotics in predominant persistent negative symptoms of schizophrenia: results from the GIANT trial. *J Clin Psychopharmacol*, Vol. 34 (2) 190-8.
- Schoepp, D.D., Johnson, B.G., Salhoff, C.R., Valli, M.J., Desai, M.A., Burnett, J.P., Mayne, N.G. & Monn, J.A. (1995) Selective inhibition of forskolin-stimulated cyclic AMP formation in rat hippocampus by a novel mGluR agonist, 2R,4R-4-aminopyrrolidine-2,4- dicarboxylate. *Neuropharmacology*, Vol. 34 (8) 843-50.
- Schoepp, D.D., Johnson, B.G., Wright, R.A., Salhoff, C.R., Mayne, N.G., Wu, S., Cockerman, S.L., Burnett, J.P., Belegaje, R., Bleakman, D. & Monn, J.A. (1997) LY354740 is a potent and highly selective group II metabotropic glutamate receptor agonist in cells expressing human glutamate receptors. *Neuropharmacology*, Vol. 36 (1) 1-11.
- Schoepp, D.D., Wright, R.A., Levine, L.R., Gaydos, B. & Potter, W.Z. (2003) LY354740, an mGlu2/3 receptor agonist as a novel approach to treat anxiety/stress. *Stress*, Vol. 6 (3) 189-97.
- Schultes, S., De Graaf, C., Haaksma, E.J., De Esch, I., Leurs, R. & Krämer, O. (2010) Ligand efficiency as a guide in fragment hit selection and optimization. *Drug Discov Today Technol*, Vol. 7 (3) e147-202.
- Schwartzman, R.J., Alexander, G.M., Grothusen, J.R., Paylor, T., Reichenberger, E. & Perreault, M. (2009) Outpatient intravenous ketamine for the treatment of complex regional pain syndrome: a double-blind placebo controlled study. *Pain*, Vol. 147 (1-3) 107-15.
- Schüttler, J., Stanski, D.R., White, P.F., Trevor, A.J., Horai, Y., Verotta, D. & Sheiner, L.B. (1987) Pharmacodynamic modeling of the EEG effects of ketamine and its enantiomers in man. *J Pharmacokinet Biopharm*, Vol. 15 (3) 241-53.

Shankar, G.M., Li, S., Mehta, T.H., Garcia-Munoz, A., Shepardson, N.E., Smith, I., Brett, F.M., Farrell, M.A., Rowan, M.J., Lemere, C.A., Regan, C.M., Walsh, D.M., Sabatini, B.L. & Selkoe, D.J. (2008) Amyloid-beta protein dimers isolated directly from Alzheimer's brains impair synaptic plasticity and memory. *Nat Med*, Vol. 14 (8) 837-42.

Sheinin, A., Shavit, S. & Benveniste, M. (2001) Subunit specificity and mechanism of action of NMDA partial agonist D-cycloserine. *Neuropharmacology*, Vol. 41 (2) 151-8.

Sheline, C.T., Behrens, M.M. & Choi, D.W. (2000) Zinc-induced cortical neuronal death: contribution of energy failure attributable to loss of NAD(+) and inhibition of glycolysis. *J Neurosci*, Vol. 20 (9) 3139-46.

Sheng, M. (2001) The postsynaptic NMDA-receptor--PSD-95 signaling complex in excitatory synapses of the brain. *J Cell Sci*, Vol. 114 (Pt 7) 1251.

Shigeri, Y., Seal, R.P. & Shimamoto, K. (2004) Molecular pharmacology of glutamate transporters, EAATs and VGLUTs. *Brain Res Brain Res Rev*, Vol. 45 (3) 250-65.

Shigeri, Y., Shimamoto, K., Yasuda-Kamatani, Y., Seal, R.P., Yumoto, N., Nakajima, T. & Amara, S.G. (2001) Effects of threo-beta-hydroxyaspartate derivatives on excitatory amino acid transporters (EAAT4 and EAAT5). *J Neurochem*, Vol. 79 (2) 297-302.

Shim, S.S., Hammonds, M.D. & Kee, B.S. (2008) Potentiation of the NMDA receptor in the treatment of schizophrenia: focused on the glycine site. *Eur Arch Psychiatry Clin Neurosci*, Vol. 258 (1) 16-27.

Shimamoto, K. & Ohfun, Y. (1996) Syntheses and conformational analyses of glutamate analogs: 2-(2-carboxy-3-substituted-cyclopropyl)glycines as useful probes for excitatory amino acid receptors. *J Med Chem*, Vol. 39 (2) 407-23.

Shleper, M., Kartvelishvili, E. & Wolosker, H. (2005) D-serine is the dominant endogenous coagonist for NMDA receptor neurotoxicity in organotypic hippocampal slices. *J Neurosci*, Vol. 25 (41) 9413-7.

Shoulson, I., Penney, J., McDermott, M., Schwid, S., Kayson, E., Chase, T., Fahn, S., Greenamyre, J.T., Lang, A., Siderowf, A., Pearson, N., Harrison, M., Rost, E., Colcher, A., Lloyd, M., Matthews, M., Pahwa, R., McGuire, D., Lew, M.F., Schuman, S., Marek, K., Broshjeit, S., Factor, S., Brown, D., Feigin, A., Mazurkiewicz, J., Ford, B., Jennings, D., Dilllon, S., Comella, C., Blasucci, L., Janko, K., Shulman, L., Wiener, W., Bateman-Rodriguez, D., Carrion, A., Suchowersky, O., Lafontaine, A.L., Pantella, C., Siemers, E., Belden, J., Davies, R., Lannon, M., Grimes, D., Gray, P., Martin, W., Kennedy, L., Adler, C., Newman, S., Hammerstad, J., Stone, C., Lewitt, P., Bardram, K., Mistura, K., Miyasaki, J., Johnston, L., Cha, J.H., Tennis, M., Panniset, M., Hall, J., Tetrud, J., Friedlander, J., Hauser, R., Gauger, L., Rodnitzky, R., Deleo, A., Dobson, J., Seeberger, L., Dingmann, C., Tarsy, D., Ryan, P., Elmer, L., Ruzicka, D., Stacy, M., Brewer, M., Locke, B., Baker, D., Casaceli, C., Day, D., Florack, M., Hodgeman, K., Laroia, N., Nobel, R., Orme, C., Rexo, L., Rothenburgh, K., Sulimowicz, K., Watts, A., Wratt, E., Tariot, P., Cox, C., Leventhal, C., Alderfer, V., Craun, A.M., Frey, J., Mccree, L., McDermott, J., Cooper, J., Holdich, T., Read, B., et al. (2001) A randomized, controlled trial of remacemide for motor fluctuations in Parkinson's disease. *Neurology*, Vol. 56 (4) 455-62.

Sigma-Aldrich (2017) *Buffer Reference Center*. [online] <http://www.sigmaaldrich.com/life-science/core-bioreagents/biological-buffers/learning-center/buffer-reference-center.html> [accessed 15-01-17]

Sigtermans, M., Dahan, A., Mooren, R., Bauer, M., Kest, B., Sarton, E. & Olofsen, E. (2009a) S(+)-ketamine effect on experimental pain and cardiac output: a population pharmacokinetic-pharmacodynamic modeling study in healthy volunteers. *Anesthesiology*, Vol. 111 (4) 892-903.

Sigtermans, M.J., Van Hilten, J.J., Bauer, M.C., Arbous, M.S., Marinus, J., Sarton, E.Y. & Dahan, A. (2009b) Ketamine produces effective and long-term pain relief in patients with Complex Regional Pain Syndrome Type 1. *Pain*, Vol. 145 (3) 304-11.

- Simmons, R.M., Webster, A.A., Kalra, A.B. & Iyengar, S. (2002) Group II mGluR receptor agonists are effective in persistent and neuropathic pain models in rats. *Pharmacol Biochem Behav*, Vol. 73 (2) 419-27.
- Singh, A. & Abraham, W.C. (2017) Astrocytes and synaptic plasticity in health and disease. *Exp Brain Res*, Vol. 235 (6) 1645-1655.
- Singh, A., Upadhyay, V., Upadhyay, A.K., Singh, S.M. & Panda, A.K. (2015) Protein recovery from inclusion bodies of Escherichia coli using mild solubilization process. *Microb Cell Fact*, Vol. 14 41.
- Singh, J.B., Fedgchin, M., Daly, E., Xi, L., Melman, C., De Bruecker, G., Tadic, A., Sienaert, P., Wiegand, F., Manji, H., Drevets, W.C. & Van Nueten, L. (2016) Intravenous Esketamine in Adult Treatment-Resistant Depression: A Double-Blind, Double-Randomization, Placebo-Controlled Study. *Biol Psychiatry*, Vol. 80 (6) 424-31.
- Singh, N.S., Paul, R.K., Sichler, M., Moaddel, R., Bernier, M. & Wainer, I.W. (2012) Capillary electrophoresis-laser-induced fluorescence (CE-LIF) assay for measurement of intracellular D-serine and serine racemase activity. *Anal Biochem*, Vol. 421 (2) 460-6.
- Skarzynski, T. & Thorpe, J. (2006) Industrial perspective on X-ray data collection and analysis. *Acta Crystallogr D Biol Crystallogr*, Vol. 62 (Pt 1) 102-7.
- Smith, M.A., Mack, V., Ebner, A., Moraes, I., Felicetti, B., Wood, M., Schonfeld, D., Mather, O., Cesura, A. & Barker, J. (2010) The structure of mammalian serine racemase: evidence for conformational changes upon inhibitor binding. *J Biol Chem*, Vol. 285 (17) 12873-81.
- Smith, S.M., Uslaner, J.M., Yao, L., Mullins, C.M., Surles, N.O., Huszar, S.L., McNaughton, C.H., Pascarella, D.M., Kandebo, M., Hinchliffe, R.M., Sparey, T., Brandon, N.J., Jones, B., Venkatraman, S., Young, M.B., Sachs, N., Jacobson, M.A. & Hutson, P.H. (2009) The behavioral and neurochemical effects of a novel D-amino acid oxidase inhibitor compound 8 [4H-thieno [3,2-b]pyrrole-5-carboxylic acid] and D-serine. *J Pharmacol Exp Ther*, Vol. 328 (3) 921-30.
- Snyder, E.M., Nong, Y., Almeida, C.G., Paul, S., Moran, T., Choi, E.Y., Nairn, A.C., Salter, M.W., Lombroso, P.J., Gouras, G.K. & Greengard, P. (2005) Regulation of NMDA receptor trafficking by amyloid-beta. *Nat Neurosci*, Vol. 8 (8) 1051-8.
- Sobolevsky, A.I., Rosconi, M.P. & Gouaux, E. (2009) X-ray structure, symmetry and mechanism of an AMPA-subtype glutamate receptor. *Nature*, Vol. 462 (7274) 745-56.
- Sparey, T., Abeywickrema, P., Almond, S., Brandon, N., Byrne, N., Campbell, A., Hutson, P.H., Jacobson, M., Jones, B., Munshi, S., Pascarella, D., Pike, A., Prasad, G.S., Sachs, N., Sakatis, M., Sardana, V., Venkatraman, S. & Young, M.B. (2008) The discovery of fused pyrrole carboxylic acids as novel, potent D-amino acid oxidase (DAO) inhibitors. *Bioorg Med Chem Lett*, Vol. 18 (11) 3386-91.
- St Clair, D., Blackwood, D., Muir, W., Carothers, A., Walker, M., Spowart, G., Gosden, C. & Evans, H.J. (1990) Association within a family of a balanced autosomal translocation with major mental illness. *Lancet*, Vol. 336 (8706) 13-6.
- Stauffer, V.L., Millen, B.A., Andersen, S., Kinon, B.J., Lagrandeur, L., Lindenmayer, J.P. & Gomez, J.C. (2013) Pomaglumetad methionil: no significant difference as an adjunctive treatment for patients with prominent negative symptoms of schizophrenia compared to placebo. *Schizophr Res*, Vol. 150 (2-3) 434-41.
- Steffek, A.E., Haroutunian, V. & Meador-Woodruff, J.H. (2006) Serine racemase protein expression in cortex and hippocampus in schizophrenia. *Neuroreport*, Vol. 17 (11) 1181-5.

Stevens, E.R., Esguerra, M., Kim, P.M., Newman, E.A., Snyder, S.H., Zahs, K.R. & Miller, R.F. (2003) D-serine and serine racemase are present in the vertebrate retina and contribute to the physiological activation of NMDA receptors. *Proc Natl Acad Sci U S A*, Vol. 100 (11) 6789-94.

Strange, M., Brauner-Osborne, H. & Jensen, A.A. (2006) Functional characterisation of homomeric ionotropic glutamate receptors GluR1-GluR6 in a fluorescence-based high throughput screening assay. *Comb Chem High Throughput Screen*, Vol. 9 (2) 147-58.

Strick, C.A., Li, C., Scott, L., Harvey, B., Hajós, M., Steyn, S.J., Piotrowski, M.A., James, L.C., Downs, J.T., Rago, B., Becker, S.L., El-Kattan, A., Xu, Y., Ganong, A.H., Tingley, F.D., Ramirez, A.D., Seymour, P.A., Guanowsky, V., Majchrzak, M.J., Fox, C.B., Schmidt, C.J. & Duplantier, A.J. (2011) Modulation of NMDA receptor function by inhibition of D-amino acid oxidase in rodent brain. *Neuropharmacology*, Vol. 61 (5-6) 1001-15.

Strohmaier, J., Georgi, A., Schirmbeck, F., Schmael, C., Jamra, R.A., Schumacher, J., Becker, T., Höfels, S., Klopp, N., Illig, T., Propping, P., Cichon, S., Nöthen, M.M., Rietschel, M. & Schulze, T.G. (2007) No association between the serine racemase gene (SRR) and schizophrenia in a German case-control sample. *Psychiatr Genet*, Vol. 17 (2) 125.

Stríšovský, K., Jirásková, J., Barinka, C., Majer, P., Rojas, C., Slusher, B.S. & Konvalinka, J. (2003) Mouse brain serine racemase catalyzes specific elimination of L-serine to pyruvate. *FEBS Lett*, Vol. 535 (1-3) 44-8.

Stríšovský, K., Jirásková, J., Mikulová, A., Rulísek, L. & Konvalinka, J. (2005) Dual substrate and reaction specificity in mouse serine racemase: identification of high-affinity dicarboxylate substrate and inhibitors and analysis of the beta-eliminase activity. *Biochemistry*, Vol. 44 (39) 13091-100.

Ströhle, A., Schmidt, D.K., Schultz, F., Fricke, N., Staden, T., Hellweg, R., Priller, J., Rapp, M.A. & Rieckmann, N. (2015) Drug and Exercise Treatment of Alzheimer Disease and Mild Cognitive Impairment: A Systematic Review and Meta-Analysis of Effects on Cognition in Randomized Controlled Trials. *Am J Geriatr Psychiatry*, Vol. 23 (12) 1234-49.

Sudhof, T.C. (2004) The synaptic vesicle cycle. *Annu Rev Neurosci*, Vol. 27 509-47.

Suzuki, M., Sasabe, J., Miyoshi, Y., Kuwasako, K., Muto, Y., Hamase, K., Matsuoka, M., Imanishi, N. & Aiso, S. (2015) Glycolytic flux controls D-serine synthesis through glyceraldehyde-3-phosphate dehydrogenase in astrocytes. *Proc Natl Acad Sci U S A*, Vol. 112 (17) E2217-24.

Suzuki, R., Matthews, E.A. & Dickenson, A.H. (2001) Comparison of the effects of MK-801, ketamine and memantine on responses of spinal dorsal horn neurones in a rat model of mononeuropathy. *Pain*, Vol. 91 (1-2) 101-9.

Szabo, M., Svensson Akusjarvi, S., Saxena, A., Liu, J., Chandrasekar, G. & Kitambi, S.S. (2017) Cell and small animal models for phenotypic drug discovery. *Drug Des Devel Ther*, Vol. 11 1957-1967.

Szanto, K., Mulsant, B.H., Houck, P., Dew, M.A. & Reynolds, C.F. (2003) Occurrence and course of suicidality during short-term treatment of late-life depression. *Arch Gen Psychiatry*, Vol. 60 (6) 610-7.

Tabata-Imai, A., Inoue, R. & Mori, H. (2014) Increased sensitivity to inflammatory pain induced by subcutaneous formalin injection in serine racemase knock-out mice. *PLoS One*, Vol. 9 (8) e105282.

Takayasu, N., Yoshikawa, M., Watanabe, M., Tsukamoto, H., Suzuki, T., Kobayashi, H. & Noda, S. (2008) The serine racemase mRNA is expressed in both neurons and glial cells of the rat retina. *Arch Histol Cytol*, Vol. 71 (2) 123-9.

Tamura, Y., Ogita, K. & Ueda, T. (2014) A new VGLUT-specific potent inhibitor: pharmacophore of Brilliant Yellow. *Neurochem Res*, Vol. 39 (1) 117-28.

- Tanaka, K., Watase, K., Manabe, T., Yamada, K., Watanabe, M., Takahashi, K., Iwama, H., Nishikawa, T., Ichihara, N., Kikuchi, T., Okuyama, S., Kawashima, N., Hori, S., Takimoto, M. & Wada, K. (1997) Epilepsy and exacerbation of brain injury in mice lacking the glutamate transporter GLT-1. *Science*, Vol. 276 (5319) 1699-702.
- Taylor, M.F. (1999) Antisense oligonucleotides for target validation and gene function determination. *IDrugs*, Vol. 2 (8) 777-81.
- Texido, L., Martin-Satue, M., Alberdi, E., Solsona, C. & Matute, C. (2011) Amyloid beta peptide oligomers directly activate NMDA receptors. *Cell Calcium*, Vol. 49 (3) 184-90.
- Thase, M.E., Entsuah, A.R. & Rudolph, R.L. (2001) Remission rates during treatment with venlafaxine or selective serotonin reuptake inhibitors. *Br J Psychiatry*, Vol. 178 234-41.
- Thompson, L.T., Moskal, J.R. & Disterhoft, J.F. (1992) Hippocampus-dependent learning facilitated by a monoclonal antibody or D-cycloserine. *Nature*, Vol. 359 (6396) 638-41.
- Thompson, M., Marecki, J.C., Marinesco, S., Labrie, V., Roder, J.C., Barger, S.W. & Crow, J.P. (2012) Paradoxical roles of serine racemase and D-serine in the G93A mSOD1 mouse model of amyotrophic lateral sclerosis. *J Neurochem*, Vol. 120 (4) 598-610.
- Thompson, S.W., Woolf, C.J. & Sivilotti, L.G. (1993) Small-caliber afferent inputs produce a heterosynaptic facilitation of the synaptic responses evoked by primary afferent A-fibers in the neonatal rat spinal cord in vitro. *J Neurophysiol*, Vol. 69 (6) 2116-28.
- Traynelis, S.F., Wollmuth, L.P., McBain, C.J., Menniti, F.S., Vance, K.M., Ogden, K.K., Hansen, K.B., Yuan, H., Myers, S.J. & Dingledine, R. (2010) Glutamate receptor ion channels: structure, regulation, and function. *Pharmacol Rev*, Vol. 62 (3) 405-96.
- Tremolizzo, L., Sala, G., Zoia, C.P. & Ferrarese, C. (2012) Assessing glutamatergic function and dysfunction in peripheral tissues. *Curr Med Chem*, Vol. 19 (9) 1310-5.
- Truin, M., Janssen, S.P., Van Kleef, M. & Joosten, E.A. (2011) Successful pain relief in non-responders to spinal cord stimulation: the combined use of ketamine and spinal cord stimulation. *Eur J Pain*, Vol. 15 (10) 1049.e1-9.
- Trullas, R. & Skolnick, P. (1990) Functional antagonists at the NMDA receptor complex exhibit antidepressant actions. *Eur J Pharmacol*, Vol. 185 (1) 1-10.
- Tsai, G., Lane, H.Y., Yang, P., Chong, M.Y. & Lange, N. (2004) Glycine transporter I inhibitor, N-methylglycine (sarcosine), added to antipsychotics for the treatment of schizophrenia. *Biol Psychiatry*, Vol. 55 (5) 452-6.
- Tsai, G., Yang, P., Chung, L.C., Lange, N. & Coyle, J.T. (1998) D-serine added to antipsychotics for the treatment of schizophrenia. *Biol Psychiatry*, Vol. 44 (11) 1081-9.
- Tsai, G.E., Yang, P., Chang, Y.C. & Chong, M.Y. (2006) D-alanine added to antipsychotics for the treatment of schizophrenia. *Biol Psychiatry*, Vol. 59 (3) 230-4.
- Tsai, G.E., Yang, P., Chung, L.C., Tsai, I.C., Tsai, C.W. & Coyle, J.T. (1999) D-serine added to clozapine for the treatment of schizophrenia. *Am J Psychiatry*, Vol. 156 (11) 1822-5.
- Tsuzuki, H., Maekawa, M., Konno, R. & Hori, Y. (2012) Functional roles of endogenous D-serine in pain-induced ultrasonic vocalization. *Neuroreport*, Vol. 23 (16) 937-41.

- Tuominen, H.J., Tiihonen, J. & Wahlbeck, K. (2005) Glutamatergic drugs for schizophrenia: a systematic review and meta-analysis. *Schizophr Res*, Vol. 72 (2-3) 225-34.
- Tverskoy, M., Oren, M., Vaskovich, M., Dashkovsky, I. & Kissin, I. (1996) Ketamine enhances local anesthetic and analgesic effects of bupivacaine by peripheral mechanism: a study in postoperative patients. *Neurosci Lett*, Vol. 215 (1) 5-8.
- Umbricht, D., Alberati, D., Martin-Facklam, M., Borroni, E., Youssef, E.A., Ostland, M., Wallace, T.L., Knoflach, F., Dorflinger, E., Wettstein, J.G., Bausch, A., Garibaldi, G. & Santarelli, L. (2014) Effect of bitopertin, a glycine reuptake inhibitor, on negative symptoms of schizophrenia: a randomized, double-blind, proof-of-concept study. *JAMA Psychiatry*, Vol. 71 (6) 637-46.
- Uo, T., Yoshimura, T., Shimizu, S. & Esaki, N. (1998) Occurrence of pyridoxal 5'-phosphate-dependent serine racemase in silkworm, *Bombyx mori*. *Biochem Biophys Res Commun*, Vol. 246 (1) 31-4.
- Vagenende, V., Yap, M.G. & Trout, B.L. (2009) Mechanisms of protein stabilization and prevention of protein aggregation by glycerol. *Biochemistry*, Vol. 48 (46) 11084-96.
- Van Der Auwera, S., Teumer, A., Hertel, J., Homuth, G., Volker, U., Lucht, M.J., Degenhardt, F., Schulze, T., Rietschel, M., Nothen, M.M., John, U., Nauck, M. & Grabe, H.J. (2016) The inverse link between genetic risk for schizophrenia and migraine through NMDA (N-methyl-D-aspartate) receptor activation via D-serine. *Eur Neuropsychopharmacol*, Vol. 26 (9) 1507-15.
- Van Dyke, M.W., Sirito, M. & Sawadogo, M. (1992) Single-step purification of bacterially expressed polypeptides containing an oligo-histidine domain. *Gene*, Vol. 111 (1) 99-104.
- Vance, K.M., Hansen, K.B. & Traynelis, S.F. (2012) GluN1 splice variant control of GluN1/GluN2D NMDA receptors. *J Physiol*, Vol. 590 (16) 3857-75.
- Vance, K.M., Simorowski, N., Traynelis, S.F. & Furukawa, H. (2011) Ligand-specific deactivation time course of GluN1/GluN2D NMDA receptors. *Nat Commun*, Vol. 2 294.
- Vega, C.A., Butler, R.A., Perez, B. & Torres, C. (2002) Thermodynamics of the dissociation of protonated tris(hydroxymethyl)aminomethane in 25 and 50 wt % 2-propanol from 5 to 45.degree.C.
- Verrall, L., Walker, M., Rawlings, N., Benzel, I., Kew, J.N., Harrison, P.J. & Burnet, P.W. (2007) d-Amino acid oxidase and serine racemase in human brain: normal distribution and altered expression in schizophrenia. *Eur J Neurosci*, Vol. 26 (6) 1657-69.
- Vogensen, S.B., Jensen, H.S., Stensbol, T.B., Frydenvang, K., Bang-Andersen, B., Johansen, T.N., Egebjerg, J. & Krosgaard-Larsen, P. (2000) Resolution, configurational assignment, and enantiopharmacology of 2-amino-3-[3-hydroxy-5-(2-methyl-2H-tetrazol-5-yl)isoxazol-4-yl]propionic acid, a potent GluR3- and GluR4-preferring AMPA receptor agonist. *Chirality*, Vol. 12 (10) 705-13.
- Volbracht, C., Van Beek, J., Zhu, C., Blomgren, K. & Leist, M. (2006) Neuroprotective properties of memantine in different in vitro and in vivo models of excitotoxicity. *Eur J Neurosci*, Vol. 23 (10) 2611-22.
- Vollenweider, F.X., Leenders, K.L., Oye, I., Hell, D. & Angst, J. (1997) Differential psychopathology and patterns of cerebral glucose utilisation produced by (S)- and (R)-ketamine in healthy volunteers using positron emission tomography (PET). *Eur Neuropsychopharmacol*, Vol. 7 (1) 25-38.
- Vorlová, B., Nachtigallová, D., Jirásková-Vaníčková, J., Ajani, H., Jansa, P., Rezáč, J., Fanfrlík, J., Otyepka, M., Hobza, P., Konvalinka, J. & Lepšík, M. (2015) Malonate-based inhibitors of mammalian serine racemase: kinetic characterization and structure-based computational study. *Eur J Med Chem*, Vol. 89 189-97.

- Vyklicky, V., Korinek, M., Smejkalova, T., Balik, A., Krausova, B., Kaniakova, M., Lichnerova, K., Cerny, J., Krusek, J., Dittert, I., Horak, M. & Vyklicky, L. (2014) Structure, function, and pharmacology of NMDA receptor channels. *Physiol Res*, Vol. 63 Suppl 1 S191-203.
- Wallace, M.S., Rowbotham, M.C., Katz, N.P., Dworkin, R.H., Dotson, R.M., Galer, B.S., Rauck, R.L., Backonja, M.M., Quessy, S.N. & Meisner, P.D. (2002) A randomized, double-blind, placebo-controlled trial of a glycine antagonist in neuropathic pain. *Neurology*, Vol. 59 (11) 1694-700.
- Walsh, D.M., Klyubin, I., Fadeeva, J.V., Cullen, W.K., Anwyl, R., Wolfe, M.S., Rowan, M.J. & Selkoe, D.J. (2002) Naturally secreted oligomers of amyloid beta protein potently inhibit hippocampal long-term potentiation in vivo. *Nature*, Vol. 416 (6880) 535-9.
- Wang, C.X. & Shuaib, A. (2005) NMDA/NR2B selective antagonists in the treatment of ischemic brain injury. *Curr Drug Targets CNS Neurol Disord*, Vol. 4 (2) 143-51.
- Wang, C.Y., Ku, S.C., Lee, C.C. & Wang, A.H. (2012) Modulating the function of human serine racemase and human serine dehydratase by protein engineering. *Protein Eng Des Sel*, Vol. 25 (11) 741-9.
- Wang, H.W., Pasternak, J.F., Kuo, H., Ristic, H., Lambert, M.P., Chromy, B., Viola, K.L., Klein, W.L., Stine, W.B., Krafft, G.A. & Trommer, B.L. (2002) Soluble oligomers of beta amyloid (1-42) inhibit long-term potentiation but not long-term depression in rat dentate gyrus. *Brain Res*, Vol. 924 (2) 133-40.
- Wang, J., Goffer, Y., Xu, D., Tukey, D.S., Shamir, D.B., Eberle, S.E., Zou, A.H., Blanck, T.J. & Ziff, E.B. (2011) A single subanesthetic dose of ketamine relieves depression-like behaviors induced by neuropathic pain in rats. *Anesthesiology*, Vol. 115 (4) 812-21.
- Wang, W. & Barger, S.W. (2011) Roles of quaternary structure and cysteine residues in the activity of human serine racemase. *BMC Biochem*, Vol. 12 63.
- Watkins, L.R. & Maier, S.F. (2005) Immune regulation of central nervous system functions: from sickness responses to pathological pain. *J Intern Med*, Vol. 257 (2) 139-55.
- Watt, A.D., Perez, K.A., Rembach, A., Sherrat, N.A., Hung, L.W., Johanssen, T., Mclean, C.A., Kok, W.M., Hutton, C.A., Fodero-Tavoletti, M., Masters, C.L., Villemagne, V.L. & Barnham, K.J. (2013) Oligomers, fact or artefact? SDS-PAGE induces dimerization of beta-amyloid in human brain samples. *Acta Neuropathol*, Vol. 125 (4) 549-64.
- Wendler, A. & Wehling, M. (2010) The translatability of animal models for clinical development: biomarkers and disease models. *Curr Opin Pharmacol*, Vol. 10 (5) 601-6.
- Wesnes, K.A., Edgar, C., Dean, A.D. & Wroe, S.J. (2009) The cognitive and psychomotor effects of remacemide and carbamazepine in newly diagnosed epilepsy. *Epilepsy Behav*, Vol. 14 (3) 522-8.
- Whiteford, H.A., Degenhardt, L., Rehm, J., Baxter, A.J., Ferrari, A.J., Erskine, H.E., Charlson, F.J., Norman, R.E., Flaxman, A.D., Johns, N., Burstein, R., Murray, C.J. & Vos, T. (2013) Global burden of disease attributable to mental and substance use disorders: findings from the Global Burden of Disease Study 2010. *Lancet*, Vol. 382 (9904) 1575-86.
- Wilding, T.J. & Huettner, J.E. (1996) Antagonist pharmacology of kainate- and alpha-amino-3-hydroxy-5-methyl-4-isoxazolepropionic acid-preferring receptors. *Mol Pharmacol*, Vol. 49 (3) 540-6.
- Willard, L.B., Hauss-Wegrzyniak, B., Danysz, W. & Wenk, G.L. (2000) The cytotoxicity of chronic neuroinflammation upon basal forebrain cholinergic neurons of rats can be attenuated by glutamatergic antagonism or cyclooxygenase-2 inhibition. *Exp Brain Res*, Vol. 134 (1) 58-65.
- Willard, S.S. & Koochekpour, S. (2013) Glutamate, glutamate receptors, and downstream signaling pathways. *Int J Biol Sci*, Vol. 9 (9) 948-59.

Williams, D.C., Van Frank, R.M., Muth, W.L. & Burnett, J.P. (1982) Cytoplasmic inclusion bodies in *Escherichia coli* producing biosynthetic human insulin proteins. *Science*, Vol. 215 (4533) 687-9.

Williams, S.M., Diaz, C.M., Macnab, L.T., Sullivan, R.K. & Pow, D.V. (2006) Immunocytochemical analysis of D-serine distribution in the mammalian brain reveals novel anatomical compartmentalizations in glia and neurons. *Glia*, Vol. 53 (4) 401-11.

Winter, H.C. & Ueda, T. (1993) Glutamate uptake system in the presynaptic vesicle: glutamic acid analogs as inhibitors and alternate substrates. *Neurochem Res*, Vol. 18 (1) 79-85.

Wisniewski, K. & Car, H. (2002) (S)-3,5-DHPG: a review. *CNS Drug Rev*, Vol. 8 (1) 101-16.

Wittekindt, B., Malany, S., Schemm, R., Otvos, L., Maccacchini, M.L., Laube, B. & Betz, H. (2001) Point mutations identify the glutamate binding pocket of the N-methyl-D-aspartate receptor as major site of conantokin-G inhibition. *Neuropharmacology*, Vol. 41 (6) 753-61.

Wo, Z.G. & Oswald, R.E. (1995) Unraveling the modular design of glutamate-gated ion channels. *Trends Neurosci*, Vol. 18 (4) 161-8.

Wojcik, S.M., Rhee, J.S., Herzog, E., Sigler, A., Jahn, R., Takamori, S., Brose, N. & Rosenmund, C. (2004) An essential role for vesicular glutamate transporter 1 (VGLUT1) in postnatal development and control of quantal size. *Proc Natl Acad Sci U S A*, Vol. 101 (18) 7158-63.

Wolosker, H. (2011) Serine racemase and the serine shuttle between neurons and astrocytes. *Biochim Biophys Acta*, Vol. 1814 (11) 1558-66.

Wolosker, H., Blackshaw, S. & Snyder, S.H. (1999a) Serine racemase: a glial enzyme synthesizing D-serine to regulate glutamate-N-methyl-D-aspartate neurotransmission. *Proc Natl Acad Sci U S A*, Vol. 96 (23) 13409-14.

Wolosker, H., Dumin, E., Balan, L. & Foltyn, V.N. (2008) D-amino acids in the brain: D-serine in neurotransmission and neurodegeneration. *FEBS J*, Vol. 275 (14) 3514-26.

Wolosker, H. & Mori, H. (2012) Serine racemase: an unconventional enzyme for an unconventional transmitter. *Amino Acids*, Vol. 43 (5) 1895-904.

Wolosker, H., Sheth, K.N., Takahashi, M., Mothet, J.P., Brady, R.O., Ferris, C.D. & Snyder, S.H. (1999b) Purification of serine racemase: biosynthesis of the neuromodulator D-serine. *Proc Natl Acad Sci U S A*, Vol. 96 (2) 721-5.

Wood, P.L., Hawkinson, J.E. & Goodnough, D.B. (1996) Formation of D-serine from L-phosphoserine in brain synaptosomes. *J Neurochem*, Vol. 67 (4) 1485-90.

Wootz, H., Enjin, A., Wallen-Mackenzie, A., Lindholm, D. & Kullander, K. (2010) Reduced VGLUT2 expression increases motor neuron viability in Sod1(G93A) mice. *Neurobiol Dis*, Vol. 37 (1) 58-66.

Wu, P.L., Tang, H.S., Lane, H.Y., Tsai, C.A. & Tsai, G.E. (2011) Sarcosine therapy for obsessive compulsive disorder: a prospective, open-label study. *J Clin Psychopharmacol*, Vol. 31 (3) 369-74.

Wu, S. & Barger, S.W. (2004) Induction of serine racemase by inflammatory stimuli is dependent on AP-1. *Ann N Y Acad Sci*, Vol. 1035 133-46.

Wu, S., Basile, A.S. & Barger, S.W. (2007) Induction of serine racemase expression and D-serine release from microglia by secreted amyloid precursor protein (sAPP). *Curr Alzheimer Res*, Vol. 4 (3) 243-51.

- Wu, S.Z., Bodles, A.M., Porter, M.M., Griffin, W.S., Basile, A.S. & Barger, S.W. (2004) Induction of serine racemase expression and D-serine release from microglia by amyloid beta-peptide. *J Neuroinflammation*, Vol. 1 (1) 2.
- Xu, Q. & Yaksh, T.L. (2011) A brief comparison of the pathophysiology of inflammatory versus neuropathic pain. *Curr Opin Anaesthesiol*, Vol. 24 (4) 400-7.
- Yamada, K., Ohnishi, T., Hashimoto, K., Ohba, H., Iwayama-Shigeno, Y., Toyoshima, M., Okuno, A., Takao, H., Toyota, T., Minabe, Y., Nakamura, K., Shimizu, E., Itokawa, M., Mori, N., Iyo, M. & Yoshikawa, T. (2005) Identification of multiple serine racemase (SRR) mRNA isoforms and genetic analyses of SRR and DAO in schizophrenia and D-serine levels. *Biol Psychiatry*, Vol. 57 (12) 1493-503.
- Yamanaka, M., Miyoshi, Y., Ohide, H., Hamase, K. & Konno, R. (2012) D-Amino acids in the brain and mutant rodents lacking D-amino-acid oxidase activity. *Amino Acids*, Vol. 43 (5) 1811-21.
- Yang, B., Ren, Q., Ma, M., Chen, Q.X. & Hashimoto, K. (2016) Antidepressant Effects of (+)-MK-801 and (-)-MK-801 in the Social Defeat Stress Model. *Int J Neuropsychopharmacol*, Vol. 19 (12).
- Yang, C., Shirayama, Y., Zhang, J.C., Ren, Q., Yao, W., Ma, M., Dong, C. & Hashimoto, K. (2015) R-ketamine: a rapid-onset and sustained antidepressant without psychotomimetic side effects. *Transl Psychiatry*, Vol. 5 e632.
- Yang, Y., Adelstein, S.J. & Kassis, A.I. (2009) Target discovery from data mining approaches. *Drug Discov Today*, Vol. 14 (3-4) 147-54.
- Yang, Z., Zhou, X. & Zhang, Q. (2013) Effectiveness and safety of memantine treatment for Alzheimer's disease. *J Alzheimers Dis*, Vol. 36 (3) 445-58.
- Yao, Y., Harrison, C.B., Freddolino, P.L., Schulten, K. & Mayer, M.L. (2008) Molecular mechanism of ligand recognition by NR3 subtype glutamate receptors. *EMBO J*, Vol. 27 (15) 2158-70.
- Yeung, L.Y., Wai, M.S., Fan, M., Mak, Y.T., Lam, W.P., Li, Z., Lu, G. & Yew, D.T. (2010) Hyperphosphorylated tau in the brains of mice and monkeys with long-term administration of ketamine. *Toxicol Lett*, Vol. 193 (2) 189-93.
- Yoshikawa, M., Takayasu, N., Hashimoto, A., Sato, Y., Tamaki, R., Tsukamoto, H., Kobayashi, H. & Noda, S. (2007) The serine racemase mRNA is predominantly expressed in rat brain neurons. *Arch Histol Cytol*, Vol. 70 (2) 127-34.
- Yu, H., Zhang, H., Yang, Y., Li, W., Yang, G. & Lu, L. (2015) [Association of gene polymorphisms with the susceptibility of schizophrenia in Han Chinese population]. *Zhonghua Yi Xue Za Zhi*, Vol. 95 (47) 3803-7.
- Yuan, H., Hansen, K.B., Vance, K.M., Ogden, K.K. & Traynelis, S.F. (2009) Control of NMDA receptor function by the NR2 subunit amino-terminal domain. *J Neurosci*, Vol. 29 (39) 12045-58.
- Yurkewicz, L., Weaver, J., Bullock, M.R. & Marshall, L.F. (2005) The effect of the selective NMDA receptor antagonist traxoprodil in the treatment of traumatic brain injury. *J Neurotrauma*, Vol. 22 (12) 1428-43.
- Zanders, E.D., Bailey, D.S. & Dean, P.M. (2002) Probes for chemical genomics by design. *Drug Discov Today*, Vol. 7 (13) 711-8.
- Zanos, P., Moaddel, R., Morris, P.J., Georgiou, P., Fischell, J., Elmer, G.I., Alkondon, M., Yuan, P., Pribut, H.J., Singh, N.S., Dossou, K.S., Fang, Y., Huang, X.P., Mayo, C.L., Wainer, I.W., Albuquerque, E.X., Thompson, S.M., Thomas, C.J., Zarate, C.A., Jr. & Gould, T.D. (2016) NMDAR inhibition-independent antidepressant actions of ketamine metabolites. *Nature*, Vol. 533 (7604) 481-6.

- Zarate, C.A., Singh, J.B., Carlson, P.J., Brutsche, N.E., Ameli, R., Luckenbaugh, D.A., Charney, D.S. & Manji, H.K. (2006) A randomized trial of an N-methyl-D-aspartate antagonist in treatment-resistant major depression. *Arch Gen Psychiatry*, Vol. 63 (8) 856-64.
- Zhang, C., Li, Z., Wu, Z., Chen, J., Wang, Z., Peng, D., Hong, W., Yuan, C., Yu, S., Xu, Y., Xu, L., Xiao, Z. & Fang, Y. (2014a) A study of N-methyl-D-aspartate receptor gene (GRIN2B) variants as predictors of treatment-resistant major depression. *Psychopharmacology (Berl)*, Vol. 231 (4) 685-93.
- Zhang, H.X., Lyons-Warren, A. & Thio, L.L. (2009) The glycine transport inhibitor sarcosine is an inhibitory glycine receptor agonist. *Neuropharmacology*, Vol. 57 (5-6) 551-5.
- Zhang, J.C., Li, S.X. & Hashimoto, K. (2014b) R (-)-ketamine shows greater potency and longer lasting antidepressant effects than S (+)-ketamine. *Pharmacol Biochem Behav*, Vol. 116 137-41.
- Zhang, J.H., Chung, T.D. & Oldenburg, K.R. (1999) A Simple Statistical Parameter for Use in Evaluation and Validation of High Throughput Screening Assays. *J Biomol Screen*, Vol. 4 (2) 67-73.
- Zhang, X.L., Sullivan, J.A., Moskal, J.R. & Stanton, P.K. (2008) A NMDA receptor glycine site partial agonist, GLYX-13, simultaneously enhances LTP and reduces LTD at Schaffer collateral-CA1 synapses in hippocampus. *Neuropharmacology*, Vol. 55 (7) 1238-50.
- Zhang, Y.L. & Zhang, Z.Y. (1998) Low-affinity binding determined by titration calorimetry using a high-affinity coupling ligand: a thermodynamic study of ligand binding to protein tyrosine phosphatase 1B. *Anal Biochem*, Vol. 261 (2) 139-48.
- Zhao, W., Konno, R., Zhou, X.J., Yin, M. & Wang, Y.X. (2008) Inhibition of D-amino-Acid oxidase activity induces pain relief in mice. *Cell Mol Neurobiol*, Vol. 28 (4) 581-91.
- Zhao, W.J., Gao, Z.Y., Wei, H., Nie, H.Z., Zhao, Q., Zhou, X.J. & Wang, Y.X. (2010) Spinal D-amino acid oxidase contributes to neuropathic pain in rats. *J Pharmacol Exp Ther*, Vol. 332 (1) 248-54.
- Zhou, H.Y., Chen, S.R. & Pan, H.L. (2011) Targeting N-methyl-D-aspartate receptors for treatment of neuropathic pain. *Expert Rev Clin Pharmacol*, Vol. 4 (3) 379-88.
- Zhou, Y. & Danbolt, N.C. (2013) GABA and Glutamate Transporters in Brain. *Front Endocrinol (Lausanne)*, Vol. 4 165.

10 APPENDIX

10.1 Profile of pET-24a plasmid

The pET-24a dsDNA bacterial vector was used for *in vitro* SR expression via a T7 promoter; it contains a gene for kanamycin resistance and is comprised of 5310 base pairs. Key features of the plasmid are presented in Table 10.1.

Table 10.1. Features of pET-24a bacterial plasmid used for expression of SR.

Feature	Name	Description	Start position	End position
Bacterial origin	pBR322 ori	pBR322-type origin of replication	0	0
Bacterial operon	Lac op	Lac operator (after T7, before tags and MCS ¹)	0	0
Trxn termination sequence	T7 term	T7 terminator sequence	26	72
Tag	His tag	His tag CDS ²	140	157
MCS	MCS	MCS (XhoI, NotI, EagI, HindIII, Sall, SacI, EcoRI, BamHI)	158	203
Tag	T7 tag	T7 tag CDS	207	239
Promoter	T7 pr	T7 promoter 5'[TAATACGACTCACTATAGGG]3'	311	327
Repressor protein gene	LacI	LacI CDS	714	1793
Selectable marker	KanR	Kanamycin resistance gene	3936	4748
ssDNA origin	F1 ori	F1 origin for ssDNA production	4844	5299

¹ Multiple cloning site

² Coding DNA sequence

10.2 Published SR biochemical assays

Table 10.2. Summary of SR coupled biochemical assays.

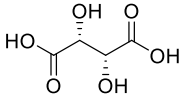
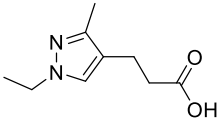
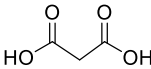
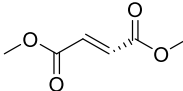
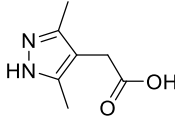
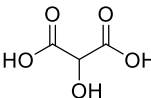
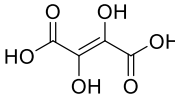
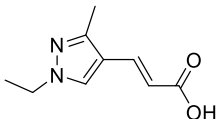
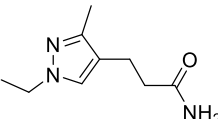
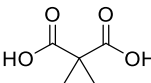
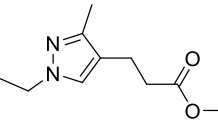
The literature surrounding SR was reviewed for biochemical assays that might have relevance to development of the chemiluminescence assay used throughout this thesis, and an overview of the findings is presented below.

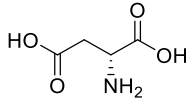
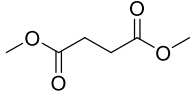
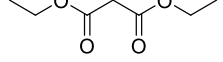
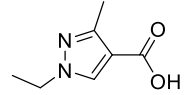
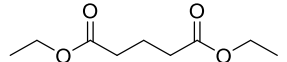
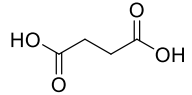
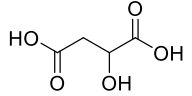
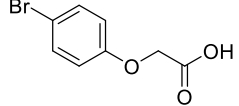
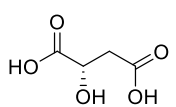
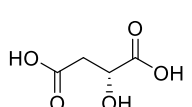
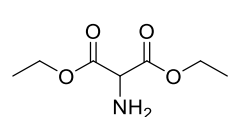
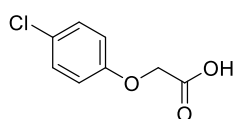
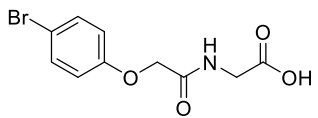
SR [μ M]	Buffer (pH)	Additives	Detection	Temp.	Reference
4	20mM MOPS (8.1)	1 μ M FAD, 5 μ M PLP, 30 μ M DTT	Colorimetric (OPD)	37°C	Cook 2012
2.6	50mM Tris-HCl (8.0)	1mM EDTA, 15 μ M PLP, 2mM DTT	Luminescence (luminol)	37°C	Wolosker 1999
1.5	50mM TEA (8.0)	2mM ATP, 50 μ M PLP, 150mM NaCl, 2mM MgCl ₂	Chromophoric	37°C	Bruno 2017
2.3	50mM TEA (8.0)	1mM ATP, 50 μ M PLP, 150mM NaCl, 1mM MgCl ₂	Chromophoric	37°C	Marchetti 2013
0.3-0.5	50mM TEA (8.0)	2mM ATP, 50 μ M PLP, 2mM DTT, 1mM MgCl ₂ , 150mM NaCl	Fluorescence	37°C	Marchetti 2014
0.1	100mM CHES (9.0)	1mM ATP, 10 μ M PLP, 1mM MgCl ₂ , 0.05% Pluronic F-127, 0.5% BSA	Fluorescence	37°C	Smith 2010
?	100mM HEPES (8.0)	1mM ATP, 10 μ M PLP, 1mM MgCl ₂	Pyruvate/NADH/LDH	37°C	Wang 2012
4	20mM Tris-HCl (7.4)	1mM ATP, 15 μ M PLP, 1mM MgCl ₂	Pyruvate/NADH/LDH	37°C	De Miranda 2002
?	100mM HEPES (8.0)	1mM ATP, 10 μ M PLP, 5mM DTT, 1mM MgCl ₂	Reversed-phase HPLC	37°C	Hoffman 2010
?	50mM phosphate buffer (8.0)	1mM ATP, 15 μ M PLP, 0.2mM DTT, 52mM NaCl	Chemiluminescence	37°C	Wang & Barger 2011
0.4	100mM Tris-HCl (8.5)	1mM ATP, 10 μ M PLP, 1mM MgCl ₂ , 0.05% Pluronic F-127	Chemiluminescence	RT	Koulouris 2017

10.3 SR literature inhibitors

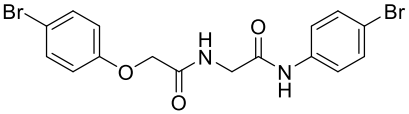
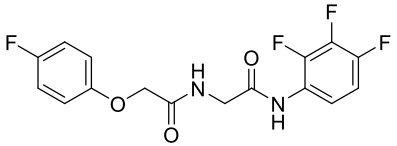
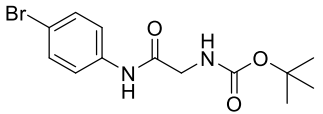
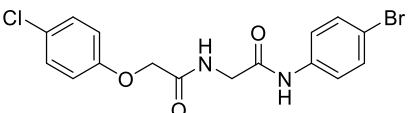
Table 10.3. Names and structures of reported SR inhibitors.

The 40 literature SR inhibitors evaluated in Chapter 6 are presented in the Table below.

Name	Number	Structure	Ref.
L(+)-dihydroxysuccinic acid	1		a
3-(1-ethyl-3-methyl-1H-pyrazol-4-yl)propanoic acid	2		b
Malonate	3		a, c, d
Dimethyl maleate	4		a
2-(3,5-demethyl-1H-pyrazol-4-yl)acetic acid	5		b
Hydroxymalonic/tartronic acid	6		d, e
(E)-2,3-dihydroxyfumaric acid	7		a
(2E)-3-(1-Ethyl-3-methyl-1H-pyrazol-4-yl)-acrylic acid	8		b
3-(1-Ethyl-3-methyl-1H-pyrazol-4-yl)-N,N-dimethylacrylamide	9		b
Dimethyl malonate	10		d
Methyl 3-(1-ethyl-3-methyl-1H-pyrazol-4-yl)propanoate	11		b

D(-)-aspartic acid	12		e
Succinic acid dimethyl ester	13		a
Diethyl malonate	14		d
1-Ethyl-3-methyl-1H-pyrazole-4-carboxylic acid	15		b
Diethyl glutarate	16		d
Succinic acid	17		a
DL-malic acid	18		a
2-(4-Bromophenoxy)acetic acid	19		f
L-malic acid	20		a
D-malic acid	21		a
Diethyl 2-aminomalonate	22		d, e
4-Chlorophenoxyacetic acid	23		f
2-[2-(4-Bromophenoxy)acetamido]acetic acid	24		f

2-(4-Fluorophenoxy)-N-[[[(2,6-difluorophenyl)carbamoyl]methyl]acetamide	25		f
2-(4-Chloromophenoxy)-N-[[[(2,6-difluorophenyl)carbamoyl]methyl]acetamide	26		f
2-[2-(4-Chlorophenoxy)acetamido]acetic acid	27		f
4-Fluoro methylphenoxyacetate	28		f
2-(4-Chlorophenoxy)-N-[[[(2,3,4-trifluorophenyl)carbamoyl]methyl]acetamide	29		f
2-(4-Bromophenoxy)-N-[[[(2,6-difluorophenyl)carbamoyl]methyl]acetamide	30		f
2-(4-Bromophenoxy)-N-[[[(2,3,4-trifluorophenyl)carbamoyl]methyl]acetamide	31		f
N-[[[(4-Bromophenyl)carbamoyl]methyl]-2-(4-fluorophenoxy)acetamide	32		f
2-Amino-N-(2,3,4-trifluorophenyl)acetamide	33		f
2-Amino-N-(4-bromophenyl)acetamide	34		f
N-[[[[(2-Fluorophenyl)carbamoyl]methyl]carbamoyl]methyl]-2-(2,3,4-trifluorophenoxy)acetamide	35		f
Tert-butyl N-[[[(2,3,4-trifluorophenyl)carbamoyl]methyl]carbamate	36		f

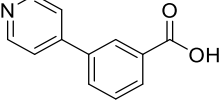

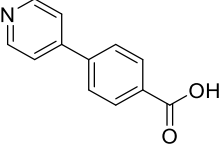

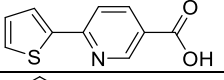

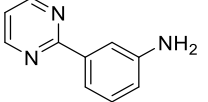

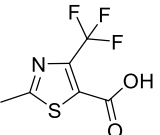

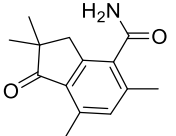

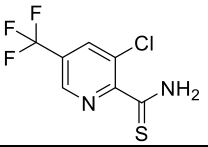

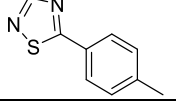

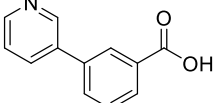

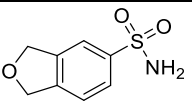

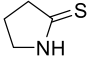

4-Bromophenyl 2-({[(4-bromophenyl)carbamoyl]methyl}amino)acetate	37		f
4-Fluorophenyl 2-({[(2,3,4-trifluorophenyl)carbamoyl]methyl}amino)acetate	38		f
Tert-butyl N-({[(4-bromophenyl)carbamoyl]methyl}carbamate	39		f
Chlorophenyl 2-({[(4-bromophenyl)carbamoyl]methyl}amino)acetate	40		f

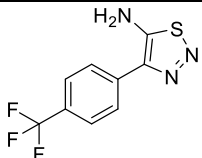
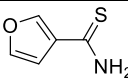
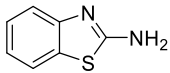
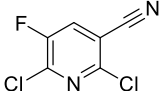
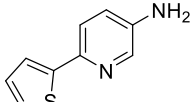
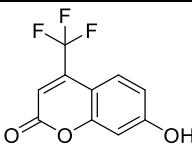
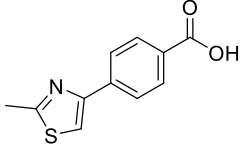
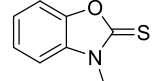
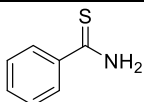
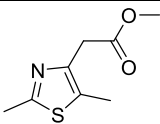
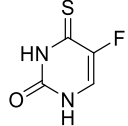
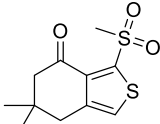
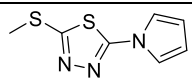
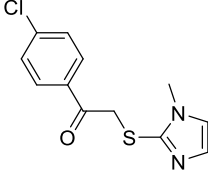
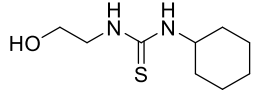
a (Strisovský *et al.*, 2005); **b** Evotec screening hits; **c** (Dellafiora *et al.*, 2015); **d** (Vorlová *et al.*, 2015); **e** (Jirásková-Vaníčková *et al.*, 2011); **f** (Mori *et al.*, 2014).

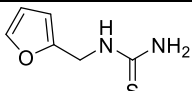
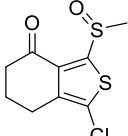
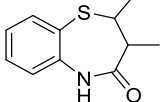
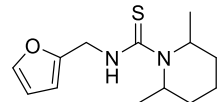
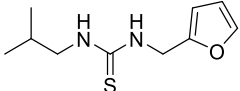
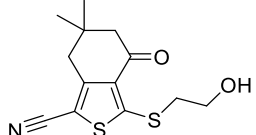
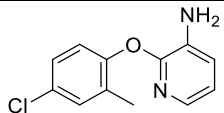
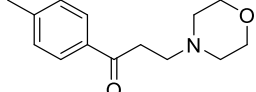
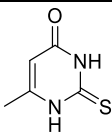
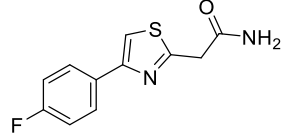
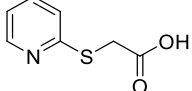
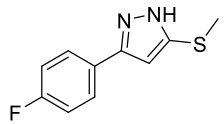
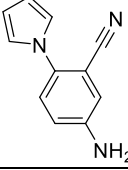
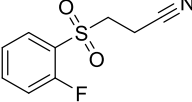
10.4 61 fragment inhibitors of SR

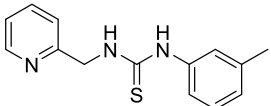
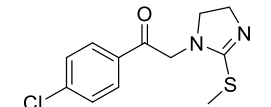
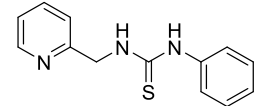
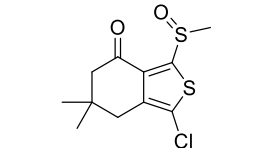
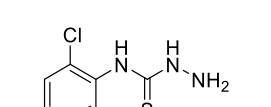
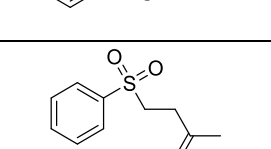
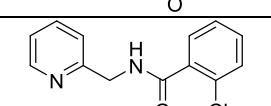
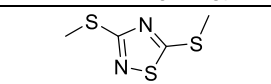
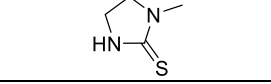
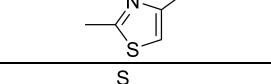
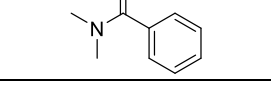
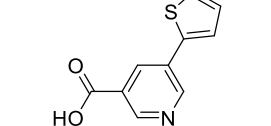
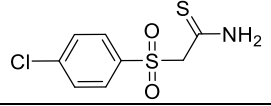
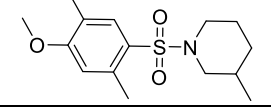
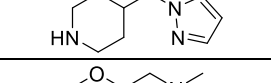
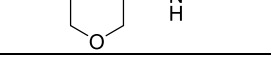
Table 10.4. Fragment inhibitors of SR identified from medium-throughput screening.

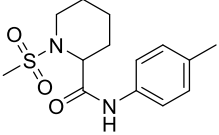
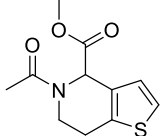
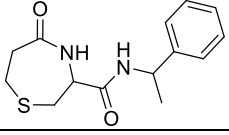
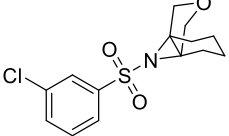
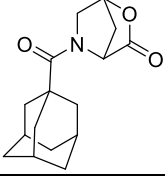
Two fragment libraries (Maybridge Ro3 and Life Chemicals 3D) were screened against SR in a coupled biochemical assay. The fragments shown below demonstrated IC_{50} values around or below 1 mM at an SR concentration of 400 nM, and did not show nonspecific inhibitory activity in the DAO counter screen. The SMARTs alert is an internal quality control measure that flags potentially problematic or reactive moieties and functional groups. Hit assessment refers to the triaging process that prioritised and progressed hits after each stage of biophysical analysis (refer to key at end of Table).

Fragment No.	Structure	IC_{50} (μ M)			SMARTs alert	Hit assessment
		N1	N2	Average		
1		1648	532	1090		
2		803	268	536		
3		701	919	810		
4		890	699	794	Aniline	
5		290	271	280		
6		427	670	549		
7		473	805	639		
8		248	211	229		
9		235	16	126		
10		1306	965	1135	Sulfamine	
11		102	39	71	Thiocarbonyl group	

12		271	58	165		◆
13		108	77	93		◆ ◆
14		1280	698	989		◆
15		872	666	769	Halo pyridine	◆
16		1428	668	1048		◆ ◆ ◆ ◆
17		1287	966	1126	Phenol ester	◆ ◆ ◆ ◆
18		41	31	36		◆
19		52	42	47	Thiocarbonyl group	◆
20		1369	626	997	Thiocarbonyl group	◆
21		458	199	329	Ester	◆
22		52	8	30	Thiocarbonyl group	◆ ◆
23		752	464	608		◆
24		1040	828	934		◆
25		1048	384	716		◆
26		951	1059	1005	Thiocarbonyl group	◆

27		326	870	598	Thiocarbonyl group	◆
28		62	35	49		◆ ◆ ◆ ◆
29		203	271	237		◆
30		230	189	209	Thiocarbonyl group	◆
31		180	246	213	Thiocarbonyl group	◆
32		499	1411	955		◆
33		1371	940	1155		◆
34		10	8	9		◆
35		344	407	376	Thiocarbonyl group	◆
36		45	12	28		◆ ◆
37		160	343	252		◆
38		360	289	324		◆
39		856	726	791	Aniline	◆ ◆ ◆ ◆
40		1047	649	848		◆

41		933	872	903	Thiocarbonyl group	◆
42		898	839	868		◆ ◆
43		411	813	612	Thiocarbonyl group	◆ ◆ ◆
44		400	67	234		◆
45		243	205	224	Hydrazone, O-N single bond, thiocarbonyl group	◆ ◆ ◆ ◆
46		53	8	30		◆
47		100	28	64		◆
48		95	4	49		◆
49		19	30	25	Thiocarbonyl group	◆
50		638	313	476		◆
51		25	8	17	Thiocarbonyl group	◆
52		11	34	22		◆ ◆
53		1208	363	785	Thiocarbonyl group	◆ ◆
54		110	122	116	Sulfamine	◆
55		838	114	476		◆
56		1597	677	1137		◆

57		329	70	199	Sulfamine	◆
58		422	449	435	Ester	◆
59		922	376	649		◆
60		1585	389	987	Sulfamine	◆
61		1761	606	1183	Ester	◆

◆ Biochemical assay: Demonstrated IC₅₀ of 1 mM or below in at least one experiment

◆ Thermal denaturation analysis: Produced a statistically significant T_m shift

◆ MST: Produced a significant F_{norm} shift

◆ MST: K_D of around 1 mM or below in at least one experiment

◆ Crystallisation trials

◆ Binding confirmed by X-ray crystallography

10.5 Crystallography results tables

Crystallography datasets were collected from single crystals by Dr Mark Roe, either in-house (Rigaku Saturn 944+ CCD detector) or at Diamond Light Source (beamline I03). Dataset statistics are presented as averages while statistics for the highest resolution shell are shown in parentheses.

10.5.1 SR-malonate complex

Table 10.5. Data collection and validation statistics for SR-malonate complex.

(Left) Data collection statistics from a single crystal obtained in-house. (Right) Validation statistics generated by MolProbity. The Clashscore and MolProbity score were in the 99th and 98th percentile, respectively. Percentile statistics are for structures solved to 2.15–2.65 Å.

Dataset Parameter	Value	MolProbity Parameter	Value
Space group	P21	Clashscore, all atoms	3.53
a, b, c (Å)	48.17 156.60 85.91	Poor rotamers (%)	3.6
α , β , γ (°)	90.00 98.11 90.00	Ramachandran outliers (%)	0.16
Mosaicity	0.71	Ramachandran favoured (%)	96.8
Resolution range	74.74 – 2.10 (2.18 – 2.10)	No. of C β deviations (> 0.25 Å)	0.0
Average redundancy	5.41 (2.54)	MolProbity score	1.77
% completeness	99.7 (96.9)	Residues with bad bonds (%)	0.04
R _{merge}	0.123 (0.641)	Residues with bad angles (%)	0.18
R _{meas}	0.135 (0.792)		
R _{measA}	0.127 (0.755)		
Reduced χ^2	0.97 (1.28)		
I/ σ I	6.4 (0.6)		
R _{work} /R _{free}	0.28/0.32		

10.5.2 SR holoenzyme

Table 10.6. Data collection and validation statistics for SR holoenzyme.

(Left) Data collection statistics from a single crystal obtained at Diamond Light Source. (Right) Validation statistics generated by MolProbity. The Clashscore and MolProbity score were in the 99th and 92nd percentile, respectively. Percentile statistics are for structures solved to 1.65–2.15 Å.

Parameter	Value	MolProbity Parameter	Value
Space group	P21	Clashscore, all atoms	2.15
a, b, c (Å)	68.99 53.84 79.40	Poor rotamers (%)	3.9
α, β, γ (°)	90.00 106.13 90.00	Ramachandran outliers (%)	0.16
Mosaicity	3.19	Ramachandran favoured (%)	97.1
Resolution range	76.27 – 2.20 (2.28 – 2.20)	No. of C β deviations (> 0.25 Å)	0.0
Average redundancy	6.42 (3.51)	MolProbity score	1.6
% completeness	99.8 (99.8)	Residues with bad bonds (%)	0.01
R _{merge}	0.144 (0.500)	Residues with bad angles (%)	0.09
R _{meas}	0.157 (0.584)		
R _{measA}	0.143 (0.549)		
Reduced X ²	0.88 (0.64)		
I/ σ I	5.6 (1.2)		
R _{work} /R _{free}	0.28/0.32		

10.5.3 SR complex with 3-pyridin-4-yl benzoic acid

Table 10.7. Data collection and validation statistics for SR-F01 complex.

(Left) Data collection statistics from a single crystal obtained at Diamond Light Source. (Right) Validation statistics generated by MolProbity. The Clashscore and MolProbity score were in the 99th and 92nd percentile, respectively. Percentile statistics are for structures solved to 1.65–2.15 Å.

Parameter	Value	MolProbity Parameter	Value
Space group	P21	Clashscore, all atoms	3.95
a, b, c (Å)	48.19 155.24 86.06	Poor rotamers (%)	2.5
α, β, γ (°)	90.00 98.36 90.00	Ramachandran outliers (%)	0.0
Resolution range	155.2 – 1.81 (2.28 – 2.20)	Ramachandran favoured (%)	97.7
% completeness	96.5 (99.3)	No. of C β deviations (> 0.25 Å)	0.0
R _{merge}	0.040 (0.445)	MolProbity score	1.6
R _{meas}	0.049 (0.525)	Residues with bad bonds (%)	0.03
R _{measA}	0.048 (0.534)	Residues with bad angles (%)	0.12
I/ σ I	14.7 (2.2)		
R _{work} /R _{free}	0.18/0.21		

10.6 Ramachandran plots

10.6.1 SR-malonate complex

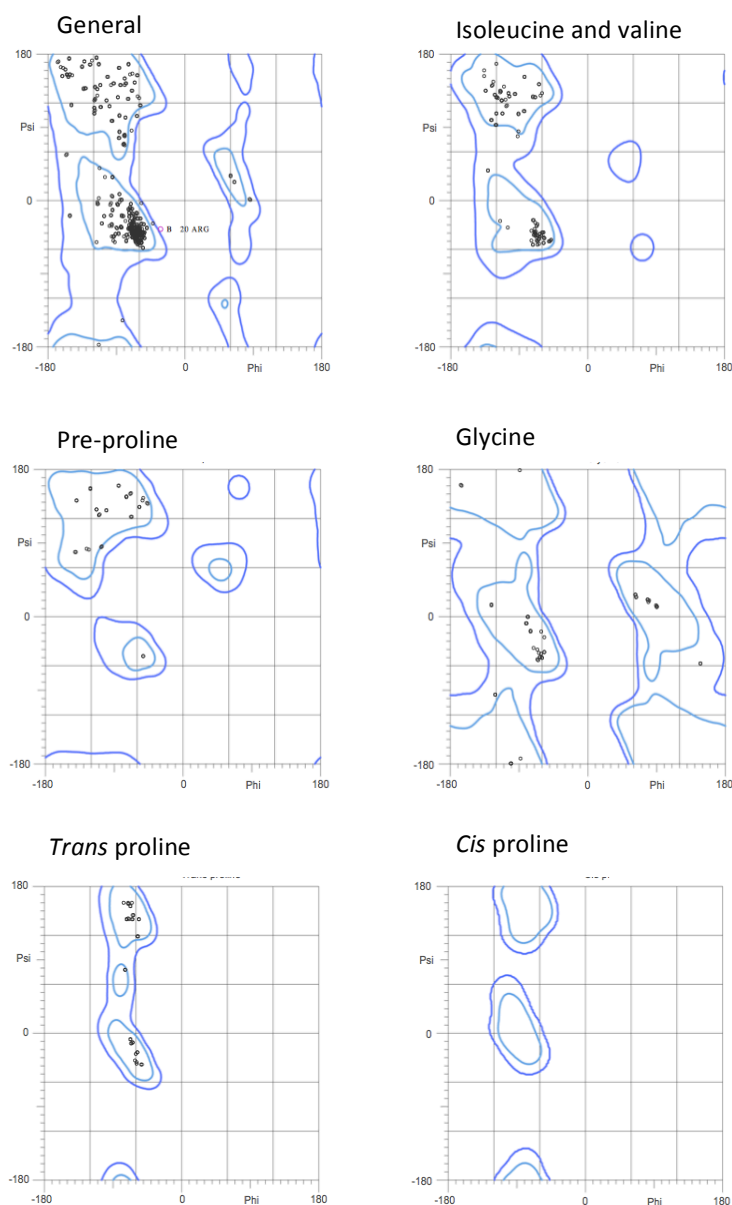


Figure 10.1. Specific Ramachandran plots for SR-malonate complex generated by MolProbity.

Evaluation of Ramachandran angles revealed there were practically no steric hindrances between atoms of the polypeptide, indicating high quality structure solution for the SR-malonate crystal. Separate Φ and Ψ distributions are shown for general, isoleucine/valine, pre-proline, glycine, and *trans/cis* proline residues. Areas encapsulated by the blue lines are the favourable regions (light blue) and limit for allowed regions (dark blue). MolProbity statistics were as follows: favoured regions (596/616 residues, 96.8%); allowed regions (615/616 residues, 99.8%); outside region (1 residue, ARG 20, 0.16%).

10.6.2 SR holoenzyme

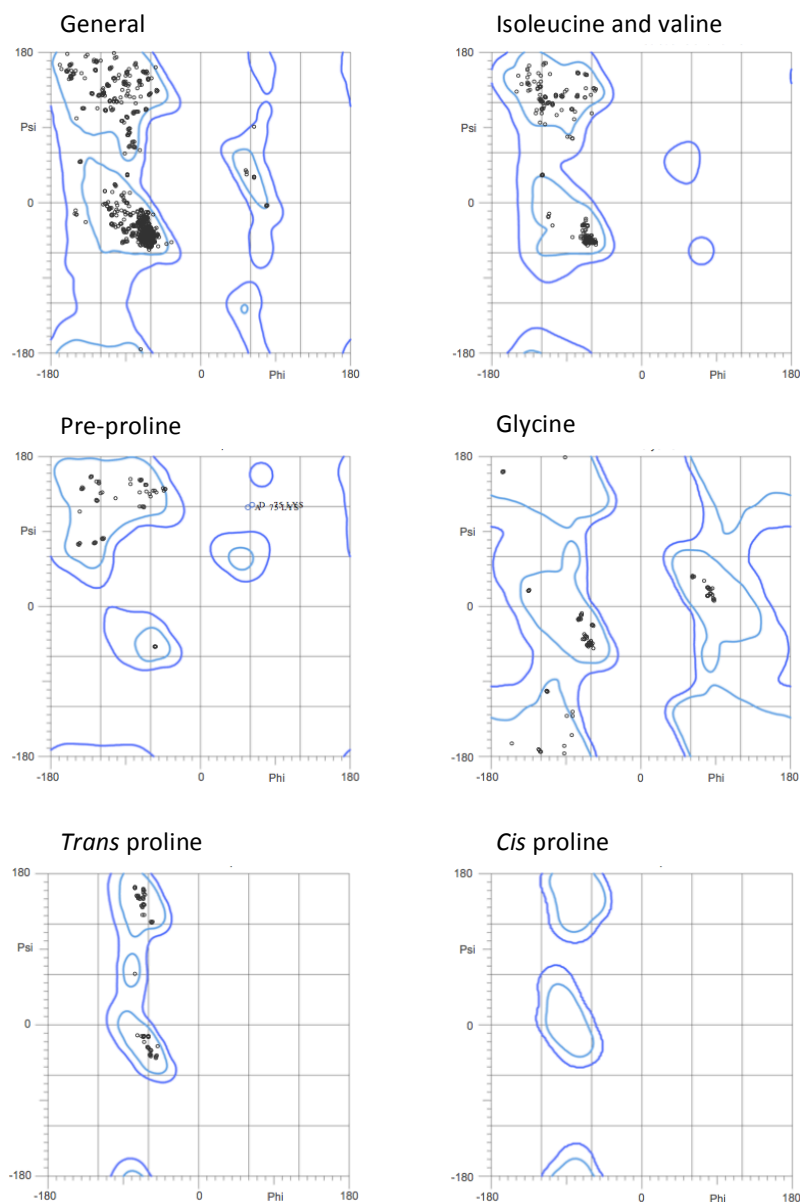


Figure 10.2. Specific Ramachandran plots for SR holoenzyme generated by MolProbity.

Evaluation of Ramachandran angles revealed negligible steric hindrances between atoms of the polypeptide (Fig. 5.6), with 99.8% of residue angles falling within allowed regions. Again, this demonstrates the SR unbound crystal structure was resolved to a high degree of quality. Separate Φ and ψ distributions are shown for general, isoleucine/valine, pre-proline, glycine, and *trans/cis* proline residues. Areas encapsulated by the blue lines are the favourable regions (light blue) and limit for allowed regions (dark blue). Favoured regions (1186/1221 residues, 97.1%); allowed regions (1219/1221 residues, 99.8%); outside region (2 residues, LYS 75 chains A and D, 0.16%).

10.7 Difference Fourier electron density map

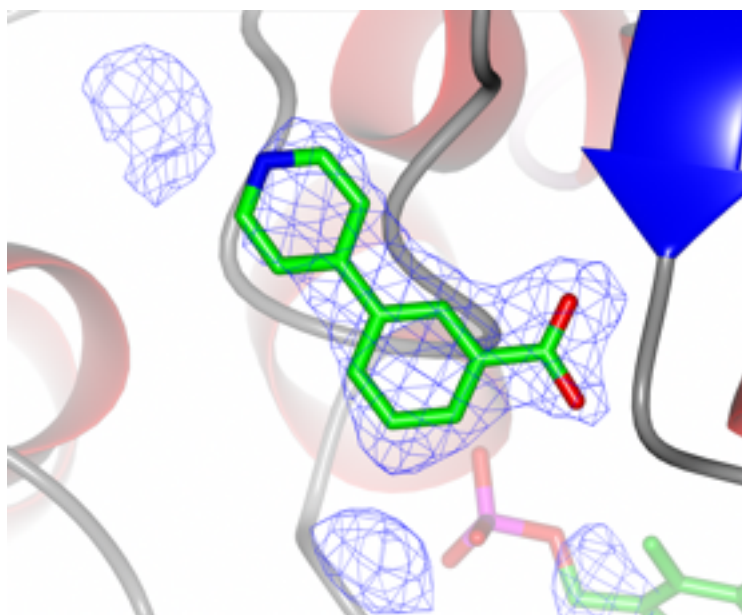


Figure 10.3 OMIT Fourier electron density map for SR ligand F01.

The OMIT map (blue mesh) contoured at 3σ was calculated using coefficients $F_{\text{obs}} - F_{\text{calc}}$ using phases from the final refined model, with the coordinates of F01 (green) deleted prior to a further round of crystallographic refinement. F_{obs} is the experimentally observed structure factor amplitude and F_{calc} is the calculated structure factor amplitude from the model. The empty density indicates the presence of a small ligand. The B-factor of F01 alone is 43%, and with respect to surrounding residues in a 5 Å range (81–83, 87, 150–153) is 27% (both side and main chains) and 30% (side chains only). That the occupancy of F01 alone is greater than those determined from the surrounding residues indicates F01 is inherently mobile, which could be attributed to the fact F01 is linked to SR only by two H-bonds on the protein surface, whereas inhibitors such as malonate bind deep in the active site where mobility is limited.